

Synthesis and Properties of Gold(III) Pincer Complexes with Sulfur Ligands

Lucy A Currie

A thesis submitted in partial fulfilment of the requirements for the
degree of Doctor of Philosophy

University of East Anglia

School of Chemistry



June 2018

This copy of the thesis has been supplied on condition that anyone who consults it is understood to recognise that its copyright rests with the author and that use of any information derived therefrom must be in accordance with current UK Copyright Law. In addition, any quotation or extract must include full attribution

Abstract

This thesis investigates the synthesis of gold(III) pincer complexes and their functionalisation and reactivity with sulfur based ligands. The first chapter gives a brief introduction to gold chemistry, focusing on C^NC gold(III) pincer complexes. The synthesis of these complexes and their subsequent functionalisation is described, emphasising their impact on our understanding of gold(III) chemistry.

Chapter Two investigates the synthesis of a series of C^NC gold(III) thiolate complexes. These complexes are photoluminescent and show either red or green emission. The emission properties are investigated in the solid state and solution. Analysis of crystal polymorphs with different emission properties show the potential for intermolecular interactions to affect the emission pathway. We identify two separate emission pathways resulting in the different emissions observed.

Chapter Three explores the potential mechanisms of reductive elimination from C^NC gold(III) complexes. Two different methodologies have been developed that trigger either C–S or C–C bond formation from a series of gold(III) complexes (chloride, thiolate, aryl and alkyl). The investigations are extended to further gold(III) heteroatom species and their reactivity is compared.

Chapter Four investigates reactions of gold(III) complexes with two different transmetallating agents: organozinc halides and silyl boronic acids. Use of these transmetallating agents, to the best of our knowledge, is unexplored with gold(III) systems. Zinc aryl halides transmetallate Au–Cl and Au–S bonds affording gold(III) aryls in one step under mild conditions. The use of a silyl boronic acid in the transmetallation of Au–O bonds produces a gold(III) silyl complex.

Chapter Five investigates the synthesis and anticancer properties of a series of C^NC gold(III) NHC complexes. We investigate the potential influence of systemic alterations to both the pincer system and NHC upon the anticancer properties and DNA intercalation. In addition, the reactivity of these complexes with thiols is probed.

Acknowledgements

Firstly, I would like to thank Professor Manfred Bochmann for the opportunity to study for a PhD in his research group. Throughout my PhD Manfred has provided advice, guidance and feedback on many aspects of my work for which I am very grateful. He has supported me to become a more independent researcher and encouraged me to present my work so thank you for all the opportunities.

Thank you to all the postdocs who I have had the opportunity to work with. Many thanks to Dr Luca Rocchigiani, who has been an invaluable source of information as well as teaching me NMR tricks and running some of the more complex NMR experiments (diffusion NMR in chapters two and three). Thanks also to Dr Benoît Bertrand for helping with some of my early synthetic problems, for running the biological assays and providing some amazing cakes and Dr Julio Fernandez-Cestau for the training in photoluminescent measurements and analysis, running several experiments at the Universidad de La Rioja, Logroño, as well as solving some crystal structures and making their pretty diagrams. In addition, thank you Dr Isabelle Fernandes for providing chemicals and company, Dr Anna Pintus for complex **39** and instigating Wednesday beer, Dr Alex Romanov for introducing me to mangosteen and all other postdocs that I have had the pleasure of working with: Dr Mateusz Cybulski, Dr Florian Chotard and Dr James Morris

Thank you also to my fellow PhD's; to Morwen Williams for providing your friendship and going climbing after work, and to James Woods for his enthusiasm and filling the lab with music.

To our collaborators, thank you for all your contributions; Professor Simon Lancaster for your time as secondary supervisor, providing extra opinions and questions; Dr Zoe Waller and Dr Elise Wright for the training in FRET assays and the opportunity to work in their lab; to Dr David Hughes for running and solving the other crystal structures; Dr Tom Penfold and Helen Duckworth for the DFT calculations in Chapter Two. In addition, I would like to express gratitude for the use of EPSRC's National Crystallography service at Southampton and the UK National Mass Spectrometry Facility at Swansea.

Outside of the lab, thank you to my family and friends who have supported me throughout my PhD studies. A huge thank you to my parents and Will who have been a source of encouragement and listened patiently to me talking about my PhD.

Contents

Lucy A Currie	
Abstract.....	i
Acknowledgements.....	ii
Abbreviations	viii
Chapter One	
Introduction.....	2
1.1 Why are we interested in gold?.....	2
1.2 Relativistic effects	2
1.3 Common oxidation states.....	3
1.4 Organometallic gold complexes	4
1.4.1 Cyclometallated gold(III) complexes.....	5
1.4.2 Gold(III) complexes using a C ^N C pincer ligand.....	5
References.....	10
Introduction.....	13
2.1 Photoluminescent metal complexes.....	13
2.1.1 Gold(III) photoluminescence.....	13
2.1.2 Photoluminescent C ^N C pincer gold(III) complexes	15
2.2 Gold(III) thiolates.....	18
2.3 Objectives	18
Results and Discussion.....	19
2.4 Synthesis of gold(III) thiolates	19
2.4.1 Solid state structures	22
2.5 Photoluminescence.....	25
2.5.1 Absorption properties of 3 – 11	26
2.5.2 Emission properties of 3 – 11	26
2.5.3 Extending the photoluminescent studies	28

2.6 Crystal packing.....	32
2.7 Diffusion NMR	36
2.8 Theoretical calculations	39
Conclusion	41
References.....	41
 Chapter Two	
Introduction.....	44
3.1 Gold Catalysis	44
3.2 Oxidative addition to gold(I) species.....	46
3.3 Reductive elimination from gold(III) species	48
3.4 Use of thiols as reducing agents	50
3.5 C-S reductive elimination from metal complexes	51
3.6 Stability of the (C [^] N [^] C)Au-X system.....	52
3.7 Objectives	53
Results and Discussion.....	54
3.8 Addition of adamantyl thiol to 2	54
3.9 Addition of other acidic compounds to 2	56
3.10 Investigating a possible mechanism for C-S reductive elimination.....	57
3.10.1 Investigating rates of C-S reductive elimination.....	57
3.10.2 Observation of a third species in the kinetic investigations.....	58
3.10.3 Reactivity of 2 with hydrochloric acid	61
3.10.4 Effect of altering the ligand system up on the rate.....	61
3.10.5 Establishing a mechanism	62
3.11 Addition of an aryl thiol to 2	64
3.12 Reactivity of adamantyl thiol with 18	65
3.13 Reactivity of adamantyl thiol with (C [^] N [^] C)AuR complexes	66
3.14 Reactivity of adamantyl thiol with (C [^] N [^] C)Au-ER (ER = OR, NR) complexes.....	69
3.15 C-S Reductive elimination via a stepwise methodology.....	71

3.16 Addition of dimethyl sulfide to 28	73
3.17 Investigating the stepwise protocol with further gold(III) heteroatom species	74
Conclusion	77
References	78
Chapter Three	
Introduction	82
4.1 Transmetallation reactions	82
4.1.1 Boronic acids in transmetallation reactions	82
4.1.2 Transmetallation using organozinc reagents	84
4.1.3 Silanes and stannanes in transmetallation reactions.....	85
4.2 Compounds containing an Si–B in transmetallation reactions.....	86
4.3 Gold-silyl complexes	88
4.4 Objectives	89
Results and Discussion	90
4.5 Reaction of 2 and 1 with aryl zinc iodide	90
4.6 Reaction of 14 with aryl zinc iodide.....	91
4.7 Reaction of 14 with boronic acids	93
4.8 Reaction of Au–O bonds with boron reagents	93
4.9 Investigating the reaction of Au(III)-O bonds with Me ₂ PhSi–Bpin	94
4.9.1 Initial experiments into insertion reactions	97
Conclusion	97
References	97
Chapter Five	
Introduction	102
5.1 Platinum based anticancer agents	102
5.2 Cyclometallated gold(III) complexes as anticancer agents	103
5.3 Gold(III) carbene complexes as anticancer agents	105

5.4 (C ^N C)gold(III) NHC complexes as anticancer agents	107
5.5 DNA binding properties.....	111
5.5.1 G-quadruplexes.....	111
5.5.2 iMotifs	113
5.6 Objectives	114
Results and discussion.....	114
5.7 Synthesis and characterisation of gold(III) carbenes (40-48)	114
5.8 Anticancer properties of 40 – 48	117
5.8.1 In vitro antiproliferative activity.....	117
5.8.2 IC ₅₀ values	119
5.9 Investigating the interactions with DNA	120
5.10 Do thiols mimic the reactivity of glutathione (GSH)?.....	125
Conclusion	126
References.....	126
Chapter Six	
6.1 General procedures	131
6.2 Synthesis and characterisation	131
6.2.1 Complexes in Chapter Two.....	131
6.2.2 Complexes in Chapter Three.....	137
6.2.3 Complexes in Chapter Four	144
6.2.4 Complexes in Chapter Five.....	147
6.3 X-ray crystallography	152
6.4 Photophysical Properties	157
6.5 Diffusion NMR	161
6.5.1 Investigating aggregation tendency Dr Luca Rocchigiani	162
6.5.2 Hydrodynamic dimensions of [ClAuSAd] _n H _n in collaboration with Dr Luca Rocchigiani.....	165

6.6 Kinetic Investigations	166
6.7 Biological testing.....	167
6.7.1 Antiproliferation assay (Dr Benoit Bertrand) ²⁰	167
6.7.2 FRET assay ²¹	167
References.....	168

Abbreviations

°	degrees
°C	degrees Celsius
Ad	adamantyl
Å	Angstrom
Ar	aryl
br	broad
calc.	calculated
C [^] N	phenyl pyridine
C [^] N ^{pz} ^C	2,6-diphenylpyrazine dianion
C [^] N ^{py} ^C	2,6-diphenylpyridine dianion
C [^] N ^{py-OMe} ^C	2,6-diphenyl- <i>p</i> -OMe-pyridine dianion
δ	chemical shift
d	doublet
DCM	dichloromethane
DMSO	dimethyl sulfoxide
eq.	equivalents
HAB ₂	[H(OEt ₂) ₂] ⁺ [H ₂ N[B(C ₆ F ₅) ₃] ₂] ⁻
HOMO	Highest Occupied Molecular Orbital
Hz	Hertz
IPr	N, N'-bis(2,6-diisopropylphenyl)imidazole-2-ylidene
ⁱ PrOH	isopropanol
IL	intraligand
<i>J</i>	coupling constant
K	Kelvin
k	rate constant
LLCT	Ligand to ligand charge transfer
LUMO	Lowest Unoccupied Molecular Orbital
m	multiplet
Me	methyl
MeCN	acetonitrile
MLCT	Metal to Ligand Charge Transfer
NHC	N-Heterocyclic Carbene
Np-1	1-naphthyl
Np-2	2-naphthyl
<i>o</i> -	ortho

OAc	acetate anion
OAc ^F	trifluoroacetate anion
<i>p</i> -	para
Ph	phenyl
Py	pyridine
Pz	pyrazine
ppm	parts per million
Quin	quinoline
s	singlet
^t Bu	tertiary butyl
t	triplet
THF	tetrahydrofuran
UV/Vis	ultraviolet/visible
λ_{max}	wavelength of maximum absorption or emission
λ_{em}	wavelength of excitation

Chapter One:

Introduction to gold(III) pincer complexes

Introduction

1.1 Why are we interested in gold?

The noble character of gold(0) had led to the preconception that gold is unreactive. It has long been considered a stable and inert metal, which is in part due to its redox potentials. The discovery that gold salts, particularly of gold(I), were active catalysts has revived an interest in understanding the nature of gold species.¹ Subsequently, this has led to the application of gold in catalysis, anticancer agents and photoluminescent materials.

The organometallic chemistry of gold is less well developed if compared to platinum, palladium and iridium, its neighbours in the periodic table. This can be exemplified by the recent isolation of the first gold(III) alkene complex in 2013,² compared to the isoelectronic, platinum(II) equivalent, Zeise's salt, which was reported in 1827 (Figure 1.1).³ Gold(III) is frequently compared to platinum(II) as they are isoelectronic. Whilst this is useful in highlighting the development of gold chemistry the two metals differ in their reactivity, such as the oxidative addition of aryl halide bonds is more facile for Pt(0) than Au(I) and their properties differ, such as electronegativity and their respective bond strengths.

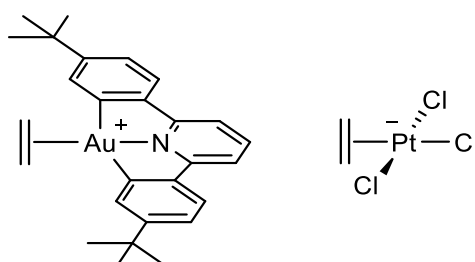


Figure 1.1. A gold(III) alkene complex and Zeise's salt.

1.2 Relativistic effects

The slow development of gold chemistry is related to the perceived inertness. This is due to relativistic effects that influence the atomic properties of gold. Relativistic effects occur in late transition metals due to high speed electrons moving close to a heavy nucleus.⁴ Gold has higher relativistic effects than its neighbours in the periodic table and is responsible for the difference in properties.⁵ One of these properties is electronegativity, gold is the most electronegative metallic element, with a similar electronegativity to carbon and hydrogen.⁶

Relativistic effects cause the contraction of penetrating orbitals, resulting in stabilisation of the 6s and 6p orbitals.⁷ This contraction of 6s and 6p orbitals increases the shielding of the nuclear charge and therefore results in the expansion of orbitals with higher angular

momentum and less penetrating radial distribution functions such as the 5d orbitals (Figure 1.2). Relativistic effects also result in increased spin orbit splitting also known as spin orbit coupling, which affects the photoluminescent properties of gold complexes (see section 2.1).

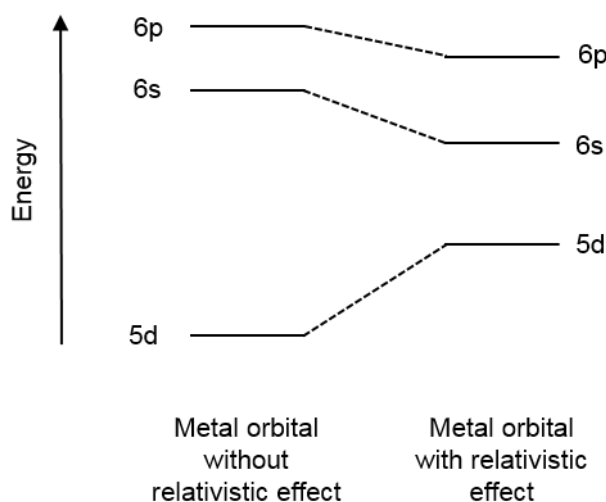


Figure 1.2. The effects upon the energy levels with and without relativistic effects of the valence shells in gold.⁸

The relativistic effect is also responsible for the yellow colour and lowered reactivity of gold, and consequently the prevalence of gold(0) found in nature.⁷ The golden colour of the metal results from a transition from the filled 5d band to the Fermi level which requires the absorption of blue and green light and reflection of red and yellow light to give the distinctive golden colour.⁹

1.3 Common oxidation states

The stability of gold(0) is indicated by the positive electropotentials (Figure 1.3).⁶ The favourable reduction potentials from gold(III) to both gold(I) and gold(0) make the synthesis of stable gold(III) complexes more difficult, with reduction products frequently observed. The comparative ease of reduction of gold(III) is evident when compared to the reduction of platinum(II) ($\text{Pt}^{2+}/\text{Pt}^0 = 1.19 \text{ V}$) to which it's reactivity is most frequently compared.

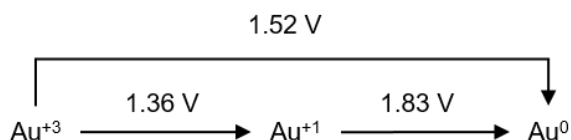


Figure 1.3. The electropotentials of gold ions in 1 M aqueous acid solutions at 25 °C.⁶

Organometallic gold chemistry is dominated by gold in oxidation states +1 and +3, due to the favourable valence electron arrangements d^{10} and d^8 respectively. Gold(I) complexes predominantly adopt a linear geometry, though there are some interesting nonlinear examples discussed in Section 3.2. Whereas gold(III) complexes adopt a square planar geometry around the metal centre, typical of 2nd and 3rd row d^8 transition metal complexes. The development of organometallic gold(III) chemistry has been slower than that of gold(I), mainly due to favourable reduction pathways of gold(III) to gold(I). There is significant interest in gold(III) because it is isoelectronic with iridium(I) and platinum(II), both of which have been extensively used in photoluminescent, catalytic and anticancer applications. Many cross-coupling catalyses involve oxidative addition and reductive elimination steps which require access of both gold(I) and (III) oxidation states, recent advances in understanding the fundamental catalytic steps have identified conditions under which this transition more facile.¹⁰

Gold(II) is less stable than gold(I) and (III), due to the d^9 electron configuration with one electron in the $d_{x^2-y^2}$ orbital and therefore it often disproportionates to a mixed valence gold(I)/(III) complex.¹⁴ Disproportionation of the naked ions is favourable and the process has been demonstrated to release 300 kcalmol⁻¹.¹¹ In fact many early complexes identified as gold(II) have now been identified as mixed gold(I)/(III) complexes. Numerous gold(II) complexes are dinuclear and are stabilised by the formation of a gold-gold bond. These complexes can be synthesised by the oxidative addition of halides to dinuclear gold(I) complexes and frequently contain bridging ligands. Recently the first complex containing an unsupported gold(II)-gold(II) bond was synthesised and isolated,¹² and subsequently a further stable example using a C[^]N[^]C pincer ligand was synthesised by Bochmann *et al.*¹³

Unusually for a metal it is possible to form the auride, an Au⁻ anion. It was initially discovered as an alkali metal salt, such as in RbAu and CsAu.¹⁴ The formation is possible due to the unusual relativistic effects of gold.

1.4 Organometallic gold complexes

Recent advances in organometallic gold chemistry have highlighted the importance of the ligand system utilised. Bulky N-heterocyclic carbene (NHC) ligands were used in the stabilisation of gold(I) hydrides by Sadighi *et al.*,¹⁵ whereas Bochmann *et al.* demonstrated that the C[^]N[^]C pincer systems (based on a pyridine diphenyl ligand system) were vital in stabilising the first gold(III) hydride.^{13a} Alternatively, Bourissou *et al.* have shown that the hemilabile P[^]N chelate systems enabled facile oxidative addition of aryl halides to gold(I), a reaction that until recently was unobserved for gold(I) systems.¹⁶ This is in contrast the

plethora of platinum based cross coupling reactions where oxidative addition of aryl halides are frequently observed. As the understanding of organometallic gold systems is improving it is challenging the initial preconception of gold's inertness.

1.4.1 Cyclometallated gold(III) complexes

The most successful approach to stabilise gold(III) complexes from reduction is the use of cyclometallating ligands.¹⁷ These ligands contribute to the stabilisation through the chelate effect and a shift in redox potentials.⁶ There are many bidentate and tridentate cyclometallated gold(III) complexes supported by a range of ligands. Figure 1.4 shows a selection of C and N based ligands, where C is an aryl ligand.¹⁸ Cyclometallation reactions conditions are strongly ligand dependant, and various methodologies have been developed.¹⁸ One approach is direct auration; this is often a two-step process where first the ligand is mixed with a gold(III) salt to form an Au–N adduct which is then heated or subjected to microwave conditions to induce C–H activation and cyclisation. This method was used in the synthesis of the three complexes on the left of Figure 1.4, to form a 5 membered cycle using C[^]N,¹⁹ or C[^]C[^]N ligands,²⁰ or a 6 membered cycle using a C[^]N ligand.²¹ Alternatively, transmetalation of a mercurated species is another common route in the formation of Au–C bonds, such as in the case of C[^]N[^]C ligands (see Scheme 1.1), this is followed by C–H activation to form the second Au–C bond. Finally, silver(I) salts can assist cyclometallation through chloride abstraction, forming a reactive site and insoluble silver chloride; this method was used in the synthesis of a C[^]N[^]N complex (right Figure 1.4).^{18,22}

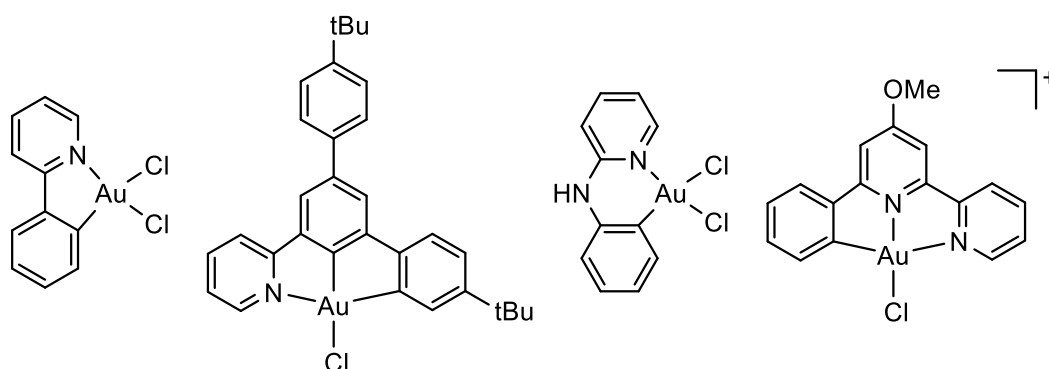


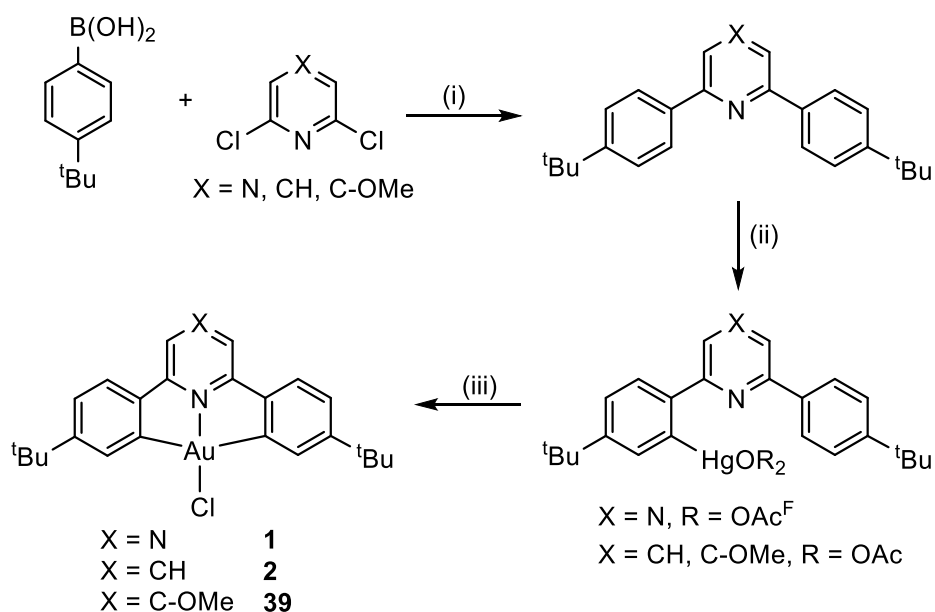
Figure 1.4. Examples of cyclometallated gold(III) complexes (anions omitted).

1.4.2 Gold(III) complexes using a C[^]N[^]C pincer ligand

The work in this thesis focuses on the use of pincer ligands based on C[^]N[^]C biscyclometalated gold(III) complex using dianionic 2,6-diaryl-substituted pyridine ligands that give neutral, highly stable complexes.¹⁷ This system is by far the most widely explored in relation to

gold(III) chemistry due to the stability of the complexes formed. However, there are other biscyclometalated systems using substituted phenyl pyridine ligands: either dianionic 3,5-diaryl-substituted phenyl pyridine ligands that give neutral, highly stable N^{^C^C} gold(III) complexes or monoanionic C^{^N^N} and N^{^C^N}, which give less stable cationic gold(III) species.

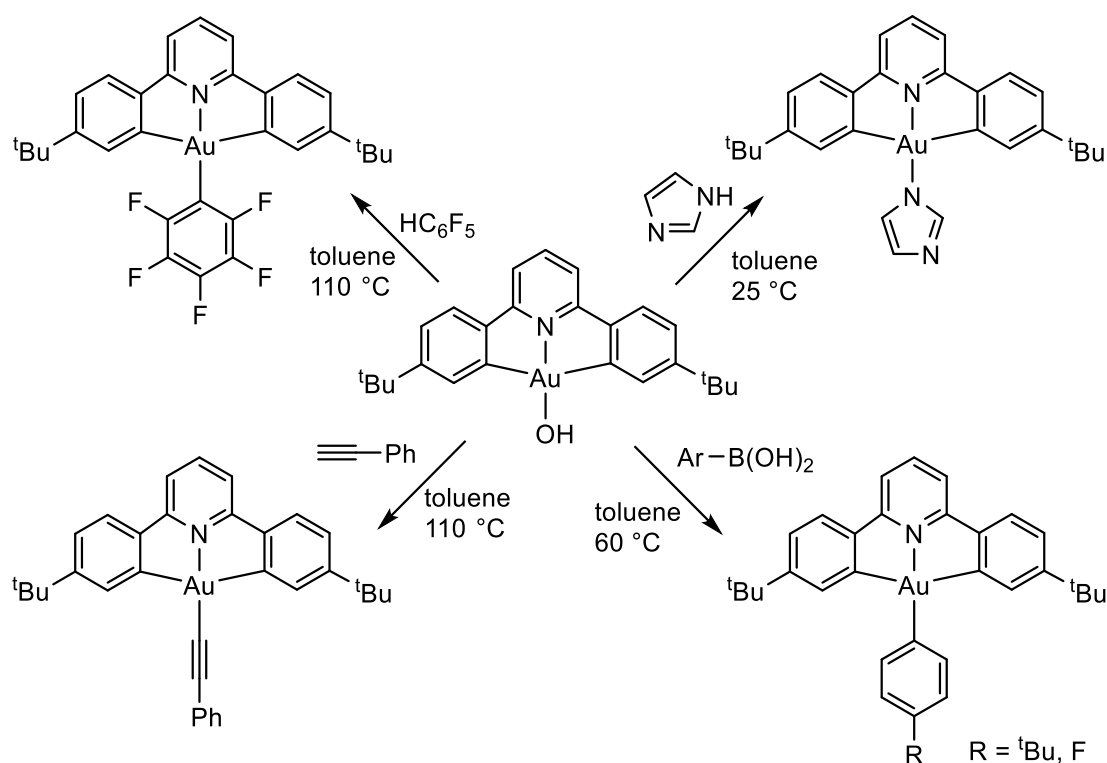
The 2,6-diphenylpyridine gold(III) complex, was first synthesised by Che *et al.*²³ and further developed by Yam *et al* to give the modified system (C^{^N^{py}^C})AuCl (**2**),²⁴ where the addition of *tert*-butyl groups improved solubility. Further derivatives have been synthesised by Bochmann *et al.* through substitution of the central pyridine for either a pyrazine²⁵ to give (C^{^N^{pz}^C})AuCl (**1**) or a *p*-OMe-pyridine²⁶ to give (C^{^N^{py-OMe}^C})AuCl (**39**) (Scheme 1.1). The syntheses of these complexes were similar, firstly the 2,6-diphenylpyridine or 2,6-diphenylpyrazine based ligand was synthesised with a Suzuki-Miyaura coupling between the 2,6-dichloropyridine (or its 4-substituted pyridine derivatives) and 4-*tert*-butylphenylboronic acid. Then the ligand was mercurated using a suitable mercury salt (Hg(OAc)₂/EtOH for the pyridine and *p*-OMe-pyridine ligands and Hg(OAc)^F₂/HOAc^F for the pyrazine ligand). Finally, transmetallation of the mercury species by KAuCl₄ and subsequent C-H activation gave the corresponding C^{^N^C} gold complexes **1**, **2** and **39**.



Scheme 1.1. The synthesis of C^{^N^C} gold(III) complexes; (i) Suzuki cross coupling (X = N: 2 molar equivalents Na₂CO₃, 0.6 mol% Pd(PPh₃)₂Cl₂ in MeCN/H₂O refluxed for 48 h; X = CH: 2 mol% Pd(PPh₃)₄, 2 molar equivalents K₃PO₄ refluxed in *i*PrOH for 12 h; X = C-OMe: 0.6 molar equivalents K₃PO₄, 5 mol% Pd(PPh₃)₄ in *i*PrOH refluxed for 48 h); (ii) mercuriation (X = N: Hg(OAc)^F₂/HOAc^F refluxed for 48 h; X = CH, C-OMe: Hg(OAc)₂/EtOH refluxed for 72 h) (iii) transmetallation (X = N: KAuCl₄ in MeCN/H₂O

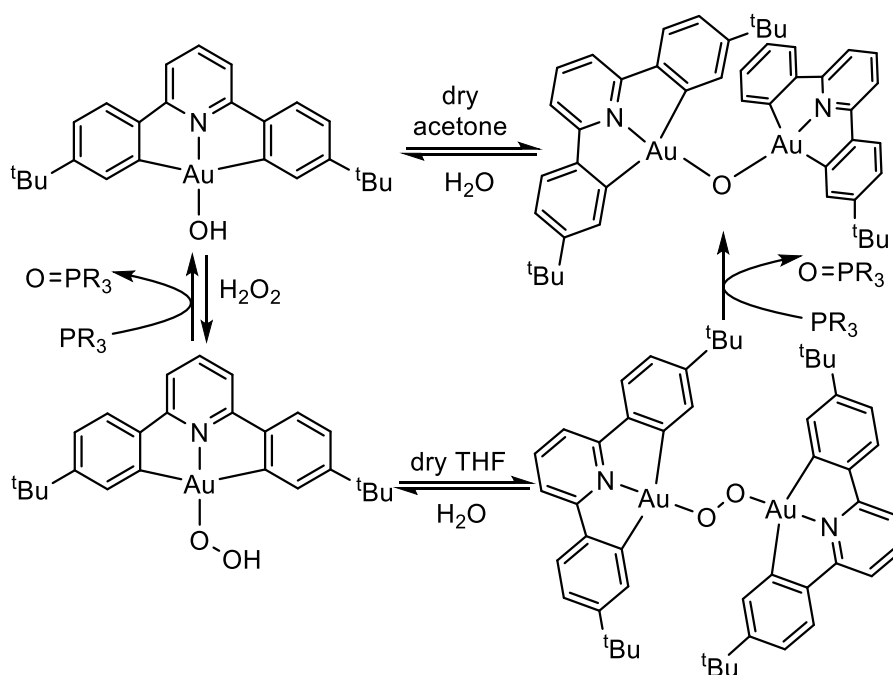
(1:1) was refluxed for 72 h; X = CH: KAuCl₄ in MeCN, refluxed for 24 h; X = C-OMe: KAuCl₄ in MeCN/H₂O (3:2) refluxed for 72 h).

Bochmann *et al.* demonstrated that the gold(III) hydroxide stabilised by the C^NPy[^]C pincer system (centre of Scheme 1.2) was a versatile starting material and key in the synthesis of many gold(III) derivatives and several highly reactive species.²⁷ It was synthesised through the reaction of (C^NPy[^]C)AuCl (**2**) with CsOH·H₂O in a THF/toluene/H₂O mixture. It has been shown to react with a range of functionalities, including C–H and N–H bonds, and boronic acids resulting in the range of (C^NPy[^]C) gold(III) complexes such as gold(III) aryls and acetylides (Scheme 1.2).



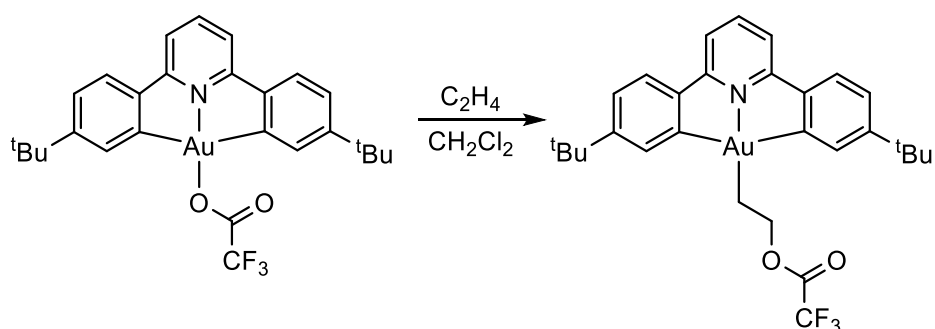
Scheme 1.2. The versatility of the C^NCAu-OH complex.

The (C^NPy[^]C)Au–OH complex has also been used in the synthesis of gold(III) hydroperoxide and gold(III) peroxide, both of which have been postulated as intermediates in heterogeneous gold-catalysed oxidations.²⁸ The hydroperoxide and hydroxide underwent dehydration reactions in dry conditions (Scheme 1.3). The dehydration of the hydroxide complexes to give a bridging μ -oxide was of significant interest because the crystal obtained had an Au–O–Au bond angle of 113.5°. This angle is close to a tetrahedral angle of 109.5° indicating that there is no π -bonding in the Au–O bond.



Scheme 1.3. The hydration and dehydration equilibria and oxygen abstraction of gold(III) oxygen containing complexes.

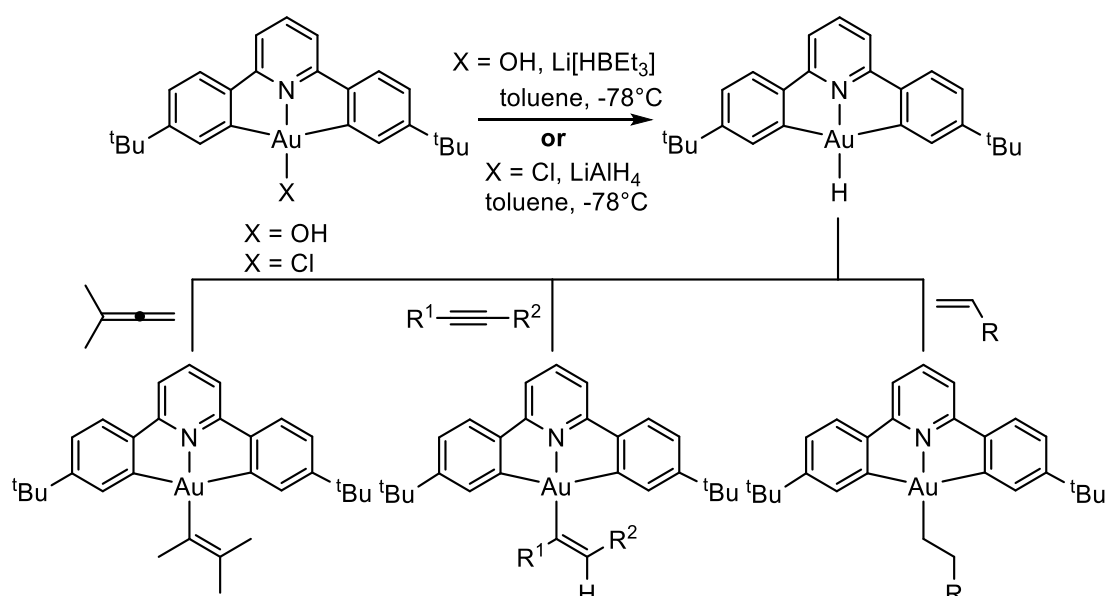
Further understanding of the Au–O bond was developed by Bochann *et al.* based on the observation that ethylene could insert into an Au–O bond in the (C[^]N^{py}^C)Au–OAc^F complex (Scheme 1.4).² This reaction helped demonstrate the bond strengths in gold(III) complexes, with the Au–C bond being stronger than the Au–O bond.⁶ This particular reactivity has been further investigated and developed by Tilset *et al.* into a catalytic system where it was shown that acetylene inserted into an Au–O bond of a C[^]N chelated gold(III) trifluoroacetate complex to give a functionalised acetylene.²⁹



Scheme 1.4. The ethylene insertion into an Au–O bond.

The first reported gold(III) hydride was synthesised by Bochmann *et al.* through the reaction of superhydride (LiHBt₃) with the (C[^]N^{py}^C)Au–OH complex (Scheme 1.5), which further highlights the versatility of the hydroxide species as a starting material.^{13a} This gold(III) hydride was both air and moisture stable, indicating the covalent nature of the Au–H bond.

However, upon treatment with dimethylallene it underwent a 1,2 insertion to produce a gold(III) vinyl complex (Scheme 1.5). Synthesis of subsequent gold(III) hydrides supported by a range of C[^]N[^]C ligand systems used 0.5 M solution of lithium aluminium hydride in tetrahydrofuran as a hydride source (Scheme 1.5).²⁶ The use of azobisisobutyronitrile (AIBN) extended the scope of the insertion reactions and enhanced the rate.^{26,30} The insertion was shown to go via an outer sphere mechanism involving radical formation which is responsible for the stereo- and regiospecific formation on the Z-vinyl isomers in the case of alkyne insertion.



Scheme 1.5. Synthesis and reactivity of gold(III) hydrides.

Oxygen abstraction from (C[^]N[^]C)Au–OH complex by phosphines (PAr₃) also gave the gold(III) hydride complex.²⁸ This indicates that the bond energy of the Au–H bond is greater than that of the Au–O bond.⁶ The same methodology was used to form a gold(III) alkyl complex from the alkoxide.³¹ In addition, the reaction of the (C[^]N[^]C)Au–H with (C[^]N[^]C)Au–OH forms a unsupported gold(II) dimer with an Au–Au bond.^{13a}

Finally, the C[^]N[^]C pincer ligand has been vital in the isolation of stable gold(III) π complexes of alkenes and alkynes by Bochmann *et al.* (Figure 1.5). Two different synthetic approaches have been used to obtain gold(III) olefin complexes, either starting with (C[^]N^{py}^C)Au–OH in the presence of an olefin and [H(OEt₂)₂]⁺X⁻, X = H₂N(B(C₆F₅)₃)₂ or B(3,5-C₆H₃(CF₃)₂)₄ at -40 °C or from (C[^]N^{py}^C)Au–OAc^F in the presence of an olefin and B(C₆F₅)₃ at -40 °C.² All alkenes: ethylene, cyclopentene and norbornene, coordinated η^2 and the solids of the complexes were stable at room temperature under a nitrogen atmosphere. The ¹H NMR spectrum showed a downfield shift in the signal corresponding to the coordinated ethylene (δ = 6.29 ppm) in comparison to free ethylene (δ = 5.38 ppm), which contrasted the ethylene

gold(I) and platinum(II) species where an upfield shift was observed for the coordinated ethylene signal. This indicated that the π -electron donation from the alkene to the gold(III) is not compensated by back-bonding. DFT calculations estimated a rotational barrier of 2.4 kJ mol⁻¹, further indicating a low back-bonding contribution from gold(III).

Synthesis of a gold(III) alkyne used a similar protocol to that of the alkene complexes. First, (C[^]N[^]C)Au–OAc^F was reacted with B(C₆F₅)₃ to form an ion pair [(C[^]N[^]C)Au⁺⋯Y] (Y = Ac^FOB(C₆F₅)₃), followed by addition of an internal alkyne (^tBuC≡CMe, AdC≡CAd Ad = adamantyl) yields a π -alkyne complex (Figure 1.5).³² Only small shifts in the ¹³C NMR spectra were observed compared to the free alkyne, which was similar to the alkene complex. Charge-decomposition analysis showed the bonding was almost entirely dependent on the π donation of the alkyne to the gold, indicating again the limited π -donation from gold(III).

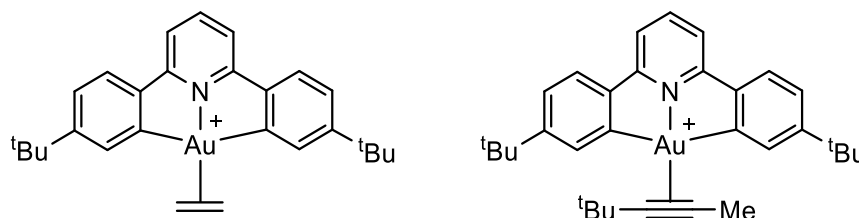


Figure 1.5, Gold(III) π complexes.

Together, these complexes demonstrate the ability of the C[^]N[^]C ligand system to form stable gold(III) complexes in a range of conditions. Furthermore, C[^]N[^]C pincer ligands play a vital role in stabilising the hydride and π complex, facilitating their isolation and studies into their properties. These complexes also reveal further characteristics of C[^]N[^]C gold(III) complexes such as the high covalent nature of the Au–H and Au–C bonds resulting from the high electronegativity of gold, the order of bond strengths Au–H > Au–C \geq Au–O and lack of π back-bonding. These particularly contrast platinum(II) complexes, against which gold(III) complexes are frequently compared.

Further modification of square planar C[^]N[^]C gold(III) systems have applications in photoluminescent materials and as anticancer agents. The stability of this system also allows investigations into the study of fundamental steps of cross coupling catalysis. These applications will be discussed in the following chapters.

References

- (1) Raubenheimer, H. G.; Schmidbaur, H. *J. Chem. Educ.* **2014**, *91*, 2024.
- (2) Savjani, N.; Rosca, D. A.; Schormann, M.; Bochmann, M. *Angew. Chem.-Int. Ed.* **2013**, *52*, 874.

- (3) (a) Zeise, W. C. *Poggendorf's Ann. Phys. Chem.* **1827**, 9, 632. (b) Seyferth, D. *Organometallics* **2001**, 20, 2.
- (4) (a) Pitzer, K. S. *Acc. Chem. Res.* **1979**, 12, 272. (b) Pyykko, P. *Angew. Chem.-Int. Ed.* **2002**, 41, 3573.
- (5) Pyykko, P. *Angew. Chem.-Int. Ed.* **2004**, 43, 4412.
- (6) Rosca, D. A.; Wright, J. A.; Bochmann, M. *Dalton Trans.* **2015**, 44, 20785.
- (7) Pyykko, P.; Desclaux, J. P. *Acc. Chem. Res.* **1979**, 12, 276.
- (8) Yam, V. W. W.; Cheng, E. C. C. *Chem. Soc. Rev.* **2008**, 37, 1806.
- (9) Gimeno, M. C.; Laguna, A. *Gold Bull.* **2003**, 36, 83.
- (10) Joost, M.; Amgoune, A.; Bourissou, D. *Angew. Chem.-Int. Ed.* **2015**, 54, 15022.
- (11) Barakat, K. A.; Cundari, T. R.; Rabaa, H.; Omary, M. A. *J. Phys. Chem. B* **2006**, 110, 14645.
- (12) Zopes, D.; Hegemann, C.; Tyrra, W.; Mathur, S. *Chem. Commun.* **2012**, 48, 8805.
- (13) (a) Rosca, D. A.; Smith, D. A.; Hughes, D. L.; Bochmann, M. *Angew. Chem.-Int. Ed.* **2012**, 51, 10643. (b) Dann, T.; Rosca, D. A.; Wright, J. A.; Wildgoose, G. G.; Bochmann, M. *Chem. Commun.* **2013**, 49, 10169.
- (14) Jansen, M. *Chem. Soc. Rev.* **2008**, 37, 1824.
- (15) Tsui, E. Y.; Muller, P.; Sadighi, J. P. *Angew. Chem.-Int. Ed.* **2008**, 47, 8937.
- (16) Zeineddine, A.; Estevez, L.; Mallet-Ladeira, S.; Miqueu, K.; Amgoune, A.; Bourissou, D. *Nat. Commun.* **2017**, 8, 8.
- (17) Kumar, R.; Nevado, C. *Angew. Chem.-Int. Edit.* **2017**, 56, 1994.
- (18) Henderson, W. *Adv. Organomet. Chem.* **2006**, 54, 207.
- (19) Constable, E. C.; Leese, T. A. *J. Organomet. Chem.* **1989**, 363, 419.
- (20) Kumar, R.; Linden, A.; Nevado, C. *Angew. Chem.-Int. Ed.* **2015**, 54, 14287.
- (21) Nonoyama, M.; Nakajima, K.; Nonoyama, K. *Polyhedron* **1997**, 16, 4039.
- (22) Liu, H. Q.; Cheung, T. C.; Peng, S. M.; Che, C. M. *J. Chem. Soc.-Chem. Commun.* **1995**, 1787.
- (23) Wong, K. H.; Cheung, K. K.; Chan, M. C. W.; Che, C. M. *Organometallics* **1998**, 17, 3505.
- (24) Wong, K. M. C.; Hung, L. L.; Lam, W. H.; Zhu, N. Y.; Yam, V. W. W. *J. Am. Chem. Soc.* **2007**, 129, 4350.
- (25) Fernandez-Cestau, J.; Bertrand, B.; Blaya, M.; Jones, G. A.; Penfold, T. J.; Bochmann, M. *Chem. Commun.* **2015**, 51, 16629.
- (26) Pintus, A.; Rocchigiani, L.; Fernandez-Cestau, J.; Budzelaar, P. H. M.; Bochmann, M. *Angew. Chem.-Int. Ed.* **2016**, 55, 12321.
- (27) Rosca, D. A.; Smith, D. A.; Bochmann, M. *Chem. Commun.* **2012**, 48, 7247.

- (28) Roşca, D.-A.; Wright, J. A.; Hughes, D. L.; Bochmann, M. *Nat. Commun.* **2013**, *4*, 2167.
- (29) (a) Langseth, E.; Nova, A.; Tråseth, E. A.; Rise, F.; Øien, S.; Heyn, R. H.; Tilset, M. *J. Am. Chem. Soc.* **2014**, *136*, 10104. (b) Holmsen, M. S. M.; Nova, A.; Balcells, D.; Langseth, E.; Øien-Odegaard, S.; Heyn, R. H.; Tilset, M.; Laurenczy, G. *ACS Catal.* **2017**, *7*, 5023.
- (30) Pintus, A.; Bochmann, M. *RSC Adv.* **2018**, *8*, 2795.
- (31) Chambrier, I.; Rosca, D. A.; Fernandez-Cestau, J.; Hughes, D. L.; Budzelaar, P. H. M.; Bochmann, M. *Organometallics* **2017**, *36*, 1358.
- (32) Rocchigiani, L.; Fernandez-Cestau, J.; Agonigi, G.; Chambrier, I.; Budzelaar, P. H. M.; Bochmann, M. *Angew. Chem.-Int. Ed.* **2017**, *56*, 13861.

Chapter Two:

Synthesis of gold(III) thiolates and their photoluminescent properties

Part of this chapter has been published as: Currie, L.; Fernandez-Cestau, J.; Rocchigiani, L.; Bertrand, B.; Lancaster, S. J.; Hughes, D. L.; Duckworth, H.; Jones, S. T. E.; Credgington, D.; Penfold, T. J.; Bochmann, M. *Chem.-Eur. J.* **2017**, *23*, 105

Introduction

2.1 Photoluminescent metal complexes

Organometallic complexes are increasingly being used in OLEDs and bioimaging due to their photophysical properties.¹ Two of the most commonly used metal complexes are six coordinate iridium(III)² and four coordinate platinum(II)³ complexes due to their broad and easily tuned emission properties; accessed by using different ligands and synthetic alterations. Likewise, many gold(III) complexes are photoluminescent.

2.1.1 Gold(III) photoluminescence

The luminescent properties of gold(III) complexes are influenced by several factors. One important aspect is the large spin-orbit coupling of gold and other third row transition metals that allows population of triplet states.⁴ The transition between the S_1 and T_1 states are formally spin-forbidden, however spin-orbit coupling enables intersystem crossing and population of the T_1 state. Subsequent phosphorescence from the T_1 to the S_0 ground state is also formally forbidden but the spin-orbit coupling again enables this transition. These transitions can be seen in the Jablonski diagram (Figure 2.1). Phosphorescent emission from the T_1 state results in a Stokes shift (the difference between the absorption and emission wavelength) and is also characterised by longer lifetimes.

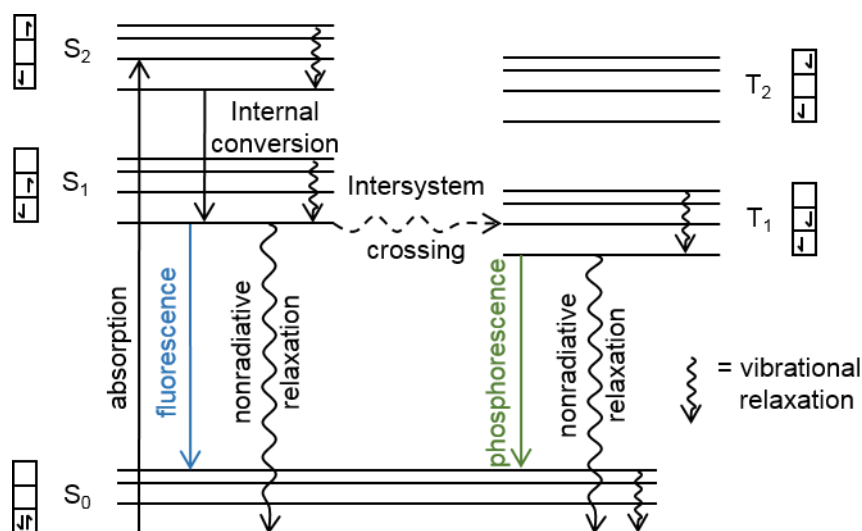


Figure 2.1. Jablonski diagram, illustrating emissive and non-emissive pathways.

There are several non-radiative pathways shown on the Jablonski diagram (Figure 2.1) including internal conversion and nonradiative vibrational relaxations. These occur because

upon excitation the electron moves to a higher energy level in the same molecular geometry as the ground state, this is not usually the lowest vibrational level of that electronic state. The molecule can lose energy through vibrational relaxation from a higher vibrational energy level (v_n) to the lowest vibrational energy level of that electronic state (v_0). If there is overlap of the S_{2,v_0} with a higher vibrational state of S_1 there can be internal conversion, the transfer of an electron from S_{n+1} to S_n . External conversion is also possible, where the molecule loses energy to the environment such as solvent.

In addition, the use of cyclometallating ligands, especially those containing an Au–C bond provide both thermodynamic and kinetic stability.⁴ Gold(III) photoluminescent complexes are dominated by those bearing bidentate and tridentate ligands. The more rigid tridentate ligands prevent the d^8 square planar complexes from undergoing molecular distortions from D_{4h} to D_{2d} , which can enable nonradiative decay.⁵

Finally, the ligand type has a large effect on the photoluminescence properties.^{5d} This can be illustrated by the $(N^N)AuCl_2$ complex that was only emissive as a solid (298 K), however upon substitution of the chlorides for mesityl groups the luminescence was enhanced with emission observed in solution at room temperature (Figure 2.2).⁶ The ligands have different σ -donating properties; chloride is a poor σ -donor whereas mesityl is a strong σ -donor. In the dichloride complex nonradiative relaxation was thought to occur from d-d states that were close in energy but lower than the intraligand (IL) or metal-to-ligand charge transfer (MLCT) states. However, a strongly σ -donating ligand such as mesityl raised the energy of the d-d states therefore facilitating radiative emission from a IL or MLCT state.

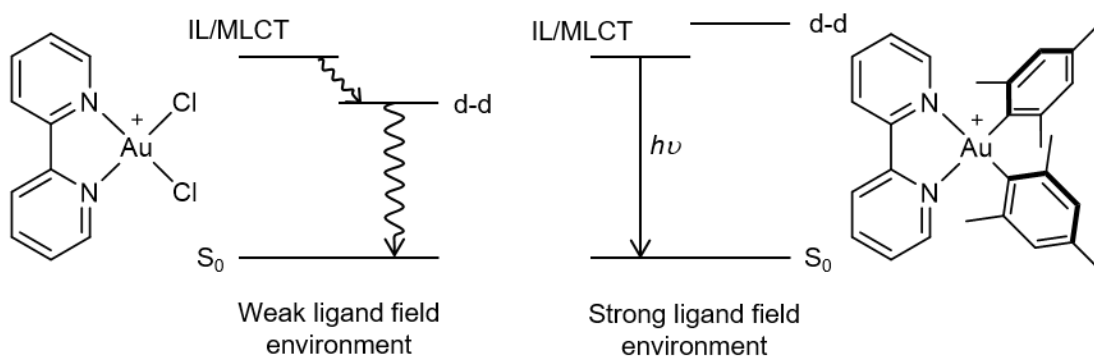


Figure 2.2. The effect of the ligand field strength on the d-d energy levels: left) weak field ligand; right) strong field ligand. IL = intra ligand and MLCT = metal-to-ligand charge transfer.^{5d}

2.1.2 Photoluminescent C[^]N[^]C pincer gold(III) complexes

C[^]N[^]C pincer ligands have been used to stabilise gold(III) complexes, functionalisation at the fourth position allows synthesis of photoluminescent complexes. Many different σ -donors have been investigated including N-heterocyclic carbenes (NHC), phosphines, aryls and alkenes, which are used to raise the d-d orbital energy and to minimise nonradiative pathways.

(C[^]N[^]C)Au–Cl (C[^]N[^]C = 2,6-diphenyl-pyridine dianion) was nonemissive at room temperature and only weakly emissive at 77 K. However, Che *et al.* demonstrated that C[^]N[^]C gold(III) phosphine complexes synthesised through chloride substitution had enhanced photoluminescent properties (Figure 2.3).⁷ Depending on the phosphine used, both monomer and binuclear species were synthesised. These gold(III) phosphines were luminescent only at 77 K ($\lambda_{\text{max}} = 484 \text{ nm}$) and had a structured emission band, which is characteristic of C=C and C=N vibrations of the C[^]N[^]C pincer ligand and is often described as vibronic progression. The emission was assigned a metal perturbed ³IL transition based on the C[^]N[^]C pincer ligand. The binuclear species containing a CH₂ linker between two phosphines was red-shifted ($\lambda_{\text{max}} = 524 \text{ nm}$) compared to the mononuclear complex and it was proposed that emission takes place from an excimer where the C[^]N[^]C ligands interact in a π - π manner.

Altering the σ -donating ligand to a NHC gives C[^]N[^]C gold(III) complexes that are emissive in solution at 298 K (Figure 2.3).⁸ The wide range of NHCs available has facilitated the synthesis of many gold(III) NHC complexes including monomeric species with imidazole and benzimidazole based NHC's and binuclear species. The monomeric and dimeric species had $\lambda_{\text{max}} > 480 \text{ nm}$ with vibronic-structured emission bands that do not shift significantly with temperature ($> 10 \text{ nm}$). The nature of the NHC has little effect of the emission which is proposed to occur from ³IL of the C[^]N[^]C cyclometallating ligand.

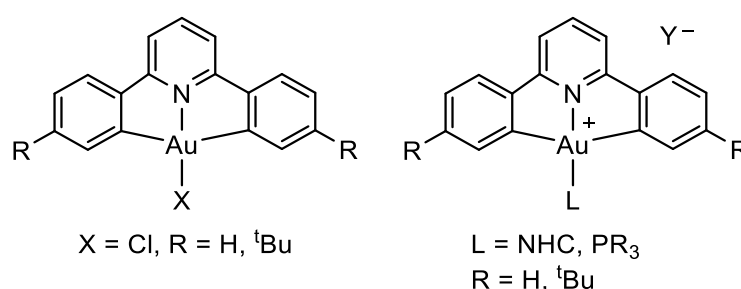


Figure 2.3. The C[^]N[^]C scaffold used with chloride, NHC and phosphine ligands.

Yam *et al.* used σ -donating alkynyl ligands to give highly luminescent complexes [(C[^]N[^]C)Au–C \equiv C–R] (Figure 2.4).⁹ The emission spectra of these complexes were dominated by a sharp, structured emission band ($\lambda_{\text{max}} > 470 \text{ nm}$) at ambient temperatures in solution, which showed little sensitivity to alkyne substituents. Emission lifetimes were on the

microsecond scale, indicative of a triplet-based emission. The transition was assigned to a ^3IL metal perturbed $\pi^* \rightarrow \pi$ transition based on the $\text{C}^{\wedge}\text{N}^{\wedge}\text{C}$ ligand.

Interestingly, complexes bearing amino substituted alkynes ($\text{C}\equiv\text{C}-\text{C}_6\text{H}_4-\text{NR}_2-p$) were found to have structureless emission bands that are significantly red-shifted (by 4500 cm^{-1}) compared to the other alkynyl compounds. The lack of fine structure and the red-shift of the emission indicates a different emission pathway. The different emission was proposed to result from the amino groups increasing the energy of the π orbital of the alkyne ligand resulting in a $^3\text{LLCT}$ from the electron-rich aminophenylacetylidyne ligand to the 2,6-diphenylpyridine ligand ($^3[\pi(\text{C}\equiv\text{C}-\text{C}_6\text{H}_4-\text{NR}_2-p) \rightarrow \pi^*(\text{C}^{\wedge}\text{N}^{\wedge}\text{C})]$).

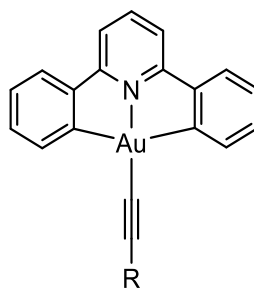


Figure 2.4. Photoemissive gold(III) complexes with a 2,6-diphenylpyridine pincer system and alkyne ligands.

Modulating the emission was also achieved through altering the $\text{C}^{\wedge}\text{N}^{\wedge}\text{C}$ ligand scaffold.¹⁰ A series of $\text{C}^{\wedge}\text{N}^{\wedge}\text{C}$ ligands with a range of different functional groups and extended aryl systems were investigated in gold(III) systems that also contain an alkynyl ligand at the fourth position. These complexes were emissive, with a range of emissions observed from $\lambda_{\text{max}} = 476\text{ nm}$ to 660 nm in solution at 298 K . The emission was proposed to occur from intraligand $^3[\pi-\pi^*]$ excited states. Again, the emission could be red-shifted if an amino substituted alkyne was used and was assigned as a $^3\text{LLCT}$. The emission in a PMMA matrix resembled that of a dichloromethane solution.

The tendency of amino substituted alkynyl complexes to give red emissive complexes led to the development of a complex using a $\text{C}\equiv\text{C}-\text{C}_6\text{H}_4\text{N}(\text{C}_6\text{H}_5)_2-p$ alkyne.¹¹ In this case, a red structureless emission band was assigned as a LLCT $^3\pi[\text{C}\equiv\text{C}-\text{C}_6\text{H}_4\text{N}(\text{C}_6\text{H}_5)_2-p] \rightarrow \pi^*(\text{C}^{\wedge}\text{N}^{\wedge}\text{C})$ transition. When incorporated into an OLED device the emission shift was shown to depend on the concentration of complexes, with a red shift of 150 nm observed at high concentrations.

Alkynyl ligands have also been used as linkers in more complex dendrimer systems which can be incorporated into OLED devices based on carbazoles,¹² extended aryl systems¹³ and other delocalised systems.¹⁴

Further derivatives of the C[^]N[^]C gold(III) pincer system have been used in combination with an aryl functionality to produce emissive complexes suitable for use in OLEDs.¹⁵ Tuning of the emission was possible by altering the functional group attached to the arene in a similar fashion to an alkynyl linker.

Bochmann *et al.* demonstrated that gold(III) complexes supported by C[^]N[^]C systems containing a central pyrazine instead of a pyridine had a more pronounced emissive properties (Figure 2.5).¹⁶ **1**, with a weak σ -donating chloride, is strongly emissive at 77 K in the solid state ($\lambda_{\text{max}} = 560$ nm) with a structured emission that is redshifted from the weakly emissive pyridine system by 40-50 nm. The redshift occurs because the π - π^* energy gap in pyrazine is 0.95 eV less than in pyridine.¹⁶⁻¹⁷ Substitution of the chloride for strongly σ -donating ligands such as cyanide or acetylide (Figure 2.5), gave complexes with enhanced photoluminescent properties. Additionally, gold(III) species with weaker σ -donors such as a pyrazolate, were emissive in solution at ambient temperatures. All the complexes emit in the yellow to green region, with the emission spectra showing vibronic progression. The transition was assigned to a metal perturbed ³IL transition centred on the 2,6-diphenylpyrazine ligand, which was further supported by DFT calculations. Modulation of the emission properties of this system was also achieved through protonation and alkylation of the pyrazine nitrogen (blue shifts emission) or addition of metal ions (a slight red shift of emission). A red shift of the emission was observed on cooling from 298 K to 77 K, this temperature dependence of the emission led to the identification of a thermally activated delayed fluorescence (TADF) process. TADF occurs when the T¹ and S¹ excited states are close in energy allowing repopulation of the S¹ from the T¹ at higher temperatures, where the emissive pathway is an S¹ to S⁰ transition.

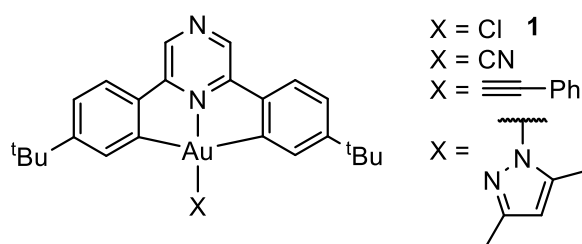


Figure 2.5. Photoemissive complexes based on the gold(III) 2,6-diphenylpyrazine system.

Subsequent to the work carried out in this chapter, Bochmann *et al.* investigated the emissive properties for pyridine and pyrazine based C[^]N[^]C gold(III) complexes with alkyl ligands (Figure 2.6).¹⁸ Substitution of position R with different alkyl groups gave a series of complexes where the emission is dependent on the $\text{p}K_{\text{a}}$ of the alkyl ligand precursor. A blue shift of the emission was observed in both ligand systems for alkyl groups with stronger electron donors, allowing fine tuning of the emission properties. Again, there was a red shift of complexes

bearing a pyrazine-based pincer ligand compared to the corresponding pyridine complexes. The emissions were assigned to ${}^3\text{IL}(\text{C}^{\wedge}\text{N}^{\wedge}\text{C})/{}^3\text{ILCT} ((\text{C}_6\text{H}_4^t\text{Bu}) \rightarrow \text{pz/py}^*)$ transitions.

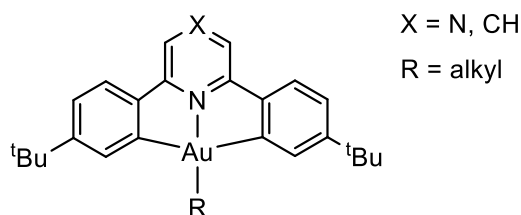


Figure 2.6. CNC gold(III) alkyl complexes.

2.2 Gold(III) thiolates

Traditionally thiolate ligands have been associated with gold(I) complexes and there is a plethora of examples. There are comparatively fewer examples for gold(III). Gold(I) and gold(III) are often described as behaving as soft or hard Lewis acids respectively, using this categorisation it may be expected that thiols would make more stable complexes with gold(I) than with gold(III). Examples of gold(III) thiolate compounds include the tetrathiolate complexes such as $[\text{Au}(\text{SAr})_4]^-$ or $[\text{X}_2\text{Au}(\mu\text{-SR})_2]_2$.¹⁹ These complexes have been used as molecular wires and in the study of redox behaviour of disulfides.

Gold(III) thiolate complexes supported by cyclometallating ligands have been predominantly used in studies into biological activity (Figure 2.7).²⁰ There is only one study into photoluminescence that included a gold(III) thiolate supported by a $\text{C}^{\wedge}\text{N}^{\wedge}\text{C}$ pincer, however it was described as non-emissive (left in Figure 2.7).⁷ In comparison, the photoluminescent properties of gold(I) thiolates have been extensively studied.²¹

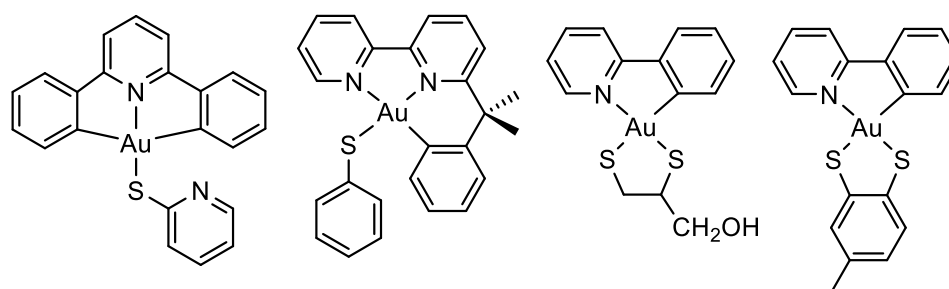


Figure 2.7. Cyclometallated gold(III) thiolates.

2.3 Objectives

The gold(III) complexes above show the nature of the pincer system and the substituents used have a large effect on the complexes photoluminescent properties. The pyrazine based

gold(III) complexes are of particular interest because were shown to be photoluminescent with weak σ -donating substituents. This work aims to investigate the use of thiolates, as weak σ -donating ligands, with pyrazine gold(III) complexes. There are significantly fewer of gold(III) thiolates compared to the plethora of gold(I) thiolates, with none of the previous gold(III) thiolate reported as photoluminescent. This work investigates the synthesis and photoluminescence properties of a series gold(III) thiolates with different thiolates and pincer ligands to investigate their effects on the photoluminescence properties. For these investigations, complexes **1** and **2** were used as the starting materials (Figure 2.8).

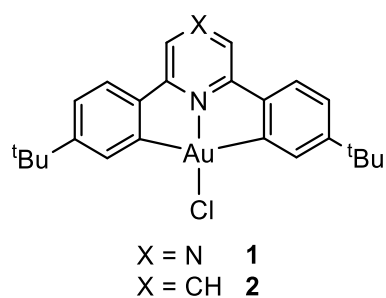
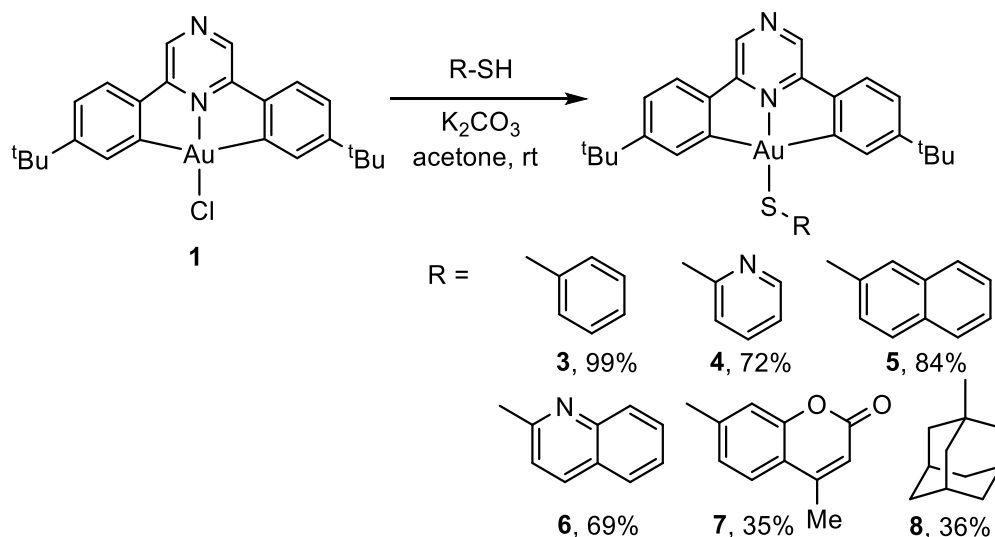


Figure 2.8. Gold(III) chlorides supported by CNC pincer ligands

Results and Discussion

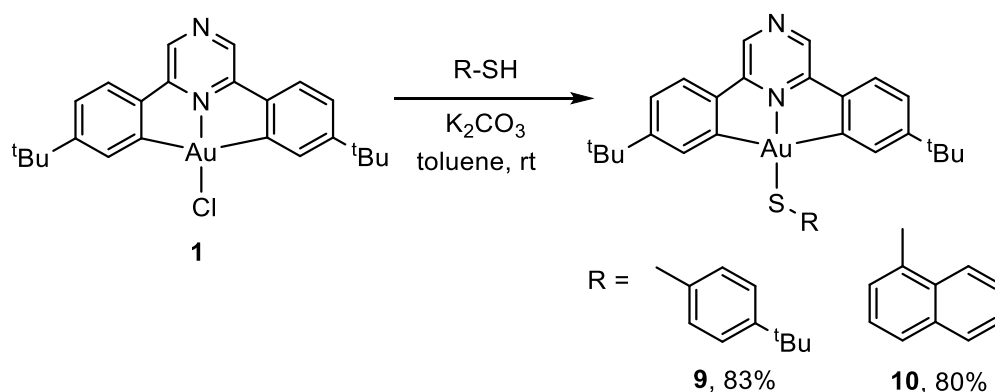
2.4 Synthesis of gold(III) thiolates

A series of gold(III) thiolates were synthesised from **1** through substitution of a chloride for a thiolate ligand. Complexes **3–8** were synthesised using the same method: **1**, the corresponding thiol and potassium carbonate were dissolved in acetone and stirred at room temperature for 3 hours (Scheme 2.1). The complexes were isolated as solids in yields 35 - 99 %. Longer reaction times of 18 hours were required for **7** and **8**, there were further purification steps and mechanical loss resulting in the lower corresponding yields.



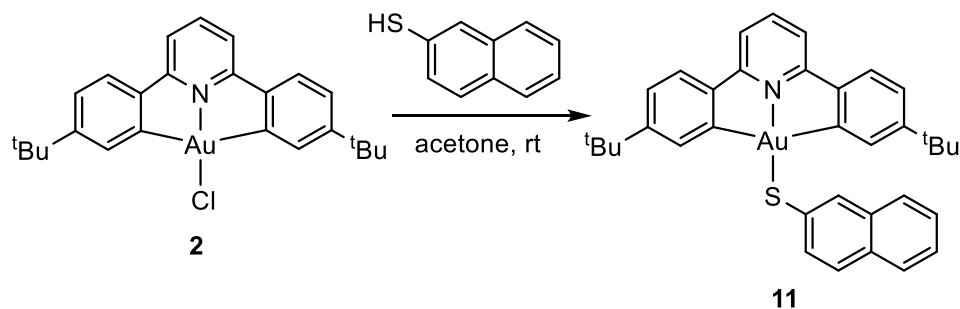
Scheme 2.1. Synthesis of gold(III) thiolates **3** – **8**.

A slightly altered method was required for the synthesis of **9** and **10**, due to the air sensitivity of thiols. Therefore the reactions were carried out under inert conditions and using dried and degassed toluene (Scheme 2.2). The reaction time remained 3 hours for these complexes, which were isolated as air-stable solids in 83 % (**9**) and 80 % (**10**) yield.



Scheme 2.2. Synthesis of gold(III) thiolates **9** and **10** under inert conditions.

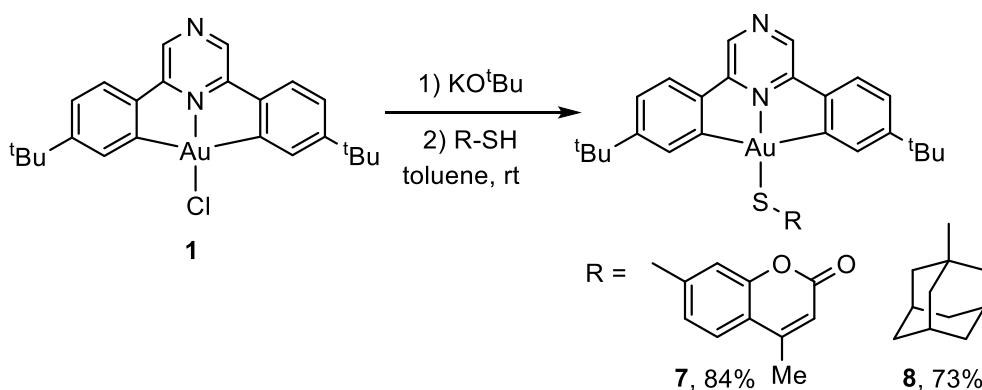
The synthesis of complex **11**, with the pyridine based pincer ligand, used the first method (**2**, 2-naphthalenethiol and potassium carbonate) but required a longer reaction time of 18 hours (Scheme 2.3). **11** was isolated as a solid in a 67 % yield.



Scheme 2.3. Synthesis of **11** using the pyridine ligand system.

The synthesis of these complexes required mild reaction conditions, using a weak base and room temperature. All these C^NC gold(III) thiolate complexes were air and moisture stable.

An additional method was developed for the synthesis of complexes that required longer reaction times. This method used a stronger base, potassium *tert*-butoxide, which required the use of inert conditions and dried and degassed solvent (Scheme 2.4). This reduced the reaction times for **7** and **8** from 18 hours to 6 hours. **7** and **8** were again isolated as solids in 84 % and 73 % yield respectively.



Scheme 2.4. Synthesis of **7** and **8** using a different method.

The complexes were characterised by ¹H and ¹³C NMR spectroscopy and elemental analysis. Across the series of complexes, the ¹H NMR spectra showed similar shifts for the pincer protons. The H⁸ proton environment (Figure 2.9) showed a dependence on the nature of the thiolate, for the alkyl thiol **8** the H⁸ shifted ~ 1.0 ppm from the average of the other complexes, with the alkyl thiol resulting in deshielding compared to the more shielding aryl thiols.

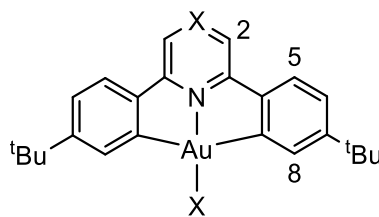


Figure 2.9. Numbering scheme used in NMR assignments.

2.4.1 Solid state structures

It was possible to obtain crystals of several of the complexes that were suitable for x-ray analysis.

In the crystallisation of **3** there were two different types of crystal formed, red plates (Figure 2.10) and yellow blocks (Figure 2.11). The red plates contained two independent molecules in the unit cell. Both crystal forms showed the expected connectivity of **3**. The main difference in the molecular geometries between the two crystal forms are the torsion angles between the Au-S-C and S-aryl planes, which are 50.1(4) and 58.2(3) ° for the two molecules in the red crystal and 94.3(6) ° in the yellow crystal. Neither crystal structure showed the presence of solvent molecules, therefore these two structures are polymorphs. Interestingly, under UV irradiation only the red crystals were emissive.

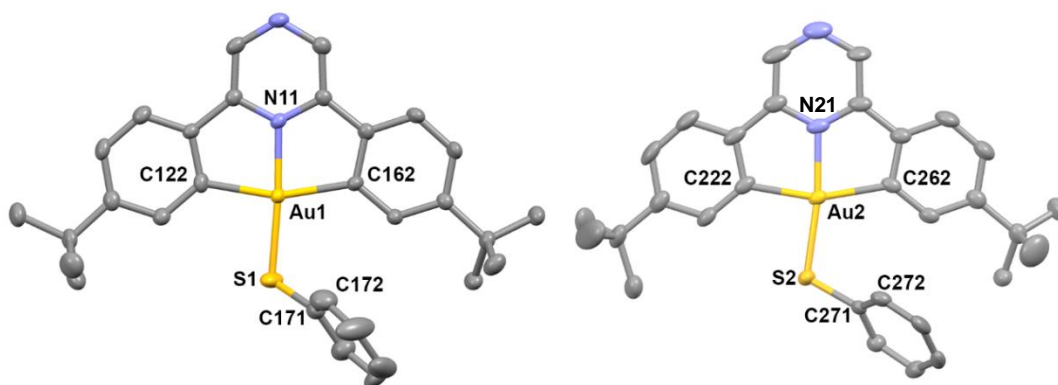


Figure 2.10. Structure of **3** in the red polymorph. The unit cell contained two independent molecules. Selected bond distances (Å) and angles (°): Au1-S1 2.273(1), Au2-S2 2.277(1), Au1-N11 2.006(3), Au2-N21 2.017(4), Au1-C122 2.086(4), Au1-C162 2.091(4), Au2-C222 2.083(4), N11-Au1-S1 175.66(8), N21-Au2-S2 172.2(1), C122-Au1-N11 80.5(1), C162-Au1-N11 80.6(1), C122-Au1-S1 95.46(9), C162-Au1-S1 103.38(9), C222-Au2-N21 80.6(1), C262-Au2-N21 80.1(1), C222-Au2-S2 91.8(1), C262-Au2-S2 107.49(9), Au1-S1-C171 110.2(2), Au2-S2-C271 110.9(1), torsion Au1-S1-C171-C172 50.1(4), torsion Au2-S2-C271-C272 58.2(3).

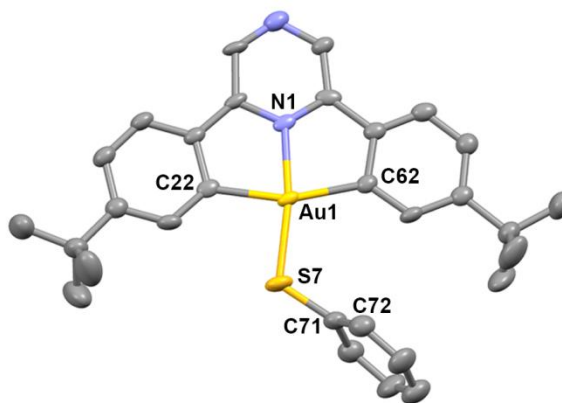


Figure 2.11. Structure of **3** in the yellow polymorph. Selected bond distances (Å) and angles (°): Au1-S7 2.276(2), Au1-N1 2.022(6), Au1-C22 2.088(7), Au1-C62 2.080(7), N1-Au1-S7 170.94(18), C22-Au1-N1 81.3(3), C62-Au1-N1 79.8(3), C22-Au1-S7 89.6(2), C62-Au1-S7 109.2(2), Au1-S7-C71 116.6(3), torsion Au1-S7-C71-C72 94.3(6).

Complex **5** also crystallised as a mixture of red and yellow crystals, similar to the crystallisation of **3**. The structures of the different polymorphs are shown in Figure 2.12. The torsion angles between the gold plane and the S-aryl plane were similar $52.3(5)^\circ$ for the red form and $56.5(3)^\circ$ for the yellow form.

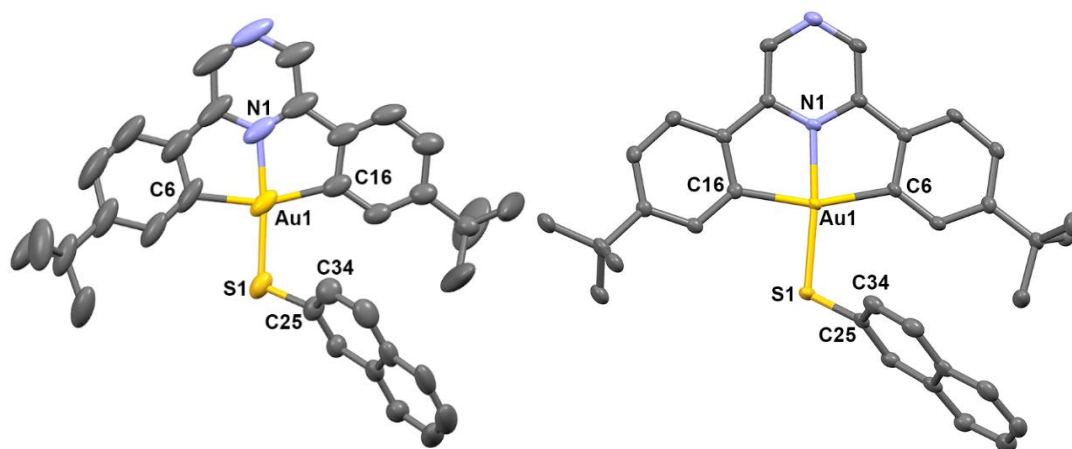


Figure 2.12. Structure of **5** (left) in the red polymorph. Selected bond distances (Å) and angles (°): Au1-S1 2.263(2), Au1-N1 2.006(6), Au1-C6 2.069(6), Au1-C16 2.080(6), N1-Au1-S1 174.3(2), C6-Au1-N1 80.6(3), C16-Au1-N1 80.1(2), C6-Au1-S1 93.8(2), C16-Au1-S1 105.6(2), Au1-S1-C25 109.5(2), torsion Au1-S1-C25-C34 $52.3(5)^\circ$; (right) yellow polymorph Au1-S1 2.2837(8), Au1-N1 2.014(3), Au1-C6 2.095(3), Au1-C16 2.086(3), N1-Au1-S1 174.05(7), C6-Au1-N1 80.7(1), C16-Au1-N1 80.2(1), C6-Au1-S1 104.68(8), C16-Au1-S1 94.53(8), Au1-S1-C25 109.8(1), torsion Au1-S1-C25-C34 $56.5(3)^\circ$.

The difference in emission between the two polymorphs of **5** (2-Np) can be clearly seen in Figure 2.13 where a mixture of the two crystalline forms are shown under white light and UV light. Under UV light the red polymorph is emissive whereas the yellow polymorph is not.

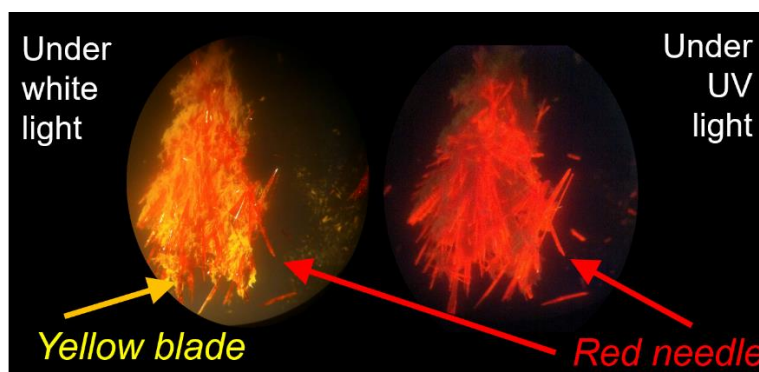


Figure 2.13. Different emission of two polymorphs of **5** under white or UV light at 298 K.

All other complexes crystallised as only one form. The structures of **4** and **7** (Figure 2.14 left and right respectively) were obtained and showed the expected connectivity and coordination environment. The crystals analysed were both yellow.

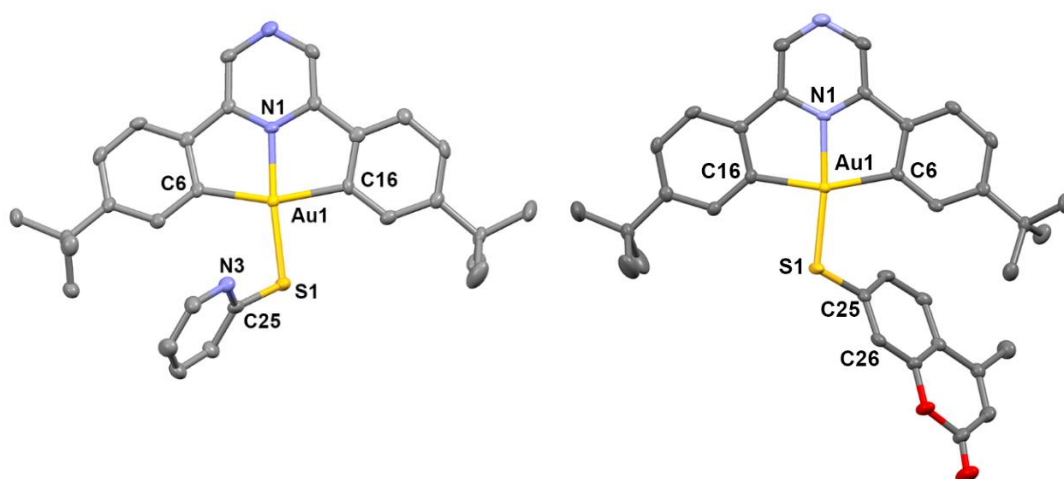


Figure 2.14. left) structure of **4**. Selected bond distances (Å) and angles (°): Au1-S1 2.289(1), Au1-N1 2.009(4), Au1-C6 2.104(4), Au1-C16 2.090(4), N1-Au1-S1 174.0(1), C6-Au1-N1 80.2(2), C16-Au1-N1 80.7(2), C6-Au1-S1 104.9(1), C16-Au1-S1 94.1(1), Au1-S1-C25 109.4(1), torsion Au1-S1-C25-N3 49.8(4). right) structure of **7** Au1-S1 2.2785(9), Au1-N1 2.009(2), Au1-C6 2.097(3), Au1-C16 2.084(3), N1-Au1-S1 173.88(7), C6-Au1-N1 80.2(1), C16-Au1-N1 80.7(1), C6-Au1-S1 105.87(8), C16-Au1-S1 93.19(8), Au1-S1-C25 111.1(1), torsion Au1-S1-C25-N3 35.2(3).

The structure of **9** again showed the expected connectivity (left, Figure 2.15). Complex **11** was the only compound that crystallised with a solvent molecule, dichloromethane (right, Figure 2.15). Both crystals were yellow.

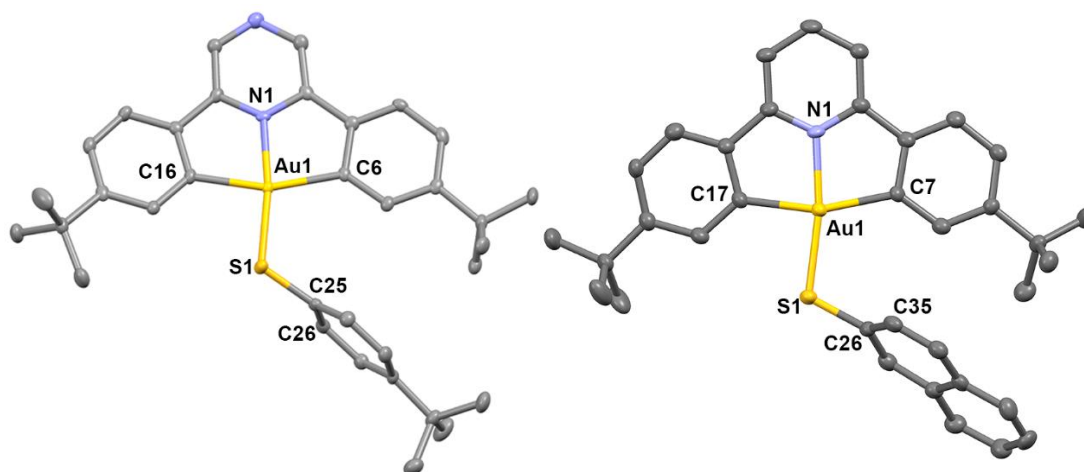


Figure 2.15. left) structure of **9**. Selected bond distances (Å) and angles (°): Au1-S1 2.2781(9), Au1-N1 2.017(2), Au1-C6 2.090(4), Au1-C16 2.090(4), N1-Au1-S1 171.62(8), C6-Au1-N1 80.4(1), C16-Au1-N1 80.5(1), C6-Au1-S1 107.9(1), C16-Au1-S1 91.2(2), Au1-S1-C25 112.7, torsion Au1-S1-C25-C26 77.2(3); right) structure of **11** · CH₂Cl₂ the CH₂Cl₂ molecule is omitted for clarity. Au1-S1 2.282(2), Au1-N1 2.019(5), Au1-C7 2.078(5), Au1-C17 2.070(5), N1-Au1-S1 170.7(1), C7-Au1-N1 80.4(2), C17-Au1-N1 80.7(2), C7-Au1-S1 108.7(1), C17-Au1-S1 90.3(2), Au1-S1-C26 112.0(2), torsion Au1-S1-C26-C35 72.5(5).

Across the series of gold(III) thiolate complexes there are no significant alterations in bond lengths. The Au-S bond ranges from 2.263(2) Å in **5** to 2.289(1) Å in **4**. The N-Au-S angle that would be 180 ° in an ideal square-planar geometry is distorted from linearity in all complexes, the largest distortion was 170.7(1) ° in **11** and least the distorted is 175.7 ° in **3**. This distortion is likely to occur from the steric repulsion between the *tert*-butyl substituents of the pincer ligand and the thiolate group. These are comparable to the previously reported gold(III) thiolate supported by a C[^]N[^]C ligand, with a very slightly longer Au-S bond 2.296(2) Å and a distorted N-Au-S angle of 176.5(1) °.⁷

2.5 Photoluminescence

The observation that the complexes appeared red was unusual as the previously reported gold(III) complexes supported by the pyrazine C[^]N[^]C ligand had been yellow in the absence of additives.¹⁶ The photoemission of these previous complexes was based on a structured emission at 540 nm. Therefore, the absorption and emission properties of these complexes was studied.

2.5.1 Absorption properties of **3** – **11**

The UV/Vis absorption spectra of **3** – **11** are similar to those of previously studied C[^]N[^]C pincer complexes. The spectra are dominated by low-energy absorption bands, with characteristic vibronic progression, these are attributed to a metal perturbed intraligand transition (¹IL) in the C[^]N[^]C pincer ligand (Chapter 6, Table 6.2). The absorption maxima of these complexes, in the 420–440 nm region, is not in agreement with the deep-red colour of complexes in a dichloromethane solution observed by the naked eye. The red colour might instead be explained by the weak, broad absorption tail in the 470–530 nm region.

The differences between the pyridine and pyrazine ligands can be clearly illustrated in Figure 2.16. The low energy band of **11** (2-Np), with a pyridine based C[^]N[^]C pincer, is significantly blue shifted in comparison to **5** (2-Np), with the same naphthyl thiolate but instead supported by a pyrazine based C[^]N[^]C pincer. The shift in absorption results from lower π^* level of pyrazine compared to pyridine.¹⁶ The tail that is tentatively assigned to the deep-red colour of **5** (2-Np) in a dichloromethane solution can be seen above 470 nm. The absence of such a tail in **1** ((C[^]N^{pz}[^]C)Au-Cl) and **11** ((C[^]N^{py}[^]C)Au-2-Np) is likely to correspond to their yellow colour.

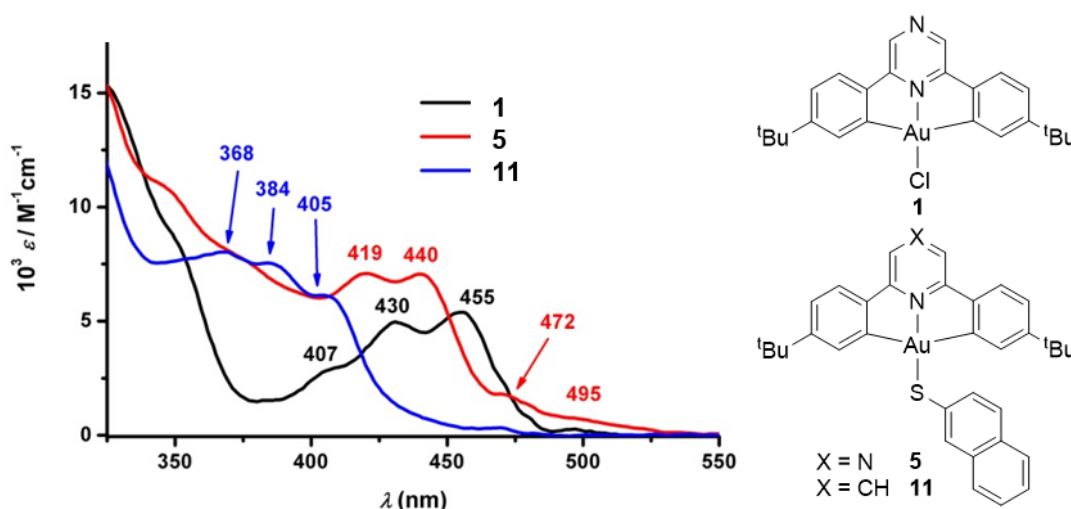


Figure 2.16. Comparison of UV/Vis absorption spectra of **1**, **5** and **11** in CH₂Cl₂ (5×10^{-5} M).

2.5.2 Emission properties of **3** – **11**

The emission properties of **3** – **11** were studied in the solid state (298 K and 77 K), in dichloromethane solution (298 K and 77 K) and as a 10% doped sample in PMMA (polymethylmethacrylate) (298 K) and are shown in Tables 6.3, 6.4 and 6.7 (Chapter 6). The

emissions of complexes **3** – **11** can be separated into two different groups based on either red or green emission.

The green emissive complexes are **4** (py) and **6** (Quin), which both contain N-heterocyclic aryl thiolates, and **11**, which is supported by a pyridine based C^NC ligand. **4** and **6** are weakly to non-emissive at room temperature in the solid state, but cooling to 77 K green emission is observed at 534 and 532 nm with a vibronic structured emission band. In a dichloromethane solution and a 10% doped PMMA matrix at 298 K a weak green emission is observed for both **4** and **6**. The green emission ($\lambda_{\text{max}} = 540$ nm) showed no concentration dependence between 10^{-4} and 10^{-2} M in a dichloromethane solution at 298 K. This is similar to the emission of the previously reported gold(III) complexes with a C^{N^{pz}}C ligand, therefore is tentatively assigned to a ³IL transition. Similar behaviour is observed for **11**, which is emissive only at 77 K, but is blue shifted from **4** and **6**. The emission assigned to a ³IL(C^{N^{py}}C) band showing a typical structured profile at 517 nm, similar previously observed emissive gold(III) complexes with this ligand.

The red emissive complexes (**3** (Ph), **5** (2-Np), **8** (Ad), **9** (^tBu) and **10** (1-Np)) are gold(III) thiolates supported by the pyrazine-based C^NC pincer system. These complexes have a range of thiolate functionalities including: aryls, substituted aryls and alkyl groups, which significantly do not contain any heteroatoms. They are emissive at room temperature in the solid state, with broad unstructured low-energy bands observed above 600 nm. Upon cooling to 77 K the emission spectra of **5** (2-Np) and **8** (Ad) remain unchanged, however there is a blue shift observed for **3** (Ph), **9** (^tBu) and **10** (1-Np). In a 10 % doped PMMA matrix at 298 K there is red emission ($\lambda_{\text{max}} > 600$ nm) observed for **3**, **5**, **8**, **9** and **10**. In a dichloromethane solution **5** (Np-2), **8** (Ad), **9** (^tBu) and **10** (Np-1) are red emissive with $\lambda_{\text{max}} > 670$ nm, upon cooling to 77 K there is a blue shift the emission, but the emission remains in the red region with $\lambda_{\text{max}} > 600$ nm. In the emission bands of several complexes in frozen conditions (at 77 K) there is the appearance of a shoulder around 540 nm, this may indicate a mixed emission based on both green and red emissive pathways.

In addition, the excitation bands for these complexes differ from the absorption spectra. This can be exemplified in the case of **5** (2-Np), where the emission at 298 K is associated with a sharp low-energy excitation band at $\lambda_{\text{ex}} = 540$ nm (top Figure 2.17). This indicates that the low-energy tail in the UV/Vis spectra is associated with the red emission. This is different from the excitation of **11** (py 2-Np), which more closely represents the previously observed absorption spectra (Figure 2.16: UV/Vis spectra; Figure 2.17 shows excitation and emission bands).

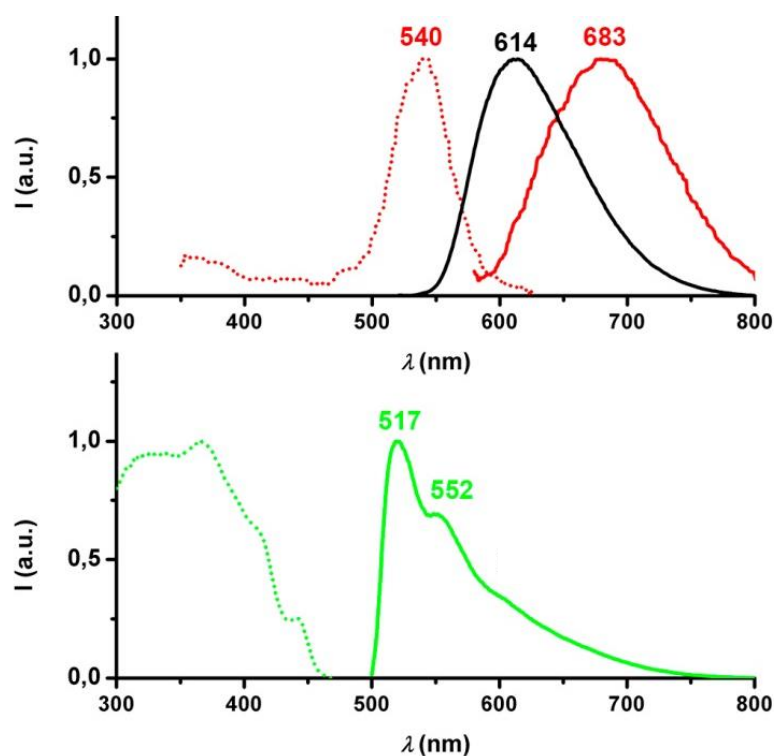


Figure 2.17. Top complex **5** (CH_2Cl_2 , 10^{-4} M): emission at 298 K (red solid line), emission at 77 K (black line), excitation at 298 K (red dotted line); Bottom complex **11** (CH_2Cl_2 , 10^{-4} M): emission at 77 K (green solid line) excitation at 77 K (green dotted line).

The two crystal polymorphs observed for **5** (2-Np) in Section 2.3.1 appeared to show different emission properties under a UV light. Microcrystalline samples of purely red crystals (obtained through slow evaporation of a saturated dichloromethane solution of **5**) or purely yellow crystals (obtained through slow evaporation a solution of **5** in petroleum ether) were prepared for photoluminescence studies. At 298 K, the red crystals were emissive with $\lambda_{\text{max}} = 650$ nm, whereas the yellow crystal were not emissive. Upon cooling to 77 K the red crystals were still red emissive ($\lambda_{\text{max}} = 653$ nm) and the yellow crystals were also emissive with a $\lambda_{\text{max}} = 539$ nm, with a structured green emission band. This reveals that the same complex has two different emission pathways, which are dependent on sample treatment.

The lifetimes of all the complexes in PMMA are the result of two different components; a prompt emission with a short lifetime of 25–50 ns (5 %), which is assigned to photoexcited singlet states, and more dominant delayed component in the range of 0.3 μs (95 %). This longer lifetime in the μs range is indicative of a triplet based emission.

2.5.3 Extending the photoluminescent studies

The two different emissions observed for these complexes were unexpected. Therefore, to gain further insight into the potential origins of the different emission pathways and, in some cases,

the dual emission pathways the dependence on concentration, solvent and temperature were probed.

The emission of **5** (2-Np) at 77 K is concentration dependant because upon decreasing its concentration in a dichloromethane solution from 10^{-2} M to 10^{-4} M there is a slight blue shift in the emission band and the appearance of a shoulder (red and black lines, Figure 2.18). Further decreasing the concentration to 10^{-5} M results in a predominantly green emission band (green line, Figure 2.18). The dominance of the red emission at high concentrations may indicate that the transition is dependent on the formation of aggregates. This is not observed at 298 K because at this temperature the green emission is very weak for all complexes, therefore the red emission will dominate. There are examples of gold(I) and platinum(II) compounds where the photoemission is linked to, and in some cases modulated by, metal-metal aggregation, however, there are no such interactions previously reported for gold(III) complexes.^{4, 22}

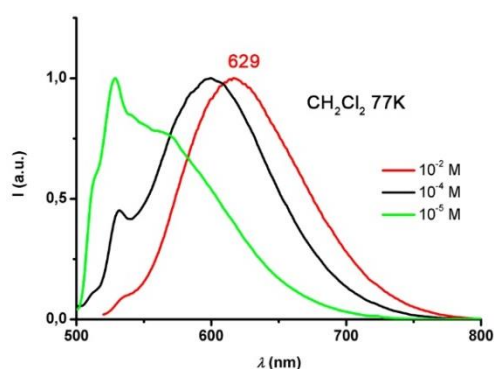


Figure 2.18. Normalized photoemission spectra of **5** (2-Np) in CH_2Cl_2 at different concentrations at 77 K.

The concentration dependence of the UV/vis absorption spectra were also probed at higher concentrations of **5** (2-Np). At higher concentrations the tail observed in the UV/Vis spectra increases in intensity, up to 10^{-3} M. At even higher concentrations absorption is also observed at longer wavelengths with the tail extending to 550 nm (Figure 2.19). The absorption at this wavelength matches the region where a band is observed in the excitation spectra in Figure 2.16. This may also indicate the presence of aggregates as an important factor on the emission pathway because of the appearance of absorption at 550 nm observed only at high concentrations.

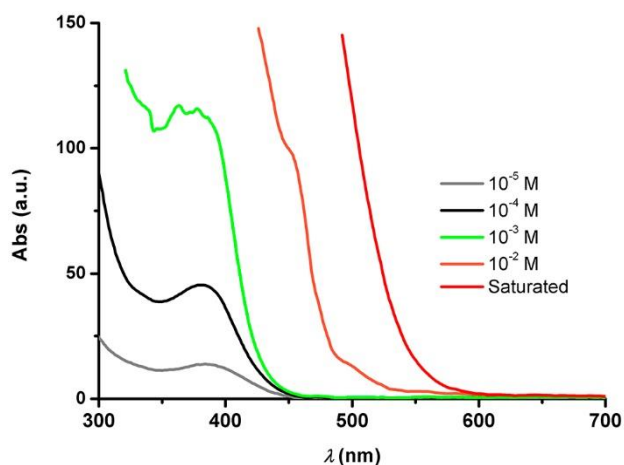


Figure 2.19. UV-Vis spectra of **5** (2-Np) in CH₂Cl₂ at different concentrations 298 K.

Following these observations, which potentially indicate the formation of aggregates influence the emission pathway, solvent effects were investigated. Different solvents were used to see if the solvent intermolecular interactions compete or influence aggregation formation. At 298 K, the emission of **5** (2-Np) in a dichloromethane solution is red ($\lambda_{\text{max}} > 680$ nm), this is slightly blue shifted in a Me-THF solution ($\lambda_{\text{max}} > 660$ nm) and further shifted in a toluene solution ($\lambda_{\text{max}} > 640$ nm). Overall the solvent effect is minimal and only red emission is observed, therefore in these conditions the solvent is not altering the emission pathway.

Upon cooling to 77 K, green emission is observed for **5** (2-Np) in Me-THF ($\lambda_{\text{max}} = 520$ nm), whereas the solutions of **5** (2-Np) in dichloromethane and toluene remain red emissive. Therefore, under these conditions the solvent is affecting the emission pathway. The potential solvent effects upon the emission of **9** (^tBu) were also investigated; at 298 K in dichloromethane (10^{-4} and 10^{-2} M) the solution is red emissive, upon cooling to 77 K a mix of red and green emission is observed at 10^{-4} M and red emission at 10^{-2} M. In a Me-THF solution there is no emission at 10^{-4} M and red emission only observed in a 10^{-2} M solution. Upon cooling to 77 K only green emission is observed at both concentrations. In this case there is both an effect of the solvent and concentration indicating that the molecular environment plays an important role.

This set of complexes have shown two emission pathways either red or green. Accessing one emission pathway has been possible through crystallisation of pure microcrystalline solids (2.5.2) or through solution treatment such as at low temperatures. Successive freeze thaw cycles also facilitated access of a single emission pathway. Freezing a solution of **9** (^tBu) (10^{-2} M) in dichloromethane to 77 K produces a red emissive sample (red line, Figure 2.20). However, upon warming to just above the melting point of the solvent and refreezing leads to a mixed emission, which appears orange to the naked eye and the emission band clearly shows

the overlapped signals of the red and green emission (blue line, Figure 2.20). Repeating this cycle several times generates a predominantly structured green emission, assigned to $^3\text{IL}(\text{C}^{\wedge}\text{N}^{\text{Pz}}\text{C})$ transition (green line, Figure 2.20). Upon warming to room temperature, the expected red emission is regenerated. This cycle can be repeated with no degradation of the complex. This is further evidence that the emission pathway may be dependent on intermolecular interactions as there is no change to the complex during the cycle. The successive freeze thaw cycles may alter the intermolecular interactions or geometry favoured by the complex.

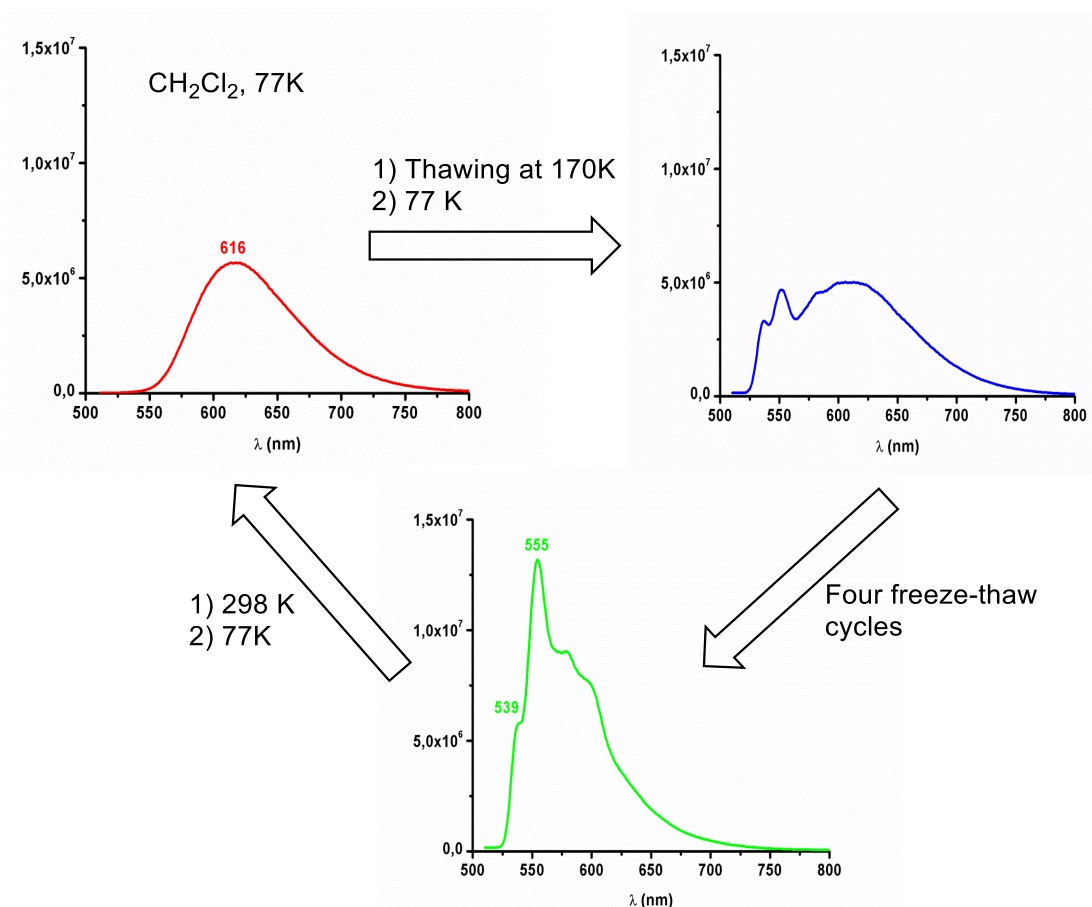


Figure 2.20. The changing emission spectra of **9** (^tBu) (10^{-2} M); Red line: upon freezing to 77 K; Blue line: thawing to melting point and refreezing at 77 K; Green line; 4 successive freeze thaw cycles and refrozen at 77 K.

Concentration appears to influence the emission pathway, with red emission dominating at high concentrations. This may indicate that aggregation of complexes is an integral requirement in this emission mode. Doping a PMMA matrix with varying concentrations of **5** (2-naphthyl thiolate, a predominantly red emissive gold(III) thiolate) and **6** (quinoline thiolate, a green emissive gold(III) thiolate) showed that the effect concentration had on different the emission modes. Upon increasing the concentration of green emitting complex **6** in a PMMA

matrix the photoluminescence quantum yield (PLQY) decreases (left Figure 2.21). In contrast increasing concentrations of **5** increases the PLQY (right Figure 2.21). The PLQY of **5** increases from $\Phi_{\text{PL}} < 0.01$ at 1 wt% loading to $\Phi_{\text{PL}} = 0.11$ at 50 wt% loading. This is also accompanied by a slight red shift with increased loadings. The decrease in the PLQY for **6** resembles the concentration-dependant quenching which has previously been observed for $\text{Ir}(\text{ppy})_3$.²³ The opposing trend in the PLQY of **5** indicates aggregation-induced photoluminescence enhancement.²⁴ The doping of different polymer matrices (polystyrene and polyvinyl carbazole (PVK)) resulted in the same trends in emission for **5** and **6**.

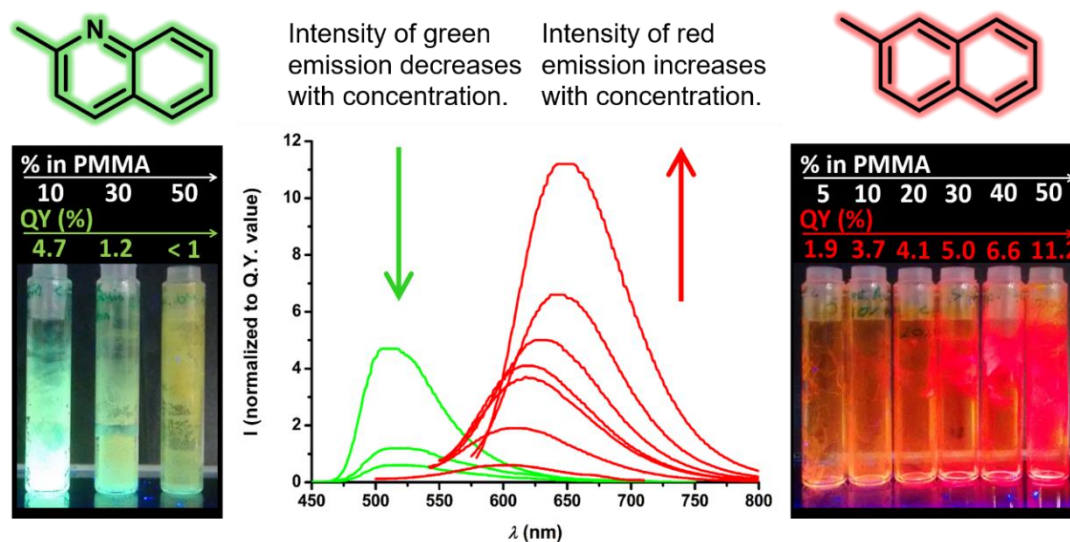


Figure 2.21. The effect of doping concentrations of **5** and **6** in a PMMA matrix upon the quantum yields (298 K).

2.6 Crystal packing

The difference in emission between the two polymorphs of **5** (2-Np) can be clearly seen in Figure 2.13 where a mixture of the two crystalline forms are shown under white light and UV light. Under UV light the red polymorph is emissive whereas the yellow polymorph is not. This difference was also observed in microcrystalline samples of **5** (Section 2.5.2). Due to the lack of compositional variation, the dramatic difference in their photophysical properties may result from different molecular interactions in the solid state.

Closer analysis of the crystal packing of the two polymorphs for both **3** (Ph) and **5** (2-Np) shows similarities between two red polymorphs. The red polymorph of **3** is made up of dimers formed by a head-to-head π -interaction with pyrazine rings of neighbouring molecules adopting a “parallel offset” orientation (Figure 2.22). The distance between the planes of the pincer ligands in these dimers is relatively short at 3.306 Å.

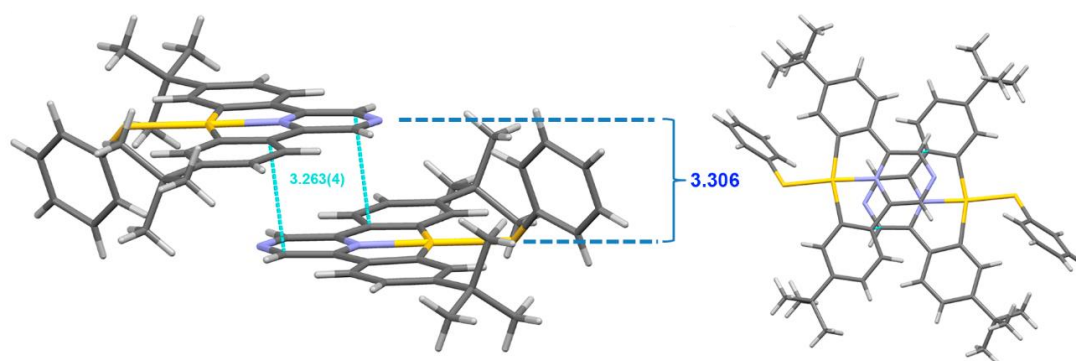


Figure 2.22. The packing of the red polymorph of **3**.

In contrast, the yellow polymorph of **3** forms one-dimensional stacks where the pyrazine ring of one molecule is superimposed on the Au-S bond of its nearest neighbour (Figure 2.23). The *o*-phenyl protons of the thiophenolate ligand interacts with two pyrazine-N atoms of its neighbour molecules in the stack in a H \cdots N \cdots H arrangement (a, Figure 2.23). The separation between molecular planes is 3.472 Å, this is larger than in the red polymorph.

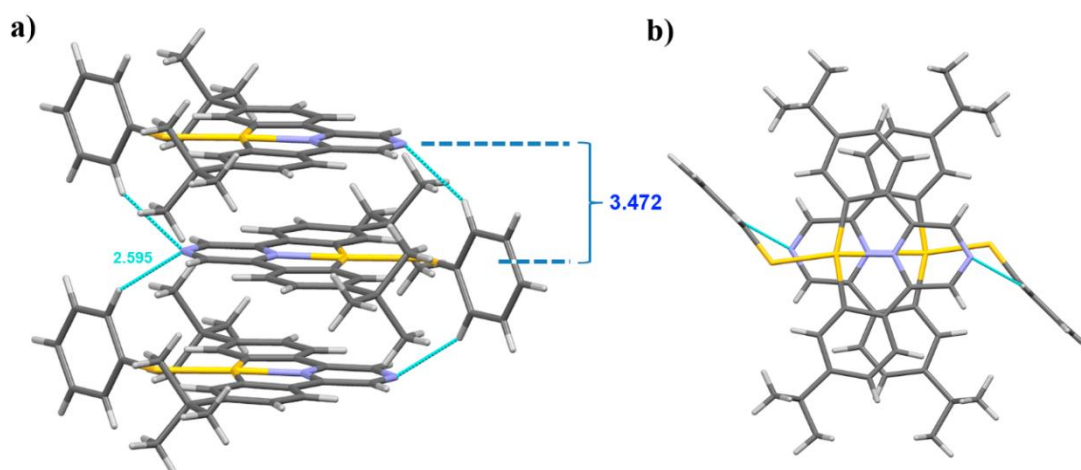


Figure 2.23. The packing of the yellow polymorph of **3**.

The red polymorph of **5** shows the same type of pyrazine-pyrazine π interactions in a parallel offset orientation as seen in the red polymorph of **3** (Figure 2.24). In the π -stacked dimers there is again a short intermolecular distance between the planes of the pincer ligands of 3.235 Å.

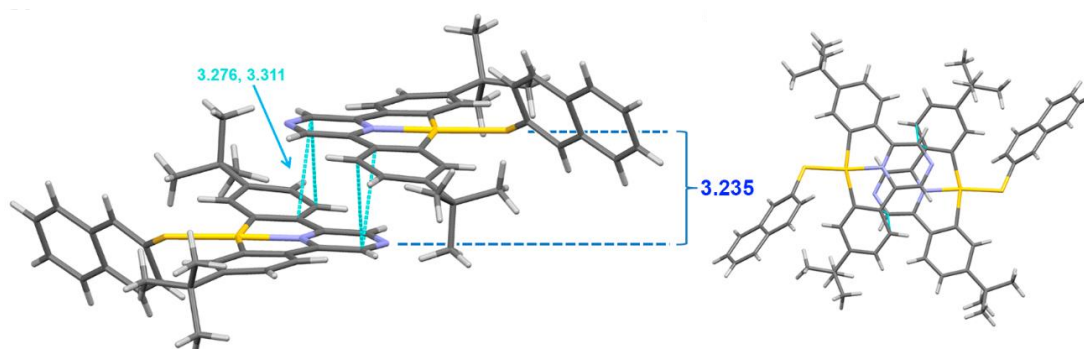


Figure 2.24. The packing of the red polymorph of **5**.

The packing of the yellow polymorph of **5** differs from the yellow polymorph of **3** as it is arranged in head-to-tail rods (Figure 2.25). This is dominated by the $S \cdots \pi$ interactions between the thiolate sulfur and the pyrazine ring of the neighbouring molecule. The distances between the planes of the pincer ligands is longer than in the corresponding red polymorph at 3.482 Å.

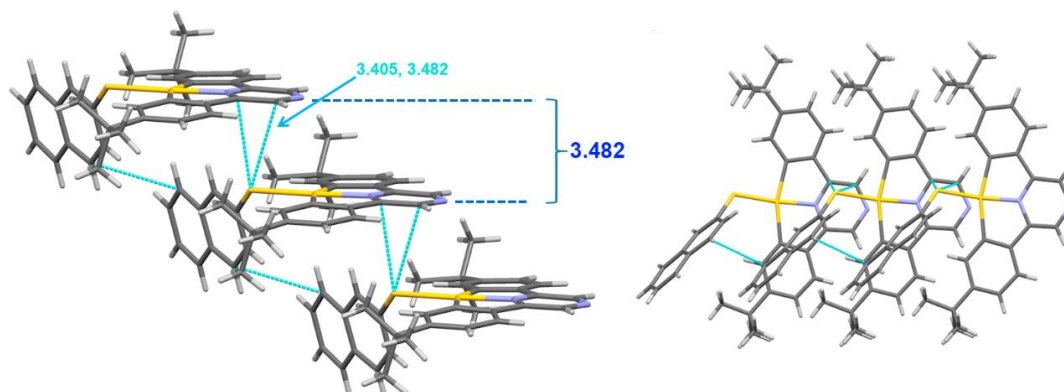


Figure 2.25. The packing of the yellow polymorph of **5**.

The other crystals obtained for complexes **4**, **7** and **9** were yellow and only one polymorph of each complex was obtained. The packing of **4** is dominated by the formation of $N \cdots H$ interactions between the nitrogen of the thiolate and C-H bonds on the pincer ligand (Figure 2.26). This is likely to be the dominant intermolecular interaction for both **4** and **6**, therefore the absence of heteroatoms in the red emissive complexes may enable different intermolecular interactions as they are not dominated by $N \cdots H$ interactions. The inter-plane distance of 3.410 Å is a similar distance to that observed in the yellow polymorphs of **3** and **5**.

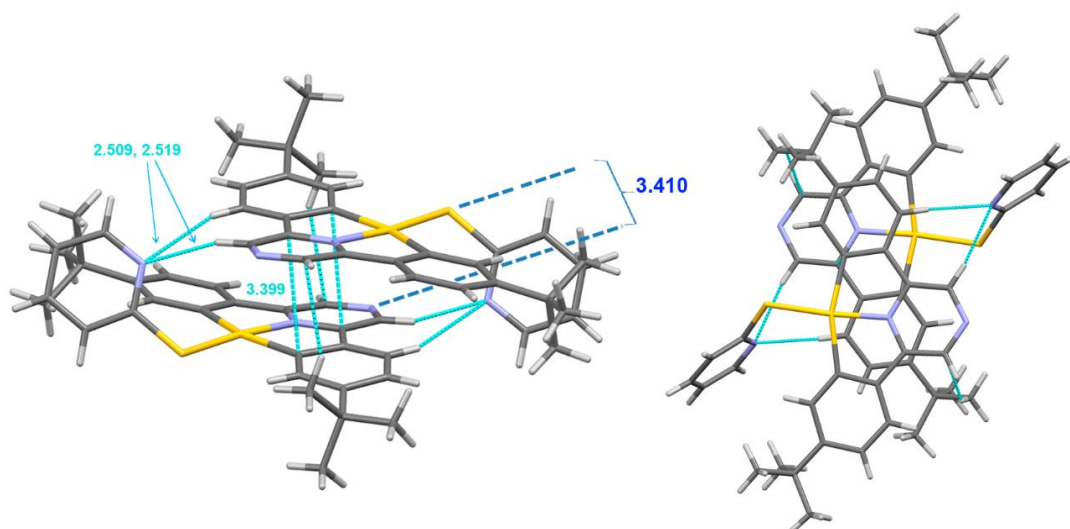


Figure 2.26. The crystal packing of **4**.

The packing of **9** was also through the formation of dimers through parallel offset π - π interactions, but here the pyrazine ring of one molecule is aligned with one of the Au-C bonds of a second molecule (Figure 2.27). The inter-plane distances are longer at 3.469 Å, which is a similar distance to the yellow polymorphs of **3** and **5** and the packing of **4**.

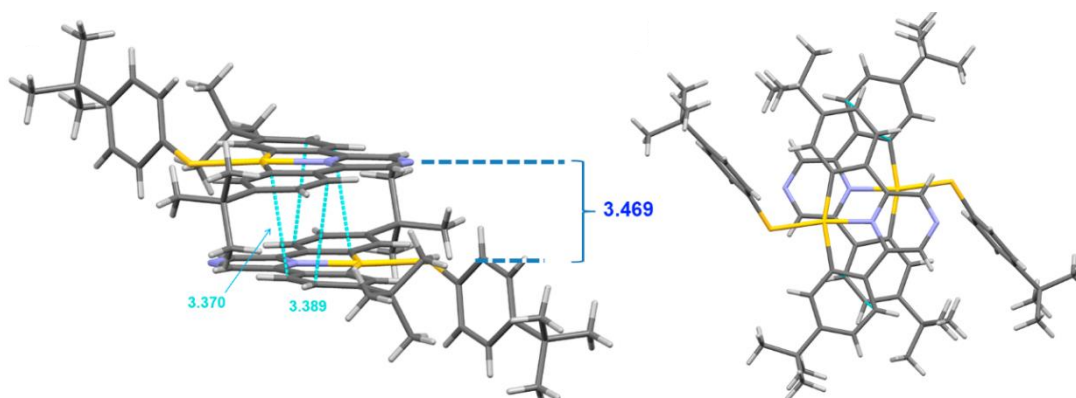


Figure 2.27. The crystal packing of **9**.

In the packing of **11** the phenyl pyridine moieties of neighbouring molecules align with an inter-planar distance is 3.349 Å (Figure 2.28). There is also one molecule of dichloromethane that cocrystallised.

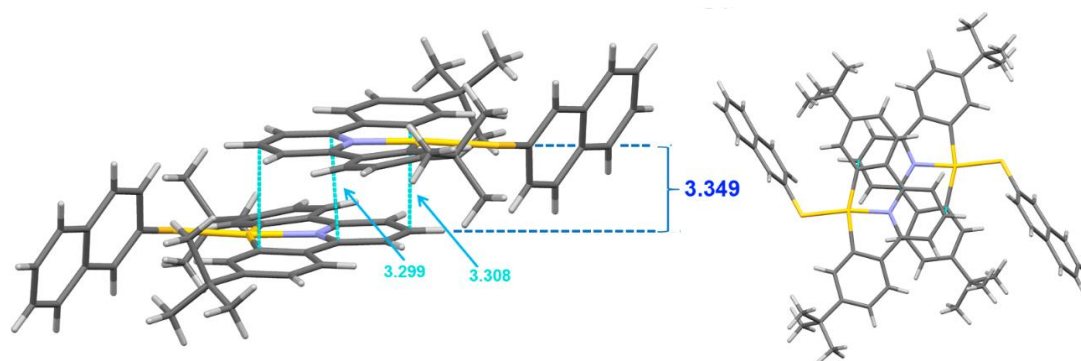


Figure 2.28. The crystal packing of **11**.

The red polymorphs of **3** (Ph) and **5** (2-Np) are both formed of dimers based on pyrazine-pyrazine π - interactions with short inter-planar distances of 3.306 Å and 3.235 Å. These are not observed in the yellow polymorphs of the corresponding molecule or in the packing of the yellow crystals **4**, **9** and **11**. The yellow polymorphs are based in the pyrazine ring interacting either with an Au-S bond or a phenyl ring of a neighbouring molecule. All the yellow crystals had larger inter-planar distances. Therefore, the formation of pyrazine-pyrazine π -interactions may be responsible for the red emission, which may occur in the formation of aggregates in solution.

2.7 Diffusion NMR

The experiments in this section were carried out in conjunction with Dr Luca Rocchigiani.

NMR spectroscopy was used to investigate whether the intermolecular interactions observed in the solid state, that are proposed to influence the photoluminescent properties, could also be observed in solution. The red emission is possibly linked to close π - π interactions in the solid state, however the red emission is also observed in solution which could indicate the persistence of intermolecular π -interactions. Two separate NMR spectroscopy methods were used to investigate the potential of aggregation in solution of complexes **1** (Cl), **3** (Ph) and **5** (2-Np).

The first method studied the concentration dependence of the chemical shift signals in the ^1H NMR spectra. The concentration was gradually increased from a 10^{-4} M solution to a saturated solution with a concentration greater than 10^{-2} M (the concentration used in photoluminescent studies). Over this gradient the greatest change in chemical shift (δ) was observed for H^2 and H^5 , which are hydrogen atoms on or next to the pyrazine ring (Figure 2.9 for NMR assignment and Figure 2.29 for the chemical shifts at different concentrations). This correlates with the head-to-head π -stacking interactions in the red polymorphs and therefore could indicate that this interaction also persists in solution. The observed shift of H^2 and H^5 is not large, which

indicates that only a proportion of the molecules are interacting in this π - π manner in solution. There was very little change in the chemical shifts of signals corresponding to the thiolate ligand with increasing concentrations; this is also agreement with the solid-state environment where the close intermolecular interactions are between the planes of the pincer ligands.

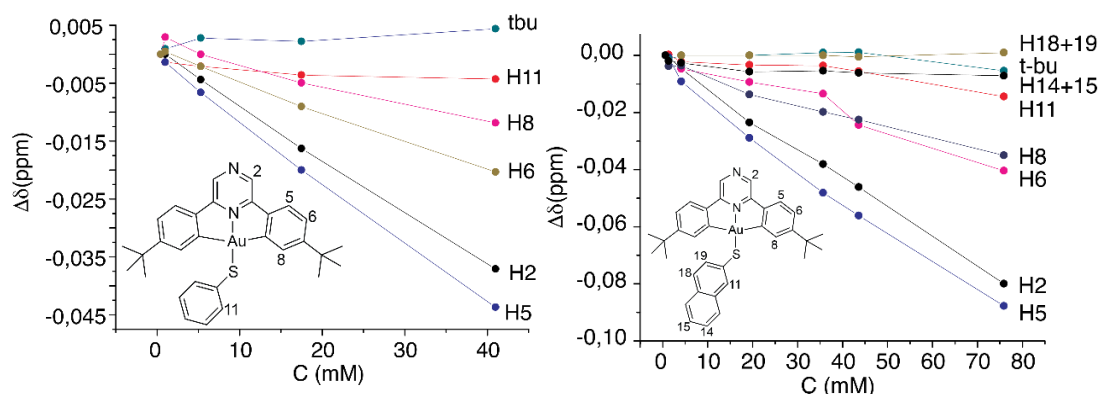


Figure 2.29. Variation in proton shifts with increasing concentration of: left) **3**; right) **5**.

Using a monomer-dimer equilibrium model it is possible to quantify the proportion of dimerization, assuming the observed chemical shift (δ) is an average between those of the monomer and dimer. This is shown by Equation 2.1 where f_m and f_d are the molar fractions of monomers and dimers, δ_M and δ_D are the limit chemical shift values of monomer and dimer, respectively. This can be manipulated to give Equation 2.2 where the observed chemical shift is a function of K , the association constant.

$$\text{a) } d_i = d_M f_M + d_D f_D = \frac{[A]}{[A]_0} d_M + \frac{2[A_2]}{[A]_0} d_D$$

$$\text{b) } d_i = d_M + (d_D - d_M) \frac{(1 + 8K[A]_0)^{1/2} - 1}{(1 + 8K[A]_0)^{1/2} + 1}$$

Equation 2.1 (a) and 2.2 (b). Used to calculate monomer-dimer equilibrium.

After fitting chemical shift versus concentration trends, the molar fractions of dimers were obtained using Equation 2.3. At the highest investigated solution of **5** (7.6×10^{-2} M) the proportion of dimers is 18 % and for **3** (5.6×10^{-2} M) the proportion of dimers is approximately 9 %.

$$f_D = -1 + \frac{2[A]_0}{[A]_0 + \frac{\sqrt{1 + 8K[A]_0} - 1}{4K}}$$

Equation 2.3. Used to calculate the molar fractions of dimers in solutions of **3** and **5**.

The rates of diffusion of **3** and **5** were also probed using PGSE (pulse gradient spin echo) NMR experiments in which the dependence of the resonance intensity (I) on a constant waiting time and on a varied gradient strength G is described by Equation 2.4.

$$\ln \frac{I}{I_0} = (gd^2)D_t \left(d - \frac{D}{3} \right) G^2$$

Equation 2.4. The dependence of D_t upon the resonance intensity (I) and a varied gradient strength (G).

Plotting $\ln(I/I_0)$ against G^2 can be used to identify the self-diffusion coefficient values (D_t) from which the structural parameters can be approximated. The relationship between D_t and hydrodynamic dimensions is expressed by the modified Stokes-Einstein equation (Equation 2.5) where k is the Boltzmann constant, T is the temperature, η is the solution viscosity, c is the “size factor”, which depends on the solute-solvent radius ratio and f is the “shape factor”. Identification of the hydrodynamic dimensions using this equation made it possible to deduce the change in dimensions over a range of concentrations.

$$D_t = \frac{kT}{\rho h f c^3 \sqrt{abd}}$$

Equation 2.4. The modified Stokes-Einstein equation.

Assuming a monomer/dimer equilibrium, the observed P values ($P = f c^3 \sqrt{abd} = kT / \pi \eta D_t$) can be treated as the average between the parameters of both monomer (P_M) and dimer (P_D), according to Equation 2.5 where x_M and x_D are the molar fractions of monomer and dimer at a given concentration. P_M parameters can be derived from X-ray structures of monomers, by approximating their shape to ellipsoids. P_D parameters have been calculated by using packing data derived by X ray diffraction.

$$P_i = P_M x_M + P_D x_D$$

Equation 2.5. The observed parameters based on a monomer/dimer equilibrium.

The structural parameters were shown to be slightly dependent upon the concentration, indicating weak self-aggregation. These experiments gave 26 % dimerization for **5** at 7.6×10^{-2} M and 21 % dimerization of **3** at 5.6×10^{-2} M.

Both methods indicate that at low concentrations the complexes are predominantly monomers. This aggregation behaviour was also observed for **1**, but to a lesser extent, this is probably because the interactions are pincer ligand based, therefore all pyrazine based complexes are able dimerise and form π - π interactions. The thiolates showed a higher percentage of

dimerization presumably due to the increased solubility of the naphthyl thiolate resulting in higher concentrations in solution and hence more dimerization.

2.8 Theoretical calculations

The work in this section was carried out by Helen Duckworth and Dr Tom Penfold.²⁵

Density function theory (DFT) and time-dependent density functional theory (TDDFT) calculations were performed to gain further insight into the effect of supramolecular interactions upon the photophysical properties of the complexes. Complex **5** (2-Np) was chosen as the model for these complexes because it had shown both red and yellow emission. Three different structural dispositions were optimised: an isolated molecule, a dimer based in the pyrazine-pyrazine aggregations that was observed in the red polymorph of **5** and a dimer based on the yellow polymorph of **5** that contained S $\cdots\pi$ interactions between a thiolate and a pyrazine of a neighbouring molecule. All optimised calculated structures agree with those in the X-ray crystal structures. This is demonstrated by both similar intramolecular distances and inter-plane distances between the structures based on dimers: red dimer had a calculated distance of 3.26 Å matching the 3.235 Å in the X-ray structure, similarly the yellow dimer had a calculated distance of 3.45 Å and 3.482 Å in the X-ray structure.

The frontier orbitals calculated for the different structures show similarities between the yellow dimer and the monomer. The LUMO for the yellow dimer is based on the cyclometallated C^NC ligand of one molecule and the HOMO is located mainly on the thiolate of the same molecule (Figure 2.30). In the monomer the similar frontier orbitals are observed. This indicates that the emission from the yellow polymorphs are based on isolated molecules, not on aggregates.

The red dimer's frontier orbitals are different, the HOMO is again located mainly on one thiolate ligand, but the LUMO is delocalised over the two pyrazine ligands of neighbouring π -stacked molecules (Figure 2.30). This bimolecular molecular orbital is likely to be responsible for the intense unstructured red photoemission.

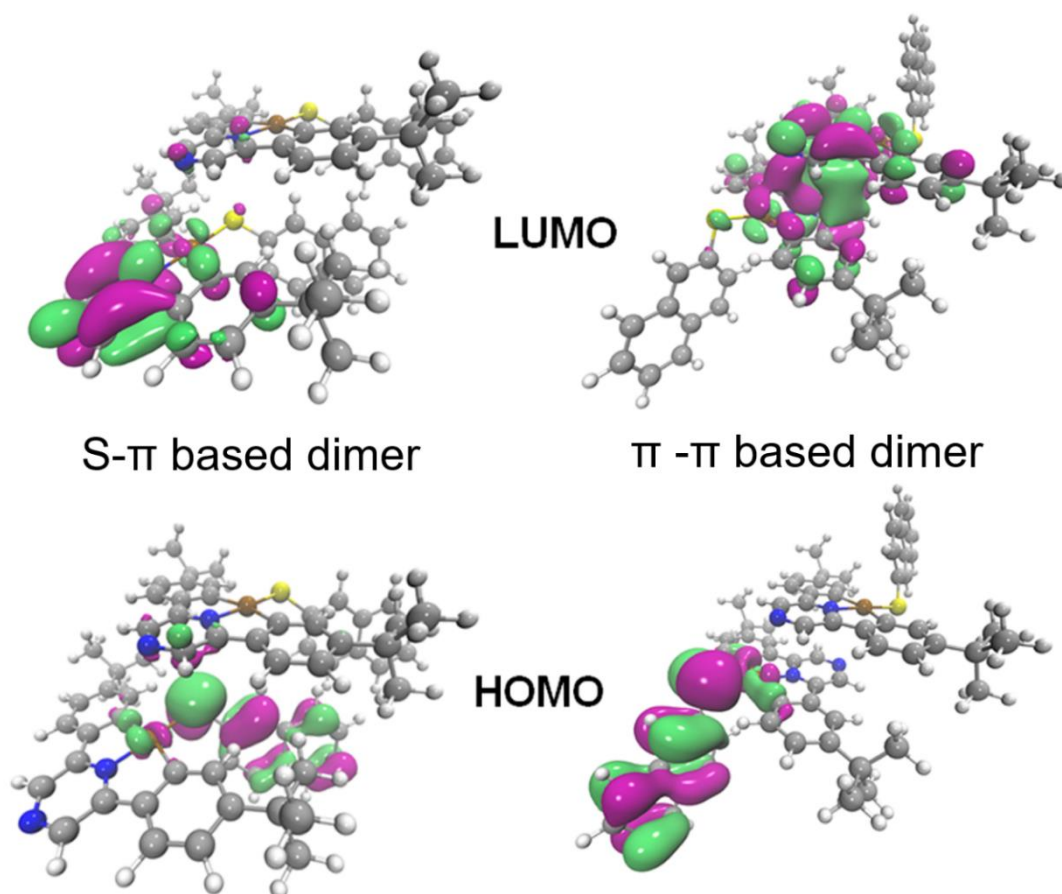


Figure 2.30. The HOMO and LUMO frontier orbitals for **5** in left) the yellow dimer based on $S \cdots \pi$ interactions; right) red dimer based on pyrazine-pyrazine interactions.

The calculated emission from the optimised triplet geometry of the red dimer of **5** is 704 nm in agreement with the red emission observed. However, for the yellow dimer and the monomer of **5** the, the transition energy is very low (>850) so the non-radiative emission rate will be larger. Calculations suggest that the emission observed arises from a transition from the second triplet state (T_2), which gives a calculated emission of 585 nm for the yellow dimer and 573 nm for the monomer. This gives a transition of HOMO-2 \rightarrow LUMO both of which are centred on the $C^{\wedge}N^{\wedge}C$ cyclometallated ligand confirming the ${}^3\pi-\pi^*(C^{\wedge}N^{pz}\wedge C)$ transition previously assigned.

The calculations support the theory that aggregation and intermolecular interactions influence the emission pathway. The aggregation through pyrazine-pyrazine $\pi-\pi$ interactions induce an alternative emission pathway to the green, structured emission based on isolated molecules assigned to a ${}^3IL(C^{\wedge}N^{\wedge}C)$ transition. The emission based on the aggregates is likely to be a charge-transfer transition from the π -stacked dimeric pyrazine moiety to a thiolate ligand ${}^3LLCT([(C^{\wedge}N^{pz}\wedge C)_2] \rightarrow SR)$. The observation of two components in the emission spectra in

either a frozen solution or polymer matrix, compared to a single, red-shifted, emission in solution can be rationalized on the basis of two emissive states of very similar energy.

Conclusion

Stable gold(III) thiolates can be synthesised using mild conditions, with those bearing a pyrazine-based pincer ligand being photoluminescent at room temperature. This emission occurs either via an $^3\text{IL}(\text{C}^{\wedge}\text{N}^{\wedge}\text{C})$ transition resulting in green structured emission or a $^3\text{LLCT}([\text{C}^{\wedge}\text{N}^{\text{pz}}\text{C}]_2) \rightarrow \text{SR}$ transition resulting in a red emission. The luminescence observed is dependent on the supramolecular arrangement both in the solid state and solution. The polymorphs obtained for **3** and **5** have different emission properties, both form a polymorph that at 298 K is red emissive and a yellow polymorph that at 298 K is nonemissive. The red emission is attributed to the formation of head-to-head π -stacked dimers of neighbouring pyrazine rings in a “parallel offset” orientation. Complexes containing a heteroatom in the thiolate ligand did not adopt these conformations as the predominant intermolecular interaction was between the heteroatom and a C-H bond of a neighbouring molecule.

The red emission was observed in a polymer matrix, in solution and in the solid state. The persistence of aggregates in solution based on π -stacked dimers was observed through NMR studies. Theoretical calculations show that dimerization through pyrazine-pyrazine π interactions produced a LUMO delocalized over two molecules further supporting the observations that aggregation is related to the red emission. In addition, successive freeze thaw cycles allowed controlled alteration of the emission pathway from red to green.

The concentration effect upon the two emission pathways was evident in PMMA matrices; while the green $^3\text{IL}(\text{C}^{\wedge}\text{N}^{\wedge}\text{C})$ emission is subject to quenching with increasing concentration, the photoluminescence quantum yield of the red emission increases with increasing concentration. To the best of our knowledge, this is first detailed study of aggregation-enhanced emission in gold(III) chemistry.

References

- (1) (a) Balzani, V.; Bergamini, G.; Ceroni, P. *Coord. Chem. Rev.* **2008**, *252*, 2456. (b) Yam, V. W. W.; Wong, K. M. C. *Chem. Commun.* **2011**, *47*, 11579. (c) Lo, K. K. W.; Choi, A. W. T.; Law, W. H. T. *Dalton Trans.* **2012**, *41*, 6021. (d) Thorp-Greenwood, F. L.; Balasingham, R. G.; Coogan, M. P. *J. Organomet. Chem.* **2012**, *714*, 12. (e) Visbal, R.; Gimeno, M. C. *Chem. Soc. Rev.* **2014**, *43*, 3551. (f) Ma, D. L.; Chan, D. S. H.; Leung, C. H. *Acc. Chem. Res.* **2014**, *47*, 3614. (g) Yam, V. W. W.; Au, V. K.

- M.; Leung, S. Y. L. *Chem. Rev.* **2015**, *115*, 7589. (h) Hemmert, C.; Gornitzka, H. *Dalton Trans.* **2016**, *45*, 440.
- (2) Lowry, M. S.; Bernhard, S. *Chem.-Eur. J.* **2006**, *12*, 7970.
- (3) Williams, J. A. G.; Develay, S.; Rochester, D. L.; Murphy, L. *Coord. Chem. Rev.* **2008**, *252*, 2596.
- (4) Lopez-de-Luzuriaga, J. M.; Monge, M.; Olmos, M. E. *Dalton Trans.* **2017**, *46*, 2046.
- (5) (a) Ballhausen, C. J.; Bjerrum, N.; Dingle, R.; Eriks, K.; Hare, C. R. *Inorg. Chem.* **1965**, *4*, 514. (b) Andrews, L. J. *J. Phys. Chem.* **1979**, *83*, 3203. (c) Williams, J. A. G. *Chem. Soc. Rev.* **2009**, *38*, 1783. (d) Bronner, C.; Wenger, O. S. *Dalton Trans.* **2011**, *40*, 12409.
- (6) Yam, V. W. W.; Choi, S. W. K.; Lai, T. F.; Lee, W. K. *J. Chem. Soc.-Dalton Trans.* **1993**, 1001.
- (7) Wong, K. H.; Cheung, K. K.; Chan, M. C. W.; Che, C. M. *Organometallics* **1998**, *17*, 3505.
- (8) Au, V. K. M.; Wong, K. M. C.; Zhu, N. Y.; Yam, V. W. W. *J. Am. Chem. Soc.* **2009**, *131*, 9076.
- (9) Yam, V. W. W.; Wong, K. M. C.; Hung, L. L.; Zhu, N. Y. *Angew. Chem.-Int. Edit.* **2005**, *44*, 3107.
- (10) Au, V. K. M.; Tsang, D. P. K.; Wong, K. M. C.; Chan, M. Y.; Zhu, N. Y.; Yam, V. W. W. *Inorg. Chem.* **2013**, *52*, 12713.
- (11) (a) Wong, K. M. C.; Hung, L. L.; Lam, W. H.; Zhu, N. Y.; Yam, V. W. W. *J. Am. Chem. Soc.* **2007**, *129*, 4350. (b) Au, V. K. M.; Wong, K. M. C.; Tsang, D. P. K.; Chan, M. Y.; Zhu, N. Y.; Yam, V. W. W. *J. Am. Chem. Soc.* **2010**, *132*, 14273.
- (12) (a) Tang, M. C.; Tsang, D. P. K.; Chan, M. M. Y.; Wong, K. M. C.; Yam, V. W. W. *Angew. Chem.-Int. Edit.* **2013**, *52*, 446. (b) Lee, C. H.; Tang, M. C.; Wong, Y. C.; Chan, M. Y.; Yam, V. W. W. *J. Am. Chem. Soc.* **2017**, *139*, 10539.
- (13) Yim, K. C.; Au, V. K. M.; Wong, K. M. C.; Yam, V. W. W. *Chem.-Eur. J.* **2017**, *23*, 5772.
- (14) (a) Tang, M. C.; Chan, C. K. M.; Tsang, D. P. K.; Wong, Y. C.; Chan, M. M. Y.; Wong, K. M. C.; Yam, V. W. W. *Chem.-Eur. J.* **2014**, *20*, 15233. (b) Tang, M. C.; Tsang, D. P. K.; Chan, M. Y.; Wong, K. M. C.; Yam, V. W. W. *Mat. Chem. Front.* **2017**, *1*, 2559.
- (15) (a) Tang, M. C.; Lee, C. H.; Lai, S. L.; Ng, M.; Chan, M. Y.; Yam, V. W. W. *J. Am. Chem. Soc.* **2017**, *139*, 9341. (b) To, W. P.; Zhou, D. L.; Tong, G. S. M.; Cheng, G.; Yang, C.; Che, C. M. *Angew. Chem.-Int. Edit.* **2017**, *56*, 14036.
- (16) Fernandez-Cestau, J.; Bertrand, B.; Blaya, M.; Jones, G. A.; Penfold, T. J.; Bochmann, M. *Chem. Commun.* **2015**, *51*, 16629.

- (17) (a) Walker, I. C.; Palmer, M. H.; Hopkirk, A. *Chem. Phys.* **1990**, *141*, 365. (b) Walker, I. C.; Palmer, M. H. *Chem. Phys.* **1991**, *153*, 169.
- (18) Fernandez-Cestau, J.; Bertrand, B.; Pintus, A.; Bochmann, M. *Organometallics* **2017**, *36*, 3304.
- (19) (a) Chen, H. W.; Papparizos, C.; Fackler, J. P. *Inorganica Chimica Acta-Articles and Letters* **1985**, *96*, 137. (b) Wang, S.; Fackler, J. P. *Inorg. Chem.* **1990**, *29*, 4404. (c) Garcia, J. J.; Hernandez, M. L.; Torrens, H.; Gutierrez, A.; Delrio, F. *Inorg. Chim. Acta* **1995**, *230*, 173. (d) Abram, U.; Mack, J.; Ortner, K.; Muller, M. *J. Chem. Soc.-Dalton Trans.* **1998**, 1011. (e) Watase, S.; Kitamura, T.; Kanehisa, N.; Nakamoto, M.; Kai, Y.; Yanagida, S. *Acta Crystallogr. Sect. C-Cryst. Struct. Commun.* **2003**, *59*, M162. (f) Bachman, R. E.; Bodolosky-Bettis, S. A.; Pyle, C. J.; Gray, M. A. *J. Am. Chem. Soc.* **2008**, *130*, 14303. (g) Le Pennec, R.; Jeannin, O.; Auban-Senzier, P.; Fourmigue, M. *New J. Chem.* **2016**, *40*, 7113.
- (20) (a) Cinellu, M. A.; Minghetti, G.; Pinna, M. V.; Stoccoro, S.; Zucca, A.; Manassero, M. *J. Chem. Soc.-Dalton Trans.* **1999**, 2823. (b) Mansour, M. A.; Lachicotte, R. J.; Gysling, H. J.; Eisenberg, R. *Inorg. Chem.* **1998**, *37*, 4625. (c) Parish, R. V.; Wright, J. P.; Pritchard, R. G. *J. Organomet. Chem.* **2000**, *596*, 165. (d) Henderson, W.; Nicholson, B. K.; Faville, S. J.; Fan, D.; Ranford, J. D. *J. Organomet. Chem.* **2001**, *631*, 41. (e) Fan, D. M.; Yang, C. T.; Ranford, J. D.; Vittal, J. J.; Lee, P. F. *Dalton Trans.* **2003**, 3376.
- (21) Tiekink, E. R. T.; Kang, J. G. *Coord. Chem. Rev.* **2009**, *253*, 1627.
- (22) (a) Kalinowski, J.; Fattori, V.; Cocchi, M.; Williams, J. A. G. *Coord. Chem. Rev.* **2011**, *255*, 2401. (b) Vezzu, D. A. K.; Deaton, J. C.; Jones, J. S.; Bartolotti, L.; Harris, C. F.; Marchetti, A. P.; Kondakova, M.; Pike, R. D.; Huo, S. Q. *Inorg. Chem.* **2010**, *49*, 5107. (c) Wong, K. M. C.; Chan, M. M. Y.; Yam, V. W. W. *Adv. Mater.* **2014**, *26*, 5558.
- (23) Takayasu, S.; Suzuki, T.; Shinozaki, K. *J. Phys. Chem. B* **2013**, *117*, 9449.
- (24) (a) Mei, J.; Hong, Y. N.; Lam, J. W. Y.; Qin, A. J.; Tang, Y. H.; Tang, B. Z. *Adv. Mater.* **2014**, *26*, 5429. (b) Zhao, Z. J.; He, B. R.; Tang, B. *Chem. Sci.* **2015**, *6*, 5347.
- (25) Currie, L.; Fernandez-Cestau, J.; Rocchigiani, L.; Bertrand, B.; Lancaster, S. J.; Hughes, D. L.; Duckworth, H.; Jones, S. T. E.; Credgington, D.; Penfold, T. J.; Bochmann, M. *Chem.-Eur. J.* **2017**, *23*, 105

Chapter Three:

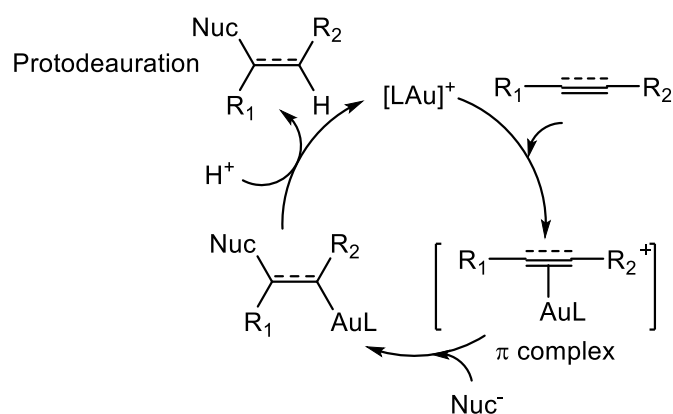
Thiol triggered C-S and C-C reductive elimination from gold(III) pincer complexes

Part of this chapter has been published as: Currie, L.; Rocchigiani, L.; Hughes, D. L.; Bochmann, M. *Dalton Trans.* **2018**, 47, 6333.

Introduction

3.1 Gold Catalysis

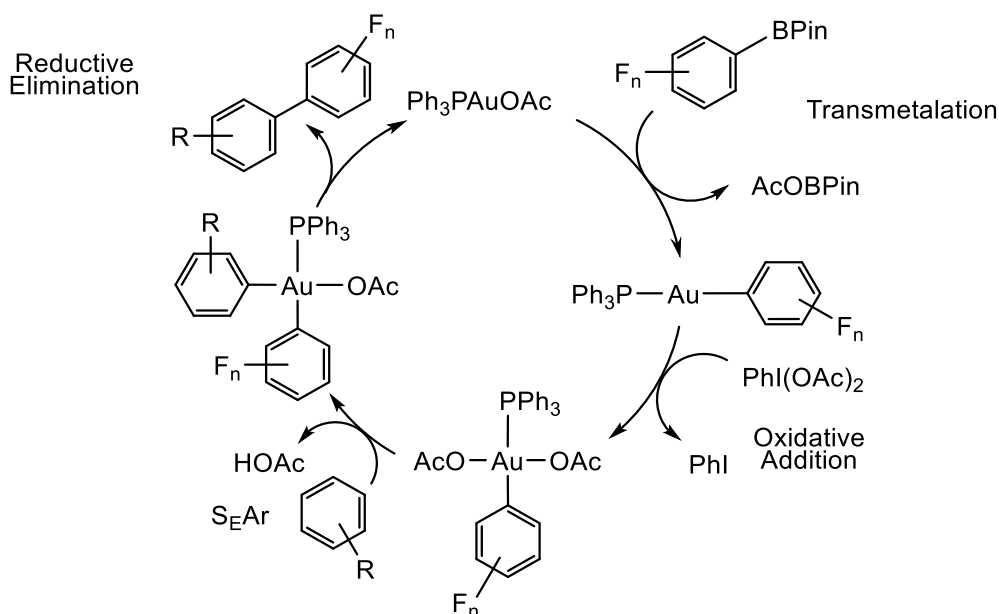
The last 10-15 years have seen a tremendous growth in the use of gold complexes as homogeneous catalysts for a multitude of organic transformations.¹ The most widespread application of gold(I) salts are as Lewis acids for the activation of unsaturated substrates (alkynes and alkenes) towards nucleophilic attack. In these systems, the key step is the formation of an intermediate π -complex, where the unsaturated bond is activated thus facilitating nucleophilic attack (Scheme 3.1). The substrate is then released through protodeauration, where an Au–C bond is broken and a C–H bond is formed, regenerating the gold(I) catalyst.² Throughout this process there is no change in the oxidation state of the metal.



Scheme 3.1. Gold(I) catalysed alkene/alkyne bond activation.

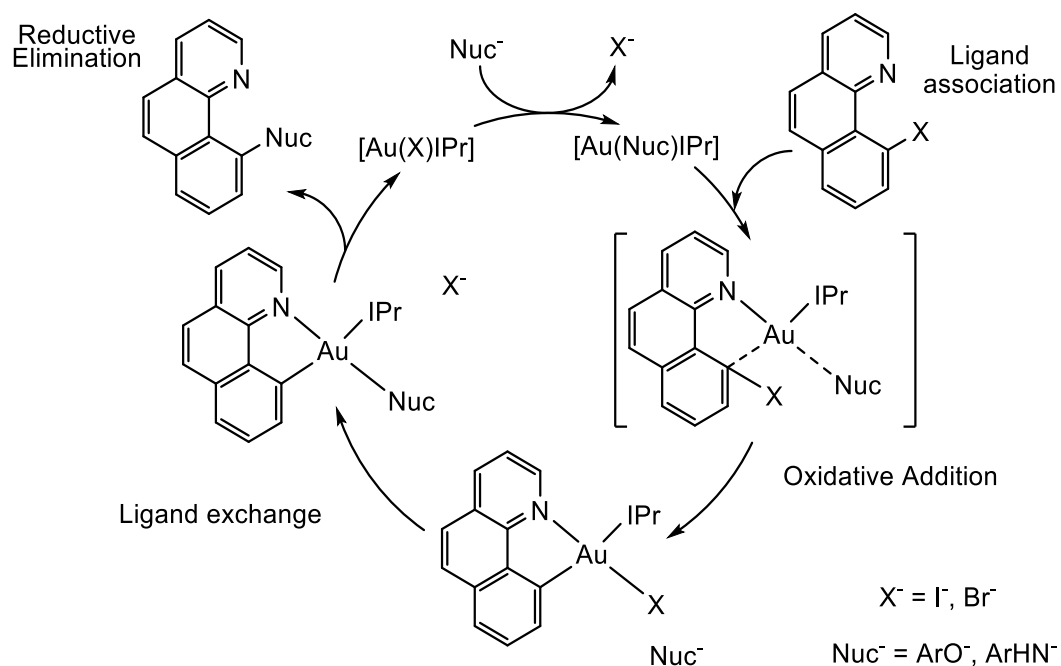
More recently there has been interest in the development of gold catalysed C–C cross coupling reactions and oxidative arylations.³ These reactions are based on key steps including: oxidative addition, transmetallation and reductive elimination. These are commonly seen in other transition metal catalysed cross coupling reactions such as the Suzuki-Miyaura reaction, but less frequently observed for gold systems.⁴ Scheme 3.2 shows a prototypical system, first a gold(I) complex undergoes transmetallation with an arylboronic acid, forming a gold(I)-aryl complex.^{3e} This species is oxidised from gold(I) to gold(III) using a strong, sacrificial oxidising agent such as a hypervalent iodine species. Subsequent electrophilic aromatic substitution forms a second Au–C bond and, finally, reductive elimination forms a C–C bond releasing the biaryl and regenerating the gold(I) species. Unlike the Suzuki-Miyaura reaction, these reactions often require the use of strong external oxidising agents, such hypervalent iodine, because oxidation of gold(I) to gold(III) is energetically unfavourable.^{3b,d,e} Even though palladium-based catalysis remains ubiquitous due to their remarkable efficiency, the

capability of gold to selectively activate C–H bonds, as well as very fast reductive elimination, has attracted notable interest.



Scheme 3.2. Gold catalyzed oxidative arylation forming C–C bonds.^{3e}

There are considerably fewer reported C–X cross coupling reactions with gold. Nevertheless, an interesting example of a gold catalyzed C–N and C–O cross coupling reaction enabled the coupling of alcohols and amines with benzoquinolines (Scheme 3.3).⁵ This system negates the use of sacrificial oxidants and highlights the importance of ligand design. Ribas *et al.*, proposed the following mechanism: initial coordination of a benzoquinoline to a gold(I) carbene complex, which undergoes oxidative addition of a C–X bond. This is followed by ligand exchange by either the alcohol or amine followed by reductive elimination, in which a new C–Nuc bond forms and a gold(I) species is regenerated (Scheme 3.3). The system was found to perform much better when benzoquinolines were used instead of phenyl pyridine ligands. This was proposed to be due to the rigidity of the benzoquinoline blocking rotation that is possible in a phenyl pyridine ligand and increased the stability of the oxidative addition product.



Scheme 3.3. Catalytic C-N and C-O bond formation without external oxidant.

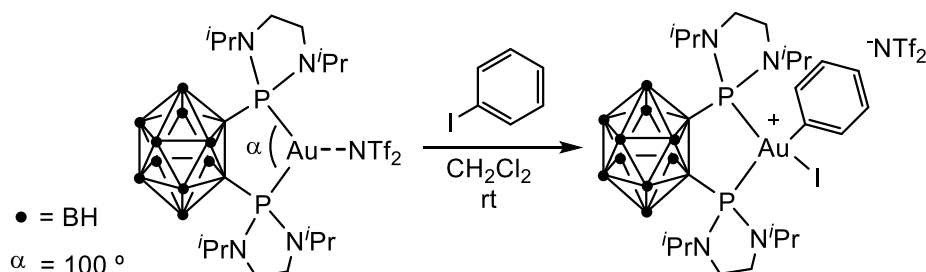
To better understand these catalytic cycles and to help develop better performing systems, there has been a concerted effort to understand the fundamental redox steps⁶ and the structure of intermediates, particularly those of gold(III).⁷ A recent review by Bourissou *et al.* covers key examples of oxidative addition, transmetalation, migratory insertion and, most interesting for this work, reductive elimination.⁶

This thesis also focuses on the sulfur based ligands, which are often considered catalyst poisons due to the formation of strong metal sulfur bonds.⁸ This is one of the major problems to overcome in the development of catalytic C-S bond forming processes. Therefore, the reactivity of gold(III) complexes with thiols is of interest.

3.2 Oxidative addition to gold(I) species

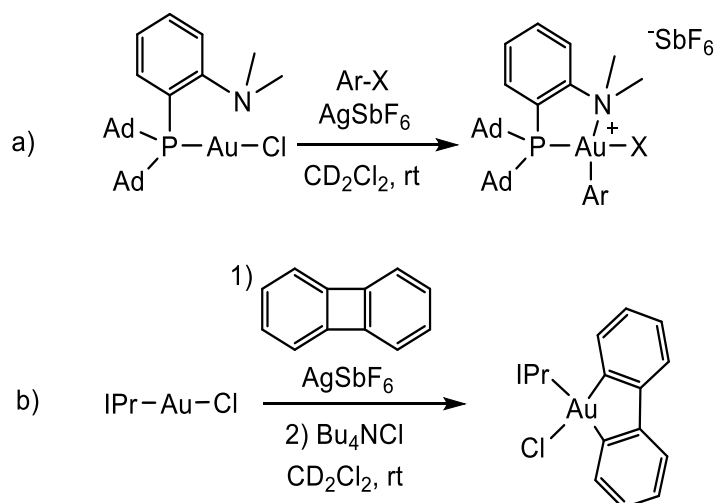
Oxidation of gold(I) to gold(III) is difficult due to the high oxidation potentials (see Section 1.3). It can be achieved using strong sacrificial oxidants such as selectfluor⁹ or hypervalent iodine,^{3b,e} however the low tolerance to a wide range of functionalities limits the scope of substrates available. Oxidative addition of C-X bonds in Suzuki-Miyaura palladium based catalysis is often rate determining,^{4b} but this is considerably more facile than in gold systems. In the Suzuki-Miyaura reaction a range of simple palladium catalysts can be used including Pd(PPh₃)₄, Pd(OAc)₂ and PdCl₂(PPh₃)₂, whereas the equivalent gold systems are unable to undergo oxidative addition.¹⁰ Various strategies have been developed to facilitate oxidative addition of a wider range of substrates. One approach to overcome this lack of reactivity used

chelating ligands with a smaller bite angle, such as in the bent diphosphine gold(I) species, to allow oxidative addition of an aryl halide (Scheme 3.4).¹¹ In this bent gold(I) system the complex had a preorganised coordination environment that favours the formation of a gold(III) product unlike linear gold(I) complexes.



Scheme 3.4. Oxidative addition of aryl halides using ligands with a bent geometry.

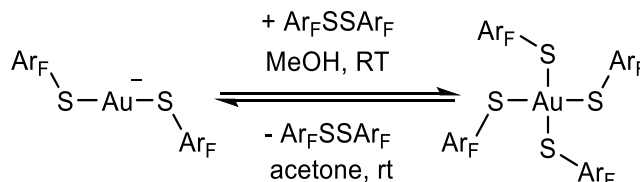
Alternatively, abstraction of a halide from hemilabile ($P^{\wedge}N$)gold(I) complexes can promote oxidative addition of aryl halides, such as in a recent system by Bourissou *et al.* (a Scheme 3.5), which was further developed into a catalytic system to produce biaryls. The first step, before oxidative addition, is abstraction of the chloride by a silver salt. The weakly coordinating anion SbF_6^- forms a weak $F_5Sb-F-Au$ interaction which is displaced by an aryl halide, this undergoes oxidative addition and is further stabilised by the hemilabile P,N ligand.¹² This methodology of halide abstraction has also been successfully applied by Toste *et al.* in the oxidative addition of strained C–C bonds (b, Scheme 3.5).¹³



Scheme 3.5. (a) Oxidative addition of aryl halides using silver to abstract a halide from the gold centre; (b) oxidative addition of a strained C–C bond.

Considering the use of sulfur based ligands in this thesis, it is also of note that oxidative addition of fluorinated disulfides to gold(I) dithiolates gives gold(III) tetrathiolates (Scheme 3.6).¹⁴ This reaction is reversible with reductive elimination regenerating a gold(I) dithiolate

and a disulfide. The relative stability of the gold(III) tetrathiolates was linked to the use of electron-deficient fluorinated thiolates. This reaction is of interest if it could be incorporated into a catalytic C-S bond forming system where the disulfide is used as an oxidant instead of a strong external oxidising agent.



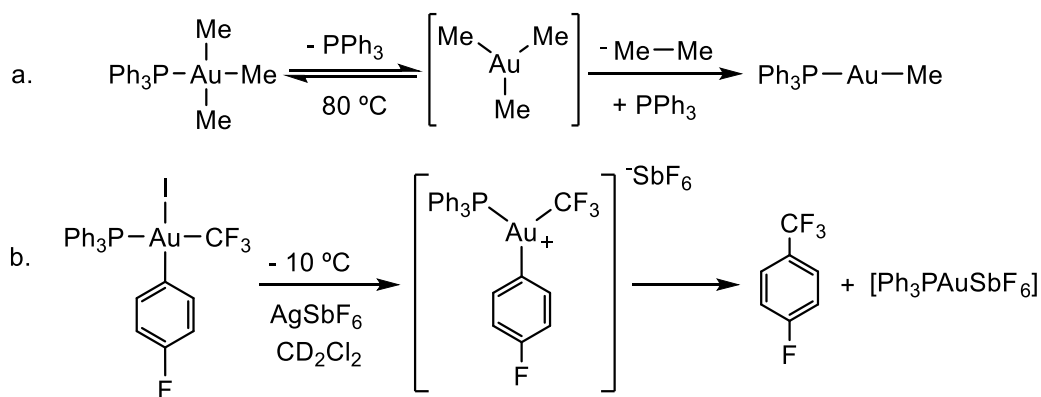
Scheme 3.6. Oxidative addition of disulfides to a gold(I) dithiolate species.

3.3 Reductive elimination from gold(III) species

Reductive elimination is the reverse of oxidative addition and in gold species is often more facile than oxidative addition. The most favourable conditions are thought to be the opposite to oxidative addition, often requiring geometrically unrestrained complexes. Consequently, the stabilisation of highly reactive gold(III) species has used chelating and pincer ligands to avoid reductive pathways.^{7,15}

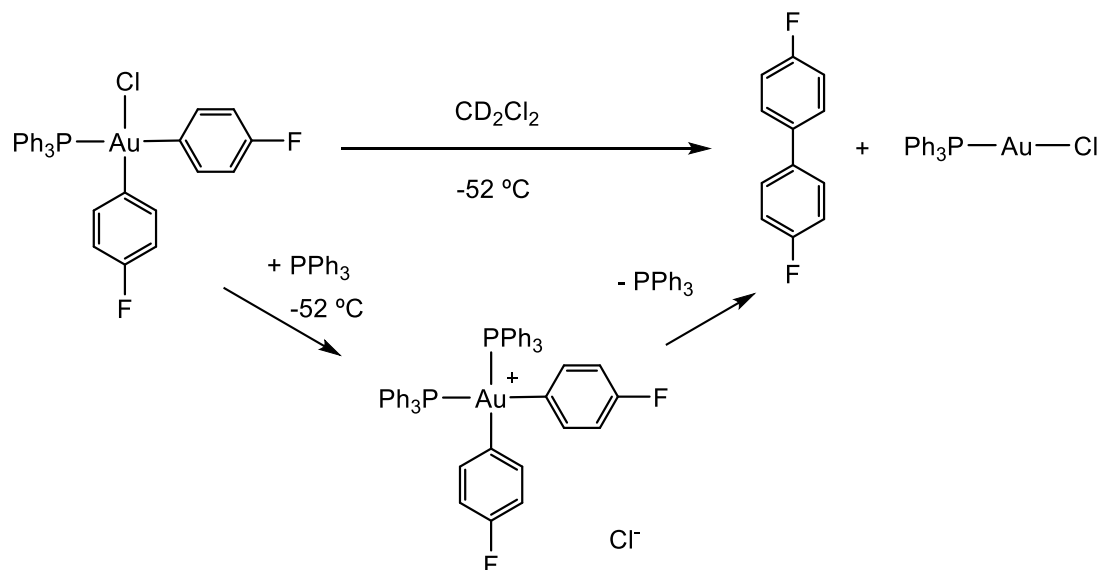
There have been investigations into many different C–C bond forming reductive elimination reactions and there are a range of different factors that have been proposed to influence it.¹⁶ These include the electronic properties of arenes that affect the formation of biaryls, it was observed that electron rich arenes underwent reductive elimination much faster than electron deficient arenes.¹⁷ The charge of the complex has also been proposed to influence the rate of reductive elimination because in some systems cationic complexes have faster rates of reductive elimination than the corresponding neutral complex.¹⁸

Identification of the mechanism for C–C reductive elimination depends strongly on the system. Various intermediates have been proposed including, for some systems, transient 3-coordinate gold(III) complexes. These highly reactive and unobservable intermediates result from the loss of one ligand through either dissociation of a phosphine ligand (a, Scheme 3.7),¹⁹ or silver abstraction of a chloride (b, Scheme 3.7)²⁰. The importance of the dissociation of a phosphine ligand can be shown through the suppression C-C reductive elimination when an excess phosphine was used. Due to fast reductive elimination from the proposed reactive intermediates formed, identification and isolation of the reactive species is challenging.



Scheme 3.7. a) Dissociation of phosphine triggering C-C reductive elimination; b) Chloride abstraction triggering C-C reductive elimination.

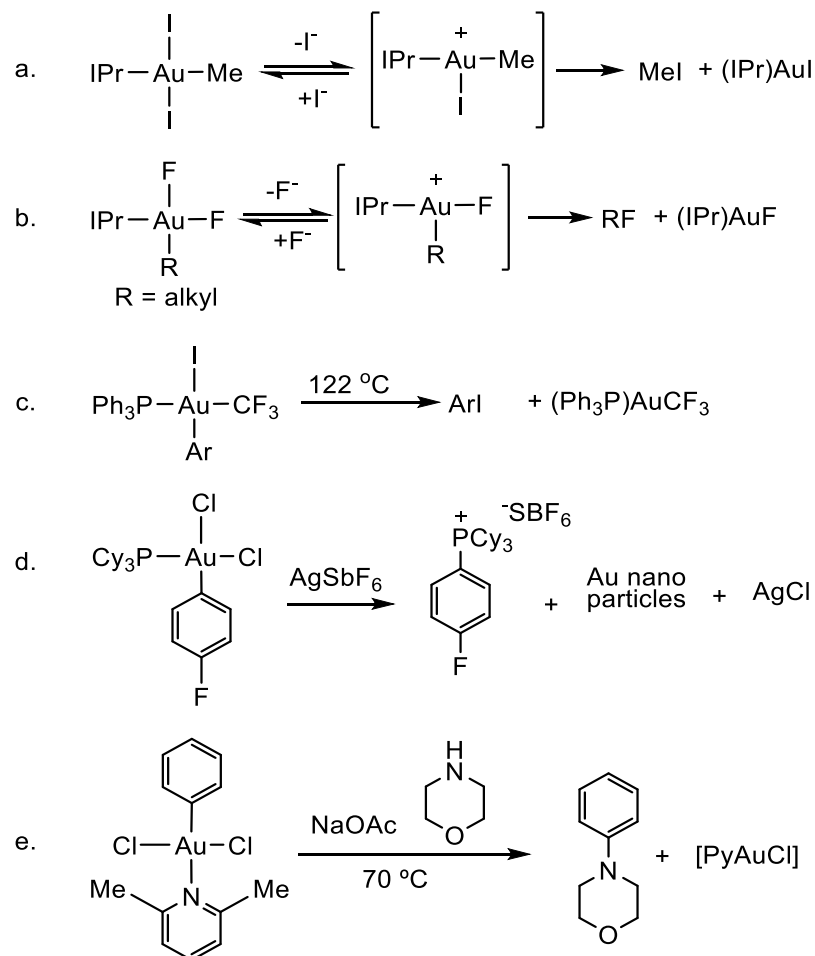
In other cases, C–C reductive elimination has been proposed to originate from 4-coordinated gold(III) complexes.²¹ Toste *et al.* reported that reductive elimination from phosphine gold(III) biaryl complexes was the fastest transition-metal C–C reductive elimination with $k \geq 0.22 \text{ s}^{-1}$ at 221 K (Scheme 3.8).²² Reductive elimination was observed at $-52 \text{ }^\circ\text{C}$ (221 K) from the starting neutral species, but addition of excess phosphine was proposed to displace a chloride by forming a cationic species, which underwent reductive elimination even faster than the neutral species.



Scheme 3.8. Fast C–C reductive elimination.

Reductive elimination of carbon-heteroatom bonds is rare compared to C–C reductive elimination, however there are several interesting examples, such as the formation of $\text{C}(\text{sp}^3)\text{-X}$ ²³ and $\text{C}(\text{sp}^2)\text{-X}$ ²⁰ carbon-halide bonds, $\text{C}(\text{sp}^2)\text{-N}$ ²⁴ and $\text{C}(\text{sp}^2)\text{-P}$ ²⁵ bonds (Scheme 3.9, a-e). All these C–X or C–E reductive elimination reactions are proposed to occur from cationic

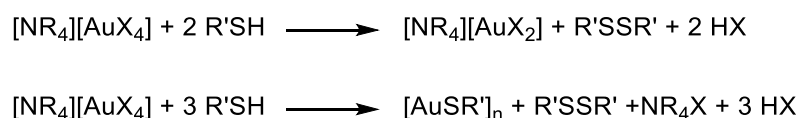
three-coordinate intermediates, formed through either silver abstraction or dissociation of a halide. By comparison C-S reductive elimination has been less well explored.



Scheme 3.9. Reductive elimination from gold(III) complexes of: a) C-I bonds; b) C-F bonds; c) C-I bonds; d) C-P bonds; e) C-N bonds.

3.4 Use of thiols as reducing agents

The reducing nature of thiols has been used in the synthesis of gold nanoparticles via the Brust-Schiffrin nanoparticle synthesis. This has been studied experimentally showing the first steps, prior to nanoparticle formation, to be reduction of gold(III) halides by thiols to gold(I) species and disulfides (Scheme 3.10).²⁶ Final reduction of the gold(I) species by sodium borohydride gives thiol protected gold nanoparticles.



Scheme 3.10. The reduction of gold(III) species to give gold(I) species and dithiolates.

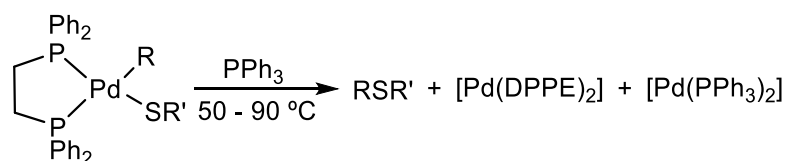
Computational studies have further investigated individual steps and have shown that the first step is displacement of a halide by a thiol, followed by the halide abstracting a proton to form $[\text{AuX}_3\text{SR}]^-$ and HX , a second substitution by HSR through this two-step process forms $\text{AuX}_2(\text{SR})_2$ and HX which is able to undergo reductive elimination to form a gold(I) species and a disulfide.²⁷

Gold(I) thiolates can form aggregates through aurophilic interactions. The nature of gold(I) thiolate species has been of interest as they can be precursors to nanoparticles.²⁸ There have been several different proposals for the stoichiometry and coordination environments of gold(I) aggregates.

In addition, there has been an increasing interest in gold metallodrugs and understanding potential interactions with biologically relevant molecules such as glutathione.²⁹ Glutathione is an SH containing tripeptide and is found in biological redox systems.³⁰ Glutathione is often overexpressed in cancer cells and has been shown to provide a deactivating pathway for cisplatin,³¹ the most successful metallodrug, by forming strong Pt-S bonds.³² It has been proposed that some gold(III) anticancer agents can be reduced by glutathione.³³

3.5 C-S reductive elimination from metal complexes

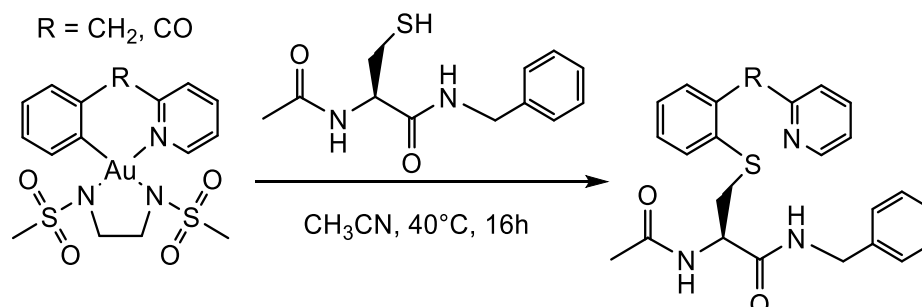
C-S reductive elimination has not been widely studied as C-C reductive elimination, but there are examples of either C-S being studied in catalytic cycles or separately for several transition metals.³⁴ In the palladium(II) system, isoelectronic to gold(III), C-S reductive elimination allowed access to a range of thioethers, including dialkyl sulfides, alkyl aryl sulfides and diaryl sulfides (Scheme 3.11).^{34c,35}



Scheme 3.11. C-S reductive elimination from P(II) complex.

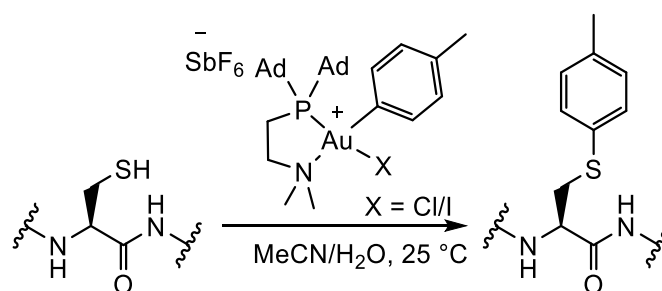
There is one previously reported example of C-S reductive elimination from gold(III).³⁶ This occurs upon the reaction of cyclometallated aryl-pyridine gold(III) chelate complexes and cysteine containing peptides with an S-H functionality (Scheme 3.12). Reductive elimination resulted in the functionalisation of the C[^]N ligand with peptides through formation of C-S bonds. The proposed intermediates were again cationic, similar to the C-X reductive elimination reactions discussed above. The mechanism of reductive elimination was not fully

explored in the paper. In addition, these authors were unable to trigger C-S reductive elimination from the analogous cyclometallated 2-phenyl pyridine complex.



Scheme 3.12. C-S reductive elimination.

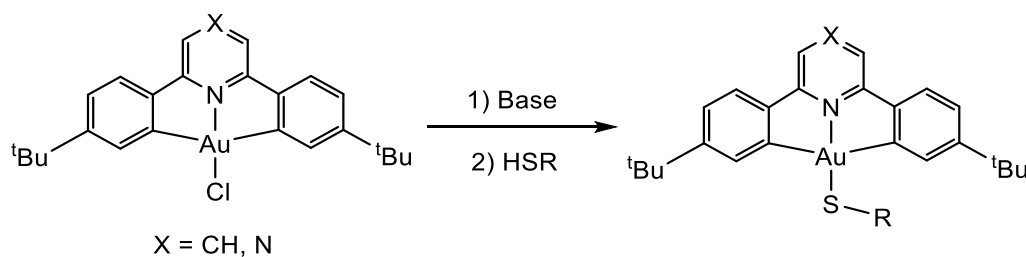
Since this work was published, Spokoyny *et al.* demonstrated that C-S reductive elimination from gold(III) complexes can be used in the cystine arylation of peptides and proteins.³⁷ This was shown to be a selective and efficient method to modify complex biomolecules with a plethora of aryls.



Scheme 3.13. C-S reductive elimination to give functionalised biological moieties.

3.6 Stability of the (C[^]N[^]C)Au-X system

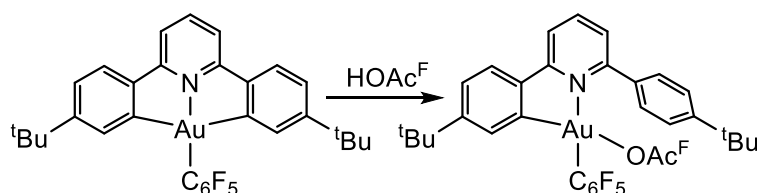
Despite the reducing properties of thiols, we have previously shown that cyclometallated C[^]N[^]C pincer ligands provide excellent protection against reduction and allow isolation of stable gold(III) thiolates (see Chapter Two and Scheme 3.14).³⁸



Scheme 3.14. Synthesis of a gold(III) thiolate stabilised by a C[^]N[^]C pincer ligand.

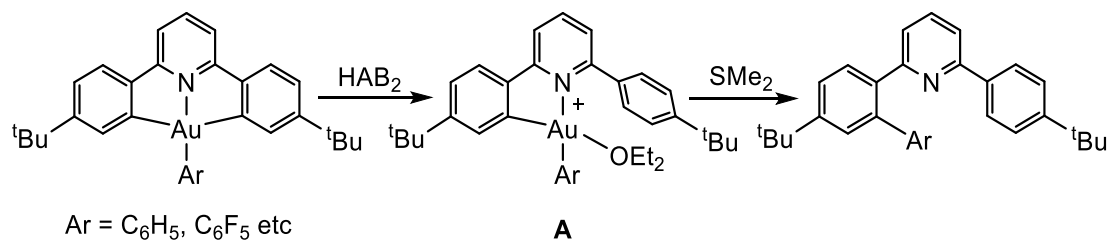
The C[^]N[^]C system has been shown to be very stable to reductive elimination allowing isolation of highly reactive species that were previously unobservable, for example the hydride,³⁹ hydroxide⁴⁰ alkyne⁴¹ and alkene⁴² complexes.

Although the C[^]N[^]C system helps stabilise gold(III) against reduction it is sensitive to strong acids and undergoes protodeauration of one Au–C bond with trifluoroacetic acid resulting in a (C[^]N) chelate with a pendant aromatic ring (Scheme 3.15).⁴³ The reaction was found to be p*K*_a dependent as the weaker acetic acid was incapable of protodeauring the Au–C bond in the same complex.



Scheme 3.15. Protodeauration of a C[^]N[^]C gold(III) by trifluoroacetic acid.

The reaction of pincer gold(III) aryl complexes with [H(OEt₂)₂]⁺[H₂N[B(C₆F₅)₃]₂]⁻ (HAB₂), a strong acid with a weakly coordinating anion, showed the Au–C bond in the pincer ligand is selectively protodeaured, this was proposed to be because it is trans to another Au–C bond (Scheme 3.16).⁴⁴ Studies into these protodeaured species showed that metalation/protodeauration is reversible and sometimes dynamic with diethyl ether mediated proton shuttling. Reductive elimination can be triggered from **A** upon addition of dimethyl sulfide, which displaces the Au–N bond induces fast C–C reductive elimination (Scheme 3.16).⁴⁵ Reductive elimination was proposed to occur from a four-coordinate cationic intermediate and the rate was strongly dependent on the nature of the substituent.



Scheme 3.16. Protodeauration and C–C reductive elimination from gold(III) stabilised by a C[^]N[^]C pincer.

3.7 Objectives

This chapter will investigate reductive elimination from C[^]N[^]C gold(III) complexes triggered by thiols. This is of interest because there has been recent development of gold catalysed cross

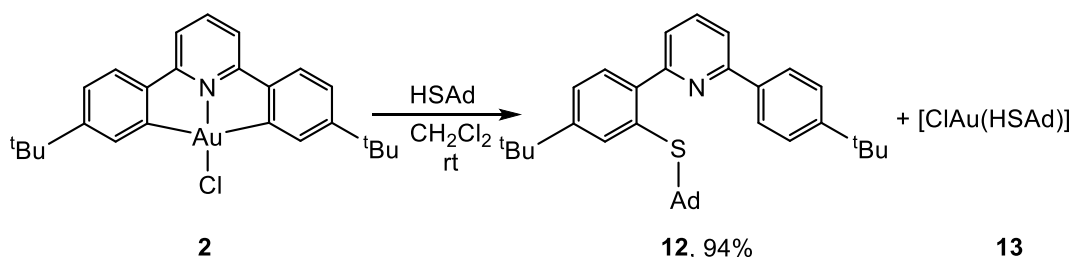
coupling reactions, which has led to a renewed interest to understand the fundamental redox steps for gold complexes.

In addition, gold(III) complexes have been shown to be anticancer agents, which in the cellular environment are subject to a high concentration of thiols such as glutathione. These have been proposed to reduce gold(III) complexes to gold(I) complexes. Therefore, it would be beneficial to have a greater understanding of how C^NC gold(III) complexes react with thiols.

Results and Discussion

3.8 Addition of adamantyl thiol to **2**

The gold(III) thiolate complexes were synthesised using a thiol in the presence of a base (see Chapter 2).³⁸ However, if **2** is reacted with adamantyl thiol (HSAd) in the absence of base the C–S reductive elimination product **12** and a gold(I) species, initially postulated to be **13**, are observed (Scheme 3.17).



Scheme 3.17. Reductive thiol-induced elimination to give **12** and **13** in the absence of a base. Ad = adamantyl.

To gain mechanistic insight into the reaction of **2** with adamantyl thiol, further reactions were explored using *in situ* NMR spectroscopy. Adamantyl thiol was used as a prototypical thiol in this system because the signals do not overlap with those of **2** and, as a solid, it is easier to handle. For complete reductive elimination two equivalents of adamantyl thiol were required. In the presence of only one molar equivalent of adamantyl thiol the reaction remains incomplete giving a mixture of starting material and reductive elimination product. Addition of further thiol to this mixture gives complete conversion to **12** and **13**.

The structure of the reductive elimination product **12** was confirmed by ¹H and ¹³C NMR spectroscopy and high resolution mass spectrometry, where the expected isotopic pattern was observed. ¹H NOESY NMR revealed the presence of spatial interactions between adamantyl

signals (H^{11}) and both H^8 and H^2 . This was ascribed to free rotation around the C3–C4 bond of **12** leading to close spatial interactions (Figure 3.1).

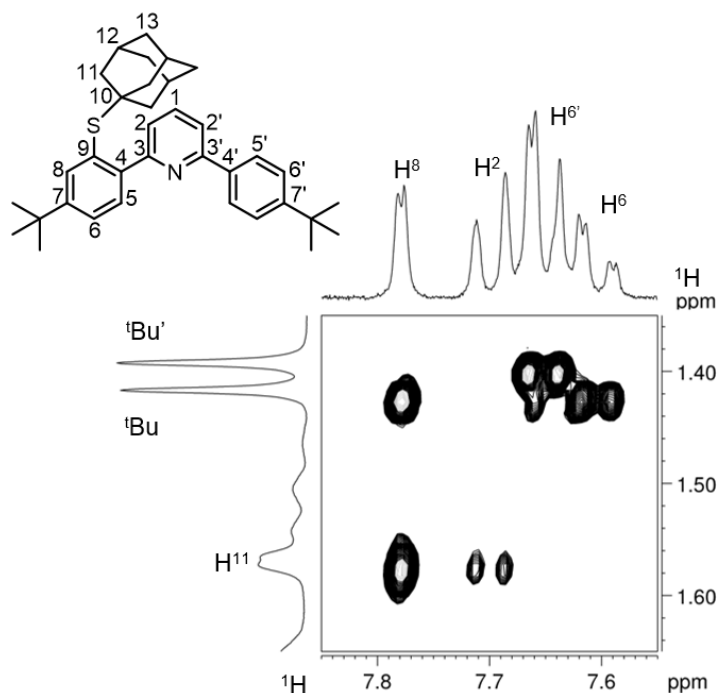


Figure 3.1. ^1H NOESY spectrum of **12** showing interactions between H^8 , H^2 and H^{11} (CD_2Cl_2 , 25 °C).

When the reaction was scaled up, **12** was isolated as a white solid in 94 % yield. The ^1H NMR spectrum of the *in situ* reaction mixture of **12** and **13** differed from that a pure sample of **12**, this is likely to be because **12** and **13** interact through coordination of a gold(I) species to the pyridine nitrogen, whereas the pure sample of **12** shows no coordination to the pyridine nitrogen. This is seen most clearly in the shift of H^1 from $\delta = 8.26$ ppm to $\delta = 7.76$ ppm (Figure 3.2).

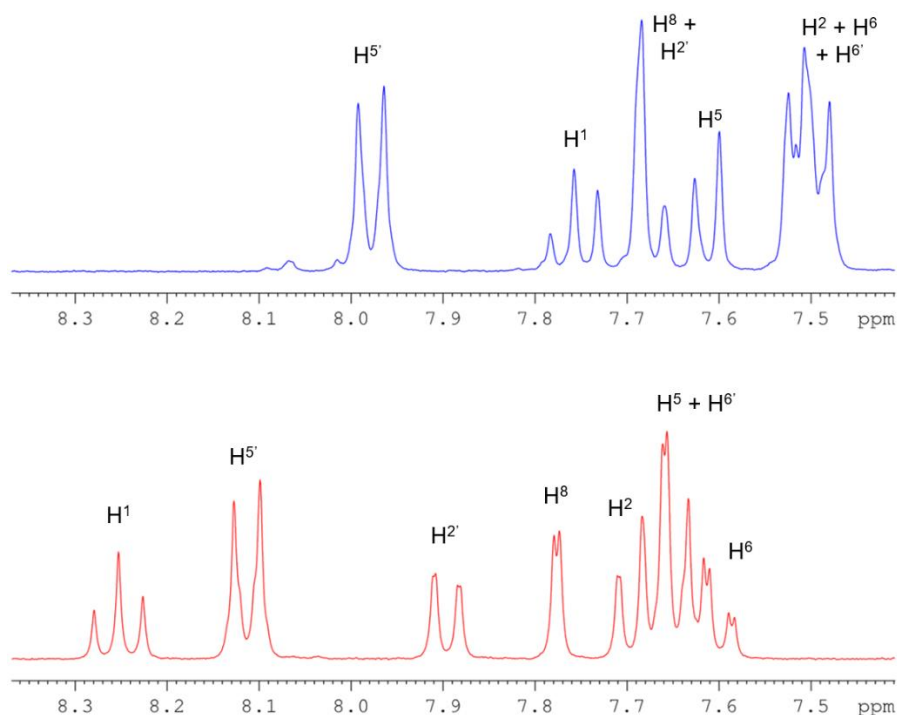


Figure 3.2. Aromatic region of ^1H NMR spectra of **12**; top) isolated sample of **12** bottom) *in situ* reaction mixture (CD_2Cl_2 , 25°C).

The gold by-product formed upon reduction is proposed to be $[\text{AuCl}(\text{HSAd})]_x$ (**13**) and over time precipitates from the solution as a white solid. This decrease in solubility could be due to nucleation resulting from aurophilic interactions between gold(I) centres forming polymers, oligomers or aggregates which precipitate as they become larger.²⁸ There are previous examples of gold(I) oligomeric species formed through reduction of a gold(III) species such as the reversible oxidative addition of fluorinated aryl disulfide to gold(I) thiolates. In this case, one decomposition product observed was proposed to be an insoluble oligomeric material $[\text{AuSR}]_n$ generated from $[\text{RSAuSR}]^-$,¹⁴ this is similar to **13**.

3.9 Addition of other acidic compounds to **2**

Reductive elimination was not observed upon addition of a range of X–H acidic compounds to **2**, even over extended periods of time. The X–H compounds investigated were carbazole, amines (acidic N–H), phenols (acidic O–H) and malonates (acidic C–H). The addition of strong acids, such as hydrochloric acid and trifluoroacetic acid, to **2** leads to protodeauration but not reductive elimination.⁴⁴

Table 3.1 shows the range of $\text{p}K_a$ values in DMSO for the different compounds that were reacted with **2**. The strong acids, hydrochloric acid and trifluoroacetic acid, with low $\text{p}K_a$ values

(1.8 and 3.45 respectively) protodeaurated **2**, whereas no reactivity was observed for many of the weaker acids with high pK_a values.

Acid	pK_a values in DMSO at 25 °C	Acid	pK_a values in DMSO at 25 °C
HCl	1.8 ⁴⁶	<i>p</i> -Me-PhSH	10.82 ⁴⁷
F ₃ CCO ₂ H	3.45 ⁴⁶	CH ₃ (CH ₂) ₃ SH	17.0 ⁴⁶
H ₃ CCO ₂ H	12.3 ⁴⁶	Carbazole	19.87 ⁴⁸
PhOH	18.0 ⁴⁶	dimethylmalonate	15.88 ⁴⁹
tBuOH	32.5 ⁵⁰		

Table 3.1. pK_a values for a range of acidic compounds.

The pK_a value for the adamantyl thiol is likely to be similar to 1-butanethiolthiol. This pK_a value is comparable to the weaker acids which showed no reactivity, therefore the acidity is not the only contributing factor to the reactivity and highlights the unexpected reactivity observed upon addition of adamantyl thiol to **2**.

3.10 Investigating a possible mechanism for C-S reductive elimination

In order to gain additional mechanistic insights, we explored the reactivity of **2** with varying concentrations of adamantyl thiol to investigate the kinetic behaviour.

3.10.1 Investigating rates of C-S reductive elimination

Kinetic studies were performed to find the order of the reaction. The decay of **2** was followed by ¹H NMR spectroscopy with the thiol in great excess of the **2** (more than 10 equivalents). Under these conditions, the reaction can be treated as pseudo first order as the concentration of adamantyl thiol does not change significantly over the course of the reaction and is treated as a constant. This gives the first order rate equation:

$$v = \frac{d[\mathbf{2}]}{dt} = -k_{obs}[\mathbf{2}] \quad k_{obs} = k[HSAd]$$

This can be rearranged to give the following equation:

$$[\mathbf{2}] = e^{-k_{obs}t}$$

Figure 3.3 (left) shows monoexponential decay of **2** over the reaction duration, which follows the equation above. This means that under these reaction conditions the process is first order in **2**, the observed rate constants ranged between $7.4 \times 10^{-4} \text{ s}^{-1}$ and $1.8 \times 10^{-3} \text{ s}^{-1}$. Therefore,

one equivalent of **2** is required in the rate determining step. The value of k_{obs} followed linearly the concentration of thiol (right, Figure 3.3), which means that under these conditions the reaction is also first order in thiol. As $k_{\text{obs}} = k[\text{HSAd}]$ the value of the rate constant for the reaction can be calculated and is $k = 3.57 \times 10^{-3} \pm 0.15 \times 10^{-3} \text{ s}^{-1}\text{mol}^{-1}\text{dm}^3$. Therefore, one equivalent of adamantyl thiol and **2** are required in the rate determining step and the overall reaction is second order.

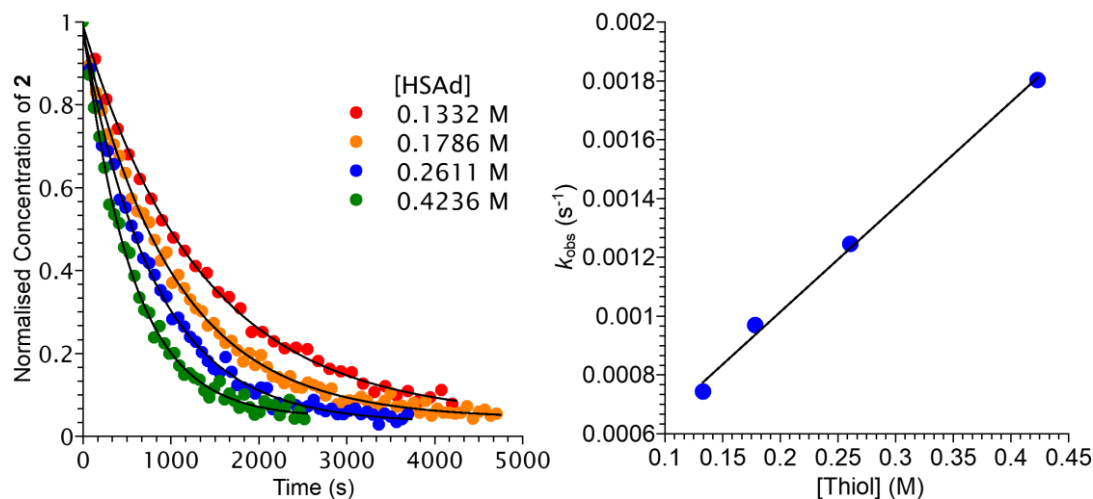


Figure 3.3. left, the decay of **2** at different concentrations of HSAd; right, the rate constants against the concentration of HSAd (CD_2Cl_2 , 25 °C).

The presence of air and water appeared to have no effect on the rate of reductive elimination, when the reaction was carried out in dry solvent under an atmosphere of dinitrogen the rate and product of the reaction were the same.

3.10.2 Observation of a third species in the kinetic investigations

At high concentrations of adamantyl thiol an additional species was observed in the ^1H NMR spectrum during the kinetic investigations. The observed mixture had signals in the ^1H NMR spectrum corresponding to **2**, **12**, **13** and a fourth species, **14**. As the concentration of adamantyl thiol was increased, whilst all other parameters remained unchanged, the proportion of **14** was observed to increase. The evolution of the mixture over the course of the reaction is shown in Figure 3.4 and shows that near the start of the reaction **2** has converted into equal proportions of **12** and **14**. Over the course of the reaction the proportion of **14** decreases and is not observed at the end of the reaction.

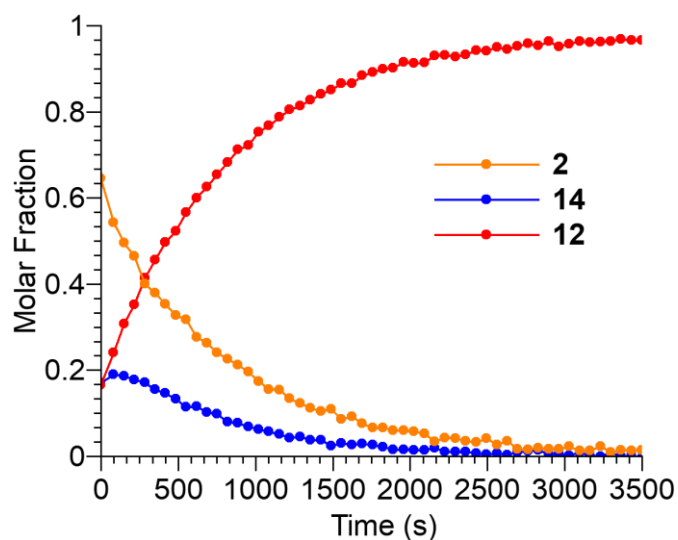
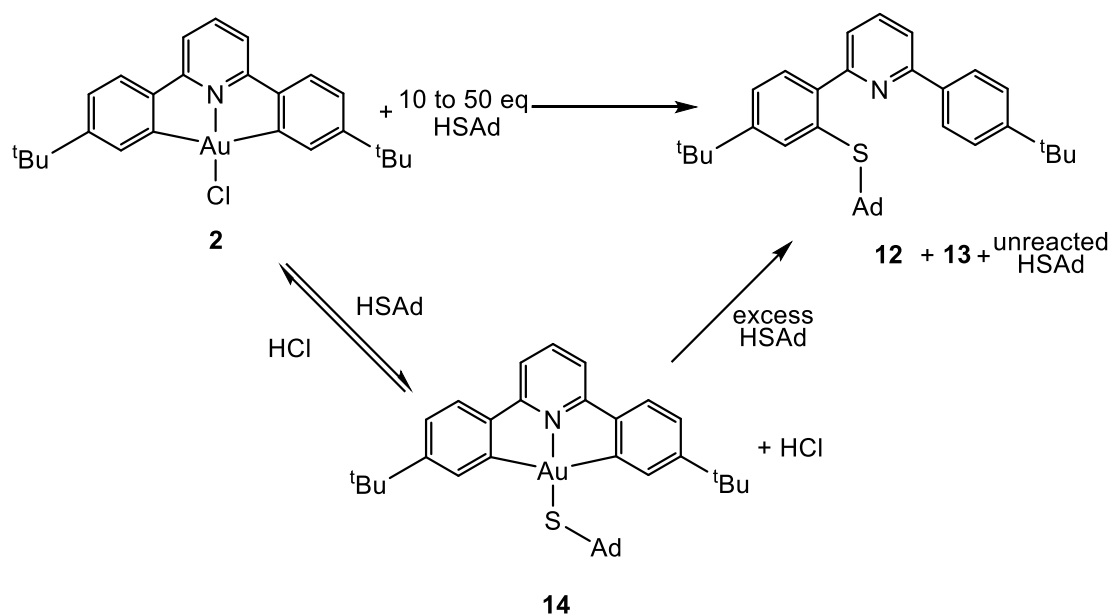


Figure 3.4. The molar fraction of different species over the reaction duration upon addition of 21 molar equivalents of thiol to **2** (CD_2Cl_2 , 25 °C).

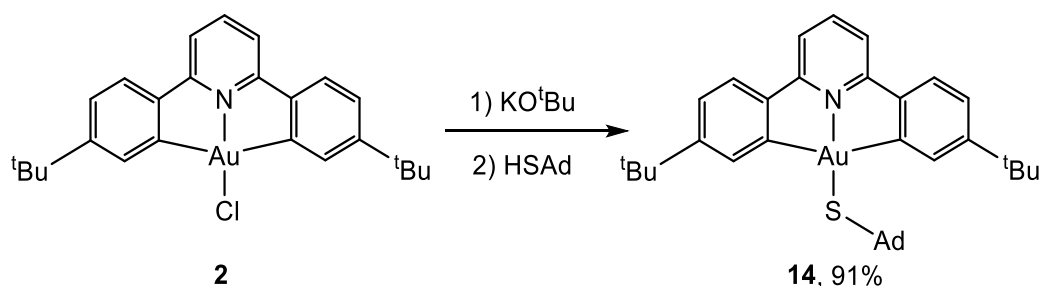
To identify this species, 50 equivalents of adamantyl thiol were added to **2** and the sample was cooled to 223 K. At this temperature, the proportions of the reagents remained near constant and **2** did not undergo reductive elimination, a small proportion of **2** precipitated due to the decreased solubility at lower temperatures. **14** was shown to be symmetric, and contain signals corresponding to one adamantyl group. Therefore, the complex was proposed to be $(\text{C}^{\wedge}\text{N}^{\text{py}}\wedge\text{C})\text{Au-SAd}$ (**14**) and was potentially formed due to the large excess of thiol displacing the chloride with a thiolate (Scheme 3.18). This reaction also resulted in the formation of one equivalent of hydrochloric acid. Similar reactivity has been proposed by calculations in the formation of gold nanoparticles, where exchange of one halide in AuX_4^- by one thiol to produce $\text{AuX}_3\text{HSR} + \text{Cl}^-$ which converts to $\text{AuX}_3\text{SR}^- + \text{HX}$.²⁷

When the mixture was warmed to 298 K the reaction proceeded to give a mixture of **12** and **13**. These observations were combined to give an initial possible reaction mechanism, where **14** may be in an intermediate (Scheme 3.18), however this was probed with further reactions.



Scheme 3.18. Initial proposal of a possible reaction mechanism of **2** with an excess of adamantyl thiol giving **14** as a possible intermediate.

14 was independently synthesised from **2** using potassium tertbutoxide and adamantyl thiol and isolated as a yellow solid in 91 % yield (Scheme 3.19).

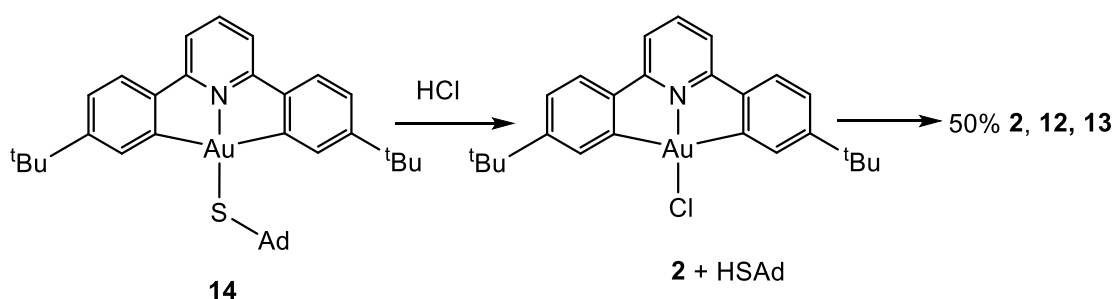


Scheme 3.19. The synthesis of **14** in dichloromethane at room temperature.

To probe the validity of the initial proposed mechanism in Scheme 3.18, it was investigated whether **14** underwent reductive elimination upon addition of adamantyl thiol. When three molar equivalents of thiol were added to **14** no reaction was observed. However, upon addition of 50 molar equivalents of adamantyl thiol to **14** the reductive elimination product **12** and a white precipitate were observed, with complete conversion obtained after two months. These reaction times are much slower than in the kinetic experiments, therefore it is unlikely that **14** is an intermediate. Instead, it was proposed that **14** formed in a proposed as a side reaction.

3.10.3 Reactivity of **2** with hydrochloric acid

The formation of **14** upon addition of a large excess of adamantyl thiol to **2**, is proposed to occur through chloride exchange also resulting in one molar equivalent of hydrochloric acid. This potential reaction was investigated by adding one molar equivalent of hydrochloric acid to a solution **14** and monitoring by ^1H NMR spectroscopy. The reaction gave almost immediate formation of **2** and release of one equivalent of adamantyl thiol. The adamantyl thiol then reacted with **2**, as previously described, to give 50% conversion to **12** and **13** (Scheme 3.20), this further emphasises the need for two molar equivalents of adamantyl thiol because of the incomplete conversion with one molar equivalent. This reaction demonstrates that the exchange of the thiol with the chloride is fast and the conversion of **2** to **14** is reversible.

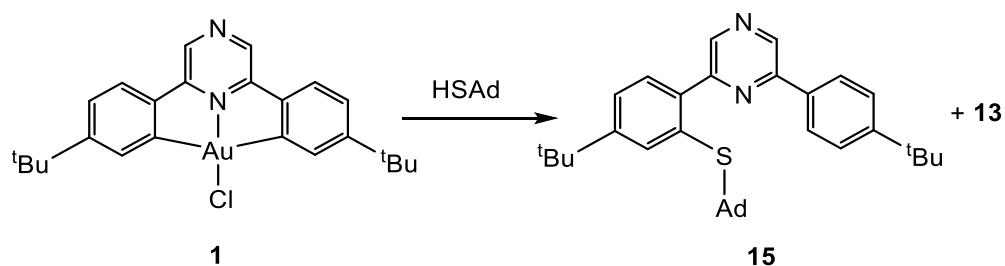


Scheme 3.20. Reaction of **14** with hydrochloric acid to give **2**, followed by subsequent reductive elimination to give **12** + **13**.

3.10.4 Effect of altering the ligand system up on the rate

The effect of altering the ligand system on the reaction was investigated to see if the Au-N displacement was kinetically relevant. **1** was used as it contains a central pyrazine instead of a pyridine. The pyrazine is less basic than pyridine, therefore has a weaker Au-N bond. If there is an alteration in the rate of the reaction between **1** and **2** it could indicate that the displacement of the Au-N bond is the rate determining step.

The reaction with three molar equivalents of adamantyl thiol with **1** gave C-S reductive elimination resulting in the formation of **15** and **13** (Scheme 3.21). **15** was characterised by ^1H , ^{13}C spectroscopy and accurate high resolution mass spectrometry, where the expected isotopic pattern was observed.



Scheme 3.21. **1** reacts with thiol to give C-S reductive elimination product **15** and gold(I) product **13**.

The consumption of **1** was studied by varying the concentration of thiol (left, Figure 3.5). Using the same methodology as in Section 3.10.1, it was demonstrated that the reaction is first order in **1** as shown by its monoexponential decay. It is also first order in adamantyl thiol (right, Figure 3.5). The rate is $k = 2.54 \times 10^{-3} \pm 0.03 \times 10^{-3} \text{ s}^{-1} \text{ mol}^{-1} \text{ dm}^3$.

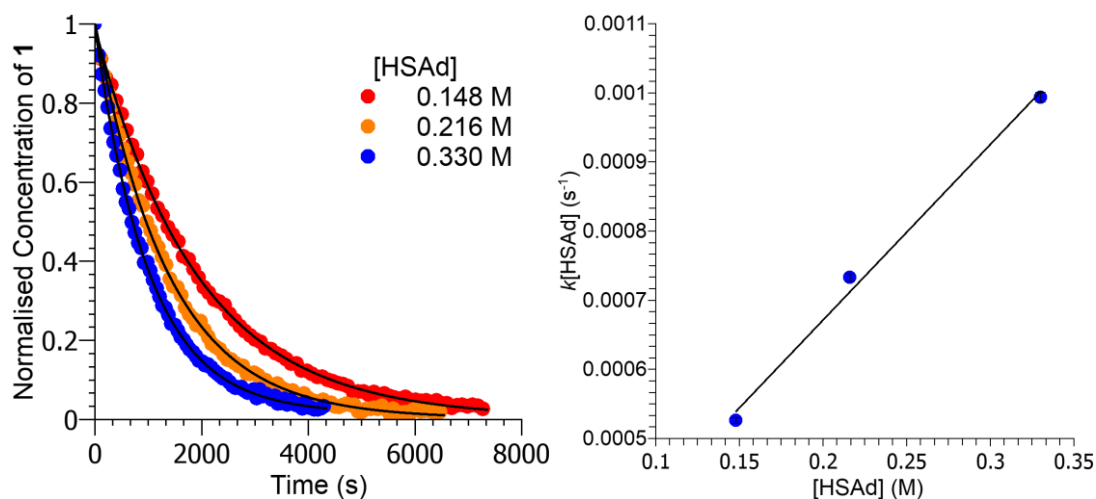


Figure 3.5. left) the decay of **1** at different concentrations of HSAd; right) the first order rate constants against the concentration of HSAd (CD₂Cl₂, 25 °C).

Despite the difference in basicity between pyridine and pyrazine, the rate of reaction of adamantyl thiol with both **2** and **1** are very similar, and therefore displacement of the Au-N ligand does not appear to be rate determining in the C-S reductive elimination mechanism.

3.10.5 Establishing a mechanism

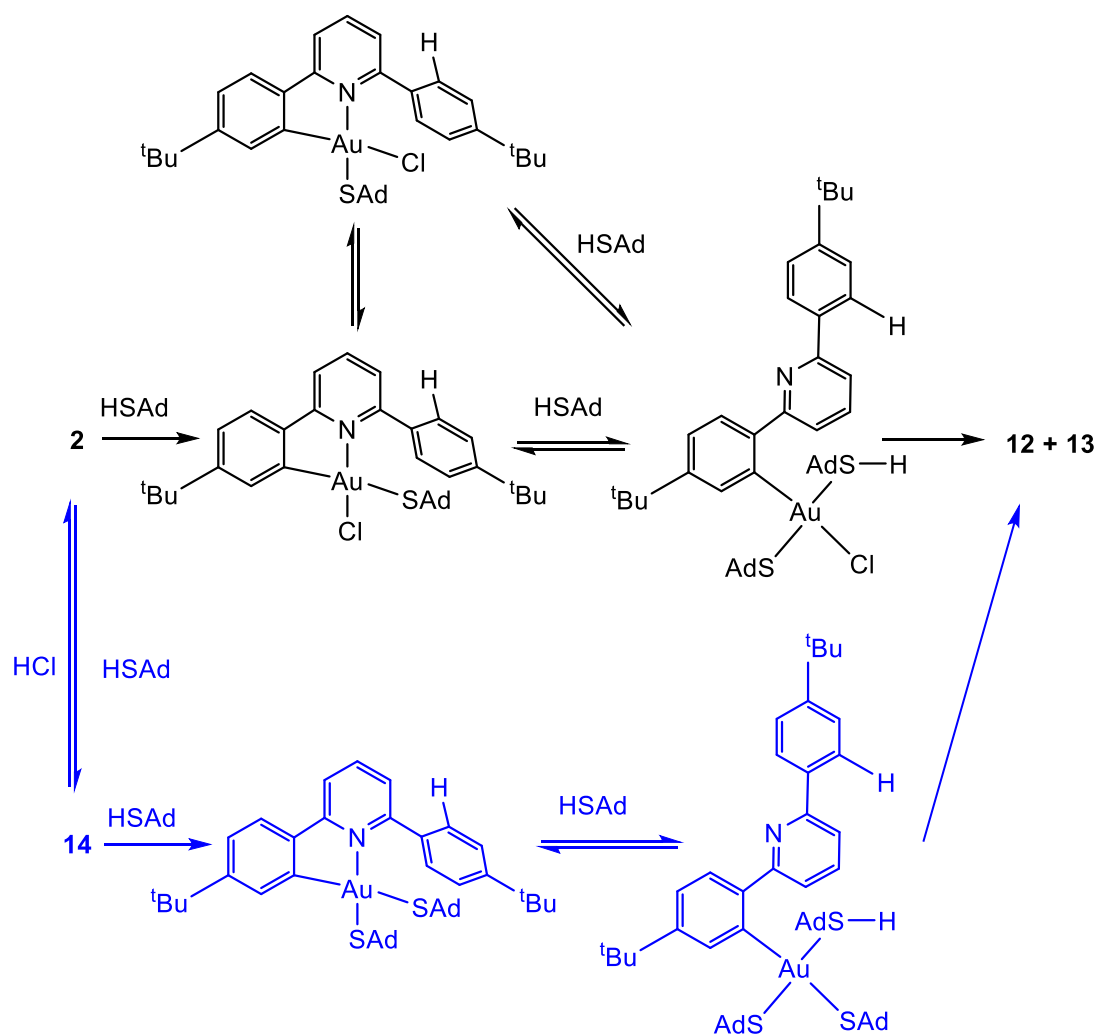
Combining these observations gives us the proposed mechanism for the C-S reductive elimination from **2** (Scheme 3.22). Importantly, two molar equivalents of adamantyl thiol are required for complete reductive elimination, however the reaction is first order in adamantyl thiol so only one molar equivalent is required in the rate determining step. The major pathway to reductive elimination is proposed to go via first a protodeauration and formation of a

bidentate gold(III) chlorothiolate intermediate. This requires one molar equivalent of adamantyl thiol and one molar equivalent of **2** as shown in the kinetic investigations where the reaction was second order. This step is comparable to previous studies, which have shown acids to protodeaurate the pincer gold(III) systems.⁴³⁻⁴⁴ Subsequent displacement of the Au–N bond by the second molar equivalent of adamantyl thiol forms a conformationally flexible system that can undergo reductive elimination. It is likely that the reductive elimination results from a four-coordinate species as the rate increases with increased thiol concentrations, however we are unable to isolate any species that would prove this hypothesis. The final step is reductive elimination to form a regiospecific C–S bond.

The thiol-induced reductive elimination of the **2** and **1** proceed at comparable rates, suggesting that displacement of the Au–N bond is not rate-limiting. Therefore, the rate limiting step is likely to be the protodeauration by adamantyl thiol.

The observation of **14** at the beginning of the reaction when a large excess of adamantyl thiol is used led to the proposal of a side pathway to reductive elimination (the lower half of Scheme 3.22). In this side reaction, **2** was converted to **14** when a great excess of thiol was used. This was reversible as it forms one equivalent of hydrochloric acid which converts **14** back to **2**. **14** can also undergo reductive elimination upon reaction with adamantyl thiol giving C–S reductive elimination, but at a considerably slower rate.

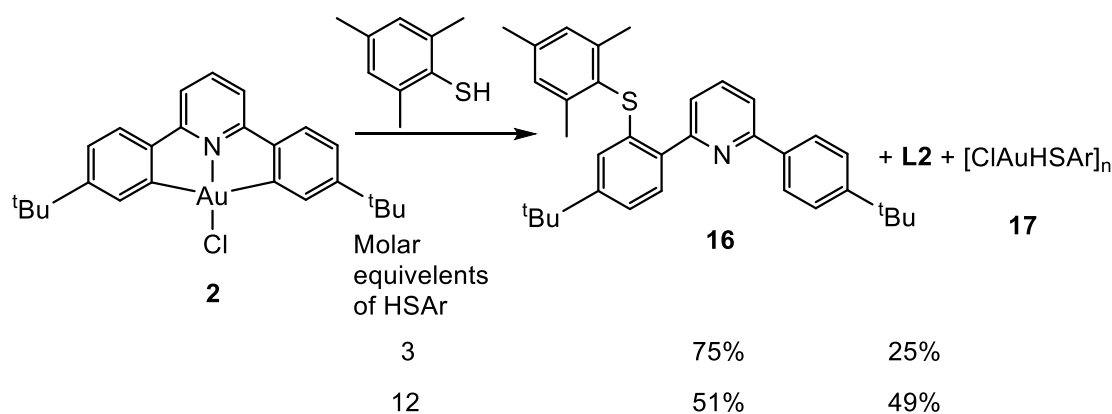
Overall, the reaction sequence is reminiscent of the reductive aryl-aryl coupling process proposed by Vicente et al. for the reaction of bis-aryl gold(III) complexes (C[^]N)Au(aryl)Cl with phosphines.^{21,51}



Scheme 3.22. Proposed mechanism of C-S reductive elimination from **2**, the black pathway is the major pathway and the blue pathway is the potential minor pathway.

3.11 Addition of an aryl thiol to **2**

The reactivity of **2** with the aryl thiol, 2,4,6-trimethylthiophenol, was investigated to compare to adamantyl thiol, an alkyl thiol. Upon addition of three molar equivalents of 2,4,6-trimethylthiophenol to **2** reductive elimination was observed to give **16**, **17** and free ligand (**L2**) (Scheme 3.23). Increasing the proportion of 2,4,6-trimethylthiophenol added to **2** to 12 molar equivalents altered the proportion of **16** and **L2**, there was an increase in free ligand (**L2**) observed and a decrease of **16**.

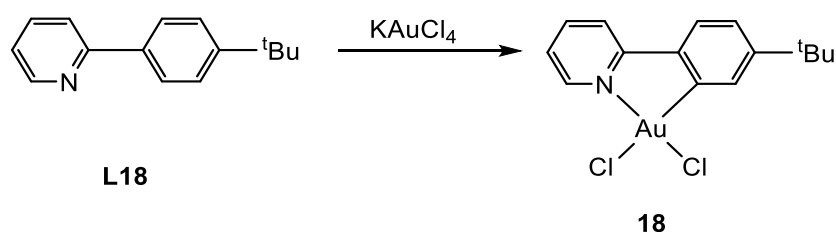


Scheme 3.23. The reaction of **2** with 2,4,6-trimethylthiophenol.

The formation of free ligand was not observed upon the reaction of **2** with adamantyl thiol. The different reactivity observed could be because of the stronger trans influence of the aryl thiolate in the proposed chlorothiolate intermediate. This proposed intermediate could be formed upon protodeauration of one Au-C bond and coordination of an aryl thiol at the remaining vacant position. In this proposed intermediate the aryl thiolate is trans to an Au-C bond and it is expected that the aryl thiolate would have a stronger trans influence than an alkyl thiolate. When the trans influence is coupled with the lower pKa of 2,4,6-trimethylthiophenol a second protodeauration may be possible. It could also indicate that under these conditions the rate of displacement of Au-N is similar to that of protodeauration of the second Au-C bond.

3.12 Reactivity of adamantyl thiol with **18**

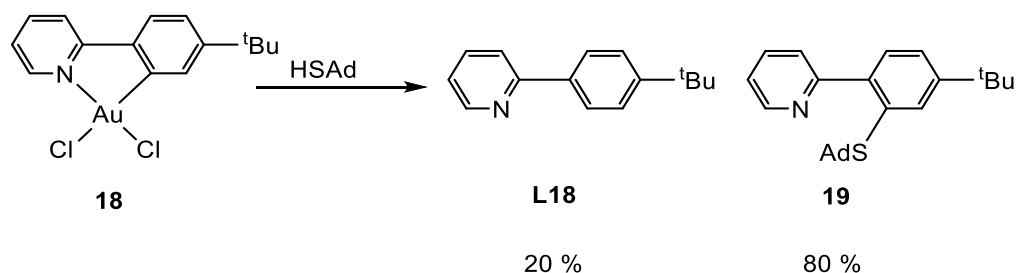
The addition of adamantyl thiol to **1** and **2**, which are both supported C^NC based pincers, triggered C-S reductive elimination. Therefore, we decided to investigate the reactivity of the bidentate system **18** with a C^N chelate (**18** was synthesized by Morwen Williams, Scheme 3.24).⁵²



Scheme 3.24. Synthesis of **18**.

The reactivity of the bidentate chelate system **18** (Scheme 3.25) was investigated by adding 12 molar equivalents of adamantyl thiol to a solution of **18** and the reaction monitored by ¹H

NMR spectroscopy. Upon addition of adamantyl thiol, there was an immediate colour change observed. The ^1H NMR of this reaction showed a mixture of **18** and a new product, this was proposed to result from displacement of the Au-N bond by an adamantyl thiol.



Scheme 3.25. Reaction of **18** with adamantyl thiol.

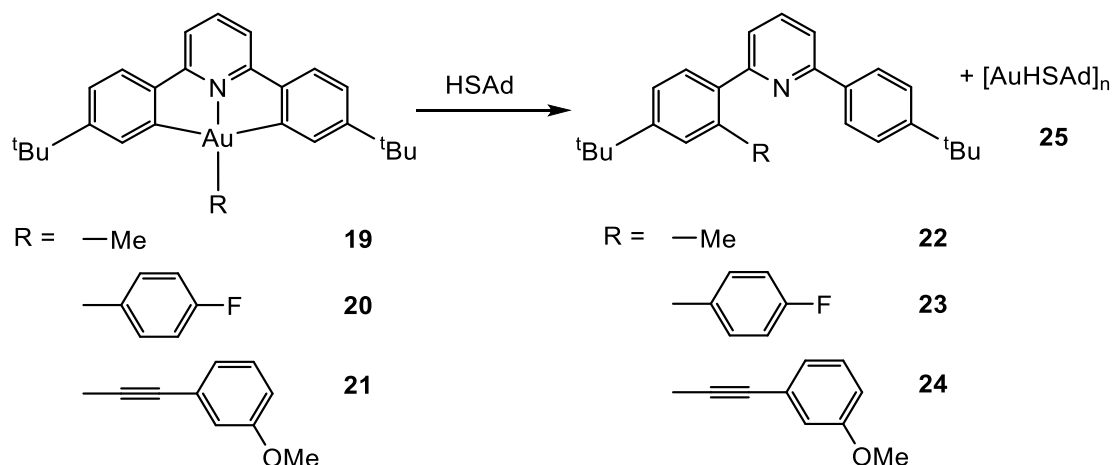
In an attempt to increase the rate of reaction it was heated at 60°C . Over the course of the reaction four possible intermediates were observed, until after two months the reaction was complete. The final composition of the reaction was 80% C-S reductive elimination **19** and 20% **L18**. **19** was characterised by ^1H , ^{13}C NMR spectroscopy and high resolution mass spectrometry, which showed the expected isotopic pattern.

The potential mechanism for this reaction could result from initial displacement of the Au-N bond by adamantyl thiol. The subsequent species formed in the reaction with adamantyl thiol could be a C[^]N chelate species with either a dichloride, two isomers of the monochloridethiolate or as a dithiolate. These species could be in equilibrium, but formation of either reductive elimination to give **19** or protodeauration to give **L18** is likely to be irreversible. The difference in reactivity between **2** and **18** is likely to occur due to lack of an Au-C bond in a trans position to another Au-C. This makes protodeauration more difficult and instead the adamantyl thiol can directly displace the Au-N bond. After forming a monochloridethiolate or dithiolate the Au-C bond is trans to an Au-S bond, potentially allowing protodeauration and formation of **L18**. The extended time for C-S reductive elimination and mixture of products does not make **18** an ideal system to study C-S reductive elimination. Therefore, the C[^]N[^]C pincer system is more useful in studying C-S reductive elimination and protodeauration. This reaction is different to the previous example of C-S reductive elimination where no reactivity was observed upon the addition of cysteine containing peptides to the phenyl pyridine gold(III) complex.³⁶

3.13 Reactivity of adamantyl thiol with (C[^]N[^]C)AuR complexes

Under the same experimental conditions that triggered C-S reductive elimination from **2**, adamantyl thiol was added to (C[^]N[^]C)Au-R (R = Me (**19**), C₆H₄-*p*-F (**20**) and C≡CC₆H₄-*m*-OMe (**21**)) complexes and the reactions were monitored by ^1H NMR spectroscopy. Thiol

addition triggered selective C–C reductive elimination from all complexes to give **22**, **23**, **24** and the gold(I) by product **25** (Scheme 3.26). These conditions are milder than stepwise protocol of HAB₂ and dimethylsulfide previously used to facilitate C–C reductive elimination and tolerated the acetylide functionality that previously reacted directly with HAB₂.⁴⁵ The rate of reductive elimination was substituent dependant, with C(sp²)–C(sp²) reductive elimination taking 6 days, C(sp²)–C(sp³) reductive elimination taking 24 days and C(sp²)–C(sp) reductive elimination taking 6 months for just 50% conversion.



Scheme 3.26. The reactions of C^NC gold(III) complexes with adamantyl thiol to give C–C reductive elimination.

A similar mechanism to that proposed for C–S reductive elimination is anticipated, with protodeauration by one molar equivalent of adamantyl thiol followed by displacement of the Au–N bond by a second molar equivalent of adamantyl thiol. This would give a possible intermediate (Figure 3.6) which could potentially undergo either C–S or C–C reductive elimination (the proton drawn on the thiol could also potentially be on the pyridine nitrogen). As only the C–C bond forming product is observed we propose that C–C reductive elimination is favoured over C–S. This could be because the rate of reductive elimination forming a C–C bond is faster than C–S. Previous examples forming biaryls through reductive elimination of a C–C bond from gold were shown to be exceptionally fast.²² It is presumed that the rate determining step is again protodeauration as only the starting material and the product are observed in the ¹H NMR spectrum.

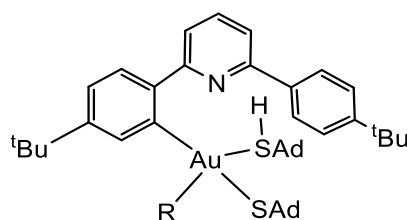


Figure 3.6. Potential intermediate.

The nature of the gold(I) species formed upon C– reductive elimination was explored with diffusion NMR to establish a hydrodynamic volume of the gold(I) thiolate. The reaction of **20** with adamantyl thiol was used because there were no overlapping signals observed in the ^1H NMR spectrum at the end of this reaction, which produced **23**, free thiol and the gold(I) thiolate species. This allowed the reaction mixture to be probed using PGSE (pulse gradient spin echo) NMR experiments where the dependence of the resonance intensity (I) on a constant waiting time and on a varied gradient strength G (Equation 3.1) can be used to identify the self-diffusion coefficient values (D_i)

$$\ln \frac{I}{I_0} = (gd^2)D_i \left(d - \frac{D}{3} \right) G^2$$

Equation 3.1. The dependence of D_i upon the resonance intensity (I) and a varied gradient strength (G).

Plotting $\ln(I/I_0)$ against G^2 can be used to identify the self-diffusion coefficient values (D_i) from which the structural parameters can be approximated. The relationship between D_i and hydrodynamic dimensions is expressed by the modified Stokes-Einstein equation (Equation 3.2) where k is the Boltzmann constant, T is the temperature, η is the solution viscosity, c is the “size factor”, which depends on the solute-solvent radius ratio and f is the “shape factor”.

$$D_i = \frac{kT}{\rho h f c^3 \sqrt{abd}}$$

Equation 3.2. The modified Stokes-Einstein equation.

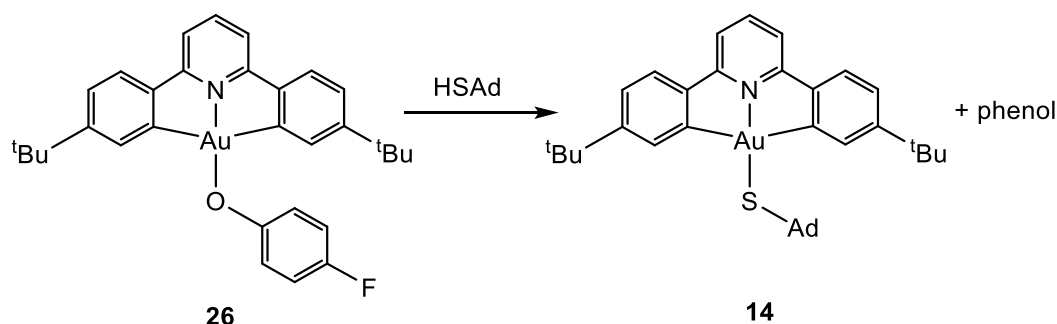
The hydrodynamic volume calculated for the species present in the mixture are 184 \AA^3 for adamantyl thiol and 727 \AA^3 for **23** (Table 3.2). The Au(I) complex had a hydrodynamic volume of 1500 \AA^3 , which is about 8 times larger than free thiol. Therefore, it can be reasonably assumed that the Au(I) product exists as a small $[\text{ClAu}(\text{HSAd})]_n$ cluster, with an average n close to 7. These species may grow to a point that they become the insoluble as a white precipitate is observed after the reaction.

Species	Hydrodynamic Radius	Hydrodynamic Volume
AuSAd	7.1 Å	1500 Å ³
HSAd	3.53 Å	184 Å ³
23	5.58 Å	727 Å ³

Table 3.2. The hydrodynamic radii and volumes of species measured by PGSE NMR experiments.

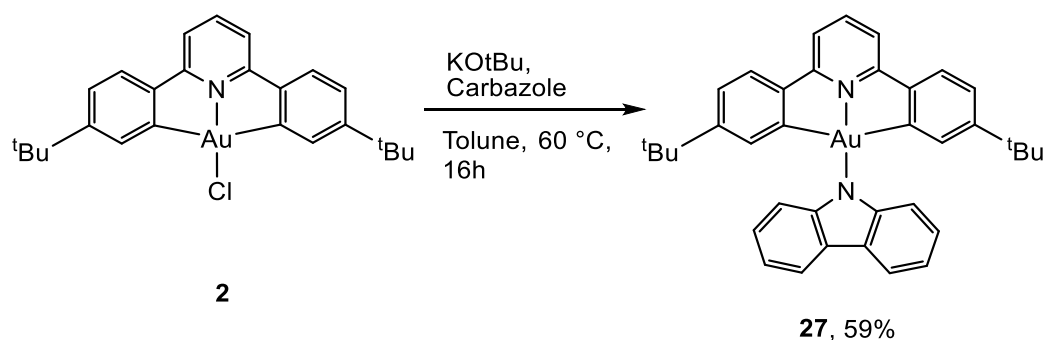
3.14 Reactivity of adamantyl thiol with (C^NC)Au–ER (ER = OR, NR) complexes

The study was extended to further gold(III) heteroatom species in the hope of triggering C–E reductive elimination. Addition of three molar equivalents of adamantyl thiol to (C^NC)Au–O–C₆H₄-*p*-F (**26**) gave **14** almost immediately (Scheme 3.27). The reaction is analogous to the synthesis of **14** with the phenolate used instead of the *tert*-butoxide (Scheme 3.19). This reaction demonstrates that the Au–S bond is stronger than the Au–O bond. No further reactivity between **14** and the excess two molar equivalents of adamantyl thiol was observed over the time that this reaction was monitored.



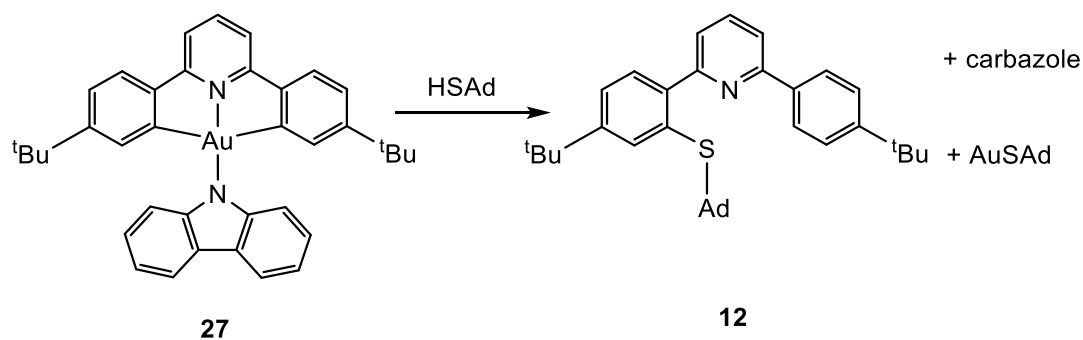
Scheme 3.27. Reaction of **26** with adamantyl thiol to give **14**.

The pincer gold(III) carbazole complex **27** was synthesised to investigate the potential for C–N reductive elimination. **27** was isolated as an orange solid, 59 % yield (Scheme 3.28). The carbazole was chosen as a gold(III)–NR₂ species because the lone pair is delocalised, and it was hoped that **27** would not be protonated as in the case of **26**.



Scheme 3.28. The synthesis of **27**.

Addition of three molar equivalents of adamantyl thiol to **27** gave C-S reductive elimination over 7 days (Scheme 3.29). The mechanism is thought to be similar to that proposed for C-S reductive elimination from **2**. After protodeauration and displacement of the Au-N bond forms a geometrically unrestrained complex that could potentially undergo either C-S or C-N reductive elimination, however in this case C-S is favoured over C-N bond formation.



Scheme 3.29. Reaction of **27** with adamantyl thiol to give **12**.

Combining these observations allows proposals of potential trends in reductive elimination reactions from gold(III) complexes. The rate of reductive elimination changes depending on the starting gold(III) complex, and protodeauration appears to be the rate determining step. The nature of the substituent cis to the Au-C bond influences the rate of protodeauration.

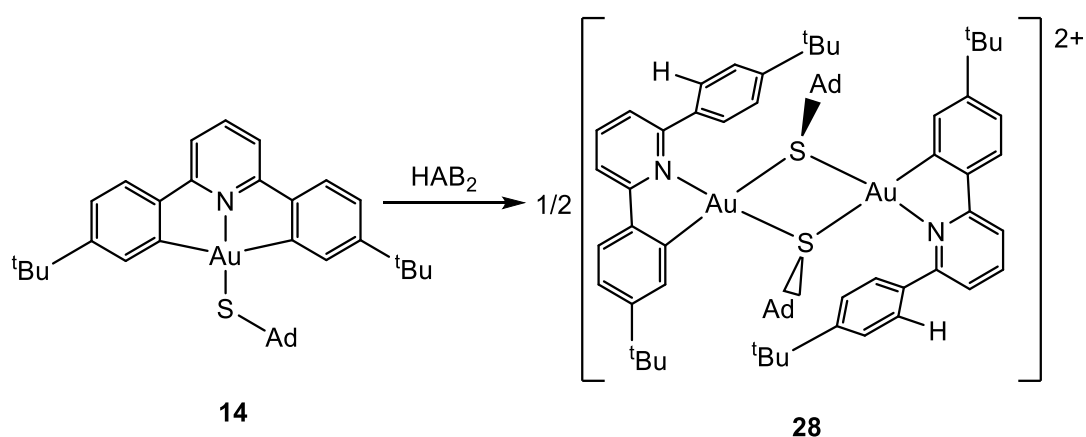
Reductive elimination is the final and irreversible step in each reaction. Bond formation is proposed to occur from a four-coordinate species (analogous to Figure 3.6 and Scheme 3.22). In this intermediate there is the potential for different bonds to be formed through reductive elimination. In complexes **19-21** there is potential to form either C-C or C-S bonds, however C-C bonds are favoured. When **2**, **14** and **27** were used, only **12** was observed, indicating that, C-S bond formation is favoured over C-N or C-Cl bond formation. In all reactions where adamantyl thiol was added to a gold(III) complex there was strong selectivity in the bond forming step.

The most interesting observations from this work are that thiols can cleave Au–C bonds and trigger C–S reductive elimination from neutral gold(III) complexes. In addition, when adamantyl thiol is added to a (C^{^N^C})Au–R complex C–C reductive elimination is triggered. These mild conditions are tolerant of a range of different functionalities, specifically the reductive elimination of C(sp²)-C(sp) bond that was not possible with previous methods.

3.15 C-S Reductive elimination via a stepwise methodology

In the mechanism in Scheme 3.22, it was proposed that C–S reductive elimination takes place via protodeauration followed by displacement of the Au–N bond. The mechanism for this was based on observations and previous work triggering C–C reductive elimination from gold(III) aryl complexes.⁴⁵ Adamantyl thiol appeared to combine these properties. Extending this stepwise protocol to the gold(III) thiolate complex **14** allowed us to further test the proposal that protodeauration and displacement lead to reductive elimination in a stepwise manner.

Addition of HAB₂ to a solution of **14** was monitored by ¹H NMR spectroscopy over 2 weeks until no further changes were observed (Scheme 3.30). In the ¹H NMR spectrum after addition the HAB₂ **14** was not observed, therefore protodeauration of **14** was fast. The major product formed was speculated to be a dimeric species **28**. This is a much longer reaction than the previous reaction of HAB₂ with (C^{^N^C})Au–Ar where the formation of an ether complex **A** (Scheme 3.16) was formed immediately, therefore as protodeauration was fast, it was proposed that dimerization was slow.



Scheme 3.30. The reaction of **14** with HAB₂ to give **28** (anions have been omitted).

Complex **28** results from the dimerization of two protodeaured species. Its structure was proposed based on several features in the ¹H NMR spectrum. Firstly, the two *t*-butyl signals ($\delta = 1.36$ ppm and 1.14 ppm) indicate the formation of an asymmetric species. Secondly, sharp signals corresponding to diethyl ether indicate that the final product does not contain

coordinated diethyl ether. Finally, in the aromatic region of **28** it was not possible to observe all expected peaks at 298 K (top, Figure 3.7), however upon cooling to 260 K all expected ^1H signals are observed. The slow exchange of the protodeaurated aryl ring was proposed to be because of restricted rotation of the aryl in the sterically demanding dimer.

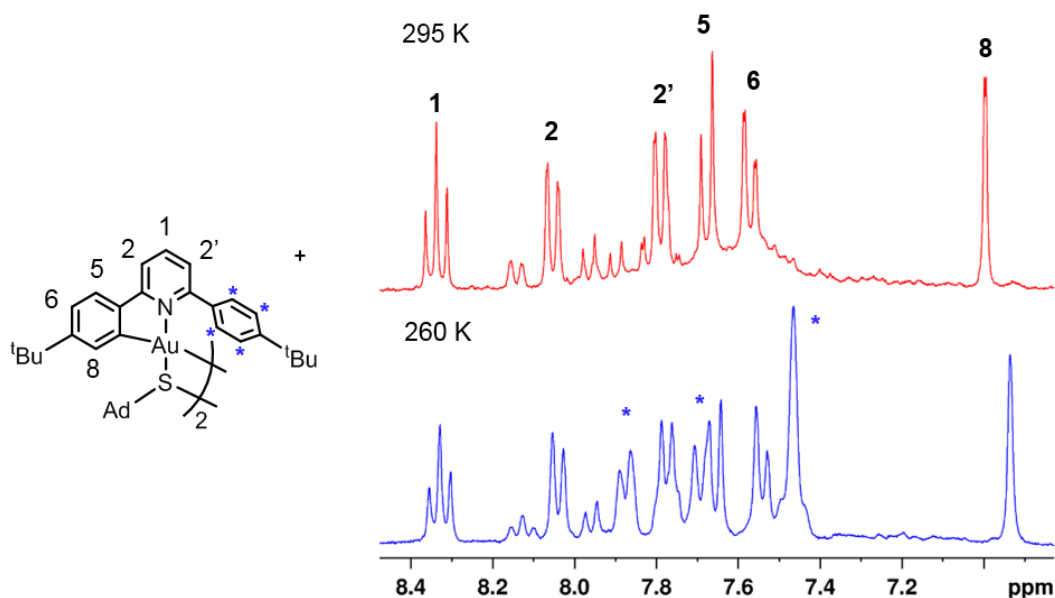


Figure 3.7. ^1H NMR spectrum of the aryl region of **28** at 295 K (red) and 260 K (blue).

Crystallization of **28** allowed structural characterisation and confirmation the structure suggested by NMR spectroscopy (Figure 3.8). The complex cation consists of two gold centres linked by bridging thiolates. The unit cell contains a dication (lying about a centre of symmetry) and two $\text{NH}_2(\text{B}(\text{C}_6\text{F}_5)_3)_2$ anions. Each gold centre is in a square-planar environment bonding to pyridine N-atom, the *o*-carbon atom of one of its phenyl group substituents, and the bridging sulfur atoms of the two S-adamantyl ligands. The pendant aryl ring is twisted out of the plane of the C[^]N ligand by $51.3(4)^\circ$ around the C(16)–C(161) bond to accommodate the steric bulk of the two bridging adamantyl thiolates. The two adamantyl groups are mutually trans and almost perpendicular to the central Au_2S_2 plane, with Au–S(1)–C(1) angles of $103.2(3)$ and $98.9(3)^\circ$. The sterically congested ligand sphere leads to distortions of the normally planar gold coordination sphere, e.g. the C(9)–Au–S angle is reduced to from the expected 180° to 163.44° . The bridging Au–S bonds are quite different in length and reflect the trans influence of the C[^]N ligand, with the one *trans* to the pyridine N-atom being 0.15 \AA shorter than the bond *trans* to the phenyl C-atom.

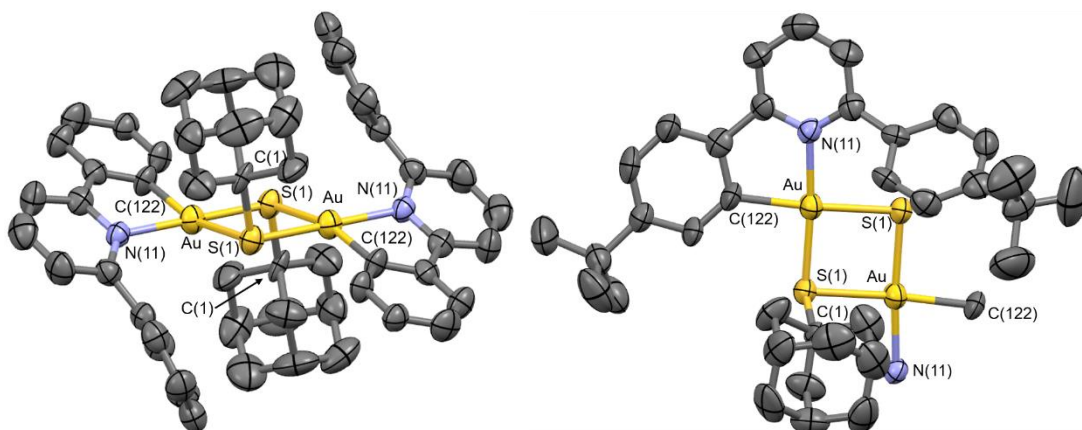


Figure 3.8. Side and partial top view of the cation in **28**. Left) H atoms, *tert*-butyl groups and anions are omitted for clarity. Right) H atoms and anions are omitted for clarity.

Ellipsoids are drawn at 50%. Selected bond distances [Å] and angles [°]: Au-C(122) 2.066(8), Au-N(11) 2.108(7), Au-S(1) 2.323(2), Au-S(1) 2.469(2), S(1)-C(1) 1.880(9); C(122)-Au-N(11) 81.2(3), C(122)-Au-S(1) 94.3(3), N(11)-Au-S(1) 174.4(2), C(122)-Au-S(1) 163.4(3), N(11)-Au-S(1) 101.2(2), S(1)-Au-S(1) 84.02(8)

Previously, there has been one other structurally characterised gold(III) bridged thiolate (Figure 3.9).⁵³ In that example the gold(III) centres are in a typical square planar environment and the bridging thiolates bend out of the plane.

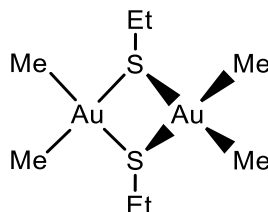
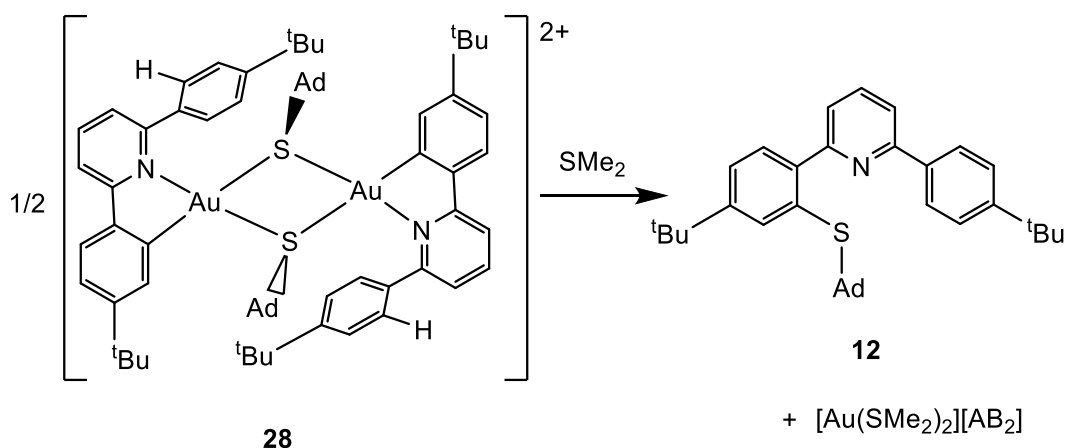


Figure 3.9. A structurally characterised dimeric gold(III) thiolate, the second gold centre is out of the plane of the page.

3.16 Addition of dimethyl sulfide to **28**

Reductive elimination from **28** can be triggered upon addition of excess dimethyl sulfide (Scheme 3.31). A possible mechanism for this is through dimethyl sulfide displacing an Au-N and Au-S bond to form an unstable intermediate which can undergo reductive elimination. Reductive elimination results in C-S bond formation giving **12** and a gold(I) species, likely to be $[\text{Au}(\text{SMe}_2)_2][\text{AB}_2]$.



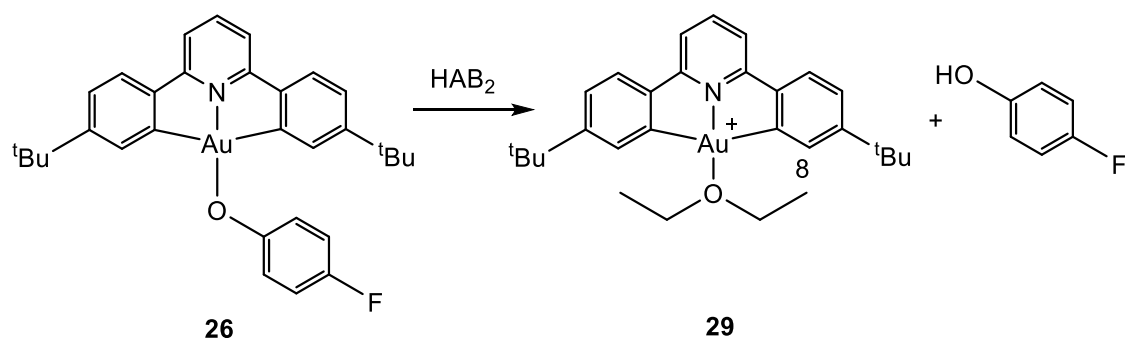
Scheme 3.31. Addition of SMe_2 to **28** to give C-S bond formation.

This is an example of reductive elimination from a cationic intermediate, which have previously been shown to be faster than neutral analogues. Qualitative studies showed the rate of reductive elimination increases with increasing amount of dimethyl sulfide which could indicate a four-coordinate intermediate.

This stepwise approach of protodeauration of an Au–C bond and subsequent displacement of Au–N and Au–S bonds demonstrates that combining these two steps leads to reductive elimination and supports the mechanism proposed in Scheme 3.22.

3.17 Investigating the stepwise protocol with further gold(III) heteroatom species

The stepwise protocol was extended to other heteroatom species with the aim of inducing further C–E (E = N, O) bond formation, however different reactivity patterns were observed. Addition of HAB_2 to a solution of **26** resulted in the formation of a diethyl ether complex **29** (Scheme 3.32).⁵⁴ **29** is unstable and decomposed over 3 hours at room temperature.



Scheme 3.32. The reaction of **26** with HAB_2 .

The unusual high frequency shift of the diethyl ether CH_2 signal at $\delta = 4.68$ ppm in the ^1H NMR spectrum is in agreement with the ^1H NOESY spectrum of **29**, which showed a through space interaction between the diethyl ether CH_2 and H^8 (Figure 3.10).

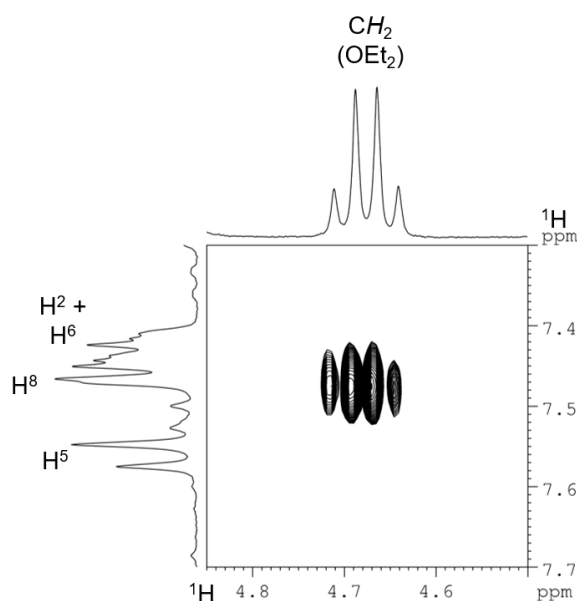
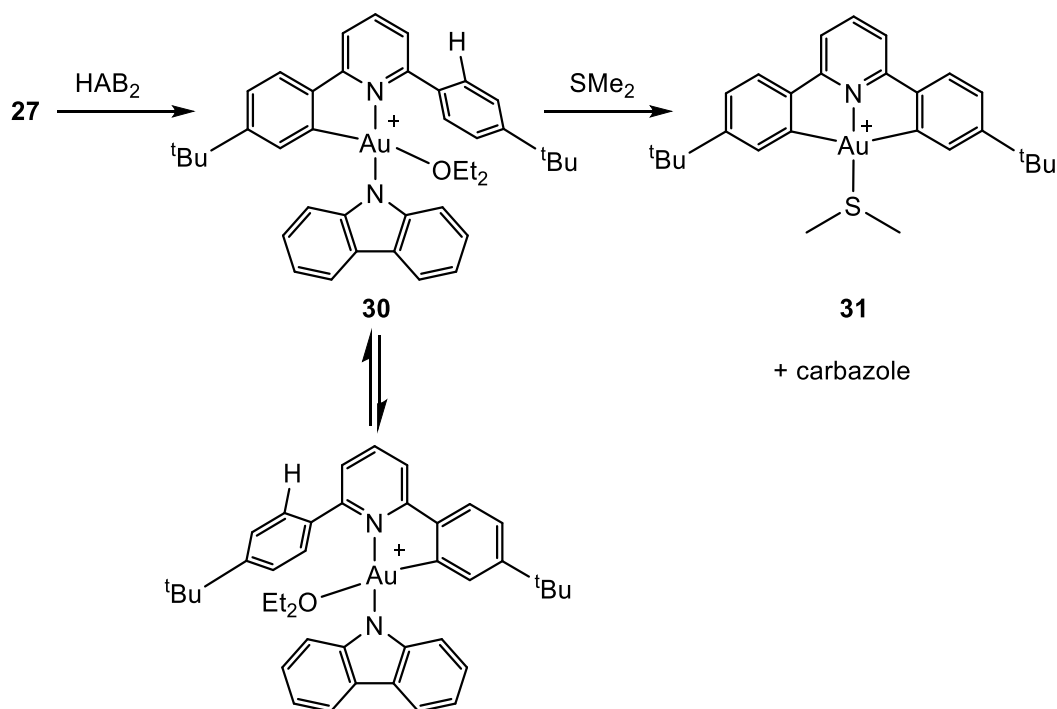


Figure 3.10. The interaction between H^8 and CH_2 of the coordinated ether molecule in complex **29**.

The stepwise protocol is unsuitable for triggering C–O reductive elimination. This is possibly because the oxygen lone pair is the most basic site in this molecule, therefore first to be protonated and is subsequently displaced by a molecule of diethyl ether forming **29** and phenol. Consequently, for protodeauration to occur there must not be a more basic site than the Au–C bond, such as an available oxygen lone pair in **26**. This is similar reactivity to the reaction of **26** with adamantyl thiol where **14** was formed instead of C–S reductive elimination.

To avoid the reactivity observed with **26**, the complex **27**, with a carbazole functionality, was used to investigate the stepwise protocol. Addition of HAB_2 to **27** gave the protodeaured species **30**, demonstrating that the carbazole nitrogen is not preferentially protonated (Scheme 3.33).



Scheme 3.33. Reaction of **27** with HAB_2 , followed by addition of dimethyl sulfide.

In the ^1H NOESY spectrum of **30** chemical exchange was observed between the two tertiary butyl signals. This is shown through negative cross peaks between the inequivalent tertiary butyl signals (Figure 3.11). This exchanging environment is likely to occur through reversible protodeauration of the two Au-C bonds facilitated by diethyl ether, as seen upon protodeauration of **2**.⁴⁴

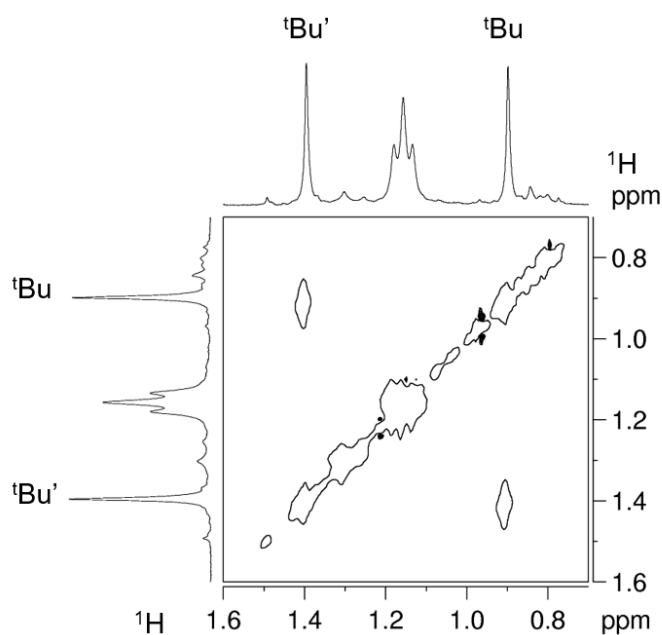


Figure 3.11. NOE spectrum of **30**, the negative peaks are white and between the two tertiary butyl signals which are exchanging with each other.

It is possible to calculate the rate of chemical exchange using Equation 3.3, where τ_m is the mixing time, I_{XX} is the intensity of diagonal peaks and I_{XY} is the intensity of cross peaks, the relative integral intensities are extracted from the NOE spectrum.⁵⁵ Here the rate is 1.23 s^{-1} , which is slightly faster than that previously observed for proton shuttling in **2**.⁴⁴

$$k = \frac{1}{\tau_m} \ln \frac{r+1}{r-1} \quad r = \frac{I_{AA}I_{BB}}{I_{AB}I_{BA}}$$

Equation 3.3. Used to calculate the rate of chemical exchange in NOESY spectrum.

Addition of dimethyl sulfide resulted in C–H activation, formation of **31** and release of the carbazole (Scheme 3.30).⁴² This reactivity was unexpected as previously the dimethylsulfide had displaced the Au–N(pyridine) bond. Potentially the formation of a gold(III) dimethylsulfide cation is more stable and proton is transferred to the carbazole, therefore halting the fluctational behaviour observed for **30**.

These reactions show that many factors are important when attempting to trigger reductive elimination from C[^]N[^]C gold(III) systems. In the first step to form a protodeaurated species there must not be a more basic site than the Au–C bond such as in **26**, in the absence of such functionality it is possible to form the protodeaurated species **28** and **30**. In the second step, addition of dimethyl sulfide, it is possible to displace an Au–N bond in **28**, however in **30** it led to C–H activation, therefore the protocol is not easily extended to other systems. The stepwise method can be used to trigger reductive elimination from **14** leading to C–S bond formation.

Conclusion

We have shown that selective C–S bond formation is possible via reductive elimination from gold(III) species, by two different methods. Addition of adamantyl thiol triggered reductive elimination from **2** at ambient temperatures. We have proposed a mechanism for this reaction by combining a series of observations. This reaction was extended to other C[^]N[^]C gold(III) pincer systems from which it was possible to trigger C–C reductive elimination. This reactivity is unique to thiols, so far, no other acidic compounds trigger this reactivity. A stepwise methodology was also used to trigger C–S reductive elimination. Structural characterisation of an intermediate showed an interesting thiolato-bridged dimer species where the large steric demands distorted the normally square planar geometry around gold(III). Application of this stepwise methodology to other gold(III) heteroatom species showed interesting reactivity, but no reductive elimination.

References

- (1) (a) Hashmi, A. S. K.; Schwarz, L.; Choi, J. H.; Frost, T. M. *Angew. Chem.-Int. Edit.* **2000**, *39*, 2285. (b) Hashmi, A. S. K. *Gold Bull.* **2004**, *37*, 51. (c) Hashmi, A. S. K. *Angew. Chem.-Int. Edit.* **2005**, *44*, 6990. (d) Hashmi, A. S. K. *Chem. Rev.* **2007**, *107*, 3180. (e) Gorin, D. J.; Sherry, B. D.; Toste, F. D. *Chem. Rev.* **2008**, *108*, 3351. (f) Jimenez-Nunez, E.; Echavarren, A. M. *Chem. Rev.* **2008**, *108*, 3326. (g) Widenhoefer, R. A. *Chem.-Eur. J.* **2008**, *14*, 5382. (h) Hashmi, A. S. K. *Angew. Chem.-Int. Edit.* **2010**, *49*, 5232. (i) Wang, W. B.; Hammond, G. B.; Xu, B. *J. Am. Chem. Soc.* **2012**, *134*, 5697. (j) Hashmi, A. S. K. *Acc. Chem. Res.* **2014**, *47*, 864. (k) Wang, Y. M.; Lackner, A. D.; Toste, F. D. *Acc. Chem. Res.* **2014**, *47*, 889.
- (2) Halliday, C. J. V.; Lynam, J. M. *Dalton Trans.* **2016**, *45*, 12611.
- (3) (a) Hopkinson, M. N.; Gee, A. D.; Gouverneur, V. *Chem.-Eur. J.* **2011**, *17*, 8248. (b) Ball, L. T.; Lloyd-Jones, G. C.; Russell, C. A. *Science* **2012**, *337*, 1644. (c) Levin, M. D.; Toste, F. D. *Angew. Chem.-Int. Edit.* **2014**, *53*, 6211. (d) Cambeiro, X. C.; Ahlsten, N.; Larrosa, I. *J. Am. Chem. Soc.* **2015**, *137*, 15636. (e) Hofer, M.; Genoux, A.; Kumar, R.; Nevado, C. *Angew. Chem.-Int. Edit.* **2017**, *56*, 1021.
- (4) (a) Miyaura, N.; Yanagi, T.; Suzuki, A. *Synth. Commun.* **1981**, *11*, 513. (b) Miyaura, N.; Suzuki, A. *Chem. Rev.* **1995**, *95*, 2457. (c) Suzuki, A. *J. Organomet. Chem.* **1999**, *576*, 147.
- (5) Serra, J.; Parella, T.; Ribas, X. *Chem. Sci.* **2017**, *8*, 946.
- (6) Joost, M.; Amgoune, A.; Bourissou, D. *Angew. Chem.-Int. Edit.* **2015**, *54*, 15022.
- (7) Rosca, D. A.; Wright, J. A.; Bochmann, M. *Dalton Trans.* **2015**, *44*, 20785.
- (8) Beletskaya, I. P.; Ananikov, V. P. *Chem. Rev.* **2011**, *111*, 1596.
- (9) (a) Ball, L. T.; Green, M.; Lloyd-Jones, G. C.; Russell, C. A. *Org. Lett.* **2010**, *12*, 4724. (b) Leyva-Perez, A.; Domenech, A.; Al-Resayes, S. I.; Corma, A. *ACS Catal.* **2012**, *2*, 121.
- (10) Johnson, M. T.; van Rensburg, J. M. J.; Axelsson, M.; Ahlquist, M. S. G.; Wendt, O. F. *Chem. Sci.* **2011**, *2*, 2373.
- (11) (a) Teles, J. H. *Angew. Chem.-Int. Edit.* **2015**, *54*, 5556. (b) Joost, M.; Zeineddine, A.; Estevez, L.; Ladeira, S. M.; Miqueu, K.; Amgoune, A.; Bourissou, D. *J. Am. Chem. Soc.* **2014**, *136*, 14654.
- (12) Zeineddine, A.; Estevez, L.; Mallet-Ladeira, S.; Miqueu, K.; Amgoune, A.; Bourissou, D. *Nat. Commun.* **2017**, *8*, 8.
- (13) Wu, C. Y.; Horibe, T.; Jacobsen, C. B.; Toste, F. D. *Nature* **2015**, *517*, 449.
- (14) Bachman, R. E.; Bodolosky-Bettis, S. A.; Pyle, C. J.; Gray, M. A. *J. Am. Chem. Soc.* **2008**, *130*, 14303.

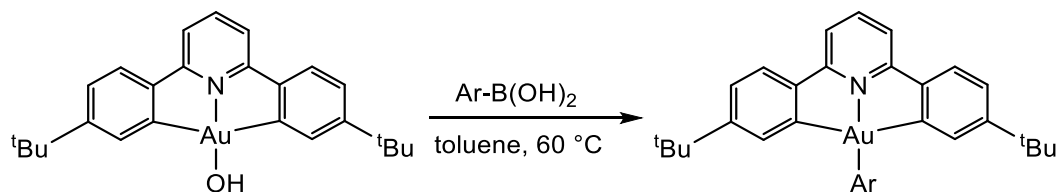
- (15) Kumar, R.; Nevado, C. *Angew. Chem.-Int. Edit.* **2017**, *56*, 1994.
- (16) Nijamudheen, A.; Karmakar, S.; Datta, A. *Chem.-Eur. J.* **2014**, *20*, 14650.
- (17) Hofer, M.; Gomez-Bengoa, E.; Nevado, C. *Organometallics* **2014**, *33*, 1328.
- (18) Kuch, P. L.; Tobias, R. S. *J. Organomet. Chem.* **1976**, *122*, 429.
- (19) Komiya, S.; Albright, T. A.; Hoffmann, R.; Kochi, J. K. *J. Am. Chem. Soc.* **1976**, *98*, 7255.
- (20) Winston, M. S.; Wolf, W. J.; Toste, F. D. *J. Am. Chem. Soc.* **2015**, *137*, 7921.
- (21) Vicente, J.; Bermudez, M. D.; Escribano, J. *Organometallics* **1991**, *10*, 3380.
- (22) Wolf, W. J.; Winston, M. S.; Toste, F. D. *Nat. Chem.* **2014**, *6*, 159.
- (23) (a) Scott, V. J.; Labinger, J. A.; Bercaw, J. E. *Organometallics* **2010**, *29*, 4090. (b) Mankad, N. P.; Toste, F. D. *Chem. Sci.* **2012**, *3*, 72. (c) Bhattacharjee, R.; Nijamudheen, A.; Datta, A. *Chem.-Eur. J.* **2017**, *23*, 4169.
- (24) Lavy, S.; Miller, J. J.; Pazicky, M.; Rodrigues, A. S.; Rominger, F.; Jakel, C.; Serra, D.; Vinokurov, N.; Limbach, M. *Adv. Synth. Catal.* **2010**, *352*, 2993.
- (25) Kawai, H.; Wolf, W. J.; DiPasquale, A. G.; Winston, M. S.; Toste, F. D. *J. Am. Chem. Soc.* **2016**, *138*, 587.
- (26) (a) Goulet, P. J. G.; Lennox, R. B. *J. Am. Chem. Soc.* **2010**, *132*, 9582. (b) Schaaff, T. G.; Shafiqullin, M. N.; Khoury, J. T.; Vezmar, I.; Whetten, R. L.; Cullen, W. G.; First, P. N.; GutierrezWing, C.; Ascensio, J.; JoseYacaman, M. J. *J. Phys. Chem. B* **1997**, *101*, 7885.
- (27) Barngrover, B. M.; Aikens, C. M. *J. Am. Chem. Soc.* **2012**, *134*, 12590.
- (28) (a) Schmidbaur, H.; Schier, A. *Chem. Soc. Rev.* **2008**, *37*, 1931. (b) Schmidbaur, H.; Schier, A. *Chem. Soc. Rev.* **2012**, *41*, 370.
- (29) Bertrand, B.; Williams, M.; and Bochmann, M.; **2018**, *Chem. Eur. J.* Accepted Manuscript; 10.1002/chem.201800981.
- (30) Schafer, F. Q.; Buettner, G. R. *Free Radic. Biol. Med.* **2001**, *30*, 1191.
- (31) Siddik, Z. H. *Oncogene* **2003**, *22*, 7265.
- (32) Ishikawa, T.; Wright, C. D.; Ishizuka, H. *J. Biol. Chem.* **1994**, *269*, 29085.
- (33) (a) Casini, A.; Cinellu, M. A.; Minghetti, G.; Gabbiani, C.; Coronello, M.; Mini, E.; Messori, L. *J. Med. Chem.* **2006**, *49*, 5524. (b) Zou, T. T.; Lum, C. T.; Chui, S. S. Y.; Che, C. M. *Angew. Chem.-Int. Edit.* **2013**, *52*, 2930.
- (34) (a) Alvaro, E.; Hartwig, J. F. *J. Am. Chem. Soc.* **2009**, *131*, 7858. (b) Zhao, X. D.; Dong, V. M. *Angew. Chem.-Int. Edit.* **2011**, *50*, 932. (c) Mann, G.; Baranano, D.; Hartwig, J. F.; Rheingold, A. L.; Guzei, I. A. *J. Am. Chem. Soc.* **1998**, *120*, 9205. (d) Desnoyer, A. N.; Love, J. A. *Chem. Soc. Rev.* **2017**, *46*, 197. (e) Hartwig, J. F. *Nature* **2008**, *455*, 314. (f) Macgregor, S. A.; Neave, G. W.; Smith, C. *Faraday Discuss.* **2003**, *124*, 111. (g) Font, M.; Acuna-Pares, F.; Parella, T.; Serra, J.; Luis, J. M.; Lloret-Fillol,

- J.; Costas, M.; Ribas, X. *Nat. Commun.* **2014**, *5*, 10. (h) Okamoto, K.; Housekeeper, J. B.; Luscombe, C. K. *Appl. Organomet. Chem.* **2013**, *27*, 639.
- (35) Baranano, D.; Hartwig, J. F. *J. Am. Chem. Soc.* **1995**, *117*, 2937.
- (36) Kung, K. K. Y.; Ko, H. M.; Cui, J. F.; Chong, H. C.; Leung, Y. C.; Wong, M. K. *Chem. Commun.* **2014**, *50*, 11899.
- (37) Messina, M. S.; Stauber, J. M.; Waddington, M. A.; Rheingold, A. L.; Maynard, H. D.; Spokoiny, A. M. *J. Am. Chem. Soc.* **2018**, *140*, 7065.
- (38) Currie, L.; Fernandez-Cestau, J.; Rocchigiani, L.; Bertrand, B.; Lancaster, S. J.; Hughes, D. L.; Duckworth, H.; Jones, S. T. E.; Credgington, D.; Penfold, T. J.; Bochmann, M. *Chem.-Eur. J.* **2017**, *23*, 105.
- (39) Rosca, D. A.; Smith, D. A.; Hughes, D. L.; Bochmann, M. *Angew. Chem.-Int. Edit.* **2012**, *51*, 10643.
- (40) Rosca, D. A.; Smith, D. A.; Bochmann, M. *Chem. Commun.* **2012**, *48*, 7247.
- (41) Rocchigiani, L.; Fernandez-Cestau, J.; Agonigi, G.; Chambrier, I.; Budzelaar, P. H. M.; Bochmann, M. *Angew. Chem.-Int. Edit.* **2017**, *56*, 13861.
- (42) Savjani, N.; Rosca, D. A.; Schormann, M.; Bochmann, M. *Angew. Chem.-Int. Edit.* **2013**, *52*, 874.
- (43) Smith, D. A.; Rosca, D. A.; Bochmann, M. *Organometallics* **2012**, *31*, 5998.
- (44) Rocchigiani, L.; Fernandez-Cestau, J.; Budzelaar, P. H. M.; Bochmann, M. *Chem. Commun.* **2017**, *53*, 4358.
- (45) Rocchigiani, L.; Fernandez-Cestau, J.; Budzelaar, P. H. and Bochmann, M. **2018**, *Chem. Eur. J.*; 10.1002/chem.201801277.
- (46) Bordwell, F. G. *Acc. Chem. Res.* **1988**, *21*, 456.
- (47) Bordwell, F. G.; Hughes, D. L. *J. Org. Chem.* **1982**, *47*, 3224.
- (48) Bordwell, F. G.; Drucker, G. E.; Fried, H. E. *J. Org. Chem.* **1981**, *46*, 632.
- (49) Arnett, E. M.; Maroldo, S. G.; Schilling, S. L.; Harrelson, J. A. *J. Am. Chem. Soc.* **1984**, *106*, 6759.
- (50) Olmstead, W. N.; Margolin, Z.; Bordwell, F. G. *J. Org. Chem.* **1980**, *45*, 3295.
- (51) Vicente, J.; Bermudez, M. D.; Escribano, J.; Carrillo, M. P.; Jones, P. G. *J. Chem. Soc.-Dalton Trans.* **1990**, 3083.
- (52) Au, V. K. M.; Wong, K. M. C.; Zhu, N. Y.; Yam, V. W. W. *Chem.-Eur. J.* **2011**, *17*, 130.
- (53) Chen, H. W.; Pappas, C.; Fackler, J. P. *Inorganica Chimica Acta-Articles and Letters* **1985**, *96*, 137.
- (54) Chambrier, I.; Rosca, D. A.; Fernandez-Cestau, J.; Hughes, D. L.; Budzelaar, P. H. M.; Bochmann, M. *Organometallics* **2017**, *36*, 1358.
- (55) Perrin, C. L.; Dwyer, T. J. *Chem. Rev.* **1990**, *90*, 935.

Chapter Four:

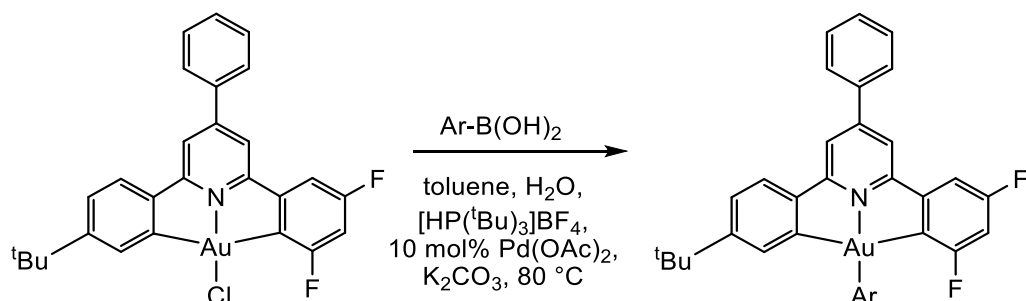
Transmetallation of Au–Cl, Au–S and Au–O bonds

photoemissive. This protocol has since been applied to the synthesis of highly luminescent gold(III) aryls that have been used in OLED devices.⁹



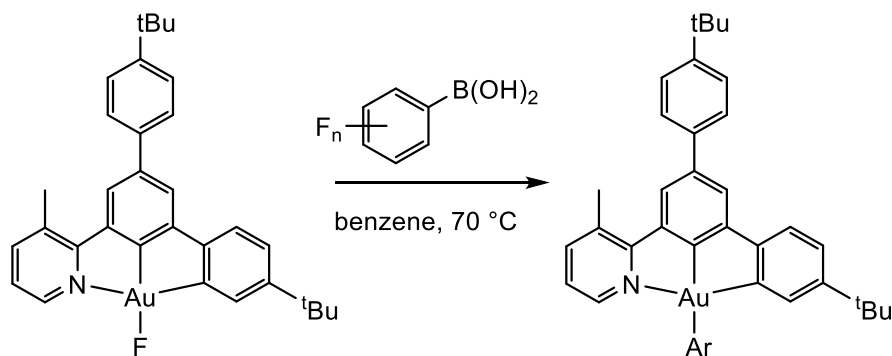
Scheme 4.2. The transmetalation of a gold(III) hydroxide by boronic acids.

Alternately, gold(III) aryls can be synthesised through the coupling of an Au–Cl bond with a boronic acid by using a palladium catalyst in the presence of a base at elevated temperatures (Scheme 4.3).¹⁰ The gold(III) aryls produced are again highly luminescent.



Scheme 4.3. The coupling of an Au–Cl bond with a boronic acid using a palladium catalyst.

Under more forcing conditions (heating to 150 °C), the base and catalyst free transmetalation of gold(III) chloride using a boronic acid was achieved.¹¹ This reaction is only compatible with electron-deficient aryl boronic acids, limiting the scope of the reaction. A C[^]C[^]N gold(III) fluoride complex required slightly less harsh conditions (heating to 70 °C) to facilitate the transmetalation of an Au–F bond by a boronic acid, however it only proceeded with electron-deficient fluoroaryl boronic acids (Scheme 4.4).¹²



Scheme 4.4. Transmetalation of an Au–F bond with fluorinated boronic acids.

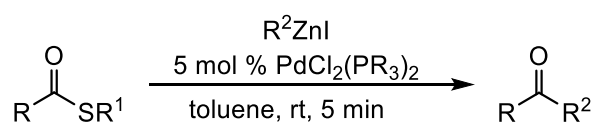
A C[^]N-stabilised gold(III) difluoride underwent facile transmetallation using boronic acids (conversion is observed at room temperature), however it is also able to undergo reductive elimination with C-C coupling products observed.¹² Similarly, the transmetallation of Au-F bonds by boronic acids in other gold complexes has been proposed, however only the C-C coupling products formed upon reductive elimination are observed.¹³

More recently, boronic acids have been used in a range of catalytic gold coupling reactions. Chapter Three, Figure 3.2, showed the use of a boronic acid in catalytic oxidative arylation.¹⁴ Boronic acids have also been used in the gold catalysed coupling of allyl halides with aryl boronic acids¹⁵ and coupling of terminal alkynes with boronic acids.¹⁶

4.1.2 Transmetallation using organozinc reagents

Organozinc reagents are also widely used in synthetic chemistry, although they are less air stable than boronic acids, but they are more tolerant of functional groups than the corresponding magnesium or lithium reagents.¹⁷ Different organozinc reagents have varying reactivity; dialkyl zinc reagents are much more reactive than the corresponding alkyl zinc halides. In palladium catalysis, organozinc reagents are used as transmetallation reagents in the Negishi coupling reaction that couples an organozinc reagent and an organohalide to form a new C-C bond.¹⁸ In this reaction oxidative addition of the organohalide C-X bond forms a palladium(II) complex, this is followed by transmetallation of a Pd-X bond by an organozinc halide which forms a Pd-C bond and subsequent reductive elimination forms a new C-C bond.

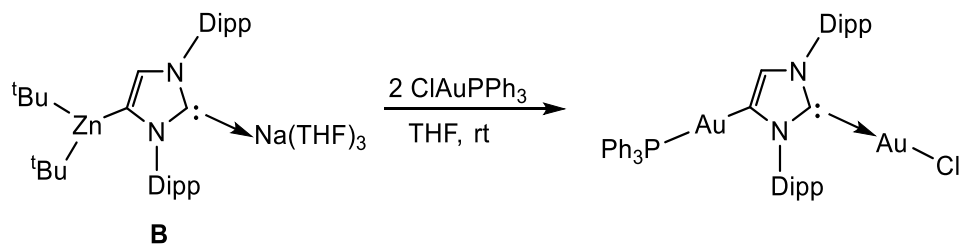
Another palladium catalysed reaction that is relevant to this work is the Fukuyama reaction because it involves the formation of a metal-thiolate species and M-S bond transmetallation. The Fukuyama reaction couples a thioester and organozinc reagent to form a ketone (Scheme 4.5).¹⁹ The mechanism is proposed to go via oxidative addition of a thioester to palladium, followed by the transmetallation of a Pd-S bond by organozinc reagent and subsequent reductive elimination forming a C-C bond. The thioester can be synthesised from carboxylic acids with the overall transformation of carboxylic acid to ketone.



Scheme 4.5. The Fukuyama reaction.

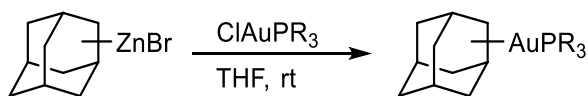
Despite the wide use of organozinc reagents with other transition metals the reports of reactivity with gold are limited to two reactions. Firstly, the reaction of (Ph₃P)AuCl with **B**

results in both transmetallation and displacement of the phosphine to give two Au–C bonds (Scheme 4.6).²⁰



Scheme 4.6. The reaction of an organozinc reagent with a gold(I) complex.

The second example uses adamantylzinc bromides (both 1-AdZnBr and 2-AdZnBr, Ad = adamantyl), which can be reduced to the corresponding diadamantylzincs to give four different organozinc reagents.²¹ All four of these complexes can be used in the transmetallation of $(R_3P)AuCl$ to give a new Au–C bond (Scheme 4.7). When the adamantylzinc bromides were used the product could not be isolated and instead were only observed *in situ*. The diadamantylzinc compounds proved to be superior reagents for transmetallation of the Au–Cl bond allowing isolation of $(R_3P)AuAd$.

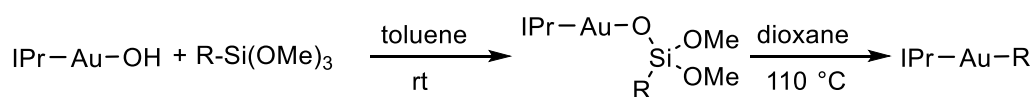


Scheme 4.7. An organozinc reagent transmetallating an Au–Cl bond.

4.1.3 Silanes and stannanes in transmetallation reactions

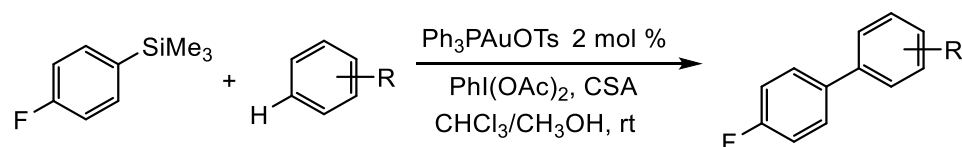
Other p-block compounds have been investigated as transmetallation reagents with both gold and other transition metals. Silyl reagents are used in transition metal cross couplings catalysis,²² such as the palladium catalysed Hiyama coupling, which uses organic halides and organosilanes to give a carbon–carbon bond.²³

The reactivity of gold complexes and a range of silanes has shown them to be transmetallation reagents.¹ The stoichiometric transmetallation of Au–O bonds with $R-Si(OMe)_3$ has been demonstrated for gold(I) species (Scheme 4.8).²⁴ The intermediates in this reaction can be isolated and characterised and contain an oxygen bonded to both gold and silane. A wide range of functional groups were shown to be transferred to gold, including aryls, vinyls and allyls.



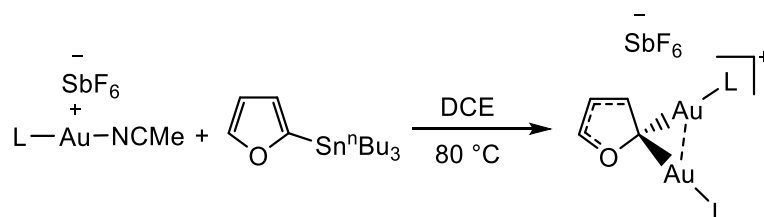
Scheme 4.8. Transmetallation of Au–O bonds with silanes.

Trimethylarylsilanes were used to transfer an aryl group to gold in gold-catalysed oxidative arylation (Scheme 4.9).²⁵ A comprehensive mechanistic study into this catalytic reaction allowed elucidation of the mechanism. A simplified description of this includes: oxidation of the gold(I) complex by a hypervalent iodine species, this undergoes electrophilic aromatic substitution of a silane and subsequent C–H auration of an aryl C–H bond; finally, reductive elimination forms a C–C bond and regenerates the gold(I) complex.



Scheme 4.9. Arylsilanes in gold catalysed oxidative arylation.

The use of stannanes in palladium catalysis is well known; the Stille reaction couples stannanes with organic electrophiles.²⁶ Stannanes have also been used in the transmetalation of gold species, such as in the formation of the *gem*-diaurated furyl complex (Scheme 4.10).²⁷ Identification of this reaction was part of a study on gold(I) catalysed cyclisation and stannyl transfer.



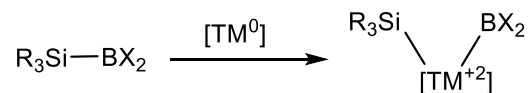
Scheme 4.10. Transmetalation of a gold(I) species using stannanes.

Other transmetalation reactions using both stannanes and gold have involved bimetallic catalysis where catalytic amounts of Pd/Au allow the addition of stannanes to alkynes.²⁸ In this reaction the gold was proposed to activate the alkyne.

4.2 Compounds containing an Si–B in transmetalation reactions

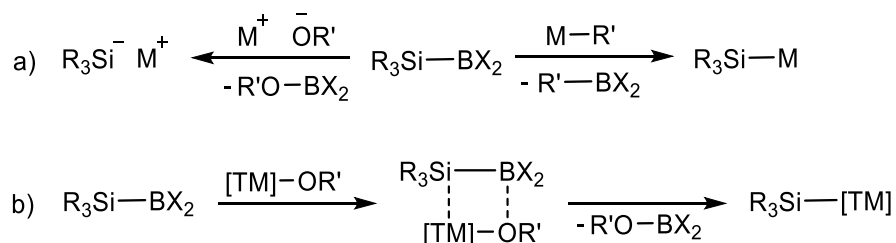
In the synthesis of new C–E bonds (E = B, Si, Sn), compounds containing bonds between two main group elements (boron, silicon, tin) can be used.²⁹ One example is the use of unsymmetrical diboranes, which have proved versatile reagents in the formation of C–B bonds.³⁰ Alternatively, compounds containing an Si–B bond have been developed where the difference in electronegativity between silicon and boron leads to highly stereoselective reactions.²⁹ Application of Si–B compounds has been widely used in organic synthesis.³¹ The most extensive studies have used Si–B activation to functionalise unsaturated bonds.

These Si–B bond containing compounds can react with transition metal complexes and display a range of reactivity. With low-valent metals oxidative addition of the Si–B bond leads to the formation of M–Si and M–B bonds (Scheme 4.11).³² These complexes can react with C=C bonds through migratory insertion, which forms a C–B bond and subsequent reductive elimination to form a C–Si bond, leading to functionalisation of an unsaturated bond.



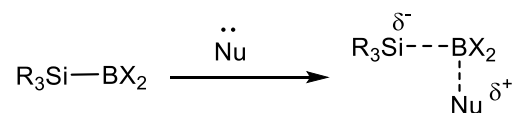
Scheme 4.11. Oxidative addition of an Si–B bond to a transition metal.

Alternatively, strong nucleophiles can react with Si–B compounds by attacking the more electrophilic Lewis acidic boron.²⁹ When metal complexes are used this results in transmetallation forming a M–Si bond.³³ There are two different mechanisms proposed for this reaction, either transmetallation with anionic nucleophiles or transmetallation through σ -bond metathesis (Scheme 4.12).²⁹ The transmetallation with anionic nucleophiles has predominantly been observed for alkali or alkali earth metal alkoxides and carbanions, whereas σ -bond metathesis has predominantly been observed for transition metal alkoxides and hydroxides. In these transmetallation reactions a M–Si bond is always formed in preference to an M–B bond. This has been used to make several Cu–Si complexes which have subsequently been used in a range of catalytic studies.³⁴ To the best of our knowledge there have been no studies using gold complexes.



Scheme 4.12. Transmetallation using Si–B compounds via: a) anionic nucleophiles or b) through σ -bond metathesis.

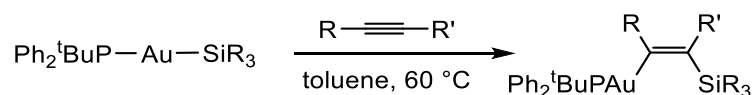
The Si–B bond can also be activated by non-metal nucleophiles to release a silicon nucleophile, allowing intermolecular silyl transfer (Scheme 4.13).³⁵ This differs from much of the silicon chemistry where silanes are used as electrophiles (see Scheme 4.9 for a silicon based electrophile).



Scheme 4.13. Metal free activation of the Si–B bond.²⁹

4.3 Gold-silyl complexes

Two methods have previously been used in the synthesis of complexes containing Au–Si bonds, either silyl lithium reagents or oxidative addition of a Si–Si bond. Gold(I) silyl complexes were synthesised in the 1980s using silyl lithium reagents and phosphine gold(I) chlorides.³⁶ More recently a series of phosphine gold(I) silyl complexes have been synthesised the same methodology by Bourissou *et al.* to investigate their reactivity.³⁷ A sterically demanding silyl group (Si^tBuPh₂) was used to increase the stability of the gold(I) silyl complex. These complexes were shown to undergo syn-insertion of alkynes into the Au–Si bond to form air stable gold(I) vinyl complexes (Scheme 4.14). A range of alkynes were investigated, with internal alkynes taking longer to react (up to 4 weeks at 65 °C). These gold(I) complexes were used in the transmetalation of stannanes and as transmetalation reagents in the palladium catalysed coupling with an aryl iodide or an allyl bromide. Decreasing the steric bulk of the silyl group by using a triphenyl silyl (R₃P–Au–SiPh₃) increased the reactivity towards insertion reactions and the insertion of allenes was observed.

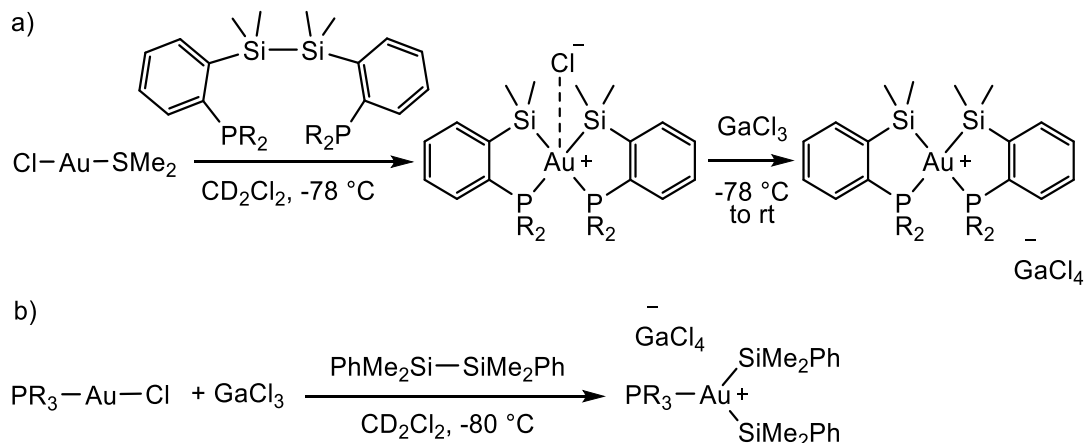


Scheme 4.14. The insertion of alkynes into Au–Si bonds.

Studies into the mechanism of this reaction showed that first the alkyne coordinates the phosphine gold(I) silyl species to form a π complex, which then inserts into the Au–Si bond.³⁸ The syn insertion is a result of a concerted inner-sphere mechanism.

Gold(III) complexes containing Au–Si bonds have been observed upon the oxidative addition of Si–Si σ bonds to gold(I) species.³⁹ The reaction of a disilane-bridged diphosphine with the chlorogold(I) dimethylsulfide complex resulted in intramolecular oxidative addition of the Si–Si σ bond (a, Scheme 4.15). The initial complex formed is thermally unstable and upon warming to room temperature the gold(III) complex is reduced to gold(I) diphosphine containing a disiloxane, which is formed with either water or oxygen acting as the oxygen source. Addition of gallium trichloride vastly increased the stability of the gold(III) complex, due to formation of the stable poorly coordinating GaCl₄[−] anion.

Based on the previous observations, a phosphine gold(I) chloride was activated by gallium trichloride at $-80\text{ }^{\circ}\text{C}$, through chloride abstraction (b, Scheme 4.15). This facilitates subsequent intermolecular oxidative addition of a disilane to form a gold(III) bissilyl complex. This complex was unstable at temperatures above $-60\text{ }^{\circ}\text{C}$.



Scheme 4.15. Oxidative addition of a Si–Si σ bonds to form Au–Si bonds: a) intramolecular oxidative addition; b) intermolecular oxidative addition.

4.4 Objectives

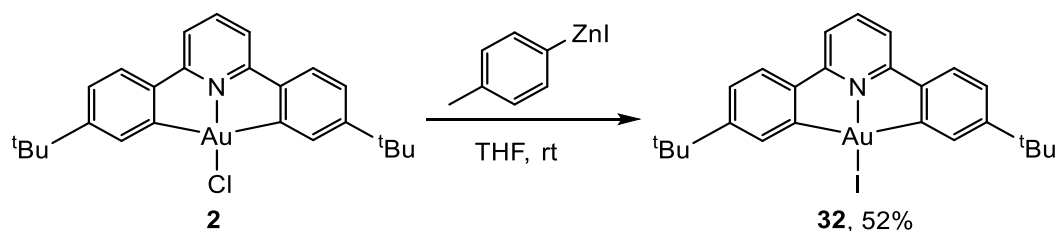
Transmetallation is a key step in transition metal catalysed cross-coupling reactions. In palladium-catalysed coupling reactions a wider range of transmetallation reagents are used to install a range of functionality. By comparison, the transmetallation of gold complexes is underexplored. Much of the attention so far focused on boronic acids, however new examples of transmetallation could lead to systems with a tolerance to different functionalities. With the current advances in gold catalysed coupling reactions it is important to understand this key step. There are few examples of transmetallation of gold species by organozinc halides and no studies with gold(III) species, therefore this work is going to probe their reactivity.

Another transmetallation reagent that has received significant amounts of interest are Si-B reagents due to the polarisation of the bond to give an electronegative silicon centre. Therefore, this chapter is going to investigate the potential of transmetallation of gold(III) species with Si-B compounds. There have been no reports of the reactivity of the Au–Si bonds in gold(III) complexes, this is presumably due to the decrease in stability of the complexes that have so far been synthesised. It is hoped that the C^NC pincer provides additional stability to probe the reactivity of complexes isolated.

Results and Discussion

4.5 Reaction of **2** and **1** with aryl zinc iodide

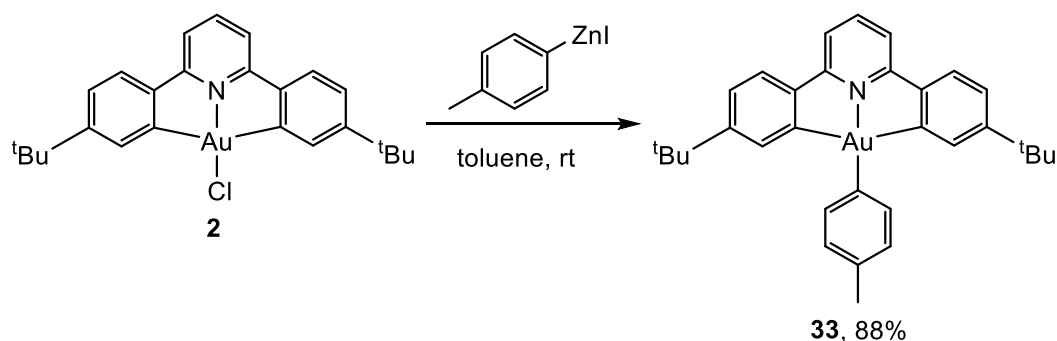
To investigate the reactivity of organozinc compounds with gold(III) complexes, two molar equivalents of 0.5 M THF solution *p*-Me-phenyl zinc iodide were added to a solution of **2** in tetrahydrofuran (Scheme 4.16). This resulted in the formation of complex **32**, where *p*-Me-phenyl zinc iodide acted as an iodide source. **32** was isolated as a solid in 52% yield and characterised by ^1H and ^{13}C NMR spectroscopy and elemental analysis.



Scheme 4.16. The reactivity of organozinc reagents with **2**.

The largest change in the ^1H NMR spectrum between **2** and **32** was the shift in the H^8 proton, in closest position to the halide. In **32** it is observed at $\delta = 8.52$ ppm (CD_2Cl_2) compared to the reported ^1H NMR spectrum of **2** where it is observed at $\delta = 7.77$ ppm ($\text{DMSO}-d_6$), it is important to note that there is a change in solvent.⁴⁰ Therefore, under these conditions **2** had undergone halide exchange instead of the desired transmetallation reaction.

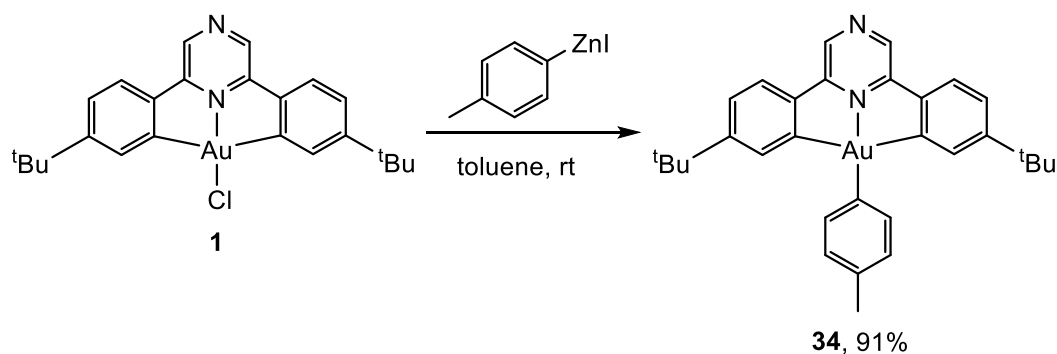
Repeating the reaction of two molar equivalents of *p*-Me-phenyl zinc iodide with **2**, but changing the solvent to toluene results in the formation of a transmetallation product **33** (Scheme 4.17). **33** was isolated as a solid in 88% yield and characterised by ^1H and ^{13}C NMR spectroscopy and elemental analysis. This reaction is also observed when toluene- d_8 was used as a solvent, therefore **33** is not the product of C–H activation of a solvent molecule.



Scheme 4.17. The reaction of an organozinc reagent with **2** to give **33**.

Therefore, *p*-Me-phenyl zinc iodide can be used in the transmetalation of an Au–Cl bond to form an C^NC gold(III) aryl complex. C^NC gold(III) aryl complexes have previously been synthesised in a two-step synthesis from **2**.⁸ The first step of this synthesis is the formation of a hydroxide species, which once isolated could be reacted with the desired boronic acid upon heating to 60 °C in toluene to give the gold(III) aryl. Previous cases of direct transmetalation of an Au–X bond (X = Cl, F) required forcing conditions.^{11, 12} Forcing conditions were used in the transmetalation of the Au–F bond, which was only compatible with electron-deficient fluoroaryl boronic acids (Scheme 4.4).¹² In addition, the gold(III) aryls formed directly from an Au–Cl bond required the use of a palladium catalyst. (Scheme 4.3).¹⁰ By comparison, these conditions are considerably more favourable.

Previously, the synthesis of gold(III) aryls from **1**, where a pyrazine is substituted for the pyridine, has proven to be more difficult as the corresponding hydroxide species cannot be formed. Therefore **1** was dissolved in toluene and reacted with two molar equivalents of *p*-Me-phenyl zinc iodide (Scheme 4.18). This reaction results in the formation of **34**, however the synthesis required a second purification step, where a solution of **34** in toluene was stirred with a water/alcohol mix to dissociate any ions bound to the pyrazine nitrogen. **34** was isolated in a 91 % yield and the ¹H and ¹³C NMR spectra confirmed its formation.



Scheme 4.18. The reaction of an organozinc reagent with **1** to give **34**.

The final ¹H NMR spectrum showed a small amount of an unidentified impurity (approximately 5 %). It is likely that these could be separated if this synthesis was to be widely applied. For example, in the synthesis of **1**, the final product is heated to 110 °C in DMSO to remove coordinated mercury ions.⁴¹

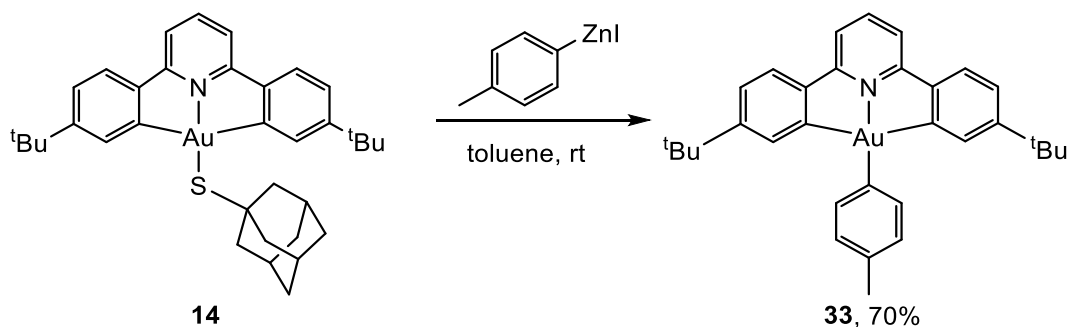
4.6 Reaction of **14** with aryl zinc iodide

Metal-sulfur bonds are typically considered strong bonds and the exposure of catalysts to sulfur containing species can result in catalyst poisoning.⁴² Despite this, the hard-soft acid-base description is sometimes used to describe metal complexes. Using this analogy, where

gold(III) is described as a hard acid and a thiolate as a soft base, one may expect the Au(III)–sulfur bonds, to be weaker than an Au(III)–O bond (two hard species). However, we have previously shown that the reaction of thiols with gold(III) phenolate complexes results in the formation of an Au–S bond (Section 3.13). The dissociation of Au–S bond in the diatomic AuS species has been experimentally determined as 308(5) kJ/mol,⁴³ higher than that of Au–O bonds in diatomic AuO species experimentally determined as 225 kJ/mol,⁴⁴ comparison of these values may be limited as they were obtained using different methods.

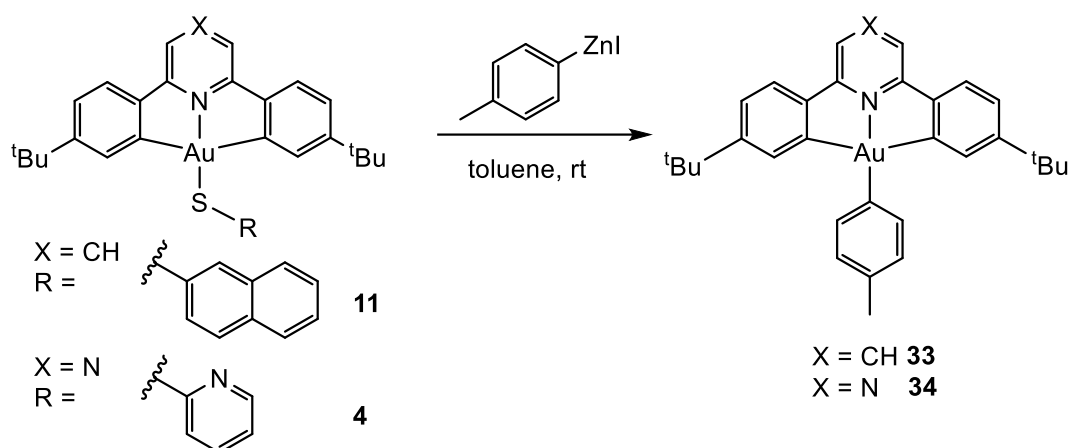
Therefore, further understanding of the nature of the Au–S bond would be advantageous. The (C[^]N[^]C)Au–SR complexes synthesised in Chapters Two and Three are stable to air and water, but the Au–S bond can be broken in the presence of a strong acid (HCl in section 3.9.3). As well as understanding the nature of the Au–S bond, it would be interesting to exchange an Au–S bond for a potentially more synthetically useful Au–C bond through transmetallation.

Following the success of the reactions of organozinc reagents with **1** and **2**, two molar equivalents of *p*-Me-phenyl zinc iodide were added to a solution of **14** in toluene (Scheme 4.19). The transmetallation product **33** was isolated as a solid in 70% yield. To the best of our knowledge, this is the first example of transmetallation of an Au–S bond.



Scheme 4.19. The reaction of an organozinc reagent with **14** to give **33**.

To investigate the range of gold(III) thiolate species that can be used in this reaction **11** and **4** were dissolved in toluene-*d*₈ and reacted with two molar equivalents of *p*-Me-phenyl zinc iodide (Scheme 4.20). This led to the formation of transmetallation products **33** and **34** respectively. Therefore, these reaction conditions are tolerant of alkyl, aryl and heterocycle thiolates.



Scheme 4.20. The reaction of gold(III) thiolates **11** and **4** with an organozinc reagent.

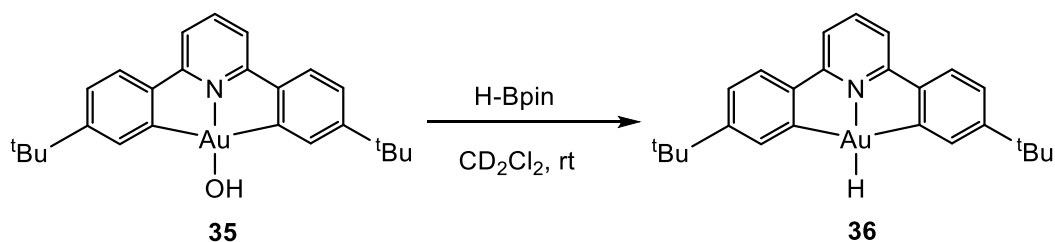
When the reactions in Scheme 4.19 and 4.20 were studied by *in situ* ^1H NMR spectroscopy, the spectrum of the finished reaction had no signals corresponding to the thiolate or formation of free thiol. Instead a black precipitate was observed; this could be because of formation of reduction products. The removal of the thiolate species with the zinc prevents the potential for reductive elimination from the gold(III) aryl species formed as seen in Chapter 3.

4.7 Reaction of **14** with boronic acids

Boronic acids have proved to be versatile transmetallation agents capable of the transmetallation of Au–O, Au–F and Au–Cl bonds. The reaction of **14** with 1.5 molar equivalents *p*-methoxyphenyl boronic acid in toluene at room temperature showed no change in the ^1H NMR spectrum over 24 hours. After heating the reaction for 60 °C for 48 hours there was still no change observed in the ^1H NMR spectrum. Therefore, boronic acids are unsuitable reagents for the transmetallation of Au–S bonds under these conditions.

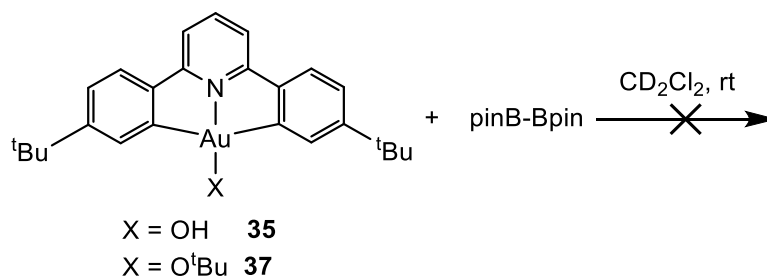
4.8 Reaction of Au–O bonds with boron reagents

Boron reagents are widely used in synthetic chemistry and boronic acids have previously been used in the transmetallation of an Au–O bond.^{8,14} Therefore, reactivity with gold(III) complexes containing an Au–O bonds with several boron based reagents were investigated. The reaction of the gold(III) hydroxide **35** with pinacolborane (H–Bpin) at room temperature resulted in the formation of a gold(III) hydride **36** (Scheme 4.21). The formation of the hydride is likely to be through transfer of the hydride from the pinacolborane and formation of a strong B–O bond in HO–Bpin. As there are several previously reported syntheses of **36**, this reaction was not investigated further.⁴⁵



Scheme 4.21. The reaction of **35** with H-Bpin.

Addition of bis(pinacolato)diborane to $(\text{C}^{\wedge}\text{N}^{\wedge}\text{C})\text{Au-OR}$ ($\text{R} = \text{H}$ and ${}^t\text{Bu}$) in a J Young NMR tube was monitored by ${}^1\text{H}$ and ${}^{11}\text{B}$ NMR spectroscopy, but no changes were observed (Scheme 4.22). Upon heating to $60\text{ }^\circ\text{C}$ there was still no change observed in the ${}^1\text{H}$ or ${}^{11}\text{B}$ NMR spectra. Therefore, despite the potential to form a strong B–O bond, the B–B bond is more stable than the B–H bond and formation of an Au–B bond was not favoured under these conditions.



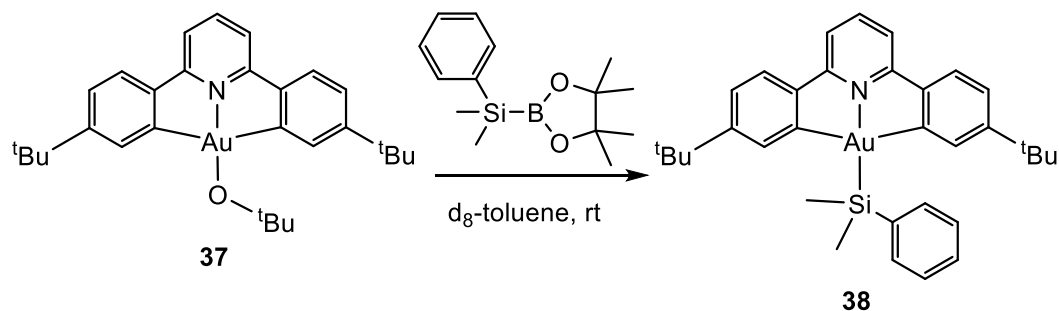
Scheme 4.22. The no reaction between either **35** or **37** with bis(pinacolato)diborane.

Previous reports of the reaction of bis(pinacolato)diborane with potassium *tert*-butoxide results in quaternarization one boron centre through the formation of a third B–O bond, which consequently alters the polarisation of the B–B bond.^{30b} These have been considered as mild sources of nucleophilic boron compared to the stronger boryls.⁴⁶ As these $\text{sp}^2\text{-sp}^3$ diboranes have been used as boron nucleophiles their reactivity with Au–O bonds was probed. The reaction of $(\text{C}^{\wedge}\text{N}^{\wedge}\text{C})\text{Au-OR}$ ($\text{R} = \text{H}$ and ${}^t\text{Bu}$) and $(\text{Bpin})_2$ in the presence of potassium *tert*-butoxide resulted the formation of the previously reported anionic boron species but this did not react further with the gold complex **37**.

4.9 Investigating the reaction of Au(III)-O bonds with $\text{Me}_2\text{PhSi-Bpin}$

Dimethylphenylsilyl boronic pinacol ester ($\text{Me}_2\text{PhSi-Bpin}$) is commercially available, and previous reports of its transmetallation of M–O bonds made it an interesting reagent to investigate with this system.²⁹ The transmetallation of gold(III) complexes by boronic acids had found **35** to be a successful starting point.⁸ Therefore, this was the first starting material chosen. The reaction of **35** in toluene- d_8 with two molar equivalents of $\text{Me}_2\text{PhSi-Bpin}$ was monitored by ${}^1\text{H}$ NMR spectroscopy but unfortunately gave a complicated mixture of products

as well as decomposition of the gold(III) species. The reaction of (C[^]N[^]C)Au–(OAc^F) in toluene-*d*₈ with two molar equivalents of Me₂PhSi-Bpin also resulted in decomposition. However, the reaction of (C[^]N[^]C)Au–(O^tBu) (**37**) in toluene-*d*₈ with two molar equivalents of Me₂PhSi-Bpin cleanly formed a single product over 24 hours (Scheme 4.23). The structure of **38** was confirmed by ¹H and ¹³C NMR spectroscopy.



Scheme 4.23. The synthesis of **38**.

¹H NOESY NMR revealed the presence of spatial interactions between the methyl groups on the silicon (H¹⁴) and both those of the C[^]N[^]C pincer ligand (H⁸) and the *o*-phenyl protons (H¹¹) (Figure 4.1).

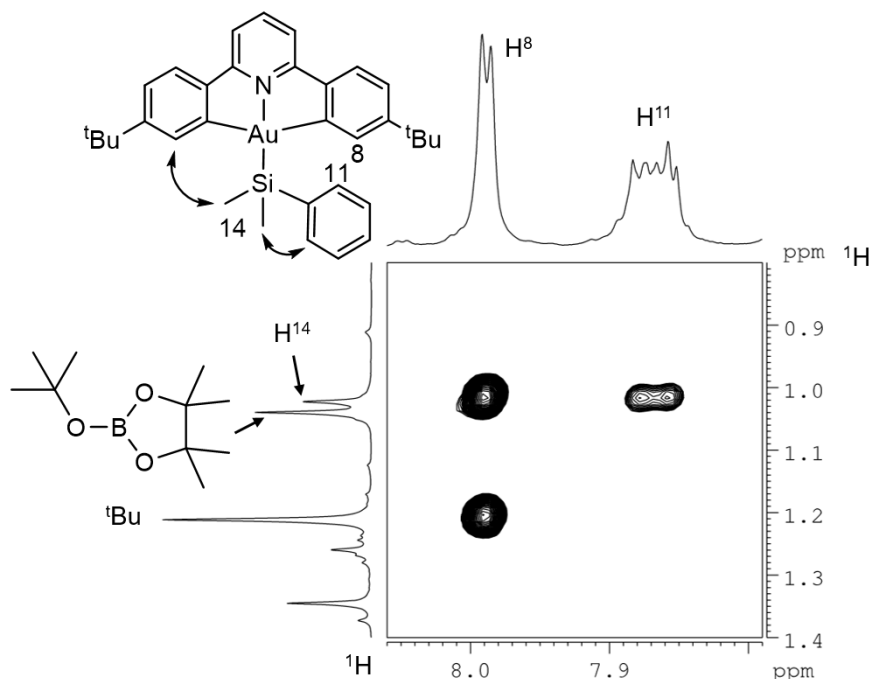


Figure 4.1. ¹H NOESY spectrum showing spatial interactions between H⁸ and the functional groups on the silicon in complex **38** (C₆D₅CD₃, 25 °C).

Diffusion NMR using PGSE (pulse gradient spin echo) NMR experiments confirmed that all signals ascribed to **38** diffused at the same rate, indicating that an Au–Si bond had been

formed. The signals corresponding to the solvent, unreacted Me₂PhSi–Bpin and ¹BuO–Bpin all diffused at faster rates. Therefore Me₂PhSi–Bpin is a suitable reagent in the transmetallation of Au–O^tBu species to form a gold(III) silyl complex.

Optimisation of this synthesis was not as straight forward as initially expected. In the synthesis in Scheme 4.23, **37** was formed *in situ* by reacting **2** with one molar equivalent of potassium *tert*-butoxide. However, isolating a pure sample of **37** was unsuccessful despite its synthesis being reported.⁴⁷ If a sample of **37** in 90 % purity was reacted with Me₂PhSi–Bpin a mixture of decomposition products was observed and therefore was unsuccessful in the synthesis of **38**. There was no reaction upon addition of two molar equivalents of Me₂PhSi–Bpin to **2** in CD₂Cl₂ over 2 days at room temperature. Addition of potassium *tert*-butoxide to a mixture of **2** and Me₂PhSi–Bpin also resulted in the formation of decomposition products.

The optimised conditions developed required **2** and 1.5 – 2.0 molar equivalents of potassium *tert*-butoxide to be suspended in toluene. Heating to 60 °C and shaking this suspension resulted in the formation of a clear and bright-yellow solution. The ¹H NMR spectrum confirmed the conversion of **2** to **37** and the presence of excess potassium *tert*-butoxide. To this solution was added 1 – 2 molar equivalents of Me₂PhSi–Bpin and the reaction was left at room temperature until complete conversion after 24 hours. The reaction did not appear to improve greatly by increasing the molar equivalents of Me₂PhSi–Bpin to 5. However, **37** converted to **38** more cleanly if there was an excess of potassium *tert*-butoxide present. Interestingly, the excess potassium *tert*-butoxide observed in the initial ¹H NMR spectrum of **37** was immediately consumed upon addition of Me₂PhSi–Bpin. This indicates that transmetallation is aided by the presence of a base.

This synthesis differs from previous synthetic methodologies used to make gold silicon species, which have used lithiation of the silane or oxidative addition of an Si–Si bond. The reaction conditions used here are much milder and proceed at room temperature.

Decomposition was observed upon exposing **38** to air. In addition, filtering **38** without drying the filter overnight resulted in decomposition, indicating that **38** is water sensitive. The Au–Si bond is therefore less stable than Au–C and Au–S bonds which are both stable to atmospheric conditions. The weaker Au–Si bond may also be able to react with other substrates, potentially through expanding the coordination sphere of silicon, which is not possible for gold(III).

4.9.1 Initial experiments into insertion reactions

The previously isolated gold(I) silicon species were capable on inserting alkynes into the Au–Si bond. Initial studies of the reactivity of **38** with alkynes used an unactivated alkyne (2-butyne) and an activated alkyne (dimethyl acetylenedicarboxylate).

The samples of **38** were filtered prior to addition of the alkynes to remove any excess solid potassium *tert*-butoxide due to previous reports of the reactivity of Me₂PhSi–Bpin with alkenes in the presence of potassium *tert*-butoxide.⁴⁸ Filtration was often a cause of decomposition of **38**, presumably due to small quantities of water in the filter. Addition of an excess of the two alkynes (5 to 10 molar equivalents) to solution of **38** in toluene was monitored by ¹H NMR spectroscopy at room temperature. Over one month no changes were observed in the ¹H NMR spectrum, therefore we observed no insertion reactivity.

Conclusion

We have shown that the organozinc reagent *p*-Me-phenyl zinc iodide can be used in the transmetallation of Au–Cl and Au–S bonds under the conditions described above. This reduces the number of steps in the synthesis of gold(III) aryls compared to previous reports. By varying the reaction conditions either halide exchange or transmetallation products were isolated cleanly. It has been previously discussed that the transmetallation of alkyl groups to gold centres has been under-explored.¹ Therefore, extending this study to other commercially available organozinc reagents could result in new functionalised species and would explore the potential scope of this reaction.

We have also shown that it is possible to use Si–B compounds in the transmetallation of gold(III) alkoxides. This is the first report of an Au–Si bond that is stable at room temperature without being part of a chelate ligand. The water-sensitivity of these Au–Si complexes resulted in frequent decomposition and limited the reactivity studies. Further investigations into the reactivity of **38** could be of interest. Potentially synthesising C[^]N[^]C gold silyl complexes with bulkier substituents might stabilise the Au–Si bond, as previously demonstrated by Bourissou *et al.*. The possibility using more forcing conditions in the insertion reactions or investigating the insertion other unsaturated substrates such as isocyanides and carbon monoxide into Au(III)–Si bonds may also be of interest.

References

- (1) Joost, M.; Amgoune, A.; Bourissou, D. *Angew. Chem.-Int. Edit.* **2015**, *54*, 15022.

- (2) (a) Hirner, J. J.; Shi, Y. L.; Blum, S. A. *Acc. Chem. Res.* **2011**, *44*, 603. (b) Contel, M.; Stol, M.; Casado, M. A.; van Klink, G. P. M.; Ellis, D. D.; Spek, A. L.; van Koten, G. *Organometallics* **2002**, *21*, 4556.
- (3) Perez-Temprano, M. H.; Casares, J. A.; Espinet, P. *Chem.-Eur. J.* **2012**, *18*, 1864.
- (4) Miyaura, N. *J. Organomet. Chem.* **2002**, *653*, 54.
- (5) (a) Miyaura, N.; Yanagi, T.; Suzuki, A. *Synth. Commun.* **1981**, *11*, 513. (b) Miyaura, N.; Suzuki, A. *Chem. Rev.* **1995**, *95*, 2457. (c) Suzuki, A. *J. Organomet. Chem.* **1999**, *576*, 147.
- (6) (a) Partyka, D. V.; Zeller, M.; Hunter, A. D.; Gray, T. G. *Angew. Chem.-Int. Edit.* **2006**, *45*, 8188. (b) Partyka, D. V.; Zeller, M.; Hunter, A. D.; Gray, T. G. *Inorg. Chem.* **2012**, *51*, 8394.
- (7) Dupuy, S.; Crawford, L.; Buhl, M.; Slawin, A. M. Z.; Nolan, S. P. *Adv. Synth. Catal.* **2012**, *354*, 2380.
- (8) Rosca, D. A.; Smith, D. A.; Bochmann, M. *Chem. Commun.* **2012**, *48*, 7247.
- (9) To, W. P.; Zhou, D. L.; Tong, G. S. M.; Cheng, G.; Yang, C.; Che, C. M. *Angew. Chem.-Int. Edit.* **2017**, *56*, 14036.
- (10) Tang, M. C.; Lee, C. H.; Lai, S. L.; Ng, M.; Chan, M. Y.; Yam, V. W. W. *J. Am. Chem. Soc.* **2017**, *139*, 9341.
- (11) Hofer, M.; Gomez-Bengoa, E.; Nevado, C. *Organometallics* **2014**, *33*, 1328.
- (12) Kumar, R.; Linden, A.; Nevado, C. *J. Am. Chem. Soc.* **2016**, *138*, 13790.
- (13) Wu, Q.; Du, C. L.; Huang, Y. M.; Liu, X. Y.; Long, Z.; Song, F. J.; You, J. S. *Chem. Sci.* **2015**, *6*, 288.
- (14) Hofer, M.; Genoux, A.; Kumar, R.; Nevado, C. *Angew. Chem.-Int. Edit.* **2017**, *56*, 1021.
- (15) Levin, M. D.; Toste, F. D. *Angew. Chem.-Int. Edit.* **2014**, *53*, 6211.
- (16) Qian, D. Y.; Zhang, J. L. *Beilstein J. Org. Chem.* **2011**, *7*, 808.
- (17) (a) Knochel, P.; Perea, J. J. A.; Jones, P. *Tetrahedron* **1998**, *54*, 8275. (b) Pu, L.; Yu, H. B. *Chem. Rev.* **2001**, *101*, 757.
- (18) Negishi, E. I. *Acc. Chem. Res.* **1982**, *15*, 340.
- (19) (a) Tokuyama, H.; Yokoshima, S.; Yamashita, T.; Fukuyama, T. *Tetrahedron Lett.* **1998**, *39*, 3189. (b) Miyazaki, T.; Han-ya, Y.; Tokuyama, H.; Fukuyama, T. *Synlett* **2004**, 477.
- (20) Armstrong, D. R.; Baillie, S. E.; Blair, V. L.; Chabloz, N. G.; Diez, J.; Garcia-Alvarez, J.; Kennedy, A. R.; Robertson, S. D.; Hevia, E. *Chem. Sci.* **2013**, *4*, 4259.
- (21) Armstrong, D.; Taullaj, F.; Singh, K.; Mirabi, B.; Lough, A. J.; Fekl, U. *Dalton Trans.* **2017**, *46*, 6212.

- (22) (a) Denmark, S. E.; Regen, C. S. *Acc. Chem. Res.* **2008**, *41*, 1486. (b) Nakao, Y.; Hiyama, T. *Chem. Soc. Rev.* **2011**, *40*, 4893.
- (23) Hatanaka, Y.; Hiyama, T. *J. Org. Chem.* **1988**, *53*, 918.
- (24) Dupuy, S.; Slawin, A. M. Z.; Nolan, S. P. *Chem.-Eur. J.* **2012**, *18*, 14923.
- (25) (a) Ball, L. T.; Green, M.; Lloyd-Jones, G. C.; Russell, C. A. *Org. Lett.* **2010**, *12*, 4724. (b) Ball, L. T.; Lloyd-Jones, G. C.; Russell, C. A. *Science* **2012**, *337*, 1644. (c) Ball, L. T.; Lloyd-Jones, G. C.; Russell, C. A. *J. Am. Chem. Soc.* **2014**, *136*, 254.
- (26) (a) Stille, J. K. *Angew. Chem.-Int. Edit. Engl.* **1986**, *25*, 508. (b) Espinet, P.; Echavarren, A. M. *Angew. Chem.-Int. Edit.* **2004**, *43*, 4704.
- (27) Chen, Y. F.; Chen, M.; Liu, Y. H. *Angew. Chem.-Int. Edit.* **2012**, *51*, 6181.
- (28) Shi, Y. L.; Peterson, S. M.; Haberaecker, W. W.; Blum, S. A. *J. Am. Chem. Soc.* **2008**, *130*, 2168.
- (29) Oestreich, M.; Hartmann, E.; Mewald, M. *Chem. Rev.* **2013**, *113*, 402.
- (30) (a) Neeve, E. C.; Geier, S. J.; Mkhaliid, I. A. I.; Westcott, S. A.; Marder, T. B. *Chem. Rev.* **2016**, *116*, 9091. (b) Dewhurst, R. D.; Neeve, E. C.; Braunschweig, H.; Marder, T. B. *Chem. Commun.* **2015**, *51*, 9594.
- (31) Ohmura, T.; Suginome, M. *Bull. Chem. Soc. Jpn.* **2009**, *82*, 29.
- (32) (a) Suginome, M.; Nakamura, H.; Ito, Y. *Chem. Commun.* **1996**, 2777. (b) Suginome, M.; Matsuda, T.; Nakamura, H.; Ito, Y. *Tetrahedron* **1999**, *55*, 8787. (c) Onozawa, S.; Hatanaka, Y.; Tanaka, M. *Chem. Commun.* **1997**, 1229. (d) Sagawa, T.; Asano, Y.; Ozawa, F. *Organometallics* **2002**, *21*, 5879. (e) Durieux, G.; Gerdin, M.; Moberg, C.; Jutand, A. *Eur. J. Inorg. Chem.* **2008**, 4236. (f) Ansell, M. B.; Spencer, J.; Navarro, O. *ACS Catal.* **2016**, *6*, 2192.
- (33) Kawachi, A.; Minamimoto, T.; Tamao, K. *Chem. Lett.* **2001**, 1216.
- (34) (a) Kleeberg, C.; Cheung, M. S.; Lin, Z. Y.; Marder, T. B. *J. Am. Chem. Soc.* **2011**, *133*, 19060. (b) Plotzitzka, J.; Kleeberg, C. *Inorg. Chem.* **2016**, *55*, 4813.
- (35) (a) O'Brien, J. M.; Hoveyda, A. H. *J. Am. Chem. Soc.* **2011**, *133*, 7712. (b) Oshima, K.; Ohmura, T.; Suginome, M. *Chem. Commun.* **2012**, *48*, 8571.
- (36) (a) Meyer, J.; Willnecker, J.; Schubert, U. *Chem. Berichte* **1989**, *122*, 223. (b) Oroz, M. M.; Schier, A.; Schmidbaur, H. *Z.Naturforsch.(B)* **1999**, *54*, 26.
- (37) Joost, M.; Gualco, P.; Mallet-Ladeira, S.; Amgoune, A.; Bourissou, D. *Angew. Chem.-Int. Edit.* **2013**, *52*, 7160.
- (38) Joost, M.; Estevez, L.; Mallet-Ladeira, S.; Miqueu, K.; Amgoune, A.; Bourissou, D. *J. Am. Chem. Soc.* **2014**, *136*, 10373.
- (39) (a) Gualco, P.; Ladeira, S.; Miqueu, K.; Amgoune, A.; Bourissou, D. *Angew. Chem.-Int. Edit.* **2011**, *50*, 8320. (b) Gualco, P.; Ladeira, S.; Miqueu, K.; Amgoune, A.; Bourissou, D. *Organometallics* **2012**, *31*, 6001. (c) Joost, M.; Gualco, P.; Coppel, Y.;

- Miqueu, K.; Kefalidis, C. E.; Maron, L.; Amgoune, A.; Bourissou, D. *Angew. Chem.-Int. Edit.* **2014**, *53*, 747.
- (40) Wong, K. M. C.; Hung, L. L.; Lam, W. H.; Zhu, N. Y.; Yam, V. W. W. *J. Am. Chem. Soc.* **2007**, *129*, 4350.
- (41) Fernandez-Cestau, J.; Bertrand, B.; Blaya, M.; Jones, G. A.; Penfold, T. J.; Bochmann, M. *Chem. Commun.* **2015**, *51*, 16629.
- (42) Beletskaya, I. P.; Ananikov, V. P. *Chem. Rev.* **2011**, *111*, 1596.
- (43) Kokkin, D. L.; Zhang, R. H.; Steimle, T. C.; Wyse, I. A.; Pearlman, B. W.; Varberg, T. D. *J. Phys. Chem. A* **2015**, *119*, 11659.
- (44) Schwerdtfeger, P.; Dolg, M.; Schwarz, W. H. E.; Bowmaker, G. A.; Boyd, P. D. W. *J. Chem. Phys.* **1989**, *91*, 1762.
- (45) (a) Rosca, D. A.; Smith, D. A.; Hughes, D. L.; Bochmann, M. *Angew. Chem.-Int. Edit.* **2012**, *51*, 10643. (b) Pintus, A.; Rocchigiani, L.; Fernandez-Cestau, J.; Budzelaar, P. H. M.; Bochmann, M. *Angew. Chem.-Int. Edit.* **2016**, *55*, 12321.
- (46) Marder, T. B. *Science* **2006**, *314*, 69.
- (47) Chambrier, I.; Rosca, D. A.; Fernandez-Cestau, J.; Hughes, D. L.; Budzelaar, P. H. M.; Bochmann, M. *Organometallics* **2017**, *36*, 1358.
- (48) Ito, H.; Horita, Y.; Yamamoto, E. *Chem. Commun.* **2012**, *48*, 8006.

Chapter Five:

Investigating effects of the C^NC ligand upon cytotoxicity of gold(III) NHC complexes

Introduction

Recent interest in the development of gold(III) based anticancer agents has its origins in the success of cisplatin, a widely used platinum(II) anticancer agent, isoelectronic with gold(III).

5.1 Platinum based anticancer agents

The break through discovery of cis-diamminedichloroplatinum(II) (cisplatin) in 1965 helped establish a new area of anticancer drugs based on metal complexes.¹ Cisplatin has been in clinical use since 1979 and is still used today in the treatment of testicular, ovarian, lung and breast cancers.² Cisplatin is a neutral, square-planar, platinum(II) complex (left, Figure 5.1); the corresponding trans isomer is less active.³ Following its success, further square-planar platinum(II) complexes have been developed and entered clinical use including carboplatin⁴ and oxaliplatin⁵ (middle and right, Figure 5.1).

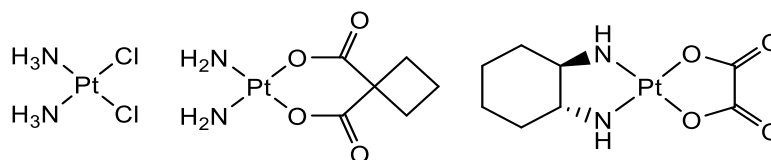


Figure 5.1. Left to right: cisplatin, carboplatin and oxaliplatin.

Understanding the mode of action of a drug is complex and many years of investigations have led to the elucidation cisplatin's mode of action (simplified scheme in Figure 5.52).^{3,6} The active species has been identified as $[\text{Pt}(\text{NH}_3)_2\text{Cl}(\text{OH}_2)]^+$, which is formed through partial hydrolysis of cisplatin. This compound is proposed to bind to nitrogen donors of purine bases (adenine and guanine) in DNA, which distorts the DNA double helix structure. The binding occurs through displacement of a water molecule in the active species. The distorted DNA structure that is formed is recognised by DNA repair enzymes and leads to cell apoptosis (cell death). The active species ($[\text{Pt}(\text{NH}_3)_2\text{Cl}(\text{OH}_2)]^+$) can also be deactivated by the formation of Pt-S bonds with glutathione (GSH), which is often over-expressed in cancerous cells.

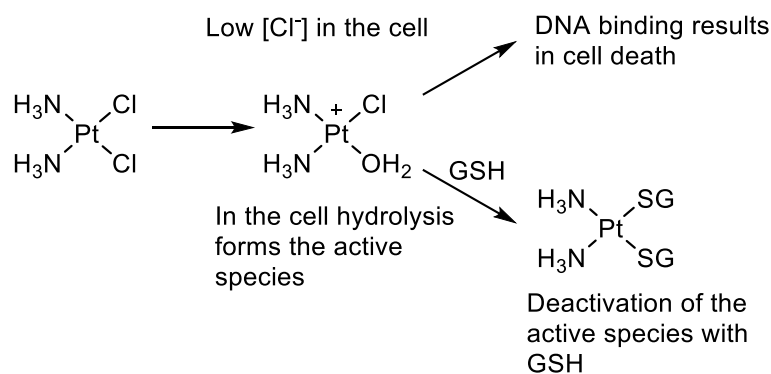


Figure 5.2. A simplified mode of action of cisplatin.

Although cisplatin can be a very powerful therapeutic agent, there are several drawbacks to its use as a chemotherapy drug, such as strong side effects including: vomiting and damage to the nervous system and kidneys, and acquired resistance (when it enters the cell in sub-toxic concentrations).² In an attempt to overcome the side effects and make systems that target cancerous cell specifically, interest has turned to more complex platinum systems as well as new metallodrugs based on other transition metals.⁷ This includes recent interest in gold(I) and gold(III) anticancer agents.⁸ This chapter focuses on gold(III) systems, with particular interest in gold(III) NHC complexes supported by C[^]N[^]C pincer ligands.

Despite its drawbacks, cisplatin is still the benchmark to which all metallodrugs are compared. For a metallodrug to be considered as a viable option it must be more active against and specific than cisplatin. The anticancer activity is quantified by an IC_{50} value which is specific for each complex and cell line. It is the concentration required to inhibit 50% of the cells from growing, therefore a successful anticancer drug would have a low IC_{50} for cancerous cell lines and a high IC_{50} for the noncancerous cell lines.

5.2 Cyclometallated gold(III) complexes as anticancer agents

Significant initial interest in gold(III) anticancer agents was based on them being isoelectronic to platinum(II) complexes, both are d^8 square planar complexes.⁸ In physiological conditions thiols are thought to reduce gold(III) complexes, however complexes containing Au-C bonds are more stable to reduction to gold(I) and gold(0) by cellular reductants such as GSH and ascorbic acid.⁹ Various cyclometallated complexes, employing a range of ligand systems including: (C[^]N), (C[^]N[^]N) and (C[^]N[^]C), have been reported to show promising anticancer properties.⁸⁻¹⁰ Figure 5.3 depicts a representative selection of gold(III) complexes that have been investigated as anticancer agents. Complex **C** is one of the initial gold(III) complexes to exhibit anticancer properties.¹¹ The complex showed high cytotoxicity against several cancerous cell lines and further analogues were synthesised through chloride substitution that

also showed anticancer properties. **C** had poor solubility in aqueous media, but solubility was increased upon chloride substitution. The substitution reactions of the chloride ligand by N, S and O donors is reminiscent of cisplatin's reactivity with water.¹¹⁻¹² The anticancer properties were proposed to be caused by the inhibition of the enzyme thioredoxin reductase (TrxR).¹³

Complex **D**, supported by a C^N ligand, showed anticancer properties against several cancer cell lines, with slightly lower activity than cisplatin.¹⁴ The cationic complex **E** stabilised by a tridentate N^NC, showed similar anticancer properties, but also activity against several cisplatin resistant cell lines.¹⁴⁻¹⁵ Both **D** and **E** were resistant to reduction by cellular thiols and investigations into their interactions with biological processes showed inhibition of TrxR.¹⁶

The anticancer properties of **F** showed greater inhibition of the growth of cancer cells over health cells.^{9,17} This complex was water soluble, which is an advantageous property for an anticancer agent. In addition, studies into its reactivity with GSH showed adduct formation. It was suggested that either **F** or its GSH adduct damaged the endoplasmic reticulum leading to cell death. Complex **G** uses the same supporting ligand but a different hydrophilic ligand, dithiocarbonate.¹⁸ Both **F** and **G** were designed as cationic complexes that combine both lipophilic and hydrophilic ligands to increase both water solubility and cell uptake.^{10a,19} Complex **G** is considerably more toxic to cancer cells than to healthy cells and showed good selectivity. It was unreactive towards GSH and was shown to target deubiquitinases, which are involved in many intercellular processes.

Complex **H** showed anticancer activity but its analogues, synthesised through chloride substitution to give thiosalicylate, dithiocarbamates and catecholate complexes, showed higher activity than **H** against the cell lines tested.²⁰ Interestingly, selectivity between cancerous and healthy cells is observed for the cationic dithiocarbamate-substituted complexes. When probing intracellular targets, this group of complexes were shown to induce reactive oxygen species (ROS) production.

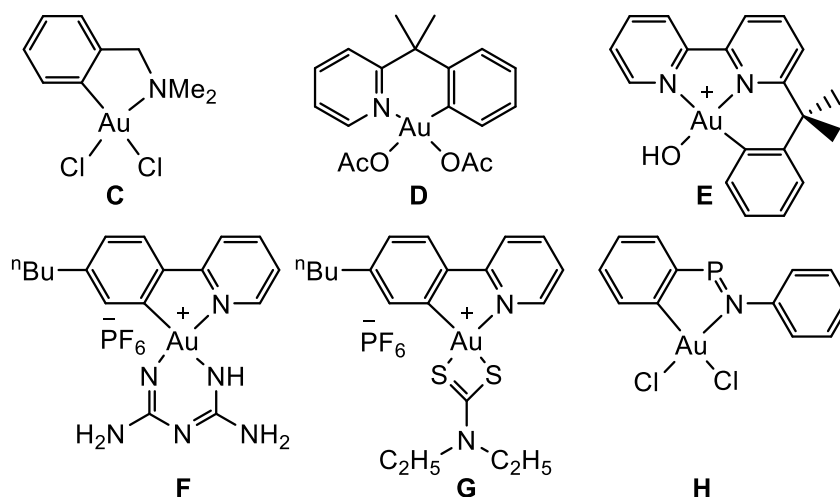


Figure 5.3. Examples of cyclometallated gold(III) complexes with anti-cancer properties.

With this range of complexes several different potential cellular targets have been suggested and investigated. Interestingly they all differ from the targets of cisplatin, which they were initially synthesised to mimic. Whereas cisplatin predominantly causes cell death through DNA binding these complexes have been shown to induce ROS production,^{20d} interact with the endoplasmic reticulum,¹⁷ or with proteins²¹ including disulfide reductases⁹ and deubiquitinases.¹⁸ It is important to note that the identification of an interaction with a cellular target does not confirm that specific interaction is responsible for cell death.

5.3 Gold(III) carbene complexes as anticancer agents

Complexes of N-heterocyclic carbenes (NHCs) have been identified as promising anticancer agents.²² The strong M-NHC σ bonds are often stable to physiological conditions and the structure of the carbenes are easily synthetically modulated.^{22a}

Several gold(III) NHC complexes studied for their anticancer properties are shown in Figure 5.4. Complex **I**, bearing one NHC group and three chlorides, inhibits cell growth of several cancerous cell lines but was less active than cisplatin.²³ Interestingly, its gold(I) analogue (with one NHC and one chloride ligand) is a more potent anticancer agent. It was proposed that the gold(III) complex (**I**) was likely to be reduced by cellular thiols, limiting its activity. Complex **J**, containing a second NHC, has lower IC_{50} values than both **I** and cisplatin.²⁴ The increase in inhibition of proliferation was linked to an increase in lipophilicity. Again, the gold(I) analogue was more active than **J** and it was proposed that **J** was reduced by cellular thiols.

The cationic complex **K** was shown to have low IC_{50} values against cancerous cells and was more active than cisplatin.²⁵ It was proposed that the active species resulted from dissociation of one NHC ligand. Cationic complexes using these ligands were two orders of magnitude

more active than neutral species, this was linked to an increased lipophilicity of two NHCs. Once again, the gold(I) analogue bearing two NHC ligands showed high activity, almost identical to **K**. This could indicate that the active species is a gold(I) complex, however the potential activity with reductants, such as cellular thiols, was not discussed.

The N[^]N[^]N based gold(III) NHC complexes **L** and **M** were designed to be reduced under physiological conditions to form a gold(I) NHC complex and release highly fluorescent 2,6-bis(imidazol-2-yl)pyridine and 2,6-bis(benzimidazol-2-yl)pyridine ligands.²⁶ Reactions of these complexes with glutathione (GSH) did reduce the complexes, releasing the fluorescent moiety, [GSAu-NHC] and GSSG. Cystine based compounds were also able to trigger reduction but ascorbic acid was insufficiently reducing. In addition, variation of the NHC R groups altered the water solubility (pharmaceutical agents are ideally water soluble), gold(III) NHC complexes with methyl substituents were water soluble, but the complexes with longer alkyl chains were insoluble. Anticancer studies showed suppression of tumour growth, with the gold(I) NHC presumed to be the active species formed *in situ*, therefore these complexes are both fluorescent probes and anti-cancer agents.

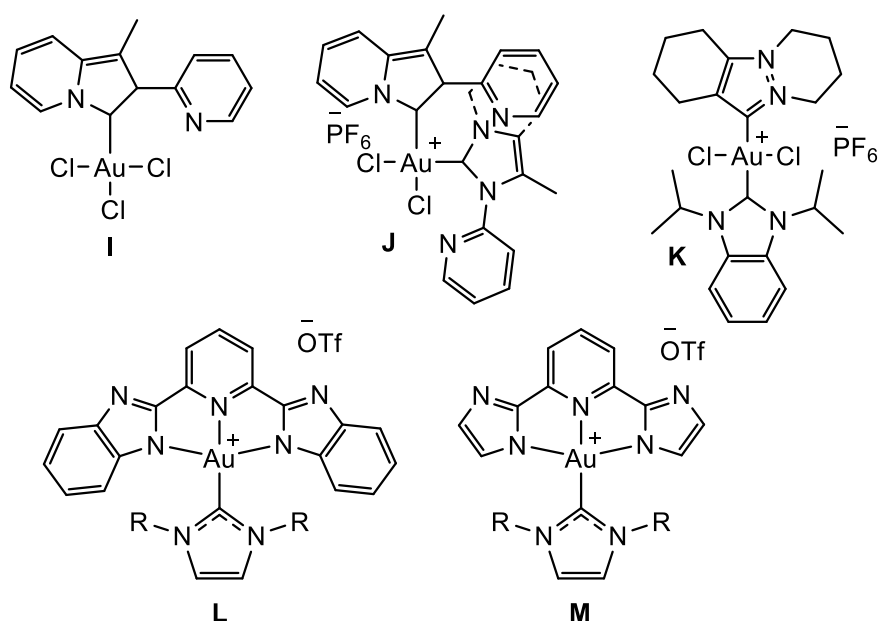


Figure 5.4. Gold(III) NHC complexes.

Many of these gold(III) NHC complexes were proposed to be reduced to gold(I) species by cellular reductants, which were the active species. In some systems the gold(I) was independently synthesised and these analogues were more active than the corresponding gold(III) NHC complexes. Therefore, understanding the reactivity of these gold(III) NHCs with cellular reductants, such as thiols, is important.

5.4 (C[^]N[^]C)gold(III) NHC complexes as anticancer agents

The C[^]N[^]C pincer system has been widely used for a broad range of applications due to its stabilisation of gold(III). Through alteration of X in (C[^]N[^]C)Au-X, a plethora of different complexes including phosphines,²⁷ pyridines,²⁷ acetylides²⁸ and thiolates²⁸ have been synthesised and tested as anticancer agents. A study into the potential anticancer properties of (C[^]N[^]C)Au-SPh demonstrated that it was not an active anticancer agent.²⁸

While the gold(III) NHC complexes in Section 5.3 were vulnerable to reduction, the C[^]N[^]C pincer allows access to stable NHC complexes. Initial studies into cationic gold(III) NHC complexes used **N** (Figure 5.5).²⁹ This complex was particularly potent, with sub-micromolar IC₅₀ values against several cancerous cell lines that were lower than cisplatin and active against cisplatin-resistant cell lines.^{29b,30} Interactions with DNA were observed, this was proposed to be through intercalation. It was also shown to poison topoisomerase I, an enzyme that unwinds DNA. Due to its high activity in vitro, in vivo studies in mice were carried out and showed suppression of tumour growth without causing weight loss or death of the mouse.

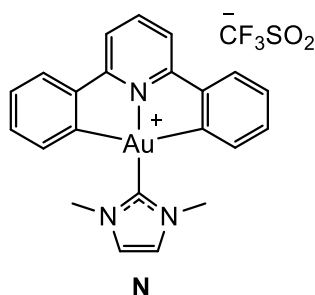


Figure 5.5. A C[^]N[^]C gold(III) NHC complex.

Further alterations on this lead complex looked at changing both the pincer ligand and the NHC. Altering the length of the alkyl groups attached to the nitrogen in the NHC showed that butyl groups had the highest activity and selectivity for inhibiting growth of cancer cells over healthy cells, while increasing the length further decreased the activity (left, Figure 5.6).³¹ An NHC linking two gold(III) pincer complexes was shown to be less toxic than **N**.^{29b} Altering the C[^]N[^]C pincer ligand resulted in higher IC₅₀ values than **N**, reducing the toxicity (right, Figure 5.6).^{29b}

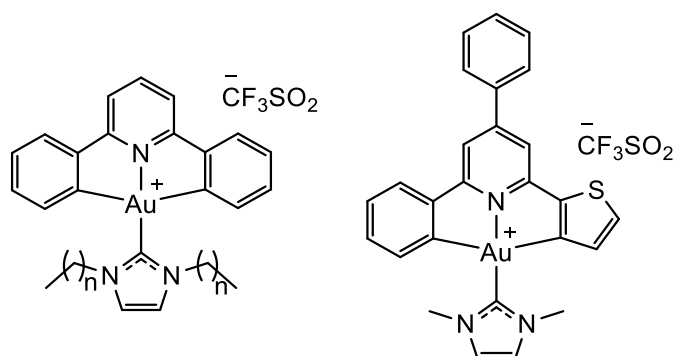


Figure 5.6. Further C^NC gold(III) NHC complexes.

To understand how the C^NC gold(III) NHC complexes target cellular mechanisms, two complexes were developed as probes (Figure 5.7).³¹ These complexes contain two separate functionalities, one photoactive and the other able to undergo click chemistry, while maintaining the basic scaffold of the C^NC gold(III) NHC complexes. Neither probe complex had an adverse effect on the bioactivity compared to the complexes they were modelling, they were both potent anticancer agents. The probes were suitable for use in both *in vivo* and *in vitro* studies. They showed that gold(III) NHCs bind to six different proteins, which had previously been identified as potential anticancer targets.

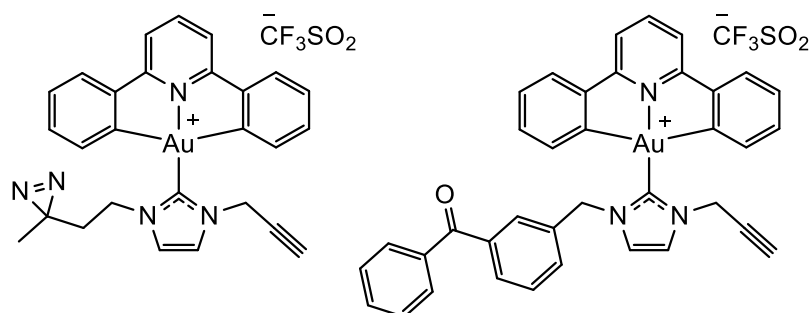


Figure 5.7. C^NC gold(III) NHC probe complexes.

The C^NC system was further altered through substitution of the central pyridine for a pyrazine and addition of *tert*-butyl groups. Two NHC complexes (**41** and **42**) using this ligand system showed anticancer properties (Figure 5.8).²⁸ Further alterations allowed investigations into the effects the substituent and the charge of the complexes upon the anticancer properties.

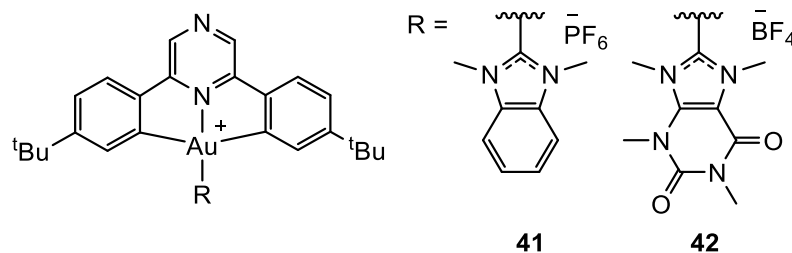


Figure 5.8. Pyrazine based C^NC gold(III) NHC complexes.

In vitro antiproliferative studies using human promyelocytic leukaemia (HL60) cells showed cell proliferation was inhibited by **41** and **42** at 10 μM concentration of complex. IC_{50} values were determined for a range of cell lines including HL60 (Human Leukaemia), MCF-7 (Human Breast Adenocarcinoma), A549 (Human Lung Adenocarcinoma Epithelial) and for comparison, healthy cells MRC-5 (Human Fetal Lung Fibroblast). Low IC_{50} values were observed for **41** against all cell lines, including healthy and cancerous, this lack of selectivity is undesirable. **41** had lower IC_{50} values than cisplatin, showing an increase in toxicity especially against cisplatin resistant cell lines. There was a difference in activity between **41** and **42**, with **41** being the more active, which was proposed to result from a higher cellular uptake of **41**. This was proposed to result from polarity differences because **42** is more hydrophilic than **41**.

Investigations into interactions with potential cellular mechanisms showed that a mixture of **41** and GSH did not react over 72 hours. This is the typical experiment time for the anticancer studies, indicating that this is not a deactivating pathway. **41** and **42** were shown to stabilise secondary DNA structures, it was proposed that both the π system and cation are required for DNA stabilisation. The final cellular target investigated was the inhibition of MDM2–p53 interaction. Disruption of the binding of MDM2 with p53, a protein that inhibits tumour growth, has been identified as a promising anticancer target. A strong interaction between **41** and MDM2 was observed, specifically with the hydrophobic area. Due to the interaction of **41** with intracellular targets it was identified as a promising lead molecule for future development of gold(III) anticancer agents.

Subsequently, C^NC stabilised gold(III) acyclic carbene complexes decorated with amino acid derivatives were developed (Figure 5.9).³² Investigations into their anticancer properties showed high activity against cancerous cells with IC_{50} values calculated for the most potent compounds for cell lines including HL60, MCF-7, A549, HCT-116 (colon), MDA-MB-231 (breast adenocarcinoma) and compared to healthy cells (MRC-5). The overall activity was similar to **41**, the selectivity for antiproliferation towards cancerous cells over healthy cells was still poor, though marginally more selective.

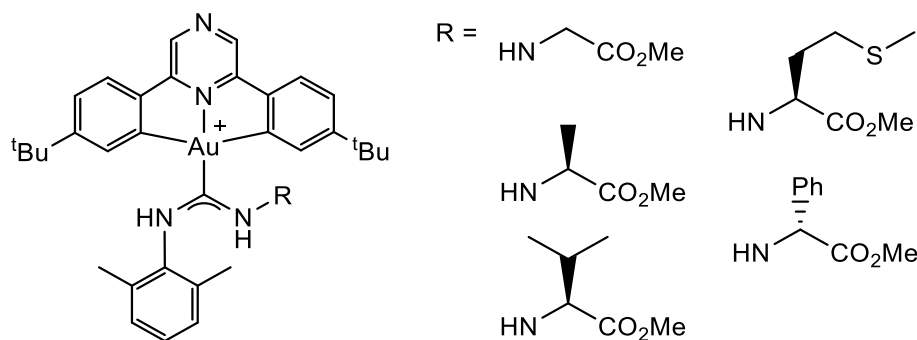


Figure 5.9. Acyclic carbenes with amino acid derivatives.

Investigations into their reactivity with GSH showed the oxidised GSSG species forming after 24 hours. Identification of the gold species formed was less conclusive but was assumed to be a gold(I) product, therefore these complexes are more sensitive to GSH than **41**. The final cellular target investigated for these species the formation of reactive oxygen species (ROS). There was no increase in ROS formation for any complex, therefore it was proposed as an unlikely cause of cytotoxicity for this class of compounds.

In this system it was possible to assess the impact of anion alteration. The anticancer properties of the same complex were investigated with both [SbF₆]⁻ and [BF₄]⁻ anions. There was no perceived difference in the antiproliferative effects at low concentrations, at higher concentrations the SbF₆ analogue gave lower cell viabilities indicating limited implication of anions into the cytotoxic mechanism.

A further approach to add complex functionality to C^NC gold(III) NHC complexes used a modified benzimidazole based NHC.³³ The position R on the NHC was decorated with bioactive moieties, including estradiol and biotin (Figure 5.10). Altering the linker length showed longer linkers (n = 5 in all cases) had the largest effect on the in vitro antiproliferation activity. The complexes showed slightly higher IC₅₀ values against MCF-7 and MRC-5 than **41** and showed no activity against A549. The uptake of complexes by cancer cells was selective towards those expressing the corresponding receptors. However, that selectivity did not translate to the higher activity in the antiproliferative assay where the compounds appeared generally less toxic than the non-vectorized complex **41**. The interactions of the vectorised complexes with a potential biological target: the G-quadruplex structure of DNA revealed a reduced interaction compared to **41**. That reduced interaction with secondary DNA structures may explain the reduced antiproliferative activity.

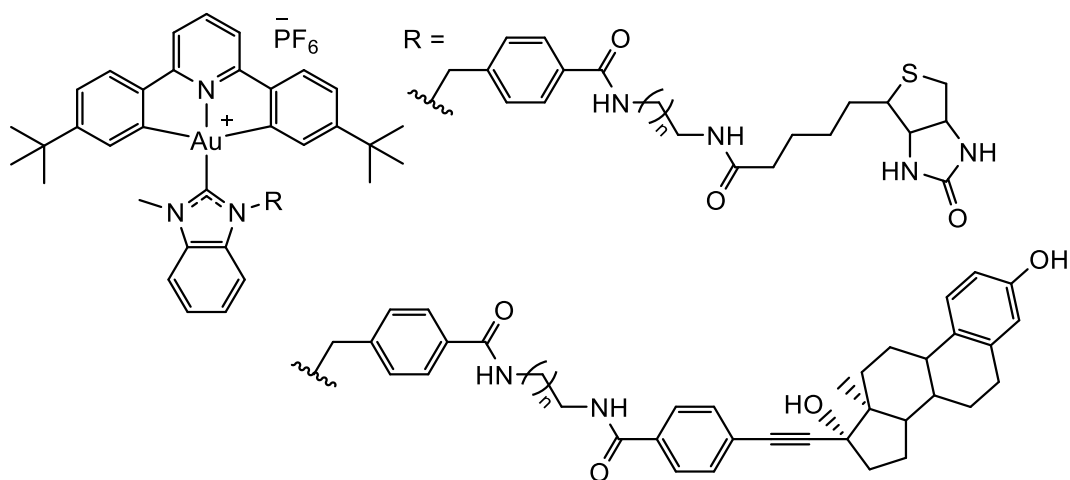


Figure 5.10. Pincer gold(III) NHC complex decorated with bioactive molecules, $n = 1, 3, 5$.

5.5 DNA binding properties

The investigations into cellular targets for **41** and **42** looked at number of potential targets, including secondary DNA structures. Both strongly interacted with G-Quadruplexes and i-motifs. These are formed from single stranded DNA rich in guanine and cytosine respectively. The potential for other nucleotides to form secondary structures has been investigated. Thymine can also form quartets however they are less stable than G-quartets because they are unable to form a stabilising interaction with alkali metal cations.³⁴

5.5.1 G-quadruplexes

G-quadruplex forming sequences are found in the telomeric region of DNA, at the ends of eukaryotic chromosomes.³⁵ Telomeres are made up of many repeating guanine units and correspondingly cytosine in the other strand. They are supposed to protect or buffer the coding region of the chromosome from degradation. These single stranded guanine rich sequences can assemble into four stranded DNA structures called G-quadruplexes.³⁴ A G-quadruplex is formed from two or more π stacked guanine tetrads (G-quartet) linked in a stable planar arrangement by hydrogen bonded Hoogsteen pairings (Figure 5.11). In addition, the presence of alkali metal cations (represented as an orange circle, Figure 5.11) are important as they coordinate to oxygen atoms and can influence the stability of the structure. The stability of the G-quadruplexes is also affected by variable length of the loops on the exterior of the G-quadruplexes, which are made of DNA bases not participating in the formation of a quartet.³⁴ The loops also allow the formation of cavities on the exterior of the G-quadruplexes which could be potentially interact with drug molecules.

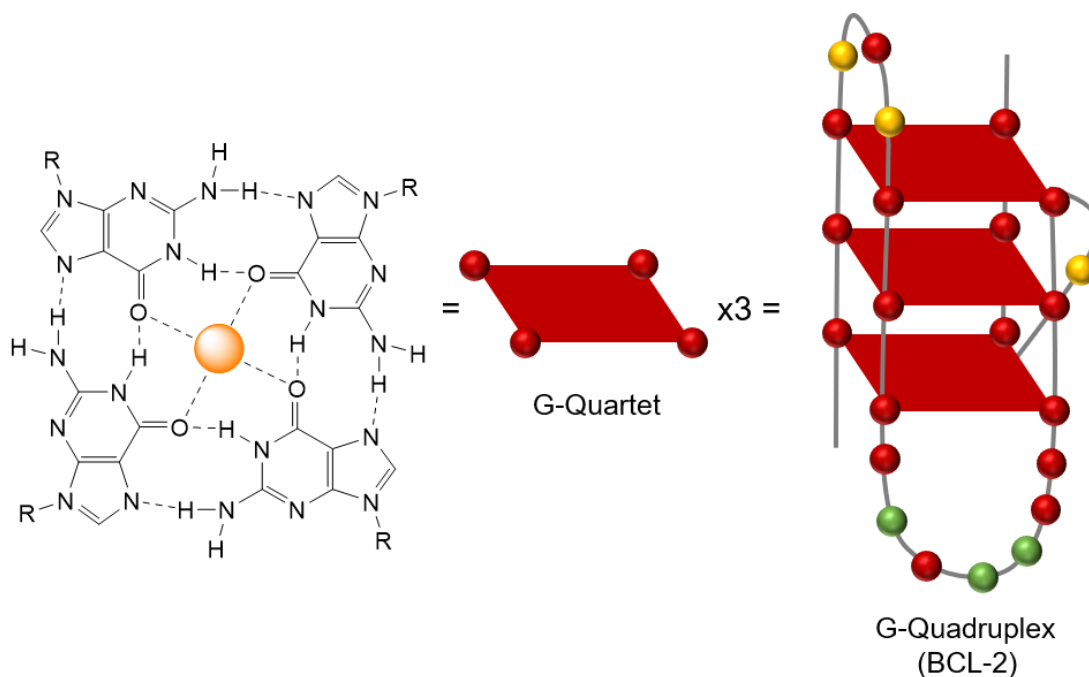


Figure 5.11. left) A G-quadruplex; middle) a representation of quartet; right) a representation of the stacked system showing stacked quartet and loops of different sizes.³⁴

Telomerase is a normally inactive enzyme that allows telomere extension and is activated in many human cancers.³⁶ Extending telomeres, extends the lifetime of a replicating cell, further removing cancer cells from normal cellular regulation. Telomerase recognizes only the linear form of DNA, so stabilizing the G-quadruplex structure in the telomeres could inhibit telomerase activity leading to the inhibition of cancer cells' immortality.³⁷

A G-quadruplex sequence is also found in the promotor region of the MYC proto-oncogene, its formation can repress the transcription of this gene.³⁸ The MYC proto-oncogene is overexpressed in almost 80% of solid tumours, therefore it is an interesting target to allow potential control of oncogene expression.

The ability of gold(I) complexes to stabilise G-quadruplexes has been investigated in the case of the caffeine-based bis(NHC)gold(I) cation (Figure 5.12). Crystallographic data showed three gold complexes per G-quadruplex interacting through π stacking into accessible tetrads.³⁹ Mass spectrometry confirmed the occurrence of aggregates of the complex with G-quadruplexes with ratios from 1:1 to 1:3 in solution.

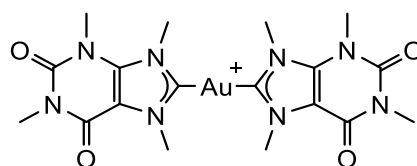


Figure 5.12. Gold(I) complex used to stabilised G-quadruplexes.

The gold(III) complexes, shown in Figure 5.13, interact with G-quadruplexes but not with double-stranded DNA.⁴⁰ The strongest binding affinity value was observed for the binuclear complex on the left. This affinity for G-quadruplexes was comparable to other metal-based complexes.⁴¹

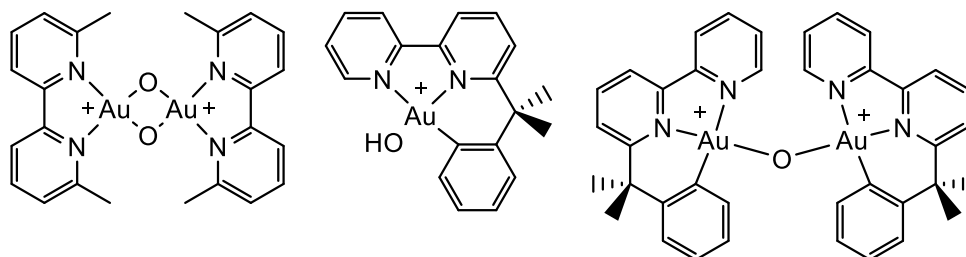


Figure 5.13. Gold(III) complexes used to stabilise G-quadruplexes.

5.5.2 iMotifs

DNA sequences rich in guanine have a complementary sequence rich in cytosine, these can also form secondary structures which are known as i-motifs (Figure 5.14).⁴² There is considerably less know about i-motifs compared to G-quadruplexes. I-motifs were first observed in acidic conditions and are formed of two parallel duplexes, arranged in an antiparallel fashion, which intercalate through hemiprotonated cytosine-cytosine base pairs (left, Figure 5.14).⁴³ The ability to trigger folding depending on the pH of the media has been investigated, allowing reversible i-motif formation.⁴²

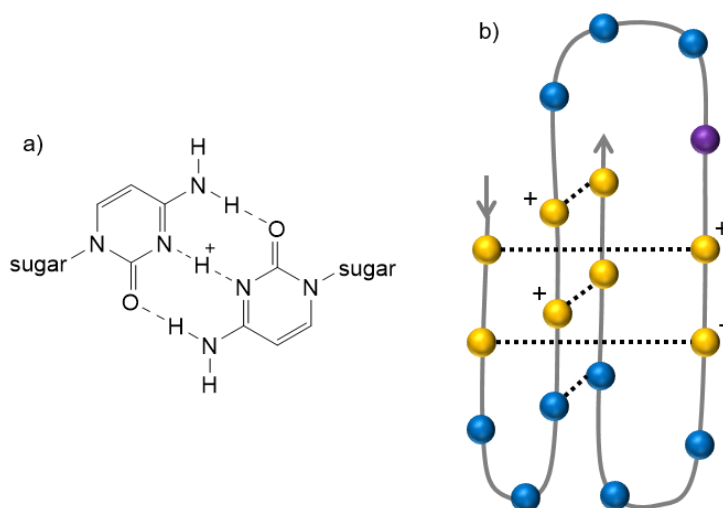


Figure 5.14. a) Hemiprotonated cytosine- cytosine base pair; b) Schematic view of an i-motif.⁴²

There are examples of interactions between other nucleotides in the loop regions contributing to stabilisation of i-motifs, such as the formation of an A-T base pair.⁴⁴ The nature of cations

present in solution is also thought to affect the conformations formed.⁴⁵ Furthermore, development of sequences of i-motifs that are stable at physiological pH instead of acidic pH have been investigated.⁴⁶ Again, stabilization of i-motifs is an interesting potential target for anticancer drugs because they have been shown to alter both telomerase activity and oncogene expression in similar manor to G-quadruplexes.⁴²

These secondary structures are of interest, but their formation requires single cytosine-rich strands of DNA to be freed from their complement. In order to understanding their formation DNA transcription has been examined, a process during which the double helix of duplex DNA is unwound releasing single stranded DNA.⁴⁷

5.6 Objectives

This work follows the previous research by the Bochmann and Che groups into gold(III) NHC complexes stabilised by pincer ligands that have shown promising anticancer properties. As discussed, alteration of the NHCs with biologically relevant molecules has been probed, but simple NHC complexes such as **N** and **41** are more potent anticancer agents. Extending the series of complexes in a systematic manner using three pincer ligands and three NHC ligands with minor changes could help to identify factors that influence anticancer properties.

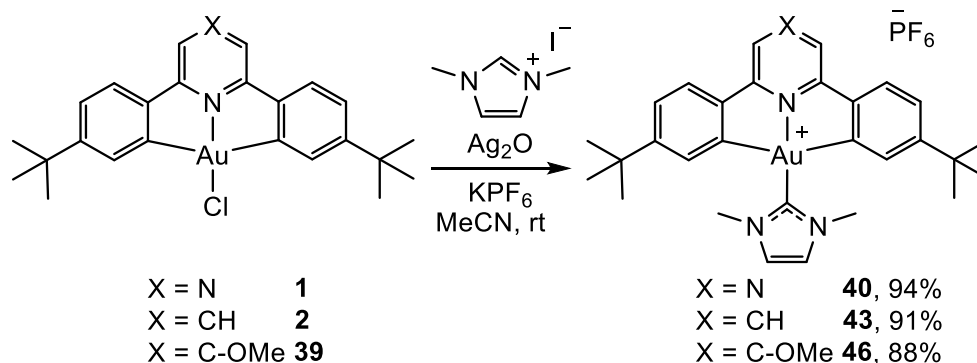
The C^NC ligand systems chosen to be investigated were 1,5-diphenyl substituted pyrazine, pyridine or *p*-methoxy substituted pyridine. Both the pyridine and pyrazine based C^NC gold(III) have been used anticancer studies, however the *p*-methoxy substituted pyridine had previously only been used in the synthesis of gold(III) hydrides.⁴⁸ Previous work has shown gold(III) NHCs based on 1,3-dimethylbenzimidazolium, 1,3-dimethylcaffeine and 1,3-dimethylimidazolium to have anticancer properties. To minimise the parameters being varied, the dimethyl NHC analogues were used for all complexes.

Results and discussion

5.7 Synthesis and characterisation of gold(III) carbenes (**40-48**)

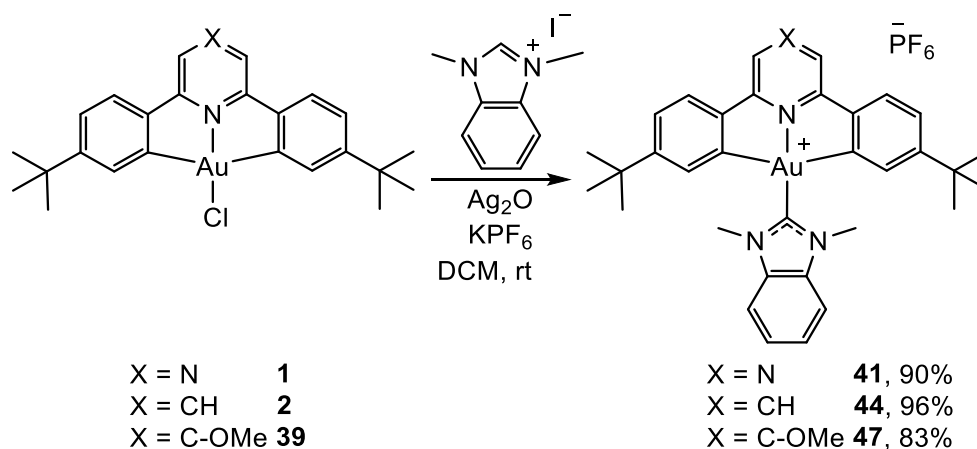
The complexes were synthesised using three separate methods, one for each of the different NHC ligands. Firstly, the 1,3-dimethylimidazolium NHC's (**40**, **43** and **46**) were synthesised by taking 1.5 molar equivalents 1,3-dimethylimidazolium iodide, one molar equivalent of Ag₂O and stirring in acetonitrile (Scheme 5.1). A slight excess of 1,3-dimethylimidazolium iodide was used due it its hydroscopic nature. The corresponding pincer gold(III) chloride (**1**, **2**, **39**) was added along with an excess of KPF₆ for anion exchange. The complexes **40**, **43** and

46 were isolated as solids in good yields (88 – 94%). This uses a different method than previously reported for the synthesis of **43**.^{29a}



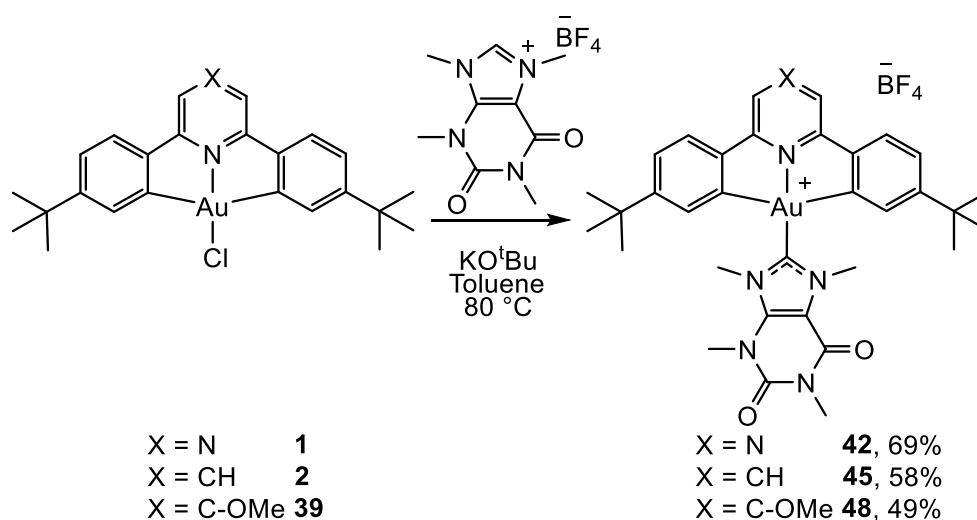
Scheme 5.1. The synthesis of **40**, **43** and **46**.

The 1,3-dimethylbenzimidazolium NHC's (**41**, **44** and **47**) were synthesised using the same methodology to the 1,3-dimethylimidazolium NHCs gold complexes above but using one molar equivalent of 1,3-dimethylbenzimidazolium iodide and dichloromethane as the solvent (Scheme 5.2). The complexes were isolated as solids in good yields (83 - 96%). This is a different method to that previously reported for **41**.²⁸



Scheme 5.2. The synthesis of **41**, **44** and **47**.

The 1,3-dimethylcaffeine based NHC's (**42**, **45** and **48**) were synthesised using a different methodology because the method described above did not translate to this system. The required gold(III) chloride (**1**, **2** or **39**) to be stirred with potassium tert-butoxide before adding [9-methylcaffeinium][BF₄]⁻ and the reaction was heated overnight (Scheme 5.3). Complexes **42**, **45** and **48** were isolated as solids in reasonable yields (49 - 69%).



Scheme 5.3. The synthesis of **42**, **45** and **48**.

The synthesis of the *p*-methoxy substituted complexes **46** and **47** required longer reaction times than their analogues based on unsubstituted pyridine and pyrazine ligands. The increase in reaction time for the final step from 16 hours to 8 days indicates that the Au–Cl bond strength increases in the *p*-OMe substituted pyridine systems.

All complexes were characterised by ^1H and ^{13}C NMR spectroscopy and elemental analysis.

A crystal of **46** suitable for X-ray crystallography was obtained (Figure 5.15). The asymmetric cell contains two molecules of **46**, with nearly identical parameters. The crystal structure showed the expected connectivity, with the gold in a distorted square planar geometry. The NHC twists out of the plane of the pincer ligand with an angle of 65.6(4) and 66.5(4)° for each of the molecules, which is similar to the previously reported **L** where the angle was 53.6°. ^{29a} Au–C and Au–N bonds in a trans position to each other across the gold centre have bond lengths of Au(1)–C(171) = 1.981(11) Å and Au(1)–N(11) = 2.001(8) Å. In the previously reported **N** with the same NHC but using a pyridine based pincer ligand Au–C(NHC) bond was 1.999(7) Å which is similar, however the trans Au–N was 1.975(4) Å is slightly shorter than the one observed here. In **41**, which used a pyrazine based pincer ligand and a 1,3-dimethylbenzimidazolium based NHC, the Au–C(NHC) was 1.995(10) Å, which is similar to the other two Au–NHC bonds and an Au–N distance of 1.991(9) Å, which is between **N** and **46**. ²⁸ In all the C^NC supported gold(III) NHC complexes the bond lengths are fairly similar, with the largest difference observed for Au–N bond across different pincer ligands, but this is still small. However, using a N^NN based pincer system with an imidazole NHC gives Au–C(NHC) bond length of 2.048 Å, which is longer (complexes shown in Figure 5.4). ²⁶

The crystal packing of **46** shows stacks of the cationic gold pincer complex. There is partial overlap of the pyridine and one phenyl ring of the two ligands, approximately 3.5 Å apart.

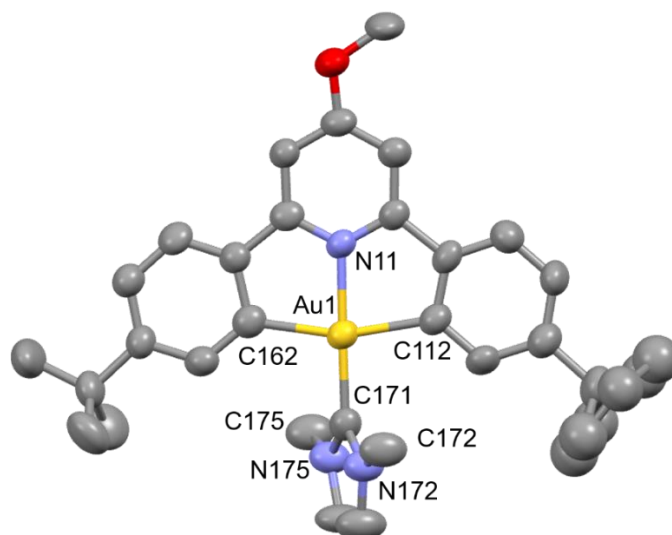


Figure 5.15. Crystal structure of **10**, PF_6^- anion is omitted for clarity. Selected bond distances [\AA] and angles [$^\circ$]: Au(1)-C(171) 1.981(11), Au(1)-N(11), 2.001(8), Au(1)-C(162) 2.071(10), Au(1)-C(122) 2.075(9), C(171)-Au(1)-N(11) 179.1(4), C(171)-Au(1)-C(162) 99.3(4), N(11)-Au(1)-C(162) 81.5(4), C(171)-Au(1)-C(122) 98.2(4), N(11)-Au(1)-C(122) 81.0(3), C(162)-Au(1)-C(122) 162.5(4).

5.8 Anticancer properties of **40** – **48**

Dr Benoit Bertrand carried out all experiments in section 5.8.

5.8.1 In vitro antiproliferative activity

The in vitro antiproliferative activity of the complexes was tested against the human lung adenocarcinoma epithelial (A549) cell line, which is cisplatin-resistant. The resistance of this cell line is thought to result from an over expression of DNA repair enzymes. As the A549 cell line had previously shown the largest difference in activity between the two gold(III) NHC complexes (**41** and **42**) it was used to see if the systematic changes across the series **40** – **48** affected their anticancer activity.²⁸

The antiproliferative activity was investigated at two concentrations 10 and 100 μM in culture medium after predilution in DMSO to reach the non-toxic concentration of 1 % DMSO. The extent of proliferation of A549 cells was determined using an MTS assay after 72 hours of incubation with the complexes (experimental section 6.7.1). In an MTS assay a purple compound is produced through the metabolism of an organic molecule (MTS) by living mitochondria. The level of absorption at a given time is proportional to the number of living cells under the specific conditions being tested, which is used in the estimation of the cell viability upon treatment with the complexes. The viabilities of the cells are shown at 10 and

100 μM concentrations for the complexes (Figure 5.16). The viability of the cells in the presence of cisplatin (prediluted in water instead of DMSO) is included for comparison.

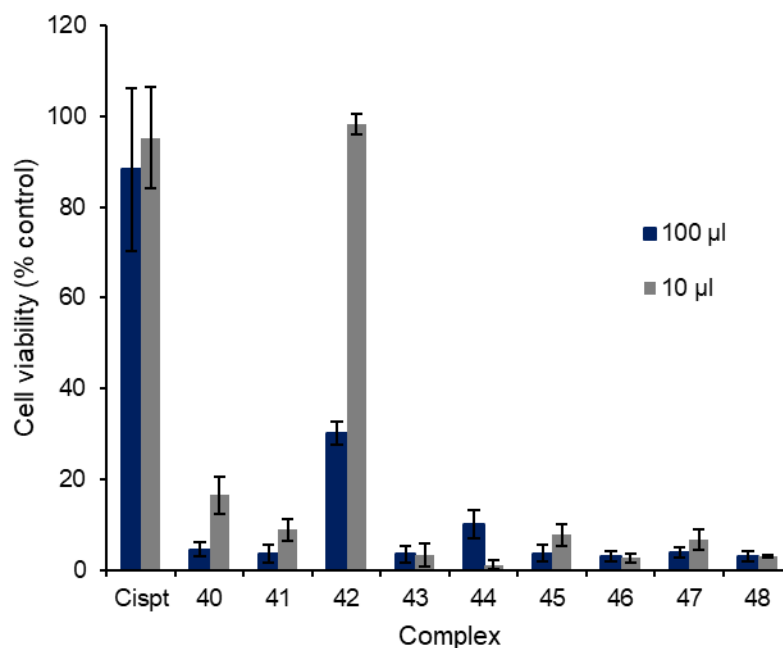


Figure 5.16. The antiproliferative activity of **40** – **48** against A549 cell line.

At 100 μM concentration of **40** – **48**, all complexes gave less than 10% cell viability except for **42** which gave 30% of cell viability after 72 hours, this is similar to what has previously been observed.²⁸ Therefore these gold(III) NHC complexes are acting as anticancer agents. The pyrazine bases complexes **40** – **42** showed lower levels of antiproliferative activity compared to the pyridine base complexes **43** – **45** and *p*-OMe-pyridine complexes **46** – **48**. For the complexes with less than 5% viability it can be considered that the complexes completely inhibited cell proliferation.

At the lower concentration of 10 μM of **40** – **48**, there was a slight increase in cell viability for most complexes, with all complexes apart from **42** showing less than 20% viability. At this concentration **42** was nontoxic to the A549 cells with no inhibition of proliferation.

Cisplatin showed no inhibition of proliferation at either 10 or 100 μM concentration as the cell line is cisplatin-resistant. The selectivity between **41** and **42** had been of interest in previous studies, but the same difference in viability was not observed between **44** and **45** and **47** and **48**. Complexes **43** – **48** showed generally lower viabilities than observed for the pyrazine based system.

5.8.2 IC₅₀ values

As complexes **40** and **43** – **48** had shown strong cytotoxic effects at 10 μM in the initial antiproliferative assay, the IC₅₀ values (the concentration to inhibit 50% of cell growth) were determined to quantify these observations. The cell viabilities were determined at a range of concentrations using an MTS assay, the experiment was repeated three times to give an average and standard deviation. These values were then used to determine the IC₅₀ for the cisplatin resistant A549 cell line using GraphPad Prism version 5.0 software to identify the concentration at which 50% of cell growth is inhibited (Table 5.1). All complexes, except **42**, were more toxic than cisplatin. Across the series of complexes, they all showed similar micromolar level IC₅₀ values. There are no strong trends across the different pincers or the NHCs. The previously observed difference between **41** and **42** was not observed for the other pincers systems.

Complex	IC ₅₀
cisplatin	33.7 \pm 3.7 ²⁸
40	5.35 \pm 0.71
41	7.8 \pm 1.3 ²⁸
42	>50 ²⁸
43	7.97 \pm 0.33
44	5.34 \pm 0.12
45	7.33 \pm 0.54
46	a
47	5.72 \pm 0.29
48	5.94 \pm 0.14

Table 5.1. IC₅₀ values for **40** – **48**. (a) Due to infected cells it was not possible to obtain and IC₅₀ value for this complex.

The previous difference between the IC₅₀ values of **41** and **42** was attributed to the difference in hydrophobicity of these two complexes.²⁸ This explanation may justify the low IC₅₀ values observed for the pyridine based complexes **43** – **45**; the pyridine ligand is more hydrophobic than the pyrazine, therefore increasing the hydrophobicity of **45** compared to **42**. The same explanation is unlikely to be the reason for the *p*-OMe-pyridine based system as a large difference in hydrophobicity is not expected. For the two complexes tested with this ligand system, **47** and **48**, both had lower IC₅₀ values than their pyrazine analogues, **41** and **42**; the value for **48** is considerably lower than **42**. Altering the size of the π system between the 1,3-

dimethylimidazolium and 1,3-dimethylbenzimidazolium did not have a significant effect upon IC_{50} values.

5.9 Investigating the interactions with DNA

41 and **42** have previously been shown to interact with DNA, specifically stabilising non-canonical secondary DNA structures: G-quadruplexes and imotifs.²⁸ This interaction was proposed as a possible mode of action that contributed to the anticancer properties of these complexes. Therefore, the interactions of complexes **40** – **48** with DNA sequences was assessed using a Förster resonance energy transfer (FRET) DNA melting assay. A FRET assay is used to calculate the change in thermal stability of secondary DNA structures in the presence of compounds.⁴⁹ The FRET assay requires the oligonucleotide being investigated be labelled with a fluorescent donor at one end (FAM (6- carboxyfluorescein) is used in this study) and an acceptor at the other end (TAMRA (6- carboxytetramethylrhodamine) is used in this study). Over the course of the melt assay, the temperature is increased incrementally from 25 °C to 95 °C and the emission of the fluorescence donor is monitored. When the single strand of DNA is in a folded conformation, such as a G-quadruplex or i-motif, the emission from the fluorescence donor is quenched. However, upon heating the DNA structure unfolds and the fluorescence donor and acceptor move further apart resulting in a fluorescent emission that is proportional to how unfolded the structure is and can be observed and monitored. T_m is the temperature at which the emission intensity is halfway between its minimum at low temperatures and its maximum at high temperatures, where 50% of the DNA is in a folded conformation.⁴⁹ ΔT_m is the difference between T_m in the presence of the complex and T_m of the control. The control contains the same concentration of labelled DNA in a buffer solution and 0.5 μ L of DMSO (same volume and solvent used to dissolve the complexes). This gives a value that quantifies the stabilisation (positive ΔT_m) or destabilisation (negative ΔT_m) of the DNA structures.

A range of FRET labelled DNA sequences were studied which could fold into different structures. These included three cytosine rich sequences capable of forming an i-motif: hTeloC_{FRET}, c-MycC_{FRET} and hif-1 α _{FRET}; a guanine rich G-quadruplex-forming sequence hTeloG_{FRET} and double stranded DNA sequence DS_{FRET}. Each of these DNA targets were studied at the transitional pH, where 50% of the population can be found in the folded conformation. Buffer solutions at known pH values were used, which also contained ions to stabilise the secondary structures at their transitional pH. The transitional pH is 6.0 for hTeloC, pH 6.6 for c-MycC and pH 7.2 for hif-1 α , hTeloG and DS.⁵⁰

An initial screening of the different DNA targets used 50 μM concentration of the complexes across all experiments. The concentration of the buffers (10 mM sodium cacodylate buffer at the indicated pH with 100 mM sodium chloride) and labelled oligonucleotide (0.2 μM) were kept constant. The ΔT_m values were calculated, predominantly, by taking the first derivative of the melting curve. However, some complexes the melting curves never plateaued and in these cases the T_m was calculated manually by taking the intensity at 95 $^\circ\text{C}$ as the final intensity. This assumes that the secondary structures are unfolded at 95 $^\circ\text{C}$, however the intensity of these curves was often much lower than other plateaued curves, so it is possible that there were still some stable secondary structures, or some of the DNA had precipitated, reducing the maximum fluorescent signal. This manual processing was used for all the melting temperatures of complexes **47** and **48**, therefore the true ΔT_m may be higher. The experiment was replicated in triplicate and the errors shown are the standard deviation of the three repeats.

The positive ΔT_m values shown in Figure 5.17 indicate that all the complexes interact and stabilise the DNA targets to some degree. The largest ΔT_m values are seen for hTeloC and c-Myc sequences, indicating strong stabilisation of i-motif structures under weakly acidic conditions. There were smaller ΔT_m values for the i-motif structure based on the hif-1 α sequence at pH 7.2. There was strong stabilisation of the G-quadruplex structure formed by the hTeloG sequence. By comparison, the interactions with double-stranded DNA was minimal, the highest values were observed for the p-OMe-pyridine based complexes **46** – **48** and **44**.

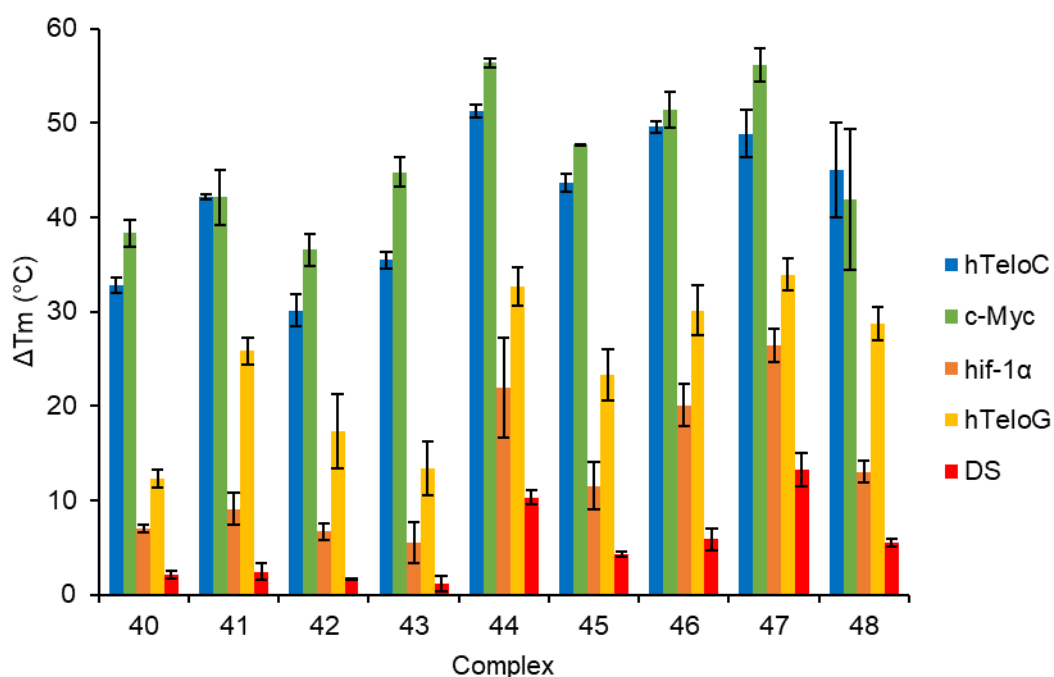


Figure 5.17. ΔT_m for complexes **40** – **48** with DNA targets.

The trends of activity can be more clearly observed by focusing on the DNA sequences with the largest ΔT_m values (hTeloC, c-Myc and hTeloG shown in Figure 5.18). For each DNA structure, the *p*-OMe-pyridine based complexes (orange Figure 5.18, **46** – **48**) provide marginally greater stabilisation than the pyridine based complexes (red Figure 5.18, **43** – **45**) which in turn are more stabilising than the pyrazine based complexes (blue Figure 5.18, **40** – **42**). The NHC with the largest ΔT_m is the 1,3-dimethylbenzimidazolium based carbene for each of the pincer systems. For the pyrazine and *p*-OMe-pyridine pincer systems the 1,3-dimethylimidazolium based NHC had a slightly larger ΔT_m than the caffeine based NHC, this order was reversed for the pyridine based pincer system, with a slightly larger stability observed for the caffeine based NHC compared to the 1,3-dimethylimidazolium.

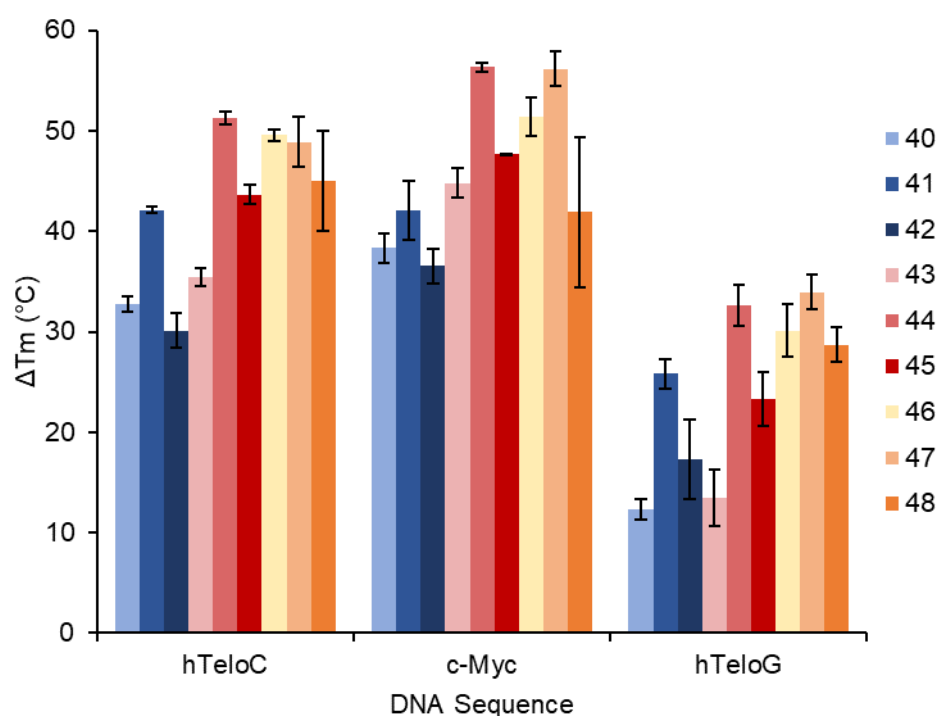


Figure 5.18. ΔT_m of hTeloC, c-Myc and hTeloG using complexes **40** – **48**, arranged by DNA.

In the previous study of **41** and **42**, it was proposed that the combination of the extended π -system, charge and potential for hydrogen bonding to the uncoordinated pyrazine nitrogen acted in cooperation to stabilise the DNA structures. This family of complexes all contain a π -system and are charged and all stabilise the structures to a varying degree. However, the pyridine-based complexes do not have an uncoordinated nitrogen to enable hydrogen bonding, however they still interact, indicating that hydrogen bonding is not essential for stabilisation.

The initial screening, used to identify changes in stabilisation for each complex and DNA sequence, exposed the secondary DNA structures a 1:250 ratio of DNA to complex. A dose response assay was investigated to establish the stabilising effect of these complexes at lower concentrations. **44** and **47** were chosen this assay because the 1,3-dimethylimidazolium NHC had shown the strongest interactions in the initial screening. It also allowed direct comparison of the three C^NC pincer ligands without altering the NHC because the dose response of **41** had previously been investigated.²⁸ Three DNA sequences hTeloC, hTeloG and double stranded DNA used were because these sequences cover three different structures, i-motif, G-quadruplex and double helical DNA. The dose response experiments were duplicated and the errors shown are the standard deviation of the two experiments.

The ΔT_m response of 0.2 μ M hTeloC labelled oligonucleotide at pH 6.0 buffer to varying doses of complexes **44** and **47** is shown in blue on the two graphs in Figure 5.19. The concentrations used are 0.25, 0.5, 1, 2, 5, 10, 20, 30 and 50 μ M of complex, however a logarithmic scale is used to see the range of concentrations graphically. The degree of stabilisation is minor at concentrations below 10 μ M for **44** and below 5 μ M for **47**. Concentrations of both **44** and **47** above 5 μ M considerably stabilise the folded conformation. This indicates that 25 equivalents of complex: oligonucleotides were required to provide stabilisation for both complexes. The experiment was repeated using the same dilutions of **44** and **47** with 0.2 μ M hTeloG labelled oligonucleotide in pH 7.2 buffer and the resultant ΔT_m are shown in red on the two graphs in Figure 5.19. There is a large ΔT_m for **44** and **47** above 10 μ M, at lower concentrations the stabilisation is much less. The experiment was repeated again using the same dilutions of **44** and **47** with 0.2 μ M double stranded labelled oligonucleotide in pH 7.2 buffer and the changes in stabilisation (ΔT_m) are shown in green in the graphs of Figure 5.19. Low ΔT_m values were observed below 30 μ M indicating that much more complex is needed to stabilise DS structures than either i-motif or G-quadruplex structures.

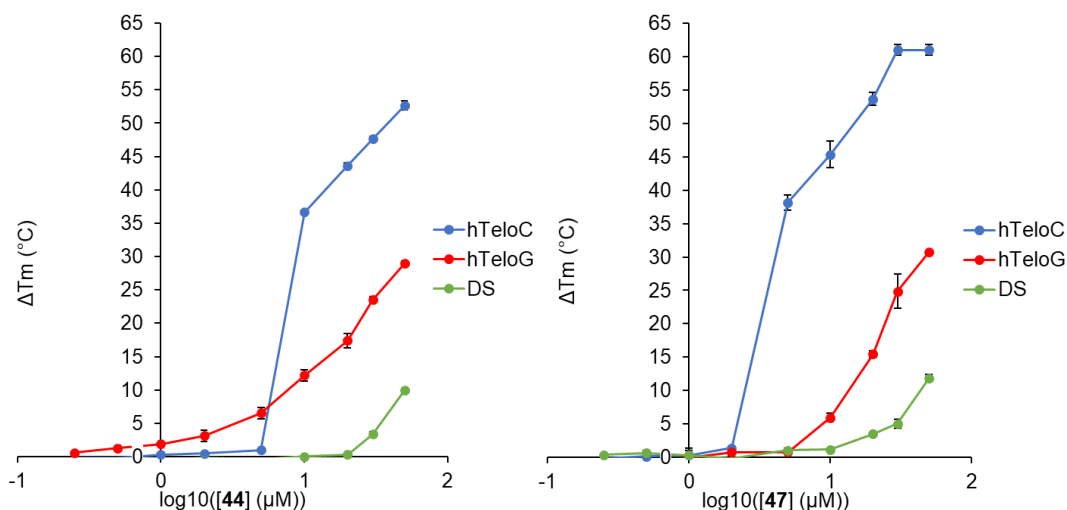


Figure 5.19. The ΔT_m of hTeloC (blue), hTeloG (red) and DS (green) DNA sequences at a range of concentrations (left) complexes **44**; (right) complex **47**.

At complex concentrations of 50 μM , the melting temperatures of the DNA structures are all positive, indicating the stabilisation of all structures; hTeloC is stabilised the most and double stranded the least. At low concentrations, less than 2 μM , there is very little stabilisation of any of the secondary structures. However, between these limits there are concentrations where the secondary structures are stabilised but there is minimal interaction with double stranded DNA.

The dose response of **41** with these DNA sequences using the same conditions has been reported.²⁸ It showed strongest interactions with the hTeloG sequence (40 °C at 20 μM) and a slightly weaker interaction with hTeloC (28 °C at 20 μM). These ΔT_m values gradually decreased with decreasing concentrations up to 2.5 μM upon which the interactions considerably decreased. Again, there was least interaction with double stranded DNA sequence (14 °C at 20 μM). At 5 μM there was stabilisation of the secondary DNA structures and minimal stabilisation of double stranded DNA.

The three (C^NC)Au-(1,3-dimethylimidazolium) complexes, **41**, **44** and **47**, all stabilise secondary DNA structures. **41** stabilised hTeloG more than **44** and **47**. Whereas **44** and **47** provided the greatest stabilisation to hTeloC. All stabilised double stranded DNA sequences the least. Complex **44**, with the pyridine C^NC pincer ligand shows the largest stabilisation of secondary structures, whilst not stabilising double stranded DNA at 20 μM .

The most important outcome of the dose response assay is the observation that there are concentrations at which only the secondary structures are stabilised, between 5 and 20 μM . This is because it indicates a preference or specificity for non-canonical DNA structures. If these compounds were to be developed as anticancer agents, their interactions with the

secondary structures may serve to direct specifically to cells that were replicating rapidly, interfering with replication and therefore selectively target cancerous cells over healthy cells.

5.10 Do thiols mimic the reactivity of glutathione (GSH)?

Glutathione (GSH) is a tripeptide with an S–H functionality that has previously been shown to reduce gold(III) anticancer agents that are stabilised by N-donor pincer ligands.²⁶ It is often over-expressed in cancerous cells and it has been demonstrated that cisplatin can react with glutathione to form of Pt–S bonds, which is a pathway in its deactivation.^{3,6}

Bochmann *et al.* previously studied the reactivity of complexes **41** with GSH in a dimethyl sulfoxide-*d*₆ (DMSO-*d*₆)/D₂O mixture as the solvent.²⁸ The ¹H NMR spectrum showed that after 6 days the major product was still **41**, however additional signals indicated further products being formed. Due to the longer reaction time required (6 days) for additional products to be formed, compared to the 3 days required in the study of the biological activity experiments, it was concluded that the reaction of **41** and GSH was unlikely to be a deactivating pathway for **41**.

A limitation of the work reported by Bochmann *et al.* is the reduced solubility of the gold(III) complexes in the DMSO/D₂O solution that is required to solubilize GSH. To overcome the solubility difference of GSH and C[^]N[^]C gold(III) NHC complexes, adamantyl thiol was used to mimic GSH. It is an alkyl-thiol and is soluble in DMSO, which is also a suitable solvent to dissolve (C[^]N[^]C)AuNHC complexes at concentrations detectable by ¹H NMR spectroscopy. We previously demonstrated that thiols react with neutral gold(III) complexes to trigger either C–C or C–S reductive elimination (Chapter 3).

Addition of 1 molar equivalent of adamantyl thiol to complexes **40** – **45** was studied by ¹H NMR spectroscopy. The reaction was left at room temperature and monitored at regular intervals. After 3 days (the time required for the antiproliferation study) there was no change in the ¹H NMR spectra for any of the complex. After 7 days there were additional signals observed in the ¹H NMR spectra of **40**, **42**, **43** and **45**. After 14 days the additional signals in the spectra for **40**, **42**, **43** and **45** had increased and there were also additional signals in the ¹H NMR spectrum of **41**. The only complex that appeared not to react with adamantyl thiol was **44**. The ¹H NMR spectra for all complexes after 14 days showed that the main species present were still the unreacted starting materials. The reaction that had progressed the furthest over 14 days was that of **43** and adamantyl thiol, the reaction mixture comprised of 87% of **43** to 13% of a new product. The compound formed was not identified but could be reduction product as observed in Chapter 3. Therefore, there is minimal reactivity between adamantyl

thiol and complexes **40** – **45**, with no reaction over the timescale of the antiproliferation study (3 days). This is similar to the reaction of **41** with GSH.²⁸

In the *in vitro* environment, the concentration of GSH is much higher than that of the complex. Therefore, the number of equivalents of adamantyl thiol was increased to 15 molar equivalents. In addition, the solvent was changed to dichloromethane to mimic the conditions used to study C-S reductive elimination. Complex **43** was chosen due to it showing the highest reactivity in the initial experiment. The reaction was monitored by ¹H NMR spectroscopy. There were no changes observed in the ¹H NMR spectrum over 2 months. Therefore it seems that the adamantyl thiol is unable to trigger reduction of (C[^]N[^]C)AuNHC complexes under these conditions in the same manner as previously observed in Chapter 3. These cationic complexes appear stable to reduction by adamantyl thiol over a time period greater than the biological assays, even at high concentrations of adamantyl thiol in a dichloromethane solution, in agreement with reactivity previously reported by Bochmann *et al.*²⁸

Conclusion

We have synthesised and characterised a series of new gold(III) NHC complexes supported by pincer ligands. The antiproliferation study and IC₅₀ values showed that these complexes are active as anticancer agents. The complexes were shown to interact and stabilise secondary DNA structures including i-motifs and G-quadruplexes. A dose response study showed that at low concentrations the secondary structures were stabilised, but there was little to no stabilisation of double-stranded DNA with these complexes, indicating a strong selectivity for non-canonical DNA structures. The lack of reactivity of these complexes with thiols, even at high concentrations, indicates a different mode of action of these complexes compared to many other gold(III) complexes have been previously proposed to interact with thioredoxin reductase. It also agrees with previous reports of the stability of C[^]N[^]C pincer ligands to biological thiols. This study further supports the potential of gold(III) NHC complexes as anticancer agents. Future work should investigate the use of NHCs decorated with biologically relevant moieties in combination with the pyridine or *p*-methoxypyridine ligand system that was shown to strongly interact with secondary DNA structures. It may also be interesting to combine this work with that of Che where increased selectivity for cancerous cells was observed for NHCs with longer alkyl groups attached to nitrogen.

References

- (1) Rosenberg, B.; Vancamp, L.; Krigas, T. *Nature* **1965**, *205*, 698.

- (2) M. Deo, K.; Ang, D.; McGhie, B.; Rajamanickam, A.; Dhiman, A.; Khoury, A.; Holland, J.; Bjelosevic, A.; Pages, B.; Gordon, C.; Aldrich-Wright, J. *Coord. Chem. Rev.* **2017**, 10.1016/j.ccr.2017.11.014.
- (3) Kelland, L. *Nat. Rev. Cancer* **2007**, 7, 573.
- (4) Harrap, K. R. *Cancer Treat. Rev.* **1985**, 12, 21.
- (5) Kidani, Y.; Inagaki, K.; Iigo, M.; Hoshi, A.; Kuretani, K. *J. Med. Chem.* **1978**, 21, 1315.
- (6) Siddik, Z. H. *Oncogene* **2003**, 22, 7265.
- (7) (a) Bruijninx, P. C. A.; Sadler, P. J. *Curr. Opin. Chem. Biol.* **2008**, 12, 197. (b) Gasser, G.; Ott, I.; Metzler-Nolte, N. *J. Med. Chem.* **2011**, 54, 3. (c) Hartinger, C. G.; Metzler-Nolte, N.; Dyson, P. J. *Organometallics* **2012**, 31, 5677.
- (8) Ott, I. *Coord. Chem. Rev.* **2009**, 253, 1670.
- (9) Zou, T. T.; Lum, C. T.; Lok, C. N.; Zhang, J. J.; Che, C. M. *Chem. Soc. Rev.* **2015**, 44, 8786.
- (10) (a) Che, C. M.; Sun, R. W. Y. *Chem. Commun.* **2011**, 47, 9554. (b) Cutillas, N.; Yellol, G. S.; de Haro, C.; Vicente, C.; Rodriguez, V.; Ruiz, J. *Coord. Chem. Rev.* **2013**, 257, 2784. (c) Bertrand, B.; Casini, A. *Dalton Trans.* **2014**, 43, 4209.
- (11) Parish, R. V.; Howe, B. P.; Wright, J. P.; Mack, J.; Pritchard, R. G.; Buckley, R. G.; Elsome, A. M.; Fricker, S. P. *Inorg. Chem.* **1996**, 35, 1659.
- (12) Parish, R. V.; Mack, J.; Hargreaves, L.; Wright, J. P.; Buckley, R. G.; Elsome, A. M.; Fricker, S. P.; Theobald, B. R. C. *J. Chem. Soc.-Dalton Trans.* **1996**, 69.
- (13) Engman, L.; McNaughton, M.; Gajewska, M.; Kumar, S.; Birmingham, A.; Powis, G. *Anti-Cancer Drugs* **2006**, 17, 539.
- (14) (a) Messori, L.; Marcon, G.; Cinellu, M. A.; Coronello, M.; Mini, E.; Gabbiani, C.; Orioli, P. *Bioorg. Med. Chem.* **2004**, 12, 6039. (b) Coronello, M.; Mini, E.; Caciagli, B.; Cinellu, M. A.; Bindoli, A.; Gabbiani, C.; Messori, L. *J. Med. Chem.* **2005**, 48, 6761.
- (15) (a) Marcon, G.; Carotti, S.; Coronello, M.; Messori, L.; Mini, E.; Orioli, P.; Mazzei, T.; Cinellu, M. A.; Minghetti, G. *J. Med. Chem.* **2002**, 45, 1672. (b) Casini, A.; Kelter, G.; Gabbiani, C.; Cinellu, M. A.; Minghetti, G.; Fregona, D.; Fiebig, H. H.; Messori, L. *J. Biol. Inorg. Chem.* **2009**, 14, 1139.
- (16) Gabbiani, C.; Mastrobuoni, G.; Sorrentino, F.; Dani, B.; Rigobello, M. P.; Bindoli, A.; Cinellu, M. A.; Pieraccini, G.; Messori, L.; Casini, A. *MedChemComm* **2011**, 2, 50.
- (17) Zhang, J. J.; Sun, R. W. Y.; Che, C. M. *Chem. Commun.* **2012**, 48, 3388.
- (18) Zhang, J. J.; Ng, K. M.; Lok, C. N.; Sun, R. W. Y.; Che, C. M. *Chem. Commun.* **2013**, 49, 5153.

- (19) Barnard, P. J.; Berners-Price, S. J. *Coord. Chem. Rev.* **2007**, *251*, 1889.
- (20) (a) Brown, S. D.; Henderson, W.; Kilpin, K. J.; Nicholson, B. K. *Inorg. Chim. Acta* **2007**, *360*, 1310. (b) Kilpin, K. J.; Henderson, W.; Nicholson, B. K. *Polyhedron* **2007**, *26*, 434. (c) Shaik, N.; Martinez, A.; Augustin, I.; Giovinazzo, H.; Varela-Ramirez, A.; Sanau, M.; Aguilera, R. J.; Contel, M. *Inorg. Chem.* **2009**, *48*, 1577. (d) Vela, L.; Contel, M.; Palomera, L.; Azaceta, G.; Marzo, I. *J. Inorg. Biochem.* **2011**, *105*, 1306.
- (21) Casini, A.; Hartinger, C.; Gabbiani, C.; Mini, E.; Dyson, P. J.; Keppler, B. K.; Messori, L. *J. Inorg. Biochem.* **2008**, *102*, 564.
- (22) (a) Teyssot, M. L.; Jarrousse, A. S.; Manin, M.; Chevry, A.; Roche, S.; Norre, F.; Beaudoin, C.; Morel, L.; Boyer, D.; Mahiou, R.; Gautier, A. *Dalton Trans.* **2009**, 6894. (b) Liu, W. K.; Gust, R. *Chem. Soc. Rev.* **2013**, *42*, 755.
- (23) Dinda, J.; Nandy, A.; Rana, B. K.; Bertolasi, V.; Das Saha, K.; Bielawski, C. W. *RSC Adv.* **2014**, *4*, 60776.
- (24) Rana, B. K.; Nandy, A.; Bertolasi, V.; Bielawski, C. W.; Das Saha, K.; Dinda, J. *Organometallics* **2014**, *33*, 2544.
- (25) Sivararn, H.; Tan, J.; Huynh, H. V. *Organometallics* **2012**, *31*, 5875.
- (26) Zou, T. T.; Lum, C. T.; Chui, S. S. Y.; Che, C. M. *Angew. Chem.-Int. Edit.* **2013**, *52*, 2930.
- (27) Li, C. K. L.; Sun, R. W. Y.; Kui, S. C. F.; Zhu, N. Y.; Che, C. M. *Chem.-Eur. J.* **2006**, *12*, 5253.
- (28) Bertrand, B.; Fernandez-Cestau, J.; Angulo, J.; Cominetti, M. M. D.; Waller, Z. A. E.; Searcey, M.; O'Connell, M. A.; Bochmann, M. *Inorg. Chem.* **2017**, *56*, 5728.
- (29) (a) Au, V. K. M.; Wong, K. M. C.; Zhu, N. Y.; Yam, V. W. W. *J. Am. Chem. Soc.* **2009**, *131*, 9076. (b) Yan, J. J.; Chow, A. L. F.; Leung, C. H.; Sun, R. W. Y.; Ma, D. L.; Che, C. M. *Chem. Commun.* **2010**, *46*, 3893.
- (30) (a) Sun, R. W. Y.; Lok, C. N.; Fong, T. T. H.; Li, C. K. L.; Yang, Z. F.; Zou, T. T.; Siu, A. F. M.; Che, C. M. *Chem. Sci.* **2013**, *4*, 1979. (b) Lum, C. T.; Sun, R. W. Y.; Zou, T. T.; Che, C. M. *Chem. Sci.* **2014**, *5*, 1579.
- (31) Fung, S. K.; Zou, T. T.; Cao, B.; Lee, P. Y.; Fung, Y. M. E.; Hu, D.; Lok, C. N.; Che, C. M. *Angew. Chem.-Int. Edit.* **2017**, *56*, 3892.
- (32) Williams, M.; Green, A. I.; Fernandez-Cestau, J.; Hughes, D. L.; O'Connell, M. A.; Searcey, M.; Bertrand, B.; Bochmann, M. *Dalton Trans.* **2017**, *46*, 13397.
- (33) Bertrand, B.; O'Connell, M. A.; Waller, Z. A. E.; Bochmann, M. *Chem.-Eur. J.* **2018**, *24*, 3613.
- (34) Balasubramanian, S.; Hurley, L. H.; Neidle, S. *Nat. Rev. Drug Discov.* **2011**, *10*, 261.
- (35) (a) Sen, D.; Gilbert, W. *Nature* **1988**, *334*, 364. (b) Sundquist, W. I.; Klug, A. *Nature* **1989**, *342*, 825.

- (36) Hanahan, D.; Weinberg, R. A. *Cell* **2000**, *100*, 57.
- (37) Zahler, A. M.; Williamson, J. R.; Cech, T. R.; Prescott, D. M. *Nature* **1991**, *350*, 718.
- (38) (a) Siddiqui-Jain, A.; Grand, C. L.; Bearss, D. J.; Hurley, L. H. *Proc. Natl. Acad. Sci. U. S. A.* **2002**, *99*, 11593. (b) Kumari, S.; Bugaut, A.; Huppert, J. L.; Balasubramanian, S. *Nat. Chem. Biol.* **2007**, *3*, 218.
- (39) Bazzicalupi, C.; Ferraroni, M.; Papi, F.; Massai, L.; Bertrand, B.; Messori, L.; Gratteri, P.; Casini, A. *Angew. Chem.-Int. Edit.* **2016**, *55*, 4256.
- (40) Gratteri, P.; Massai, L.; Michelucci, E.; Rigo, R.; Messori, L.; Cinellu, M. A.; Musetti, C.; Sissi, C.; Bazzicalupi, C. *Dalton Trans.* **2015**, *44*, 3633.
- (41) Ralph, S. F. *Curr. Top. Med. Chem.* **2011**, *11*, 572.
- (42) Day, H. A.; Pavlou, P.; Waller, Z. A. E. *Bioorg. Med. Chem.* **2014**, *22*, 4407.
- (43) Gehring, K.; Leroy, J. L.; Gueron, M. *Nature* **1993**, *363*, 561.
- (44) Kang, C. H.; Berger, I.; Lockshin, C.; Ratliff, R.; Moyzis, R.; Rich, A. *Proc. Natl. Acad. Sci. U. S. A.* **1995**, *92*, 3874.
- (45) (a) Mergny, J. L.; Lacroix, L.; Han, X. G.; Leroy, J. L.; Helene, C. *J. Am. Chem. Soc.* **1995**, *117*, 8887. (b) Saxena, S.; Bansal, A.; Kukreti, S. *Arch. Biochem. Biophys.* **2008**, *471*, 95.
- (46) Zhou, J.; Wei, C. Y.; Jia, G. Q.; Wang, X. L.; Feng, Z. C.; Li, C. *Mol. Biosyst.* **2010**, *6*, 580.
- (47) Sun, D.; Hurley, L. H. *J. Med. Chem.* **2009**, *52*, 2863.
- (48) Pintus, A.; Rocchigiani, L.; Fernandez-Cestau, J.; Budzelaar, P. H. M.; Bochmann, M. *Angew. Chem.-Int. Edit.* **2016**, *55*, 12321.
- (49) De Cian, A.; Guittat, L.; Kaiser, M.; Sacca, B.; Amrane, S.; Bourdoncle, A.; Alberti, P.; Teulade-Fichou, M. P.; Lacroix, L.; Mergny, J. L. *Methods* **2007**, *42*, 183.
- (50) Wright, E. P.; Day, H. A.; Ibrahim, A. M.; Kumar, J.; Boswell, L. J. E.; Huguin, C.; Stevenson, C. E. M.; Pors, K.; Waller, Z. A. E. *Sci Rep* **2016**, *6*, 7.

Chapter Six:
Experimental Section

6.1 General procedures

When specified, manipulations were performed by using standard Schlenk line techniques under dry N₂ or in a MBraun Unilab glovebox with a high capacity recirculator (<1.0 ppm O₂ and H₂O). Nitrogen was dried by passing through columns of supported P₂O₅, with moisture indicator, and activated 4 Å molecular sieves. Anhydrous solvents were freshly distilled from appropriate drying agents. CD₂Cl₂ and toluene-*d*₈ was stored in the glovebox over activated 4 Å molecular sieves. The balances used were a Mettler Toledo AG104 (precision 0.1 mg) or KERN ACJ 220-4M (precision 0.1 mg). (C^{N^{pZ}}C)AuCl (**1**),¹ (C^{N^{py}}C)AuCl (**2**),² (C^{N^{py}}C)AuMe (**19**),³ (C^{N^{py}}C)Au(*p*-C₆H₄F) (**20**),³ (C^{N^{py}}C)AuOC₆H₅ (**26**),⁴ (C^{N^{py}}C)AuOH (**35**),³ [H(OEt₂)₂][H₂N(B(C₆F₅)₃)₂] (HAB₂),⁵ (C^{N^{py-OMe}}C)AuCl (**39**),⁶ were synthesized according to literature procedures.

¹H, ¹H PGSE, ¹⁹F, ¹³C{¹H}, ¹H NOESY, ¹H, ¹³C HMQC and ¹H, ¹³C HMBC NMR experiments were recorded on a Bruker DPX-300 spectrometer equipped with a ¹H, BB smartprobe and Z-gradients. ¹H NMR spectra are referenced to the residual protons of the deuterated solvent. ¹³C NMR spectra are referenced to the D-coupled ¹³C signals of the solvent.

Elemental analyses were carried out at London Metropolitan University with a Perkin-Elmer 2400 CHNS/O microanalyzer.

Mass spectrometry was carried out by the EPSRC UK National Mass Spectrometry Facility at Swansea University.

6.2 Synthesis and characterisation

6.2.1 Complexes in Chapter Two

The general methods used in this chapter:

Method 1: (C^{N^{pZ}}C)AuCl (0.050 g, 0.087 mmol) and K₂CO₃ (0.024 g, 0.174 mmol) were dissolved in acetone (5 mL). The corresponding thiol (0.087 mmol) was added and the mixture was stirred at room temperature for 3 h. The acetone was removed *in vacuo* and the resulting solid was extracted into dichloromethane (5 mL). The suspension was filtered through celite and washed with dichloromethane (5 mL). The solvent was removed to give a solid. This was washed with cold hexane to give the desired product.

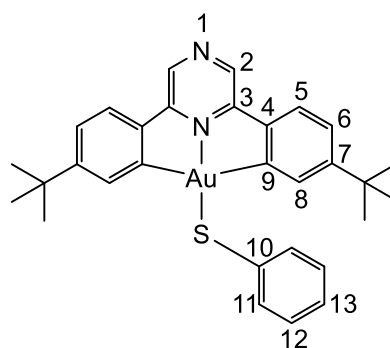
Method 2: To a flask charged with (C^{N^{pZ}}C)AuCl (0.040 g, 0.070 mmol) and potassium *t*-butoxide (0.009 g, 0.084 mmol) under N₂ was added dry toluene (5 mL), this was left to stir for 3 hours. Then the corresponding thiol (0.070 mmol) was added and reaction stirred for

further 3 hours. Solvent removed under vacuum, solid suspended in dichloromethane and passed through celite plug. The solution was evaporated to dryness to give the desired product.

Method 3: Under a nitrogen atmosphere, a flask was charged with (C^{N^{Pz}}C)AuCl (0.056 g, 0.097 mmol), K₂CO₃ (0.027 g, 0.191 mmol) and degassed acetone (5 mL). The corresponding thiol (0.097 mmol) was added and the mixture was stirred at room temperature for 3 hours. The acetone was removed *in vacuo* and the resulting solid was extracted into dichloromethane (5 mL). The suspension was filtered through celite and washed with dichloromethane (5 mL). The solvent was removed. The solid residue was washed with cold hexane to give the desired product.

(C^{N^{Pz}}C)AuSPh (**3**)

Synthesised using method 1 with thiophenol (0.013 mL, 0.087 mmol) as the corresponding thiol. **3** was isolated as a yellow powder (0.054 g, 99% yield). Single crystals suitable for X-ray diffraction were obtained from slow evaporation of a solution in dichloromethane/isopropanol (9:1). Both red and yellow crystals were obtained under the same conditions.



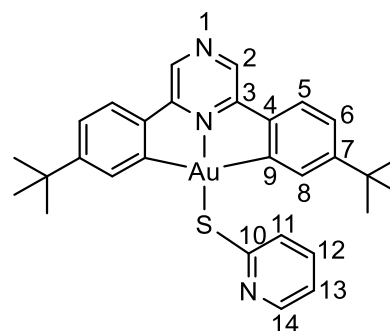
¹H NMR (CD₂Cl₂, 300.13 MHz, 298 K): δ 8.85 (s, 2 H, H²), 7.65 (m, 4 H, H⁵ + H¹¹), 7.39 (d, ⁴J_{H-H} = 1.9 Hz, 2 H, H⁸), 7.29 (dd, ³J_{H-H} = 8.2 Hz, ⁴J_{H-H} = 1.9 Hz, 2 H, H⁶), 7.21 (m, 3 H, H¹² + H¹³), 1.17 (s, 18 H, ^tBu).

¹³C{¹H} NMR (CD₂Cl₂, 75.48 MHz, 298 K): δ 169.2 (s, C⁹), 156.2 (s, C^{3/4}), 156.1 (s, C^{3/4}), 145.0 (s, C⁷), 138.8 (s, C²), 137.6 (s, C¹⁰), 135.0 (s, C^{5/11}), 131.5 (s, C⁸), 128.9 (s, C¹²), 126.7 (s, C¹³), 125.7 (s, C^{5/11}), 124.4 (s, C⁶), 35.6 (s, C(CH₃)₃), 31.1 (s, CH₃).

Elemental Microanalysis for C₃₀H₃₁N₂AuS (648.2): C, 55.55; H, 4.82; N, 4.32. Found: C, 55.47; H, 4.81; N, 4.38.

(C^{N^{Pz}}C)AuSC₅H₄N-2 (**4**)

Synthesised using method 1 and 1-mercaptopyridine (0.010 g, 0.087 mmol) as the corresponding thiol. **4** was isolated as a yellow powder (0.041 g, 0.063 mmol, 72%). Single crystals suitable for X-ray diffraction were obtained from slow evaporation of a dichloromethane and isopropanol (4:1) solution.



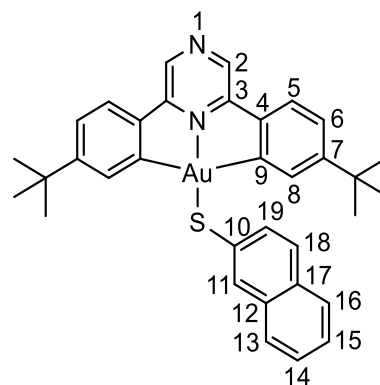
^1H NMR (CD_2Cl_2 , 300.13 MHz, 298 K): δ 8.83 (s, 2 H, H^2), 8.25 (bd, $^3J_{\text{H-H}} = 4.9$ Hz, 1 H, H^{14}), 7.64 (m, 3 H, $\text{H}^5 + \text{H}^{11}$), 7.57 (d, $^4J_{\text{H-H}} = 1.9$ Hz, 2 H, H^8), 7.40 (m, 1 H, H^{12}), 7.29 (dd, $^3J_{\text{H-H}} = 8.2$ Hz, $^4J_{\text{H-H}} = 1.9$ Hz, 2 H, H^6), 6.96 (m, 1 H, H^{13}), 1.19 (s, 18 H, ^tBu).

$^{13}\text{C}\{^1\text{H}\}$ NMR (CD_2Cl_2 , 75.48 MHz, 298 K): δ 170.1 (s, C^9), 162.4 (s, C^{10}), 156.7 (s, $\text{C}^{3/4}$), 156.4 (s, $\text{C}^{3/4}$), 149.5 (s, C^{14}), 144.8 (s, C^7), 138.8 (s, C^2), 135.8 (s, C^{12}), 132.6 (s, C^8), 127.8 (s, C^5), 125.8 (s, $\text{C}^{6/11}$), 124.5 (s, $\text{C}^{6/11}$), 119.9 (s, C^{13}), 35.7 (s, $\text{C}(\text{CH}_3)_3$), 31.1 (s, CH_3).

Elemental Microanalysis $\text{C}_{29}\text{H}_{30}\text{AuN}_3\text{S}$ (649.61): C, 53.62%; H, 4.66%; N, 6.49%. Found: C, 53.53%; H, 4.77%; N, 6.54%.

($\text{C}^{\wedge}\text{N}^{\text{pz}}\text{C}$)AuSNp-2 (**5**)

Synthesised using method 1 and 2-naphthalenethiol (0.014 g, 0.087 mmol) to give **5** as an orange solid (0.051 g, 0.073 mmol, 84%). Single crystals suitable for X-ray diffraction were obtained from slow evaporation of a dichloromethane and isopropanol (4:1) solution (yellow polymorph) and slow evaporation of a dichloromethane solution (red polymorph).



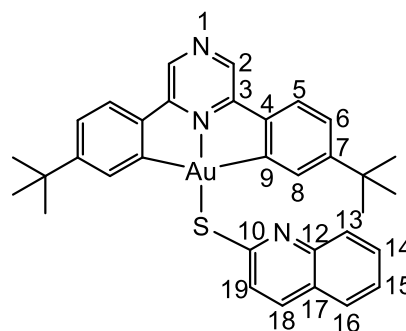
^1H NMR (CD_2Cl_2 , 300.13 MHz, 298 K): δ 8.83 (s, 2 H, H^2), 8.22 (s, 1 H, H^{11}), 7.79 (d, $^3J_{\text{H-H}} = 6.7$ Hz, 1 H, H^{16}), 7.72 (d, $^3J_{\text{H-H}} = 6.7$ Hz, 1 H, H^{13}), 7.67 (m, 2 H, $\text{H}^{18} + \text{H}^{19}$), 7.62 (d, $^3J_{\text{H-H}} = 8.2$ Hz, 2 H, H^5), 7.44 (m, 2 H, $\text{H}^{14} + \text{H}^{15}$), 7.29 (d, $^4J_{\text{H-H}} = 1.9$ Hz, 2 H, H^8), 7.24 (dd, $^3J_{\text{H-H}} = 8.2$ Hz, $^4J_{\text{H-H}} = 1.9$ Hz, 2 H, H^6), 1.00 (s, 18 H, ^tBu).

$^{13}\text{C}\{^1\text{H}\}$ NMR (CD_2Cl_2 , 75.48 MHz, 298 K): δ 169.0 (s, C^9), 156.2 (s, $\text{C}^3 + \text{C}^4$), 145.1 (s, C^7), 138.8 (s, C^2), 134.8 (s, $\text{C}^{10/12/17}$), 134.3 (s, $\text{C}^{10/12/17}$), 133.7 (s, $\text{C}^{18/19}$), 133.3 (s, C^{11}), 132.7 (s, $\text{C}^{10/12/17}$), 131.3 (s, C^8), 128.1 (s, $\text{C}^{18/19}$), 127.9 (s, C^{16}), 127.5 (s, C^{13}), 126.7 (s, $\text{C}^{14/15}$), 126.0 (s, $\text{C}^{14/15}$), 125.8 (s, C^5), 124.4 (s, C^6), 35.5 (s, $\text{C}(\text{CH}_3)_3$), 30.8 (s, CH_3).

Elemental Microanalysis: $\text{C}_{34}\text{H}_{33}\text{AuN}_2\text{S}$ (698.68): C, 58.45%; H, 4.76%; N, 4.01%. Found: C, 58.34%; H, 4.62%; N, 4.12%.

($\text{C}^{\wedge}\text{N}^{\text{pz}}\text{C}$)AuSquinoline (**6**)

Using method 1 and 2-quinolinethiol (0.014 g, 0.087 mmol) to give **6** as an orange solid (0.042 g, 0.060 mmol, 69%).



^1H NMR (CD_2Cl_2 , 300.13 MHz, 298 K): δ 8.86 (s, 2 H, H^2), 7.90-7.50 (bm, 4H, $\text{H}^{13} + \text{H}^{16} + \text{H}^{18} + \text{H}^{19}$), 7.64 (d, $^3J_{\text{H-H}} = 8.1$ Hz, 2 H, H^5), 7.52 (bs, 2 H, H^8), 7.45-7.35 (bm, 2 H, $\text{H}^{14} + \text{H}^{15}$), 7.26 (dd, $^3J_{\text{H-H}} = 8.1$ Hz, $^4J_{\text{H-H}} = 1.6$ Hz, 2 H, H^6), 1.04 (s, 18 H, ^tBu). ^1H NMR (CD_2Cl_2 , 300.13 MHz, 223 K): δ 8.83 (s, 2 H, H^2), 7.82 (d, $^3J_{\text{H-H}} = 8.6$ Hz, 1 H, $\text{H}^{13/16/18/19}$), 7.78 (d, $^3J_{\text{H-H}} = 8.6$ Hz, 1 H, $\text{H}^{13/16/18/19}$), 7.70 (d, $^3J_{\text{H-H}} = 7.4$ Hz, 1 H, $\text{H}^{13/16/18/19}$), 7.60 (m, $^3J_{\text{H-H}} = 8.3$ Hz, 4 H, $\text{H}^5 + \text{H}^{14} + \text{H}^{15}$), 7.41 (d, $^3J_{\text{H-H}} = 8.0$ Hz, 1 H, $\text{H}^{13/16/18/19}$), 7.37 (d, $^4J_{\text{H-H}} = 1.4$ Hz, 2 H, H^8), 7.21 (dd, $^3J_{\text{H-H}} = 8.2$ Hz, $^4J_{\text{H-H}} = 1.4$ Hz, 2 H, H^6), 0.95 (s, 18 H, ^tBu).

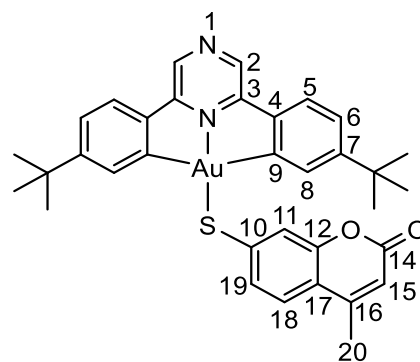
$^{13}\text{C}\{^1\text{H}\}$ NMR (CD_2Cl_2 , 75.48 MHz, 298 K): δ 170.1 (s, C^9), 156.8 (s, $\text{C}^{3/4}$), 156.4 (s, $\text{C}^{3/4}$), 144.7 (s, C^7), 138.9 (s, C^2), 132.6 (s, C^8), 127.7 (s, $\text{C}^{\text{quinoline}}$), 127.1 (s, $\text{C}^{\text{quinoline}}$), 125.9 (s, C^5), 124.4 (s, C^6), 35.6 (s, $\text{C}(\text{CH}_3)_3$), 30.9 (s, CH_3).

Elemental Microanalysis $\text{C}_{33}\text{H}_{32}\text{AuN}_3\text{S}$ (699.67): C, 56.65%; H, 4.61%; N, 6.01%. Found: C, 56.58%; H, 4.55%; N, 6.09%.

($\text{C}^{\wedge}\text{N}^{\text{pz}}\text{C}$)AuS-4-methylcoumarin (**7**)

Synthesised using method 1 and 7-mercapto-4-methylcoumarin (0.017 g, 0.087 mmol), however reaction time of 18 h was required. The product (**7**) was isolated as a yellow solid (0.022 g, 35%).

Synthesised by method 2 and 7-mercapto-4-methylcoumarin (0.013 g, 0.070 mmol) to give **7** as a yellow solid (0.043 g, 0.059 mmol, 84%).



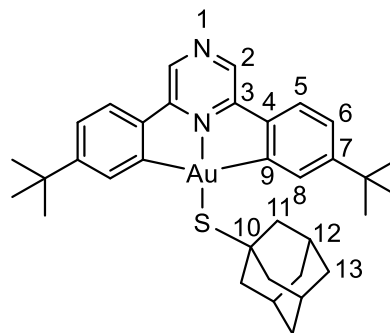
^1H NMR (CD_2Cl_2 , 300.13 MHz, 298 K): δ 8.84 (s, 2 H, H^2), 7.65 (d, $^3J_{\text{H-H}} = 8.2$ Hz, 2 H, H^5), 7.58 (d, $^4J_{\text{H-H}} = 1.7$ Hz, 1 H, H^{11}), 7.55 (dd, $^3J_{\text{H-H}} = 8.3$ Hz, $^4J_{\text{H-H}} = 1.9$ Hz, 1 H, H^{19}), 7.42 (d, $^4J_{\text{H-H}} = 1.9$ Hz, 2 H, H^8), 7.40 (d, $^3J_{\text{H-H}} = 8.3$ Hz, 1 H, H^{18}), 7.34 (dd, $^3J_{\text{H-H}} = 8.2$ Hz, $^4J_{\text{H-H}} = 1.9$ Hz, 2 H, H^6), 6.14 (bq, $^4J_{\text{H-H}} = 1.2$ Hz, 1 H, H^{15}), 2.36 (bd, $^4J_{\text{H-H}} = 1.2$ Hz, 3 H, H^{20}), 1.13 (s, 18 H, ^tBu).

$^{13}\text{C}\{^1\text{H}\}$ NMR (CD_2Cl_2 , 75.48 MHz, 298 K): δ 169.5 (s, C^9), 160.8 (s, $\text{C}^{10/12/14/17}$), 156.4 (s, $\text{C}^{3/4}$), 156.3 (s, $\text{C}^{3/4}$), 153.4 (s, $\text{C}^{10/12/14/17}$), 152.6 (s, $\text{C}^{10/12/14/17}$), 144.9 (s, $\text{C}^7 + \text{C}^{10/12/14/17}$), 138.9 (s, C^2), 131.9 (s, C^8), 130.3 (s, C^{19}), 125.9 (s, C^5), 124.6 (s, C^6), 124.3 (s, C^{18}), 121.8 (s, C^{11}), 118.1 (s, C^{16}), 113.9 (s, C^{15}), 35.7 (s, $\text{C}(\text{CH}_3)_3$), 30.9 (s, CH_3), 18.7 (s, C^{20}).

Elemental Microanalysis $\text{C}_{34}\text{H}_{33}\text{AuN}_2\text{O}_2\text{S}$ (704.73): C, 55.89%; H, 4.55%; N, 3.83%. Found: C, 56.02%; H, 4.48%; N, 3.91%.

$(C^{\wedge}N^{Pz^{\wedge}}C)AuSAd$ (**8**)

Under an atmosphere of dinitrogen, a flask was charged with $(C^{\wedge}N^{Pz^{\wedge}}C)AuCl$ (0.055 g, 0.097 mmol), K_2CO_3 (0.027 g, 0.191 mmol) and 1-adamantanethiol (0.016 g, 0.097 mmol). Degassed acetone (5 mL) was added and the mixture was stirred at room temperature for 24 hours (the reaction was incomplete after 6 h, so an excess 1-adamantanethiol was added and the reaction was left overnight). The acetone was removed *in vacuo* and the resulting solid extracted into dichloromethane (5 mL). The suspension was filtered through celite and washed with dichloromethane (5 mL). Solvent was removed to give a red solid which was further purified by flash column chromatography (1:1 dichloromethane and petroleum ether) (0.022 g, 0.031 mmol, 36%).



Synthesised with method 2 and 1-adamantanethiol (0.012 g, 0.070 mmol) gave **8** as a red solid (0.036 g, 0.051 mmol, 73%)

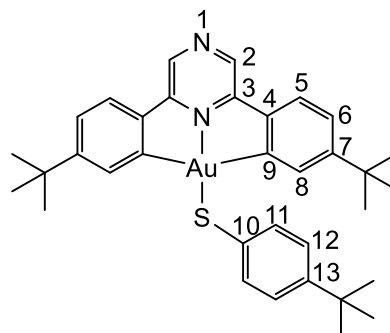
1H NMR (CD_2Cl_2 , 300.13 MHz, 298 K): δ 8.83 (s, 2 H, H^2), 8.44 (d, $^4J_{H-H} = 1.9$ Hz, 2 H, H^8), 7.63 (d, $^3J_{H-H} = 8.2$ Hz, 2 H, H^5), 7.31 (dd, $^3J_{H-H} = 8.2$ Hz, $^4J_{H-H} = 1.9$ Hz, 2 H, H^6), 2.13 (bd, $^3J_{H-H} = 2.3$ Hz, 6 H, H^{11}), 1.92 (brs, 3 H, H^{12}), 1.61 (brs, 6 H, H^{13}), 1.39 (s, 18 H, tBu).

$^{13}C\{^1H\}$ NMR (CD_2Cl_2 , 75.48 MHz, 298 K): 172.8 (s, C^9), 156.7 (s, $C^{3/4}$), 156.1 (s, $C^{3/4}$), 145.0 (s, C^7), 138.7 (s, C^2), 134.5 (s, C^8), 125.5 (s, C^5), 124.1 (s, C^6), 50.1 (s, C^{11}), 49.1 (s, C^{10}), 36.6 (s, C^{13}), 36.0 (s, $C(CH_3)_3$), 31.3 (s, CH_3), 31.2 (s, C^{12}).

Elemental Microanalysis $C_{34}H_{41}AuN_2S$ (706.74): C, 57.78%; H, 5.85%; N, 3.96%. Found: C, 57.52%; H, 5.90%; N, 4.12%.

 $(C^{\wedge}N^{Pz^{\wedge}}C)AuSC_6H_4^tBu-4$ (**9**)

Synthesised with method 3 and 4-tert-butylbenzenethiol (15 μ l, 0.097 mmol) to give **9** as a yellow solid (0.057 g, 0.081 mmol, 83%). Single crystals suitable for X-ray diffraction were obtained from slow evaporation of a dichloromethane and isopropanol (4:1) solution.



1H NMR (CD_2Cl_2 , 300.13 MHz, 298 K): δ 8.83 (s, 2 H, H^2), 7.64 (d, $^3J_{H-H} = 8.2$ Hz, 2 H, H^5), 7.56 (d, $^3J_{H-H} = 8.4$ Hz, 2 H, H^{11}), 7.43 (d, $^4J_{H-H} = 1.9$ Hz, 2 H, H^8), 7.26 (m, 4 H, $H^6 + H^{12}$), 1.29 (s, 9 H, $^tBu(SPh-4-^tBu)$), 1.17 (s, 18 H, $^tBu(C^{\wedge}N^{Pz^{\wedge}}C)$).

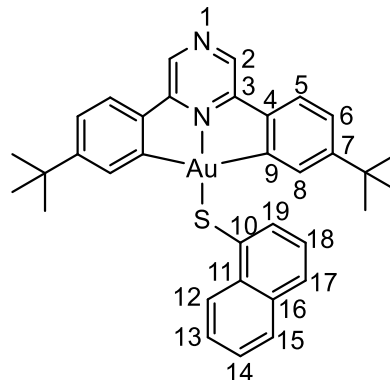
$^{13}C\{^1H\}$ NMR (CD_2Cl_2 , 75.48 MHz, 298 K): δ 169.1 (s, C^9), 156.1 (s, $C^{3/4}$), 156.0 (s, $C^{3/4}$), 149.7 (s, C^{13}), 145.1 (s, C^7), 138.8 (s, C^2), 134.7 (s, C^{11}), 133.8 (s, C^{10}), 131.4 (s, C^8), 126.1 (s,

$C^{6/12}$), 125.7 (s, C^5), 124.4 (s, $C^{6/12}$), 35.7 (s, $C(CH_3)_3(C^{\wedge}N^{pz}\wedge C)$), 34.7 (s, $C(CH_3)_3(SPh-4-{}^tBu)$), 31.4 (s, $CH_3(SPh-4-{}^tBu)$), 31.2 (s, $CH_3(C^{\wedge}N^{pz}\wedge C)$).

Elemental Microanalysis: Calc. $C_{34}H_{39}AuN_2S$ (704.73): C, 57.95%; H, 5.58%; N, 3.98%. Found: C, 57.80%; H, 5.65%; N, 4.12%.

$(C^{\wedge}N^{pz}\wedge C)AuSNp-1$ (**10**)

Synthesised with method 3 and the following quantities: $(C^{\wedge}N^{pz}\wedge C)AuCl$ (0.062 g, 0.108 mmol), K_2CO_3 (0.030 mg, 0.216 mmol) and 1-naphthalenethiol (15 μ L, 0.108 mmol). **10** was isolated as an orange solid (0.060 g, 0.086 mmol, 80%).



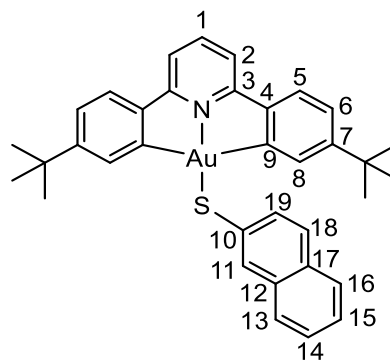
1H NMR (CD_2Cl_2 , 300.13 MHz, 298 K): δ 8.44 (s + d, 3 H, $H^2 + H^{12}$), 8.05 (d, ${}^3J_{H-H} = 7.2$ Hz, 1 H, $H^{17/19}$), 7.86 (m, 1 H, H^{15}), 7.82 (d, ${}^3J_{H-H} = 8.4$ Hz, 1 H, $H^{17/19}$), 7.63 (d, ${}^3J_{H-H} = 8.1$ Hz, 2 H, H^5), 7.49 (m, 2 H, $H^{13} + H^{14}$), 7.40 (dd, ${}^3J_{H-H} = 8.0$ Hz, 1 H, H^{18}), 7.24 (dd, ${}^3J_{H-H} = 8.1$ Hz, ${}^4J_{H-H} = 1.8$ Hz, 2 H, H^6), 7.18 (d, ${}^4J_{H-H} = 1.8$ Hz, 2 H, H^8), 1.02 (s, 18 H, tBu).

${}^{13}C\{{}^1H\}$ NMR (CD_2Cl_2 , 75.48 MHz, 298 K): δ 168.5 (s, C^9), 156.0 (s, $C^3 + C^4$), 145.2 (s, C^7), 138.8 (s, C^2), 136.4 (s, $C^{10/11/16}$), 135.6 (s, $C^{17/19}$), 134.7 (s, $C^{10/11/16}$), 134.6 (s, $C^{10/11/16}$), 130.7 (s, C^8), 128.9 (s, C^{15}), 128.8 (s, $C^{17/19}$), 127.6 (s, C^{12}), 126.7 (s, $C^{13/14}$), 126.4 (s, $C^{13/14}$), 126.1 (s, C^{18}), 125.8 (s, C^5), 124.3 (s, C^6), 35.5 (s, $C(CH_3)_3$), 30.9 (s, CH_3).

Elemental Microanalysis $C_{34}H_{33}AuN_2S$ (698.68): C, 58.45%; H, 4.76%; N, 4.01%. Found: C, 58.45%; H, 4.67%; N, 4.00%.

$(C^{\wedge}N^{py}\wedge C)AuSNp-2$ (**11**)

Synthesised using method 1 with $(C^{\wedge}N^{py}\wedge C)AuCl$ (0.050 g, 0.087 mmol) and 2-naphthalenethiol (0.014 g, 0.087 mmol) to give **11** as a pure product (0.041 g, 0.058 mmol, 67%). Single crystals suitable for X-ray diffraction were obtained from slow evaporation of a dichloromethane/isopropanol (4:1) mixture.



1H NMR (CD_2Cl_2 , 300.13 MHz, 298 K): 8.20 (s, 1 H, H^{11}), 7.88 (t, ${}^3J_{H-H} = 8.0$ Hz, 1 H, H^1), 7.75 (d, ${}^3J_{H-H} = 7.4$ Hz, 1 H, H^{16}), 7.70 (d, ${}^3J_{H-H} = 7.0$ Hz, 1 H, H^{13}), 7.64 (m, 2 H, $H^{18} + H^{19}$), 7.55 (d, ${}^3J_{H-H} = 8.1$ Hz, 2 H, H^5), 7.51 (d, ${}^3J_{H-H} = 8.0$ Hz, 2 H, H^2), 7.43 (m, 2 H, $H^{14} + H^{15}$),

7.38 (d, $^4J_{\text{H-H}} = 2.0$ Hz, 2 H, H⁸), 7.21 (dd, $^3J_{\text{H-H}} = 8.1$ Hz, $^4J_{\text{H-H}} = 2.0$ Hz, 2 H, H⁶), 1.00 (s, 18 H, ^tBu).

$^{13}\text{C}\{^1\text{H}\}$ NMR (CD₂Cl₂, 75.48 MHz, 298 K): δ 168.0 (s, C⁹), 163.6 (s, C³), 154.9 (s, C⁴), 147.3 (s, C⁷), 142.4 (s, C¹), 135.9 (s, C^{10/12/17}), 134.3 (s, C^{10/12/17}), 133.6 (s, C^{18/19}), 132.6 (s, C¹¹), 132.4 (s, C^{10/12/17}), 131.1 (s, C⁸), 127.9 (s, C^{18/19} + C¹⁶), 127.3 (s, C¹³), 126.6 (s, C^{14/15}), 125.7 (s, C^{14/15}), 125.3 (s, C⁵), 124.1 (s, C⁶), 116.7 (s, C²), 35.3 (s, C(CH₃)₃), 30.9 (s, CH₃).

Elemental Microanalysis C₃₅H₃₄AuNS (697.69): C, 60.25%; H, 4.91%; N, 2.01%. Found: C, 60.07%; H, 4.97%; N, 2.16%.

6.2.2 Complexes in Chapter Three

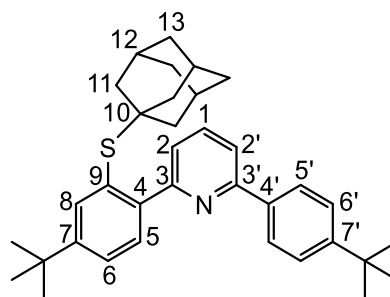
General methods used in this chapter:

Method 4 (for the *in situ* reductive elimination reactions): Under a N₂ atmosphere, a J-Young NMR tube was charged with the gold(III) complex (0.005 g) and the corresponding thiol in CD₂Cl₂ (0.6 mL). The tube was sealed, and the reaction monitored by ¹H NMR spectroscopy until the reaction was complete.

Method 5: A J-Young's NMR tube was charged with a gold complex (0.005 g), HAB₂ (1 molar equivalent) and CD₂Cl₂ (0.6 mL).⁸ The reaction monitored by ¹H NMR spectroscopy until no further changes were observed.

HC^NP^YCSAd (**12**)

Using method 4 and adamantyl thiol (0.004 g, 0.026 mmol). The reaction was monitored for 3 hours until the reaction went to completion and the fading of the yellow colour of (C^NP^YC)AuCl was observed to give a clear solution. Over 2 days a white precipitate of the proposed [ClAuSAd]_nH_n compound was observed.



¹H NMR (CD₂Cl₂, 300.13 MHz, 298 K): δ 8.26 (t, $^3J_{\text{H-H}} = 8.0$ Hz, 1 H, H¹), 8.12 (d, $^3J_{\text{H-H}} = 8.6$ Hz, 2 H, H⁵), 7.90 (dd, $^3J_{\text{H-H}} = 8.0$ Hz, $^4J_{\text{H-H}} = 0.8$ Hz, 1 H, H²), 7.78 (d, $^4J_{\text{H-H}} = 1.9$ Hz, 1 H, H⁸), 7.70 (dd, $^3J_{\text{H-H}} = 8.0$ Hz, $^4J_{\text{H-H}} = 0.8$ Hz, 1 H, H²), 7.67 (d, $^3J_{\text{H-H}} = 8.1$ Hz, 1 H, H⁵), 7.65 (d, $^3J_{\text{H-H}} = 8.6$ Hz, 2 H, H⁶), 7.60 (dd, $^3J_{\text{H-H}} = 8.1$ Hz, $^4J_{\text{H-H}} = 1.9$ Hz, 1 H, H⁶), 1.88 (bs, 3 H, H¹²), 1.57 (d, $^3J_{\text{H-H}} = 2.3$ Hz, 6 H, H¹¹), 1.50 (m, 6 H, H¹³), 1.41 (s, 9 H, ^tBu), 1.39 (s, 9 H, ^tBu').

$^{13}\text{C}\{^1\text{H}\}$ NMR (CD₂Cl₂, 75.48 MHz, 298 K): δ 156.0 (s, C⁷), 155.4 (s, C³), 154.5 (s, C⁷), 153.7 (s, C³), 142.9 (s, C¹), 137.5 (s, C⁸), 136.1 (s, C⁴), 131.5 (s, C⁵), 130.7 (s, C⁹), 130.0 (s, C⁵),

128.8 (s, C⁴), 127.6 (s, C²), 126.4 (s, C^{6+6'}), 123.9 (s, C^{2'}), 50.5 (s, C¹⁰), 44.0 (s, C¹¹), 36.2 (s, C¹³), 35.4 (s, CMe₃'), 35.2 (s, CMe₃), 31.3 (s, CMe₃ + CMe₃'), 30.5 (s, C¹²).

Bulk synthesis: Under a N₂ atmosphere, a Schlenk tube was charged with (C^{N^{py}})AuCl (0.030 g, 0.052 mmol) and adamantyl thiol (0.018 g, 0.105 mmol), which were then dissolved in dichloromethane (5 mL). The reaction was stirred at room temperature for 4 hours until the solution turned from yellow to colourless. The solvent was removed under vacuum, petrol (5 mL) was added and the suspension filtered. The solvent was removed to give **12** as a white solid (0.025 g, 94%).

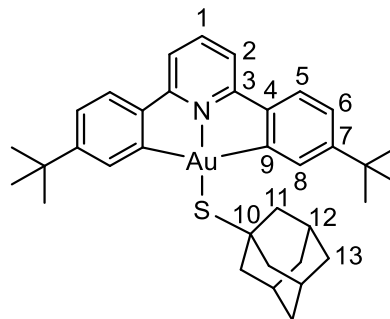
¹H NMR (CD₂Cl₂, 300.13 MHz, 298 K): δ 7.98 (d, ³J_{H-H} = 8.4 Hz, 2 H, H^{5'}), 7.76 (t, ³J_{H-H} = 7.7 Hz, 1 H, H¹), 7.68 (overlapped s, 1 H, H⁸), 7.67 (overlapped d, 1 H, H^{2'}), 7.61 (d, ³J_{H-H} = 8.0 Hz, 1 H, H⁵), 7.5 (m, 4 H, H^{6+6'+2}), 1.86 (br s, 3H, H¹²), 1.57 (br d, ³J_{H-H} = 1.4 Hz, 6 H, H¹¹), 1.51 (m, 6 H, H¹³), 1.39 (s, 9 H, 'Bu'), 1.36 (s, 9 H, 'Bu').

¹³C{¹H} NMR (CD₂Cl₂, 75.48 MHz, 298 K): δ 159.4, 156.5, 152.3, 151.3, 144.9, 137.2, 137.1, 135.9, 130.7, 128.7, 127.0, 126.2, 125.9, 125.0, 118.4, 49.7, 44.0, 36.4, 34.9, 34.8, 31.4, 31.4, 30.5.

TOF MS ASAP+: m/z [**12**+H]⁺ 510.3194 (calc. 510.3195). Spectrum displays the expected isotopic pattern.

(C^{N^{py}})AuSAd (**14**)

Synthesised by method 2 with (C^{N^{py}})AuCl (0.040 g, 0.070 mmol) and 1-adamantanethiol (0.012 g, 0.070 mmol). **14** was isolated as a bright yellow solid (0.045 g, 0.059 mmol, 91%).

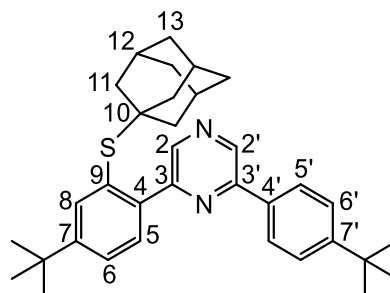


¹H NMR (CD₂Cl₂, 300.13 MHz, 298 K): δ 8.46 (d, ⁴J_{H-H} = 2.0 Hz, 2 H, H⁸), 7.83 (t, ³J_{H-H} = 8.0 Hz, 1 H, H¹), 7.54 (d, ³J_{H-H} = 8.1 Hz, 2 H, H⁵), 7.47 (d, ³J_{H-H} = 8.0 Hz, 2 H, H²), 7.27 (dd, ³J_{H-H} = 8.1 Hz, ⁴J_{H-H} = 2.0 Hz, 2 H, H⁶), 2.14 (bd, ³J_{H-H} = 2.4 Hz, 6 H, H¹¹), 1.92 (bs, 3 H, H¹²), 1.61 (s, 6 H, H¹³), 1.39 (s, 18 H, 'Bu').

¹³C{¹H} NMR (CD₂Cl₂, 75.48 MHz, 298 K): δ 171.6 (s, C⁴), 164.0 (s, C³), 154.8 (s, C⁷), 147.4 (s, C⁹), 142.6 (s, C¹), 134.1 (s, C⁸), 125.0 (s, C⁵), 123.8 (s, C⁶), 116.6 (s, C²), 50.2 (s, C¹¹), 48.5 (s, C¹⁰), 36.7 (s, C¹³), 35.9 (s, C(CH₃)₃), 31.4 (s, C(CH₃)₃), 31.2 (s, C¹²).

HC^{N^{pz}}CSAd (**15**)

Using method 4 with (C^{N^{pz}}C)AuCl (0.005 g, 0.0087 mmol) and adamantyl thiol (0.004 g, 0.026 mmol). The reaction monitored by ¹H NMR over 3 hours until the reaction was complete forming **15** and [ClAuSAd]_nH_n. Over the course of the reaction the solution turned from bright yellow to colourless. Over the following 2 days a white precipitate of [ClAuSAd]_nH_n was observed.



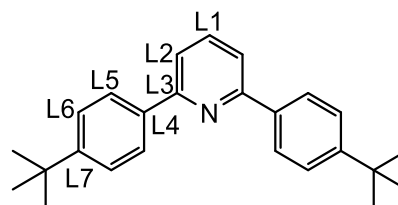
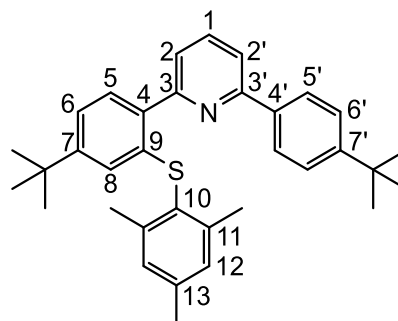
¹H NMR (CD₂Cl₂, 300.13 MHz, 298 K): δ 8.91 (s, 1 H, H²), 8.89 (s, 1 H, H^{2'}), 8.12 (d, ³J_{H-H} = 8.6 Hz, 2 H, H⁵), 7.81 (d, ³J_{H-H} = 8.1 Hz, 1 H, H⁵), 7.77 (d, ⁴J_{H-H} = 1.8 Hz, 1 H, H⁸), 7.65 (partially overlapped dd, ³J_{H-H} = 8.1 Hz, ⁴J_{H-H} = 1.8 Hz, 1 H, H⁶), 7.63 (d, ³J_{H-H} = 8.6 Hz, 1 H, H^{6'}), 1.86 (bs, 3 H, H¹²), 1.53 (d, ³J_{H-H} = 1.8 Hz, 6 H, H¹¹), 1.47 (m, 6 H, H¹³), 1.41 (s, 9 H, ^tBu), 1.38 (s, 9 H, ^tBu').

¹³C{¹H} NMR (CD₂Cl₂, 75.48 MHz, 298 K): δ 159.1 (s, C^{3/3'}), 156.2 (s, C^{3/3'/7'}), 156.1 (s, C^{3/3'/7'}), 154.7 (s, C⁷), 138.9 (s, C⁴), 137.7 (s, C⁸), 134.4 (s, C²), 131.5 (s, C^{4'}), 131.1 (s, C⁵), 128.9 (s, C⁹), 127.8 (s, C^{2'}), 127.4 (s, C^{5'}), 127.3 (s, C⁶), 127.0 (s, C^{6'}), 51.2 (s, C¹⁰), 43.9 (s, C¹¹), 36.2 (s, C¹³), 35.4 (s, CMe₃'), 35.2 (s, CMe₃), 31.2 (s, CMe₃ + CMe₃'), 30.5 (s, C¹²).

TOF MS ASAP+: m/z [**15**+H]⁺ 511.141 (calc. 511.3129). Spectrum displays the expected isotopic pattern.

HC^{N^{py}}CSMes (**16**) + HC^NCH (**L2**)

Synthesised with (C^{N^{py}}C)AuCl (0.005 g, 0.0087 mmol) and 2,4,6-trimethylthiophenol (4 μL, 0.026 mmol). The reaction was monitored by ¹H NMR over 4 hours until the reaction was complete and the solution turned from yellow to a clear colourless solution. The reaction gave **16** and free ligand (**L2**) in a ratio of 1:3.3 respectively. Over 2 days a white precipitate of an [ClAuSAr]H compound was observed.



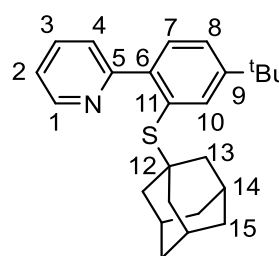
¹H NMR (CD₂Cl₂, 300.13 MHz, 298 K): δ 8.26 (t, ³J_{H-H} = 8.0 Hz, 1 H, H¹), 8.25 (t, ³J_{H-H} = 7.9 Hz, 1 H, H^{L1}), 8.07 (d, ³J_{H-H} = 8.6 Hz, 2 H, H⁵), 8.03 (d, ³J_{H-H} = 8.6 Hz, 4 H, H^{L5}), 7.90 (dd, ³J_{H-H} = 8.1 Hz, ⁴J_{H-H} = 0.9 Hz, 1 H, H²), 7.86 (dd, ³J_{H-H} = 7.9 Hz, ⁴J_{H-H} = 0.9 Hz, 1 H, H²), 7.83 (d, ³J_{H-H} = 8.0 Hz, 2 H, H^{L2}), 7.63 (d, ³J_{H-H} = 8.3 Hz, 2 H + 4 H, H^{6'+L6}), 7.53 (d, ³J_{H-H} = 8.0

Hz, 1 H, H⁵), 7.29 (dd, ³J_{H-H} = 8.0 Hz, ⁴J_{H-H} = 1.8 Hz, 1 H, H⁶), 6.98 (s, 2 H, H¹²), 6.83 (d, ⁴J_{H-H} = 1.8 Hz, 1 H, H⁸), 2.33 (s, 6 H, *o*-Me), 2.26 (s, 3 H, *p*-Me), 1.39 (s, 9 H, ¹Bu' + L¹Bu), 1.1 7 (s, 9 H, ¹Bu).

¹³C{¹H} NMR (CD₂Cl₂, 75.48 MHz, 298 K): δ 155.9 (s, C^{7/L7}), 155.7 (s, C^{7/L7/L3}), 155.4 (s, C^{7/L7/L3}), 154.9 (s, C^{7/3/3'}), 154.8 (s, C^{7/3/3'}), 154.7 (s, C^{7/3/3'}), 143.7 (s, C¹³), 143.5 (s, C^{L1}), 143.3 (s, C¹), 139.8 (s, C¹¹), 137.8 (s, C¹⁰), 132.0 (s, C⁵), 129.9 (s, C¹²), 129.8 (s, C^{5'/L5}), 129.7 (s, C^{5'/L5}), 128.6 (s, C⁴), 127.0 (s, C¹⁰), 126.4 (s, C⁶ + C^{L6}), 126.2 (s, C²), 126.1 (s, C⁴ + C^{L4}), 124.2 (s, C⁸), 123.8 (s, C^{2'}), 123.6 (s, C^{L2}), 122.4 (s, C⁶), 35.4 (s, CMe₃' + L CMe₃), 35.2 (s, CMe₃), 31.3 (s, CMe₃' + L CMe₃), 31.0 (s, CMe₃), 22.1 (s, C^{Me11}), 30.5 (s, C^{Me13}).

N^{py}CSAd (**19**)

In a J Young NMR tube, (C^N)AuCl₂ (0.005 g, 0.011 mmol) and adamantyl thiol (0.005 g, 0.031 mmol) were dissolved in CD₂Cl₂ (0.6 mL). The reaction was monitored by ¹H NMR for 5 days at room temperature. Further adamantyl thiol (0.015 g, 0.093) was added, then the NMR tube was heated to 50 °C for 4 months until no further changes were observed in the ¹H NMR spectrum. Over the course of the reaction a white precipitate was observed. **19** (80%) and **L18** (20%) were observed in the final ¹H NMR spectrum.



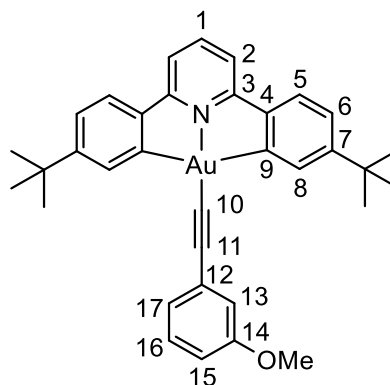
¹H NMR (CD₂Cl₂, 300.13 MHz, 298 K): δ 8.90 (d, ³J_{H-H} = 5.6 Hz, 1 H, H¹), 8.34 (pseudo triplet, ³J_{H-H} = 7.3 Hz, 1 H, H³), 8.07 (d, ³J_{H-H} = 8.2 Hz, 1 H, H⁴), 7.83 (pseudo triplet, ³J_{H-H} = 6.6 Hz, 1 H, H²), 7.79 (d, ⁴J_{H-H} = 1.8 Hz, 1 H, H¹⁰), 7.76 (d, ³J_{H-H} = 8.2 Hz, 1 H, H⁷), 7.66 (dd, ³J_{H-H} = 8.2 Hz, ⁴J_{H-H} = 1.8 Hz, 1 H, H⁸), 1.90 (overlapped with free thiol observed by NOE, H¹⁴), 1.51 (d + m, ³J_{H-H} = 2.1 Hz, 13 H, H¹³ + H¹⁵), 1.40 (s, 9 H, ¹Bu).

¹³C{¹H} NMR (CD₂Cl₂, 75.48 MHz, 298 K): δ 155.1 (s, C⁹), 153.7 (s, C⁵), 143.6 (s, C³), 141.5 (s, C¹), 138.3 (s, C¹⁰), 134.9 (s, C⁶), 131.4 (s, C⁷), 130.9 (s, C⁴), 129.7 (s, C¹¹), 127.1 (s, C⁸), 124.8 (s, C²), 51.0 (s, C¹²), 43.8 (s, C¹³), 36.2 (s, C¹⁵), 35.2 (s, CMe₃), 31.1 (s, CMe₃), 30.4 (s, C¹⁵).

TOF MS ASAP+: *m/z* [**19**+H]⁺ 378.2257 (calc. 378.2256). Spectrum displays the expected isotopic pattern.

$(C^{\wedge}N^{Pz^{\wedge}}C)AuC\equiv Cphenyl-OMe-m$ (**21**)

A flask was charged with $(C^{\wedge}N^{Py^{\wedge}}C)AuCl$ (0.040 g, 0.070 mmol), $[AgC\equiv CC_6H_4-3-OMe]_n$ ⁷ (0.050 g, 0.210 mmol) and dichloromethane (10 mL). The reaction was stirred in the dark for 21 days. The solution was filtered through celite and evaporated to dryness giving a solid which was washed with petrol. The pure product **21** was isolated as a light yellow powder (0.024 g, 51%).

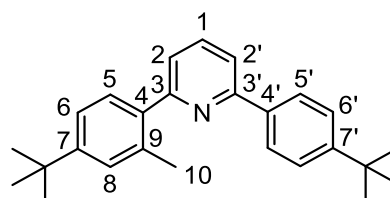


¹H NMR (CD₂Cl₂, 300.13 MHz, 298 K): δ 8.17 (d, ³J_{H-H} = 2.0 Hz, 2 H, H⁸), 7.85 (t, ³J_{H-H} = 8.0 Hz, 1 H, H¹), 7.54 (d, ³J_{H-H} = 8.2 Hz, 2 H, H⁵), 7.44 (d, ³J_{H-H} = 8.0 Hz, 2 H, H²), 7.32 (dd, ³J_{H-H} = 8.2 Hz, ⁴J_{H-H} = 2.0 Hz, 2 H, H⁶), 7.26 (dd, ³J_{H-H} = 8.0 Hz, 1 H, H¹⁶), 7.19 (d psd t, ³J_{H-H} = 7.6 Hz, ⁴J_{H-H} = 1.1 Hz, 1 H, H¹⁷), 7.14 (brm, 1 H, H¹³), 6.87 (ddd, ³J_{H-H} = 8.0 Hz, ⁴J_{H-H} = 2.4 Hz, ⁴J_{H-H} = 1.1 Hz, 1 H, H¹⁵), 3.84 (s, 3 H, O-Me), 1.39 (s, 18 H, ^tBu).

¹³C{¹H} NMR (CD₂Cl₂, 75.48 MHz, 298 K): δ 167.3 (s, C⁹), 165.2 (s, C³), 159.8 (s, C¹⁴), 155.6 (s, C⁷), 147.0 (s, C⁴), 142.7 (s, C¹), 133.7 (s, C⁸), 129.6 (s, C¹⁶), 128.1 (s, C¹²), 125.4 (s, C⁵), 124.7 (s, C¹⁷), 124.3 (s, C⁶), 116.8 (s, C¹³), 116.7 (s, C²), 114.0 (s, C¹⁵), 101.4 (s, C¹¹), 92.7 (s, C¹⁰), 55.5 (s, O-CH₃) 35.7 (s, C(CH₃)₃), 31.3 (s, C(CH₃)₃).

 $HC^{\wedge}N^{Py^{\wedge}}CMe$ (**22**)

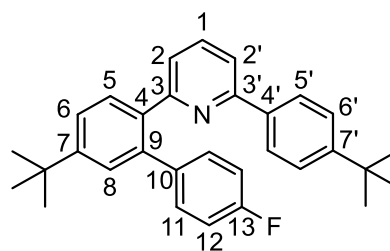
Synthesised using method 4 with $(C^{\wedge}N^{Py^{\wedge}}C)Au-Me$ (0.005 g, 0.009 mmol) and adamantyl thiol (0.006 g, 0.036 mmol). The reaction monitored by ¹H NMR over 24 days until the reaction was complete forming **22**.



¹H NMR (CD₂Cl₂, 300.13 MHz, 298 K): δ 8.02 (d, ³J_{H-H} = 8.5 Hz, 2 H, H⁵), 7.81 (t, ³J_{H-H} = 7.8 Hz, 1 H, H¹), 7.70 (dd, ³J_{H-H} = 7.9 Hz, ⁴J_{H-H} = 0.9 Hz, 1 H, H^{2/2'}), 7.50 (d, ³J_{H-H} = 8.5 Hz, 2 H, H⁶), 7.40 (d, ³J_{H-H} = 7.8 Hz, 1 H, H⁵), 7.33 (m, 3 H, H^{2/2'} + H⁶ + H⁸), 2.46 (s, 3 H, H¹⁰), 1.37 (s, 9 H, ^tBu/^tBu'), 1.36 (s, 9 H, ^tBu/^tBu').

 $HC^{\wedge}N^{Py^{\wedge}}CC_6H_4-p-F$ (**23**)

Synthesised using method 4 with $(C^{\wedge}N^{Py^{\wedge}}C)Au-C_6H_4F$ (0.005 g, 0.008 mmol) and adamantyl thiol (0.005 g, 0.032 mmol). The reaction monitored by ¹H NMR over 6 days until the reaction was complete forming **23**.



¹H NMR (CD₂Cl₂, 300.13 MHz, 298 K): δ 7.79 (d, ³J_{H-H} = 8.4 Hz, 2 H, H⁵), 7.68 (d, ³J_{H-H} = 8.1 Hz, 1 H, H⁵), 7.56 (m, 2 H, H¹ + H²), 7.53 (dd, ³J_{H-H} = 8.1 Hz, ⁴J_{H-H} = 1.9 Hz, 1 H, H⁶),

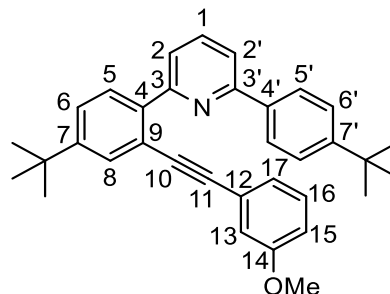
7.45 (m, 3 H, H⁶ + H⁸), 7.45 (m, 2 H, H¹¹), 6.96 (m, 3 H, H² + H¹²), 1.40 (s, 9 H, ^tBu), 1.35 (s, 9 H, ^tBu').

¹⁹F NMR (CD₂Cl₂, 282.36 MHz, 298K): δ -117.2 (br, *p*-F).

HC^{N^{py}}CC≡Cphenyl-OMe-*m* (**24**)

Synthesised using method 4 with (C^{N^{py}})Au-CC≡Cphenyl-OMe-*m* (0.005 g, 0.008 mmol) and adamantyl thiol (0.005 g, 0.030 mmol). The reaction monitored by ¹H NMR over 6 days until 50 % conversion.

Addition of further HSAd led to the formation of **24**.



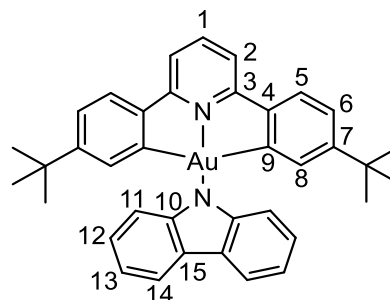
¹H NMR (CD₂Cl₂, 300.13 MHz, 298 K): δ 8.08 (d, ³J_{H-H} = 8.5 Hz, 2 H, H⁵), 7.85 (m, 3 H, H¹ + H² + H⁵), 7.75 (dd, ³J_{H-H} = 7.5 Hz, ⁴J_{H-H} = 1.2 Hz, 1 H, H²), 7.72 (d, ⁴J_{H-H} = 1.8 Hz, 1 H, H⁸), 7.54 (dd, ³J_{H-H} = 8.4 Hz, ⁴J_{H-H} = 1.8 Hz, 1 H, H⁶), 7.48 (d, ³J_{H-H} = 8.5 Hz, 2 H, H⁶), 7.20 (pseudo t, ³J_{H-H} = 7.9 Hz, 1 H, H¹⁶), 6.98 (d pseudo t, ³J_{H-H} = 7.8 Hz, ⁴J_{H-H} = 1.1 Hz, 1 H, H¹⁷), 6.89 (brm, 1 H, H¹³), 6.85 (ddd, ³J_{H-H} = 8.5 Hz, ⁴J_{H-H} = 2.5 Hz, ⁴J_{H-H} = 0.9 Hz, 1 H, H¹⁵), 3.71 (s, 3 H, O-*Me*), 1.40 (s, 9 H, ^tBu), 1.36 (s, 9 H, ^tBu').

¹³C{¹H} NMR (CD₂Cl₂, 75.48 MHz, 298 K): δ 159.8 (s, C¹⁴), 157.6 (s, C^{3/3'}), 156.9 (s, C^{3/3'}), 152.5 (s, C⁷), 151.8 (s, C⁷), 140.2 (s, C⁴), 136.9 (s, C⁴), 136.8 (s, C¹), 130.6 (s, C⁸), 130.0 (s, C⁵), 129.7 (s, C¹⁶), 126.9 (s, C⁵), 126.5 (s, C⁶), 126.0 (s, C⁶), 124.8 (s, C¹²), 124.2 (s, C¹⁷), 122.5 (s, C²), 121.1 (s, C⁹), 118.7 (s, C²), 116.4 (s, C¹³), 115.2 (s, C¹⁵), 92.0 (s, C¹¹), 90.0 (s, C¹⁰), 55.5 (s, O-*Me*), 34.9 (s, CMe₃' + CMe₃), 31.5 (s, CMe₃), 31.3 (s, CMe₃')

MS CI+: m/z [**24** + H]⁺ 474.3 (calc. 473.3).

(C^{N^{py}})Au-carbazole (**27**)

Under a N₂ atmosphere a flask was charged with (C^{N^{py}})AuCl (0.050 g, 0.087 mmol), carbazole (0.015 g, 0.087 mmol) and potassium t-butoxide (0.029 g, 0.26 mmol). Dry toluene (5 mL) was added and reaction was stirred at 60°C for 16 hours. The solution was filtered through celite and evaporated to dryness, then washed with petrol. The pure product **27** was isolated as a yellow powder (0.036 g, 59%).

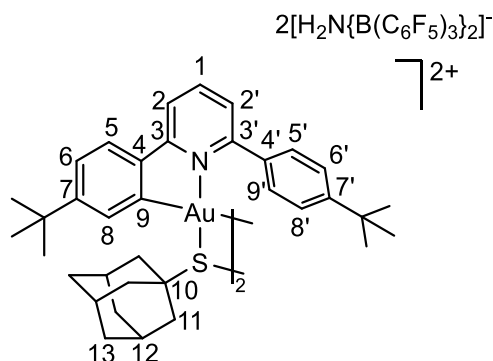


¹H NMR (CD₂Cl₂, 300.13 MHz, 298 K): δ 8.18 (d, ³J_{H-H} = 7.4 Hz, 2 H, H¹⁴), 7.94 (t, ³J_{H-H} = 8.0 Hz, 1 H, H¹), 7.58 (d, ³J_{H-H} = 8.2 Hz, 2 H, H⁵), 7.53 (d, ³J_{H-H} = 8.0 Hz, 2 H, H²), 7.49 (d, ³J_{H-H} = 8.3 Hz, 2 H, H¹¹), 7.25 (m, 4 H, H⁶⁺¹²), 7.11 (pseudo triplet, ³J_{H-H} = 7.4 Hz, 2 H, H¹³), 6.93 (d, ⁴J_{H-H} = 1.8 Hz, 2 H, H⁸), 0.96 (s, 18 H, ^tBu).

$^{13}\text{C}\{^1\text{H}\}$ NMR (CD_2Cl_2 , 75.48 MHz, 298 K): δ 168.5 (s, C^4), 165.6 (s, C^3), 155.4 (s, C^7), 146.2 (s, C^{10}), 146.2 (s, C^9), 143.4 (s, C^1), 133.1 (s, C^8), 125.3 (s, C^{15}), 125.2 (s, C^5), 124.4 (s, $\text{C}^{6/12}$), 124.3 (s, $\text{C}^{6/12}$), 120.0 (s, C^{14}), 117.2 (s, C^{13}), 116.8 (s, C^2), 35.2 (s, $\text{C}(\text{CH}_3)_3$), 30.8 (s, $\text{C}(\text{CH}_3)_3$).

$[(\text{C}^{\wedge}\text{N}^{\text{py}}\wedge\text{CH})\text{AuSAd}]_2\text{2}[\text{H}_2\text{N}\{\text{B}(\text{C}_6\text{F}_5)_3\}_2]$ (**28**)

Synthesised using method 5 with **14** (0.005 g, 0.0071 mmol), HAB_2 (0.008 g, 0.0071 mmol). The reaction monitored by ^1H NMR spectroscopy for 11 days until no further changes were observed. Crystals suitable for X-ray crystallography were obtained from a CD_2Cl_2 solution.



^1H NMR (CD_2Cl_2 , 300.13 MHz, 298 K): δ 8.33 (t, $^3J_{\text{H-H}} = 7.7$ Hz, 1 H, H^1), 8.05 (dd, $^3J_{\text{H-H}} = 8.0$ Hz, $^4J_{\text{H-H}} = 0.7$ Hz, 1 H, H^2), 7.80-7.50 (br m, 4 H, $\text{H}^{5'+6'+8'+9'}$), 7.79 (dd, $^3J_{\text{H-H}} = 7.7$ Hz, $^4J_{\text{H-H}} = 0.9$ Hz, 1 H, $\text{H}^{2'}$), 7.68 (d, $^3J_{\text{H-H}} = 8.3$ Hz, 1 H, H^5), 7.57 (dd, $^3J_{\text{H-H}} = 8.2$ Hz, $^4J_{\text{H-H}} = 1.3$ Hz, 1 H, H^6), 7.00 (d, $^4J_{\text{H-H}} = 1.2$ Hz, 1 H, H^8), 2.34 (d, $^2J_{\text{H-H}} = 11.2$ Hz, 3 H, H^{11}), 2.16 (br s, 3 H, H^{12}), 2.08 (d, $^2J_{\text{H-H}} = 11.4$ Hz, 3 H, H^{11}), 1.78 (m, 3 H, H^{13}), 1.58 (m, 3 H, H^{13}), 1.40 (s, 9 H, 'Bu), 1.18 (s, 9 H, 'Bu').

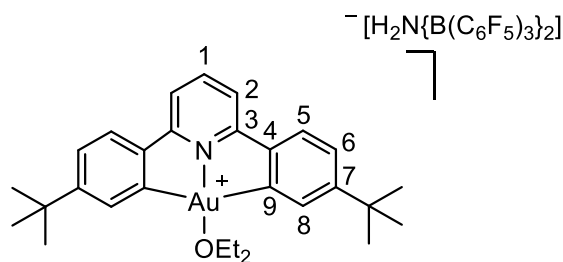
^1H NMR (CD_2Cl_2 , 300.13 MHz, 263 K): δ 8.33 (t, $^3J_{\text{H-H}} = 8.0$ Hz, 1 H, H^1), 8.04 (d, $^3J_{\text{H-H}} = 8.0$ Hz, 1 H, H^2), 7.88 (d, $^3J_{\text{H-H}} = 7.8$ Hz, 1 H, H^9), 7.78 (d, $^3J_{\text{H-H}} = 7.7$ Hz, 1 H, $\text{H}^{2'}$), 7.70 (d, $^3J_{\text{H-H}} = 8.2$ Hz, 1 H, H^8), 7.67 (d, $^3J_{\text{H-H}} = 8.5$ Hz, 1 H, H^5), 7.55 (d, $^3J_{\text{H-H}} = 8.1$ Hz, 1 H, H^6), 7.47 (br s, 2 H, $\text{H}^{5'+6'}$), 6.94 (s, 1 H, H^8), 2.31 (d, $^2J_{\text{H-H}} = 11.4$ Hz, 3 H, H^{11}), 2.14 (br s, 3 H, H^{12}), 2.01 (d, $^2J_{\text{H-H}} = 10.9$ Hz, 3 H, H^{11}), 1.74 (d, $^2J_{\text{H-H}} = 14.9$ Hz, 3 H, H^{13}), 1.55 (d, $^2J_{\text{H-H}} = 14.9$ Hz, 3 H, H^{13}), 1.36 (s, 9 H, 'Bu), 1.14 (s, 9 H, 'Bu' + Et_2O signal).

$^{13}\text{C}\{^1\text{H}\}$ NMR (CD_2Cl_2 , 75.48 MHz, 298 K): δ 162.8 (s, C^3), 161.3 (s, C^9), 160.5 (s, $\text{C}^{3'}$), 157.8 (s, $\text{C}^{7'}$), 157.3 (s, C^7), 148.2 (brd, $^1J_{\text{C-F}} = 243.8$ Hz, *o*-C-F $\text{H}_2\text{N}[\text{B}(\text{C}_6\text{F}_5)_3]_2^-$), 144.8 (s, C^1), 139.5 (brd, $^1J_{\text{C-F}} = 246.1$ Hz, *p*-C-F $\text{H}_2\text{N}[\text{B}(\text{C}_6\text{F}_5)_3]_2^-$), 139.3 (s, C^4), 137.0 (brd, $^1J_{\text{C-F}} = 248.3$ Hz, *m*-C-F $\text{H}_2\text{N}[\text{B}(\text{C}_6\text{F}_5)_3]_2^-$), 135.3 (br s, C^{Anion}), 134.4 (s, C^4), 129.2 (s, C^6), 128.7 (s, C^5), 128.3 (s, C^{Aryl}), 127.4 (s, C^{Aryl}), 127.0 (s, $\text{C}^{2'}$), 125.9 (s, C^8), 120.6 (s, C^2), 69.9 (s, C^2), 49.2 (s, C^{11}), 37.0 (s, CMe_3), 35.5 (s, CMe_3'), 35.4 (s, C^{13}), 31.7 (s, C^{12}), 31.3 (s, CMe_3), 30.1 (s, CMe_3').

To trigger reductive elimination from **28**: Addition of dimethyl sulfide (4 μL , 0.0034 mmol) to a solution of **28** in a J-Young NMR tube gave **12**. Over the course of the 4 hours the solution changed from yellow to colourless.



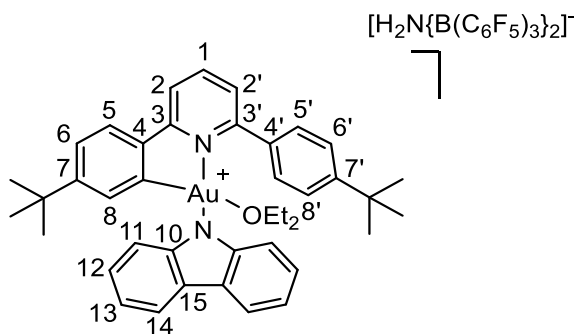
Obtained as a transient species using method 5 with **26** (0.005 g, 0.007 mmol) and HAB₂ (0.009 g, 0.007 mmol).



¹H NMR (CD₂Cl₂, 300.13 MHz, 298 K): δ 7.96 (t, ³J_{H-H} = 8.0 Hz, 1 H, H¹), 7.56 (d, ³J_{H-H} = 8.2 Hz, 2 H, H⁵), 7.47 (d, ⁴J_{H-H} = 1.6 Hz, 1 H, H⁸), 7.44 (d, ³J_{H-H} = 8.0 Hz, 2 H, H²), 7.43 (dd, ³J_{H-H} = 8.1 Hz, ⁴J_{H-H} = 1.6 Hz, 2 H, H⁶), 7.93 (pst, ³J_{H-F/H-H} = 8.0 Hz, 2 H, phenol H), 6.78 (m, 2 H, phenol H), 4.68 (q, ³J_{H-H} = 7.0 Hz, 4 H, Et), 4.68 (t, ³J_{H-H} = 7.0 Hz, 6 H, Et), 1.37 (s, 18 H, ^tBu).



Synthesised using method 5 with **28** (0.005 g, 0.007 mmol) and HAB₂ (0.009 g, 0.007 mmol), to give **30**. The species decomposed over 3 hours.



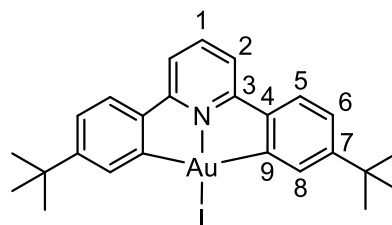
¹H NMR (CD₂Cl₂, 300.13 MHz, 298 K): δ 8.21 (d, ³J_{H-H} = 7.5 Hz, 2 H, H¹⁴), 7.98 (t, ³J_{H-H} = 8.0 Hz, 1 H, H¹), 7.90 (d, ³J_{H-H} = 7.9 Hz, 2 H, H¹¹), 7.76 (m, 3 H, H⁵⁺¹³), 7.60 (m, 5 H, H⁸⁺⁶⁺¹²⁺²), 7.41 (m, 3 H, H^{2'+5'}), 7.12 (dd, ³J_{H-H} = 8.2 Hz, ⁴J_{H-H} = 1.8 Hz, 1 H, H^{6'}), 5.62 (d, ⁴J_{H-H} = 1.0 Hz, 1 H, H⁸), 3.49 (brs, 12 H, CH₂ (OEt₂)), 1.17 (t, ³J_{H-H} = 7.1 Hz, 18 H, CH₃ (OEt₂)), 1.41 (s, 9 H, ^tBu), 0.91 (s, 9 H, ^tBu').

6.2.3 Complexes in Chapter Four



Under a N₂ atmosphere (C[∧]N^{P∨∧}C)AuCl (0.050 g, 0.087 mmol) was dissolved in dry THF (6 mL) to this solution, IZnC₆H₄-*p*-Me 0.5 M in THF (0.35, 0.174 mmol) was added and the reaction was stirred for 16 hours. In air, the solution was passed through a silica plug and the solvent was removed *in vacuo* to give a solid.

This was washed with petrol to give **32** as a light yellow solid (0.030 g, 52%).



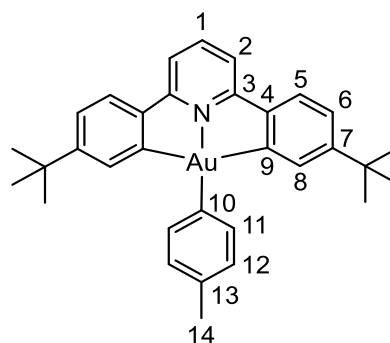
^1H NMR (CD_2Cl_2 , 300.13 MHz, 298 K): δ 8.52 (d, $^4J_{\text{H-H}} = 1.9$ Hz, 2 H, H^8), 7.87 (t, $^3J_{\text{H-H}} = 8.0$ Hz, 1 H, H^1), 7.50 (d, $^3J_{\text{H-H}} = 8.2$ Hz, 2 H, H^5), 7.40 (d, $^3J_{\text{H-H}} = 8.2$ Hz, 2 H, H^2), 7.27 (dd, $^3J_{\text{H-H}} = 8.2$ Hz, $^4J_{\text{H-H}} = 1.9$ Hz, 2 H, H^6), 1.36 (s, 18 H, ^tBu).

$^{13}\text{C}\{^1\text{H}\}$ NMR (CD_2Cl_2 , 75.48 MHz, 298 K): δ 168.7 (s, C^9), 165.2 (s, C^3), 156.4 (s, C^7), 146.9 (s, C^4), 142.8 (s, C^1), 135.9 (s, C^8), 125.6 (s, C^5), 123.9 (s, C^6), 116.7 (s, C^2), 35.9 (s, $\text{C}(\text{CH}_3)_3$), 31.3 (s, $\text{C}(\text{CH}_3)$).

Elemental Microanalysis: Calc. $\text{C}_{25}\text{H}_{27}\text{AuNI}$ (665.37): C, 45.13%; H, 4.09%; N, 2.11%. Found: C, 45.22%; H, 4.01%; N, 2.15%.

$(\text{C}^{\wedge}\text{N}^{\text{py}}\wedge\text{C})\text{AuC}_6\text{H}_4\text{-}p\text{-Me}$ (**33**)

Synthesised from $(\text{C}^{\wedge}\text{N}^{\text{py}}\wedge\text{C})\text{AuCl}$: Under a N_2 atmosphere $(\text{C}^{\wedge}\text{N}^{\text{py}}\wedge\text{C})\text{AuCl}$ (0.030 g, 0.052 mmol) was suspended in dry toluene (6 mL) to this solution, $\text{IZnC}_6\text{H}_4\text{-}p\text{-Me}$ 0.5 M in THF (0.21 mL, 0.104 mmol) was added and the reaction was stirred for 4 days. In air, the solution was passed through a silica plug and the solvent was removed *in vacuo* to give a solid. This was washed with petrol to give **33** as a light yellow solid (0.029 g, 88%).



Synthesised from $(\text{C}^{\wedge}\text{N}^{\text{py}}\wedge\text{C})\text{AuSAd}$: Under a N_2 atmosphere $(\text{C}^{\wedge}\text{N}^{\text{py}}\wedge\text{C})\text{AuSAd}$ (0.050 g, 0.071 mmol) was dissolved in dry toluene (6 mL) to this solution, $\text{IZnC}_6\text{H}_4\text{-}p\text{-Me}$ 0.5 M in THF (0.28 mL, 0.142 mmol) was added and the reaction was stirred for 4 days. In air the solution was passed through a silica plug and the solvent was removed *in vacuo* to give a solid. This was washed with petrol to give **33** as a light yellow solid (0.031 g, 70%).

NMR synthesis: In a J-Youngs NMR tube, (0.005 g) of **11** was dissolved in d_8 -toluene. $\text{IZnC}_6\text{H}_4\text{-}p\text{-Me}$ 0.5 M in THF (2 molar equivalents) was added and the reaction was monitored by ^1H NMR until completion.

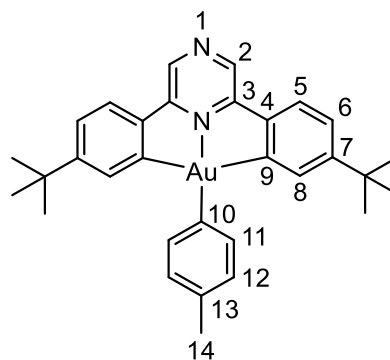
^1H NMR (CD_2Cl_2 , 300.13 MHz, 298 K): δ 7.83 (t, $^3J_{\text{H-H}} = 8.1$ Hz, 1 H, H^1), 7.59 (d, $^3J_{\text{H-H}} = 8.2$ Hz, 2 H, H^5), 7.55 (d, $^3J_{\text{H-H}} = 7.9$ Hz, 2 H, H^{11}), 7.50 (m, 4 H, $\text{H}^2 + \text{H}^8$), 7.26 (dd, $^3J_{\text{H-H}} = 8.2$ Hz, $^4J_{\text{H-H}} = 2.0$ Hz, 2 H, H^6), 7.15 (d, $^3J_{\text{H-H}} = 7.8$ Hz, 2 H, H^{12}), 2.39 (s, 3 H, H^{14}), 1.25 (s, 18 H, ^tBu).

$^{13}\text{C}\{^1\text{H}\}$ NMR (CD_2Cl_2 , 75.48 MHz, 298 K): δ 169.7 (s, C^9), 163.5 (s, C^3), 154.6 (s, C^7), 147.6 (s, C^4), 144.3 (s, C^{10}), 142.0 (s, C^1), 134.7 (s, C^{11}), 134.2 (s, C^{13}), 132.7 (s, C^8), 129.7 (s, C^{12}), 125.1 (s, C^5), 123.6 (s, C^6), 116.4 (s, C^2), 35.6 (s, $\text{C}(\text{CH}_3)_3$), 31.3 (s, $\text{C}(\text{CH}_3)$), 21.3 (s, C^{14}).

Elemental Microanalysis: Calc. $C_{32}H_{34}AuN$ (629.60): C, 61.05%; H, 5.44%; N, 2.22%. Found: C, 60.97%; H, 5.37%; N, 2.30%.

$(C^{\wedge}N^{Pz^{\wedge}}C)AuC_6H_4-p-Me$ (**34**)

Under a N_2 atmosphere $(C^{\wedge}N^{Pz^{\wedge}}C)AuCl$ (0.050 g, 0.087 mmol) was dissolved in dry toluene (6 mL) to this solution, $I ZnC_6H_4-p-Me$ 0.5 M in THF (0.35 mL, 0.174 mmol) was added. The solution was stirred for 6 hours, filtered and transferred to a flask with 10 mL water: isopropanol mixture and the reaction stirred 16 hours, whilst the solution turned from red to yellow. The mixture was separated and the organic fraction was washed with water (3 x 15 mL). The organic layer was dried over $MgSO_4$ and passed through a silica plug. Solvent was removed *in vacuo* to give **34** as a yellow solid (0.050 g, 91%).



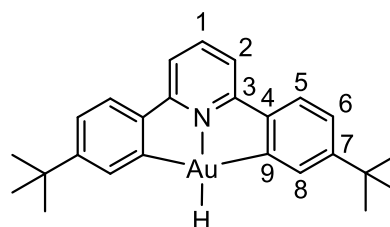
NMR synthesis: In a J-Youngs NMR tube, (0.005 g) of **4** was dissolved in d_8 -toluene. $I ZnC_6H_4-p-Me$ 0.5 M in THF (2 molar equivalents) was added and the reaction was monitored by 1H NMR until completion.

1H NMR (CD_2Cl_2 , 300.13 MHz, 298 K): δ 8.86 (s, 2 H, H^2), 7.68 (d, $^3J_{H-H} = 8.2$ Hz, 2 H, H^5), 7.54 (m, 4 H, $H^8 + H^{11}$), 7.30 (dd, $^3J_{H-H} = 8.2$ Hz $^4J_{H-H} = 2.0$ Hz, 2 H, H^6), 7.17 (d, $^3J_{H-H} = 7.7$ Hz, 2 H, H^{12}), 2.38 (s, 3 H, H^{14}), 1.26 (s, 18 H, tBu).

$^{13}C\{^1H\}$ NMR (CD_2Cl_2 , 75.48 MHz, 298 K): δ 169.5 (s, C^9), 156.3 (s, C^3), 155.8 (s, C^7), 145.3 (s, C^4), 143.6 (s, C^{10}), 138.4 (s, C^2), 134.6 (s, C^{13}), 134.4 (s, C^{11}), 131.1 (s, C^8), 129.8 (s, C^{12}), 125.6 (s, C^5), 123.9 (s, C^6), 35.7 (s, $C(CH_3)_3$), 31.2 (s, $C(CH_3)_3$), 21.3 (s, C^{14}).

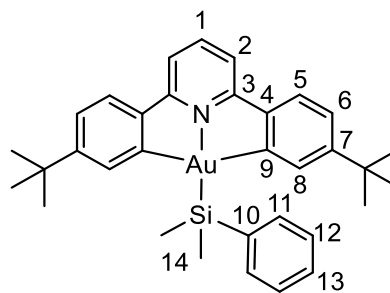
$(C^{\wedge}N^{Py^{\wedge}}C)AuH$ (**36**)

In an inert atmosphere in J-Youngs NMR tube, $(C^{\wedge}N^{Py^{\wedge}}C)Au-OH$ (0.010 g, 0.018 mmol) was dissolved in CD_2Cl_2 , to this was added HBpin (1.9 μ L, 0.018 mmol). The 1H NMR spectrum was recorded 40 minutes after addition of H-Bpin and the spectrum matched that previously reported for **36**.⁹



$(C^{\wedge}N^{py^{\wedge}}C)AuSiMePh_2$ (**38**)

In a J-Youngs NMR tube charged with $(C^{\wedge}N^{py^{\wedge}}C)AuCl$ (0.015 g, 0.026 mmol) and potassium *tert*-butoxide (0.005 g, 0.045 mmol) were suspended in dry *d*-8-toluene. The tube was heated to 60 °C until all the gold was dissolved and a clear bright yellow solution was observed.



In the 1H NMR spectrum the consumption of $(C^{\wedge}N^{py^{\wedge}}C)AuCl$ could be observed. To this solution (dimethylphenylsilyl)boronic acid pinacol ester (7.8 μ L, 0.029 mmol) was added and the reaction was monitored by 1H NMR for 24 hours until complete. Decomposition of this complex hindered further isolation.

1H NMR (C_7D_8 , 300.13 MHz, 298 K): δ 7.99 (d, $^4J_{H-H} = 1.9$ Hz, 2 H, H^8), 7.87 (m, 2 H, H^{11}), 7.30 (d, $^3J_{H-H} = 8.1$ Hz, 2 H, H^5), 7.17 (m, 3 H, $H^{12} + H^{13}$) (H^{13} indirectly observed), 7.13 (dd, $^3J_{H-H} = 8.1$ Hz, $^4J_{H-H} = 1.9$ Hz, 2 H, H^6), 6.94 (overlapped with solvent, 1 H, H^1), 6.80 (d, $^3J_{H-H} = 7.8$ Hz, 2 H, H^2), 1.21 (s, 18 H, tBu), 1.02 (s, 6 H, H^{14}).

$^{13}C\{^1H\}$ NMR (C_7D_8 , 75.48 MHz, 298 K): δ 167.4 (s, C^9), 161.9 (s, C^3), 153.7 (s, C^7), 149.6 (s, C^4), 143.3 (s, C^{10}), 140.5 (s, C^1), 137.0 (s, C^8), 135.6 (s, C^{11}), 128.7 (s, C^{13}), 127.9 (overlapped with solvent signal, observed by HMQC, C^{12}), 125.3 (s, C^5), 122.6 (s, C^6), 115.4 (s, C^2), 35.2 (s, $C(CH_3)_3$), 31.4 (s, $C(CH_3)_3$), 3.5 (s, C^{14}).

6.2.4 Complexes in Chapter Five

General methods used in this chapter:

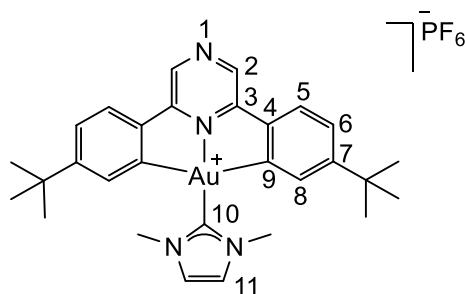
Method 6: A flask was charged with 1,3-dimethylimidazolium iodide (0.030 g, 0.131 mmol) and silver(I) oxide (0.012 g, 0.087 mmol) to which acetonitrile (20 mL) was added and stirred in the dark at room temperature for 6 h. To this solution, $(C^{\wedge}N^{\wedge}C)AuCl$ (0.087 mmol) and KPF_6 (0.080 g, 0.434 mmol) were added and reaction stirred for X h. The solvent was removed *in vacuo*, the solid was dissolved in dichloromethane and washed with water (3 x 20 mL). The dichloromethane solution was dried over $MgSO_4$ and filtered through celite. The solvent was removed *in vacuo* to give the product as a powder.

Method 7: A flask was charged with 1,3-dimethylbenzimidazolium iodide (0.024 mg, 0.087 mmol) and silver(I) oxide (0.012 g, 0.087 mmol) to which dichloromethane (10 mL) was added and stirred in the dark at room temperature for 6 h. $(C^{\wedge}N^{\wedge}C)AuCl$ (0.087 mmol) and KPF_6 (0.080 g, 0.434 mmol) were added and reaction stirred for X h. The solution was filtered through celite and the solvent was removed *in vacuo* to give the product as a powder.

Method 8: Under an N₂ atmosphere using standard Shlenk line techniques using a modified literature protocol; (C^{^N^C})AuCl (0.050 g) and potassium tert-butoxide were dissolved in dry degassed toluene (10 mL) and the reaction stirred for 3 hours. [1,3-dimethylcaffeine][BF₄]¹⁰ was added and reaction was heated to 80 °C for 16 hours. The solvent was removed *in vacuo* to give a solid. This was extracted into dichloromethane, filtered over celite and evaporated to dryness to give the pure product.

[(C^{^N^{pz}^C})Auimidazole]PF₆ (**40**)

Prepared using method 6 using the following amounts: (C^{^N^{pz}^C})AuCl (0.050 g, 0.087 mmol). For **40** the reaction time is 16 hours. **40** was isolated as a yellow powder (0.064 g, 0.082 mmol, 94%).

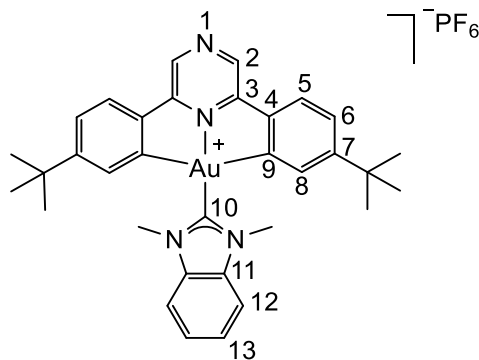


¹H NMR (CD₂Cl₂, 300.13 MHz, 298 K): δ 8.95 (s, 2 H, H²), 7.76 (d, ³J_{H-H} = 8.3 Hz, 2 H, H⁵), 7.53 (s, 2 H, H¹¹), 7.44 (dd, ³J_{H-H} = 8.2 Hz, ⁴J_{H-H} = 1.8 Hz, 2 H, H⁶), 7.02 (d, ⁴J_{H-H} = 1.8 Hz, 2 H, H⁸), 3.91 (s, 6 H, N-CH₃), 1.26 (s, 18 H, ^tBu).

¹³C{¹H} NMR (CD₂Cl₂, 75.48 MHz, 298 K): δ 165.4 (s, C⁹), 158.3 (s, C⁷), 157.3 (s, C³), 153.1 (s, C¹⁰ observed in the HMBC), 144.9 (s, C⁴), 139.7 (s, C²), 133.4 (s, C⁸), 127.2 (s, C⁵), 125.9 (s, C⁶), 125.1 (s, C¹¹), 39.0 (s, N-Me), 35.6 (s, C(CH₃)₃), 31.0 (s, C(CH₃)₃).

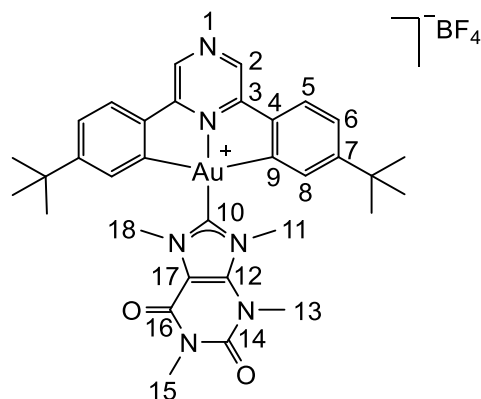
[(C^{^N^{pz}^C})Aubenzimidazole]PF₆ (**41**)

Prepared using method 7 using the following amounts: (C^{^N^{pz}^C})AuCl (0.050 g, 0.087 mmol). For **41** the reaction time is 16 hours. **41** was isolated as a yellow powder (0.065 g, 0.078 mmol, 90%).

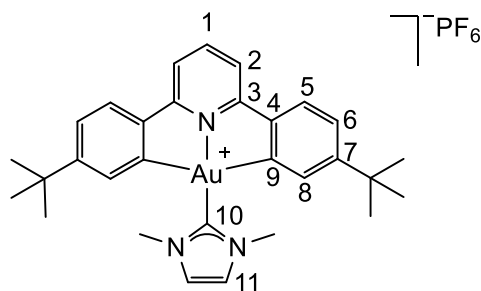


[(C^{N^{pz}}C)Aucaffeine]BF₄ (**42**)

Prepared using method 8 using the following amounts: (C^{N^{pz}}C)AuCl (0.050 g, 0.087 mmol), potassium tert-butoxide (0.012 g, 0.107 mmol), [1,3-dimethylcaffeine][BF₄] (0.026 g, 0.087 mmol). **42** was isolated as a yellow powder (0.050 g, 0.060 mmol, 69%).

[(C^{N^{py}}C)Auimidazole]PF₆ (**43**)

Prepared using method 6 using the following amounts: (C^{N^{py}}C)AuCl (0.050 g, 0.087 mmol). The reaction time for **43** is 16 hours. The product was isolated as a yellow powder (0.062 g, 0.079 mmol, 91%).



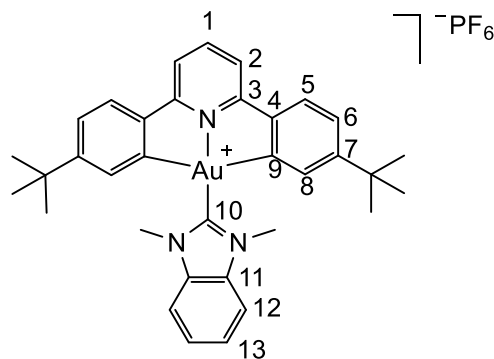
¹H NMR (CD₂Cl₂, 300.13 MHz, 298 K): δ 8.02 (t, ³J_{H-H} = 8.0 Hz, 1 H, H¹), 7.65 (d, ³J_{H-H} = 8.2 Hz, 2 H, H⁵), 7.58 (d, ³J_{H-H} = 8.0 Hz, 2 H, H²), 7.50 (s, 2 H, H¹¹), 7.39 (dd, ³J_{H-H} = 8.2 Hz, ⁴J_{H-H} = 1.7 Hz, 2 H, H⁶), 6.97 (d, ⁴J_{H-H} = 1.7 Hz, 2 H, H⁸), 3.91 (s, 6 H, N-CH₃), 1.25 (s, 18 H, ^tBu).

¹³C{¹H} NMR (CD₂Cl₂, 75.48 MHz, 298 K): δ 164.9 (s, C³), 164.4 (s, C⁹), 156.8 (s, C⁷), 154.5 (s, C¹⁰), 147.1 (s, C⁴), 144.3 (s, C¹), 132.8 (s, C⁸), 126.6 (s, C⁵), 125.5 (s, C⁶), 124.9 (s, C¹¹), 117.7 (s, C²), 38.9 (s, N-Me), 35.4 (s, C(CH₃)₃), 31.1 (s, C(CH₃)₃).

Elemental Microanalysis: Calc. C₃₀H₃₅AuN₃PF₆ (779.21): C, 46.22%; H, 4.53%; N, 5.39%. Found: C, 46.07%; H, 4.66%; N, 5.27%.

[(C^{N^{py}}C)Aubenzimidazole]PF₆ (**44**)

Prepared using method 7 using the following amounts: 1,3-dimethylbenzimidazolium iodide (0.024 g, 0.131 mmol), (C^{N^{py}}C)AuCl (0.050 g, 0.087 mmol). For **44** the reaction time is 16 hours. **44** was isolated as a yellow powder (0.069 g, 0.084 mmol, 96%).



¹H NMR (CD₂Cl₂, 300.13 MHz, 298 K): δ 8.06 (t, ³J_{H-H} = 8.0 Hz, 1 H, H¹), 7.81 (m, 2 H, H¹²), 7.72 (m, 2 H, H¹³), 7.68 (d, ³J_{H-H} = 8.3 Hz, 2 H, H⁵), 7.61 (d, ³J_{H-H} = 8.0 Hz, 2 H, H²), 7.40 (dd,

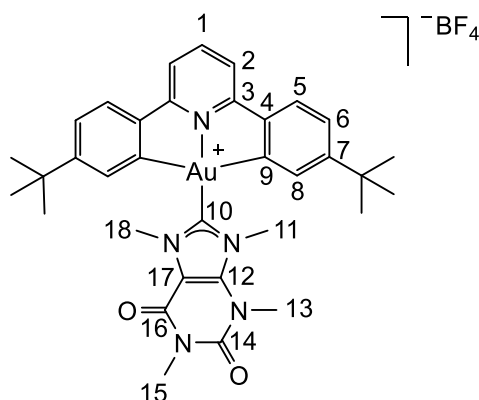
$^3J_{\text{H-H}} = 8.3 \text{ Hz}$, $^4J_{\text{H-H}} = 1.8 \text{ Hz}$, 2 H, H⁶), 6.93 (d, $^4J_{\text{H-H}} = 1.8 \text{ Hz}$, 2 H, H⁸), 4.13 (s, 6 H, N-CH₃), 1.17 (s, 18 H, ^tBu).

$^{13}\text{C}\{^1\text{H}\}$ NMR (CD₂Cl₂, 75.48 MHz, 298 K): δ 164.9 (s, C³), 164.2 (s, C⁹), 163.8 (s, C¹⁰, observed in HMBC), 156.8 (s, C⁷), 147.1 (s, C⁴), 144.6 (s, C¹), 134.7 (s, C¹¹), 132.7 (s, C⁸), 126.8 (s, C^{5/13}), 126.5 (s, C^{5/13}), 125.7 (s, C⁶), 117.9 (s, C²), 112.4 (s, C¹²), 36.2 (s, N-Me), 35.4 (s, C(CH₃)₃), 31.0 (s, C(CH₃)₃).

Elemental Microanalysis: Calc. C₃₄H₃₇AuN₃PF₆ (829.23): C, 49.22%; H, 4.50%; N, 5.07%. Found: C, 49.41%; H, 4.46%; N, 4.98%.

[(C^{^N}Py^{^C})Aucaffeine]BF₄ (**45**)

Prepared using method 8 using the following amounts: (C^{^N}Py^{^C})AuCl (0.050 g, 0.087 mmol), potassium tert-butoxide (0.012 g, 0.105 mmol), [1,3-dimethylcaffeine][BF₄] (0.026 g, 0.087 mmol). **45** was isolated as a yellow powder (0.042 g, 0.051 mmol, 58%).



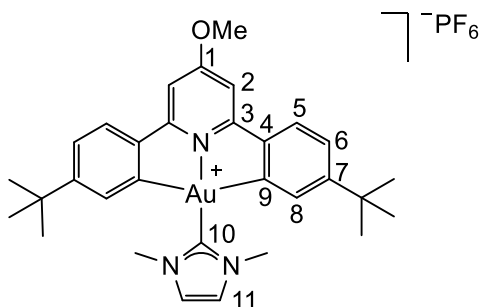
^1H NMR (CD₂Cl₂, 300.13 MHz, 298 K): δ 8.02 (t, $^3J_{\text{H-H}} = 8.0 \text{ Hz}$, 1 H, H¹), 7.66 (d, $^3J_{\text{H-H}} = 8.2 \text{ Hz}$, 2 H, H⁵), 7.58 (d, $^3J_{\text{H-H}} = 8.0 \text{ Hz}$, 2 H, H²), 7.39 (dd, $^3J_{\text{H-H}} = 8.2 \text{ Hz}$, $^4J_{\text{H-H}} = 1.5 \text{ Hz}$, 2 H, H⁶), 7.13 (d, $^4J_{\text{H-H}} = 1.5 \text{ Hz}$, 2 H, H⁸), 4.29 (s, 3 H, H¹¹), 4.19 (s, 3 H, H¹⁸), 3.94 (s, 3 H, H¹³), 3.45 (s, 3 H, H¹⁵), 1.26 (s, 18 H, ^tBu).

$^{13}\text{C}\{^1\text{H}\}$ NMR (CD₂Cl₂, 75.48 MHz, 298 K): δ 165.0 (s, C^{3/9}), 164.3 (s, C^{3/9}), 160.4 (s, C¹⁰), 157.1 (s, C⁷), 154.0 (s, C¹⁶), 151.0 (s, C¹⁴), 147.0 (s, C⁴), 144.5 (s, C¹), 141.6 (s, C¹²), 133.1 (s, C⁸), 126.7 (s, C⁵), 125.6 (s, C⁶), 117.8 (s, C²), 110.8 (s, C¹⁷), 40.2 (s, C¹¹), 38.6 (s, C¹⁸), 35.5 (s, C(CH₃)₃), 32.6 (s, C¹³), 31.1 (s, C(CH₃)₃), 29.0 (s, C¹⁵).

Elemental Microanalysis: Calc. C₃₄H₃₉AuN₅O₂BF₄ (833.28): C, 49.00%; H, 4.72%; N, 8.40%. Found: C, 49.21%; H, 4.60%; N, 8.31%.

[(C^{^N}Py^{OMe^C})Auimidazole]PF₆ (**46**)

Prepared using method 6 using the following amounts: (C^{^N}Py^{OMe^C})AuCl (0.055 g, 0.087 mmol). The reaction time for **46** is 8 days. **46** was isolated as a cream coloured powder (0.062 g, 0.077 mmol, 88%).



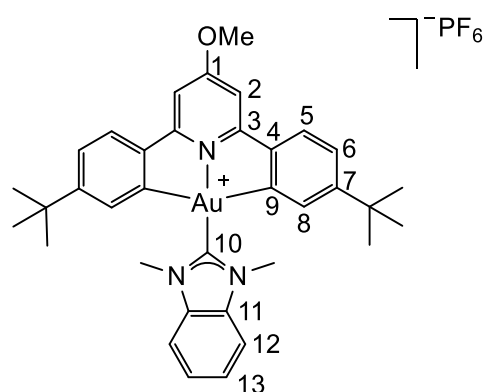
^1H NMR (CD_2Cl_2 , 300.13 MHz, 298 K): δ 7.63 (d, $^3J_{\text{H-H}} = 8.2$ Hz, 2 H, H^5), 7.49 (s, 2 H, H^{11}), 7.38 (dd, $^3J_{\text{H-H}} = 8.2$ Hz, $^4J_{\text{H-H}} = 1.8$ Hz, 2 H, H^6), 7.04 (s, 2 H, H^2), 6.97 (d, $^4J_{\text{H-H}} = 1.8$ Hz, 2 H, H^8), 4.1 (s, 3 H, O- CH_3), 3.90 (s, 6 H, N- CH_3), 1.25 (s, 18 H, ^tBu).

$^{13}\text{C}\{^1\text{H}\}$ NMR (CD_2Cl_2 , 75.48 MHz, 298 K): δ 172.1 (s, C^1), 166.4 (s, C^3), 164.3 (s, C^9), 156.7 (s, C^7), 155.3 (brs, C^{10} , located using HMBC), 147.1 (s, C^4), 132.7 (s, C^8), 126.2 (s, C^5), 125.4 (s, C^6), 124.8 (s, C^{11}), 103.6 (s, C^2), 57.3 (s, O- Me), 38.9 (s, N- Me), 35.4 (s, $\text{C}(\text{CH}_3)_3$), 31.1 (s, $\text{C}(\text{CH}_3)_3$).

Elemental Microanalysis: Calc. $\text{C}_{31}\text{H}_{37}\text{AuN}_3\text{OPF}_6$ (809.22): C, 45.99%; H, 4.61%; N, 5.19%. Found: C, 46.12%; H, 4.72%; N, 5.13%.

$[(\text{C}^{\wedge}\text{N}^{\text{py-O-Me}}\wedge\text{C})\text{Aubenzimidazole}]\text{PF}_6$ (**47**)

Prepared using method 7 using the following amounts: $(\text{C}^{\wedge}\text{N}^{\text{py-O-Me}}\wedge\text{C})\text{AuCl}$ (0.055 g, 0.087 mmol). The reaction time for **47** is 8 days. **47** was isolated as a cream coloured powder (0.062 g, 0.072 mmol, 83%).



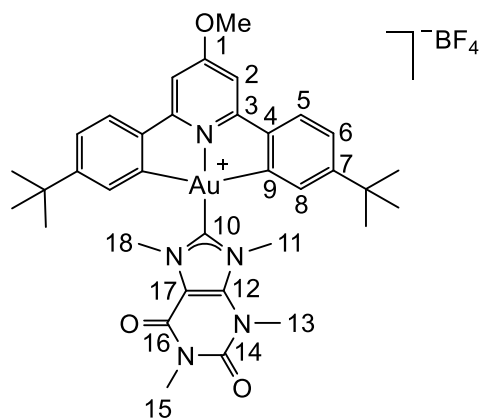
^1H NMR (CD_2Cl_2 , 300.13 MHz, 298 K): δ 7.80 (m, 2 H, H^{12}), 7.71 (m, 2 H, H^{13}), 7.66 (d, $^3J_{\text{H-H}} = 8.2$ Hz, 2 H, H^5), 7.39 (dd, $^3J_{\text{H-H}} = 8.2$ Hz, $^4J_{\text{H-H}} = 1.8$ Hz, 2 H, H^6), 7.07 (s, 2 H, H^2), 6.94 (d, $^4J_{\text{H-H}} = 1.8$ Hz, 2 H, H^8), 4.12 (s, 3 H, O- CH_3), 4.12 (s, 6 H, N- CH_3), 1.16 (s, 18 H, ^tBu).

$^{13}\text{C}\{^1\text{H}\}$ NMR (CD_2Cl_2 , 75.48 MHz, 298 K): δ 172.3 (s, C^1), 166.4 (s, C^3), 164.5 (s, C^{10}), 164.0 (s, C^9), 156.7 (s, C^7), 147.1 (s, C^4), 134.7 (s, C^{11}), 132.6 (s, C^8), 126.5 (s, $\text{C}^{5/13}$), 126.4 (s, $\text{C}^{5/13}$), 125.5 (s, C^6), 112.3 (s, C^{12}), 103.8 (s, C^2), 57.4 (s, O- Me), 36.1 (s, N- Me), 35.4 (s, $\text{C}(\text{CH}_3)_3$), 31.0 (s, $\text{C}(\text{CH}_3)_3$).

Elemental Microanalysis: Calc. $\text{C}_{31}\text{H}_{37}\text{AuN}_3\text{OPF}_6$ (859.24): C, 48.90%; H, 4.57%; N, 4.89%. Found: C, 48.91%; H, 4.56%; N, 4.98%.

$[(C^{\wedge}N^{py-OMe})Au]caffeine]BF_4$ (**48**)

Prepared using method 8 using the following amounts: $(C^{\wedge}N^{py-O-Me})AuCl$ (0.050 g, 0.083 mmol), potassium tert-butoxide (0.011 g, 0.098 mmol), [1,3-dimethylcaffeine][BF_4] (0.025 g, 0.083 mmol). **48** was isolated as a cream coloured powder (0.035 g, 0.041 mmol, 49%).



1H NMR (CD_2Cl_2 , 300.13 MHz, 298 K): δ 7.64 (d, $^3J_{H-H} = 8.2$ Hz, 2 H, H^5), 7.39 (dd, $^3J_{H-H} = 8.2$ Hz, $^4J_{H-H} = 1.8$ Hz, 2 H, H^6), 7.12 (d, $^4J_{H-H} = 1.8$ Hz, 2 H, H^8), 7.04 (s, 2 H, H^2), 4.27 (s, 3 H, H^{11}), 4.19 (s, 3 H, H^{18}), 4.11 (s, 3 H, O- CH_3), 3.93 (s, 3 H, H^{13}), 3.46 (s, 3 H, H^{15}), 1.26 (s, 18 H, iBu).

$^{13}C\{^1H\}$ NMR (CD_2Cl_2 , 75.48 MHz, 298 K): δ 172.2 (s, C^1), 166.4 (s, C^3), 164.1 (s, C^9), 161.2 (s, C^{10}), 156.9 (s, C^7), 153.9 (s, C^{16}), 151.0 (s, C^{14}), 146.9 (s, C^4), 141.6 (s, C^{12}), 132.9 (s, C^8), 126.3 (s, C^5), 125.5 (s, C^6), 110.8 (s, C^{17}), 103.7 (s, C^2), 57.4 (s, O- Me), 40.1 (s, C^{11}), 38.6 (s, C^{18}), 35.5 (s, $C(CH_3)_3$), 32.6 (s, C^{13}), 31.1 (s, $C(CH_3)_3$), 29.1 (s, C^{15}).

Elemental Microanalysis: Calc. $C_{35}H_{41}AuN_5O_3BF_4$ (863.29): C, 48.68%; H, 4.79%; N, 8.11%. Found: C, 48.70%; H, 4.77%; N, 8.06%.

6.3 X-ray crystallography

The work in the section was done by Dr Julio Fernandez-Cestau (**4**, **5**, **7**, **9** and **11**) and Dr David Hughes (**3**, **28** and **46**)

Crystals of each sample were mounted on a MiTeGen MicroMesh and fixed in the cold nitrogen stream on a diffractometer. Diffraction intensities were recorded at the specified temperature on an Oxford Diffraction Xcalibur-3/Sapphire3-CCD diffractometer, equipped with Mo- $K\alpha$ radiation and graphite monochromator or Rigaku HG Saturn724+ (2×2 bin mode). Data were processed using the CrystAlisPro-CCD and –RED software or CrystalClear-SM Expert 3.1 b27, with the absorption correction done at this stage.¹¹

The structures of all samples were determined by the direct methods routines with SHELXS or SHELXT programs and refined by full-matrix least-squares methods on F^2 in SHELXL.¹² Non-hydrogen atoms were generally refined with anisotropic thermal parameters. Hydrogen atoms were included in idealised positions. No missed symmetry was reported by PLATON.¹³

Refinement results are included in Table 6.1. Computer programs used in this analysis were run through WinGX.¹⁴ Scattering factors for neutral atoms were taken from reference 15.

	(C ^N Pz ^A C)AuSPh (3)		(C ^N Pz ^A C)AuSC ₆ H ₄ ^t Bu-4 (9)	(C ^N Pz ^A C)AuSC ₅ H ₄ N-2 (4)
	Red polymorph	Yellow polymorph		
Empirical formula	C ₃₀ H ₃₁ AuN ₂ S	C ₃₀ H ₃₁ AuN ₂ S	C ₃₄ H ₃₅ AuN ₂ S	C ₂₉ H ₃₀ AuN ₃ S
Crystal dimensions (mm), colour	0.065×0.14×0.35, red	0.35×0.09×0.08, pale yellow	0.048×0.033×0.019, yellow	0.6×0.04×0.03, yellow
F_w	648.59	648.59	700.66	649.58
T (K)	140(2)	140(2)	140(2)	100(2)
crystal system, space group	triclinic; P-1	monoclinic; P 2 ₁ /m	Monoclinic; P2 ₁ /c	Monoclinic, P2 ₁ /c
a(Å)	12.2846(2)	12.5213(8)	14.4504(6)	8.8501(2)
b(Å)	14.7009(3)	6.9443(2)	16.8527(4)	15.3636(3)
c(Å)	15.3192(2)	15.8652(6)	13.2971(4)	18.8486(3)
α (deg)	98.283(2)	90	90	90
β (deg)	109.863(2)	110.495(5)	114.412(4)	100.107(2)
γ (deg)	93.835(2)	90	90	90
volume (Å ³)	2554.81(8)	1292.19(11)	2948.71(19)	2523.06(9)
Z	4	2	4	4
D_{calcd} (Mg/m ³)	1.686	1.667	1.578	1.71
absorption coefficient (mm ⁻¹)	5.861	5.794	5.085	5.936
F(000)	1280	640	1392	1280
θ range for data collection (°)	3.143 to 29.999	3.238 to 27.496	2.129 to 27.482	2.338 to 29.557
data // restraints // params	14889 // 0 // 613	3213 // 0 // 193	6719 // 0 // 352	6272 // 0 // 313
goodness-of-fit on F^2 ^[a]	1.044	1.153	1.031	0.888
final R indexes [$I > 2\sigma(I)$] ^[a]	R1 = 0.0304, wR2 = 0.0651	R1 = 0.0372, wR2 = 0.0798	R1 = 0.0276, wR2 = 0.0531	R1 = 0.0296, wR2 = 0.1048
R indexes (all data) ^[a]	R1 = 0.0484, wR2 = 0.0701	R1 = 0.0456, wR2 = 0.0819	R1 = 0.0379, wR2 = 0.0563	R1 = 0.0354, wR2 = 0.1202
largest diff peak and hole (e.Å ⁻³)	1.661 and -1.297	2.630 and -0.993	0.746 and -1.277	1.67 and -1.753

^[a] $R1 = \Sigma(|F_o| - |F_c|) / \Sigma |F_o|$; $wR2 = [\Sigma w(F_o^2 - F_c^2)^2 / \Sigma w F_o^2]^{1/2}$; goodness of fit = $\{\Sigma [w(F_o^2 - F_c^2)^2] / (N_{\text{obs}} - N_{\text{param}})\}^{1/2}$; $w = [\sigma^2(F_o) + (g_1 P)^2 + g_2 P]^{-1}$; $P = [\max(F_o^2; 0) + 2F_c^2] / 3$.

	(C [^] N ^{pz} ^C)AuSNp-2 (5)		(C [^] N ^{pz} ^C)AuSCoum (7)	(C [^] N [^] C)AuSNp-2 · CH ₂ Cl ₂ (11 · CH ₂ Cl ₂)
	Red polymorph	Yellow polymorph		
Empirical formula	C ₃₄ H ₃₃ AuN ₂ S	C ₃₄ H ₃₃ AuN ₂ S	C ₃₄ H ₃₃ Au N ₂ O ₂ S	C ₃₆ H ₃₆ AuCl ₂ NS
Crystal dimensions (mm), colour	0.074×0.032×0.012, red	0.235×0.049 × 0.014, yellow	0.2×0.2×0.014, orange	0.15×0.02×0.02, yellow
<i>F</i> _w	698.65	698.65	730.65	782.58
T (K)	100(2)	140(2)	140(2)	100(2)
crystal system, space group	monoclinic; P 2 ₁ /n	monoclinic; P 2 ₁ /n	monoclinic; P 2 ₁ /n	triclinic; P-1
<i>a</i> (Å)	15.2707(4)	6.36960(10)	9.9308(2)	9.7612(7)
<i>b</i> (Å)	6.3728(2)	17.2085(3)	17.6575(4)	11.4058(8)
<i>c</i> (Å)	29.0818(8)	25.1788(5)	16.8512(4)	16.1645(11)
α(deg)	90	90	90	89.924(5)
β(deg)	101.425(3)	91.386(2)	103.620(2)	74.521(4)
γ(deg)	90	90	90	65.656(4)
volume (Å ³)	2774.08(14)	2759.07(8)	2871.81(11)	1568.0(2)
Z	4	4	4	2
<i>D</i> _{calcd} (Mg/m ³)	1.673	1.682	1.69	1.658
absorption coefficient (mm ⁻¹)	5.405	5.434	5.23	4.955
F(000)	1384	1384	1448	776
θ range for data collection (°)	2.3 to 29.572	2.502 to 27.482	3.127 to 29.801	2.635 to 27.538
data // restraints // params	7378 // 0 // 349	6269 // 0 // 343	7041 // 0 // 368	7141 // 0 // 376
goodness-of-fit on F ² [^a]	1.052	1.055	1.001	1.025
final R indexes [I>2σ(I)] [^a]	R1 = 0.0527, wR2 = 0.1045	R1 = 0.0237, wR2 = 0.0504	R1 = 0.0241, wR2 = 0.0405	R1 = 0.0453, wR2 = 0.1147
R indexes (all data) [^a]	R1 = 0.0635, wR2 = 0.1103	R1 = 0.0282, wR2 = 0.052	R1 = 0.0375, wR2 = 0.0429	R1 = 0.0488, wR2 = 0.1179
largest diff peak and hole (e.Å ⁻³)	3.026 and -4.187	1.344 and -0.716	1.02 and -0.727	3.213 and -2.257

[^a] R1 = Σ(|*F*_o| - |*F*_c|)/Σ|*F*_o|; wR2 = [Σw(*F*_o² - *F*_c²)/Σw*F*_o²]^{1/2}; goodness of fit = {Σ[w(*F*_o² - *F*_c²)]/(*N*_{obs} - *N*_{param})^{1/2}; w = [σ²(*F*_o) + (*g*₁*P*)² + *g*₂*P*]⁻¹; *P* = [max(*F*_o²; 0 + 2*F*_c²)/3].

	(CNCAuSAd) ₂ HAB ₂ (28)	CN ^{py-OMe} CAu–imidazole (46)
Empirical formula	C ₁₄₂ H ₉₀ Au ₂ N ₄ S ₂ B ₄ F ₆₀	C ₃₁ H ₃₇ AuN ₃ OPF ₆ , ca C _{1.55}
Crystal dimensions (mm), colour	0.19×0.10×0.07, colourless	0.055×0.065×0.35, colourless
<i>F</i> _w	3525.47	828.19
T (K)	295(1)	140(1)
crystal system, space group	triclinic; P-1	Orthorhombic, P n a 21
a(Å)	15.0100(8)	23.0946(7)
b(Å)	15.8427(8)	22.5721(7)
c(Å)	16.5234(7)	13.9068(5)
α(deg)	70.367(4)	90
β(deg)	84.345(4)	90
γ(deg)	70.653(5)	90
volume (Å ³)	3491.5(3)	7249.5(4)
Z	2	8
<i>D</i> _{calcd} (Mg/m ³)	1.677	1.518
absorption coefficient (mm ⁻¹)	2.263	4.161
F(000)	1736	3274
θ range for data collection (°)	3.515 to 22.500	3.523 to 26.000
data // restraints // params	9083 // 0 // 983	14224 // 1 // 815
goodness-of-fit on F ² [^a]	1.044	1.038
final R indexes [I>2σ(I)] [^a]	R1 = 0.065, wR2 = 0.121	R1 = 0.039, wR2 = 0.079
R indexes (all data) [^a]	R1 = 0.093, wR2 = 0.132	R1 = 0.056, wR2 = 0.084
largest diff peak and hole (e.Å ⁻³)	1.23 and -0.96	0.80 and -0.48
^[a] R1 = Σ(F _o - F _c) / Σ F _o ; wR2 = [Σw(F _o ² - F _c ²) ² / ΣwF _o ²] ^{1/2} ; goodness of fit = {Σ[w(F _o ² - F _c ²) ²] / (N _{obs} - N _{param}) ^{1/2} ; w = [σ ² (F _o) + (g ₁ P) ² + g ₂ P] ⁻¹ ; P = [max(F _o ² ; 0 + 2F _c ²)]/3.		

Table 6.1. Selected crystal data and structure refinement details.

6.4 Photophysical Properties

UV–visible absorption spectra were recorded using a Perkin-Elmer Lambda 35 UV/vis spectrometer. Excitation and emission spectra were measured using a (TCSPC) FluoroLog Horiba Jobin Yvon spectrofluorometer. Lifetime measurements were conducted with a Datastation HUB-B with a nanoLED controller and software DAS6. The nanoLEDs employed for lifetime measurements were of 370 nm with pulse lengths of 0.8–1.4 ns. Quantum yields in the solid state were measured upon excitation at 370–400 nm using an F-3018 integrating sphere mounted on a Fluorolog 3-11 Tau-3 spectrofluorimeter, at the Universidad de La Rioja by Dr Julio Fernandez-Cestau. In solution, relative quantum yields were determined with reference to $[\text{Ru}(\text{bpy})_3]^{2+}$ in H_2O ($\phi_{\text{stn}} = 2.8\%$) in accordance with reference 16.

Complex	Absorbance [nm] ($10^3 \epsilon/\text{M}^{-1} \text{cm}^{-1}$)
(C ^N Pz ^C)AuSPh 3	320 (9.1), 344 (6.2), 365 (4.3), 421 (4.3), 441 (4.3), 470(1.4), long tail up to 530.
(C ^N Pz ^C)AuSC ₅ H ₄ N-2 4	321 (11.5), 349 (8.9), 425 (5.1), 443 (5.0), 470 (1.1), tail up to 500.
(C ^N Pz ^C)AuSNp-2 5	323 (15.9), 348 (11.0), 420 (7.3), 440 (7.3), 469 (2.1), long tail up to 530.
(C ^N Pz ^C)AuSQuin-2 6	322 (13.6), 351 (11.9), 424 (5.9), 445 (5.2), 470 (1.8), tail up to 515.
(C ^N Pz ^C)AuSCoum 7	324 (23.2), 373 (17.3), 423 (7.8), 442 (7.5), 471 (2.3), long tail up to 530.
(C ^N Pz ^C)AuSAd 8	322 (7.2), 348 (4.4), 395 (2.4), 423 (2.9), 445 (3.1), 469 (0.8), tail up to 530.
(C ^N Pz ^C)AuSC ₆ H ₄ ^t Bu-4 9	321 (10.0), 348 (6.0), 421 (4.1), 440 (5.0), 471 (1.7), long tail up to 530.
(C ^N Pz ^C)AuSNp-1 10	320 (10.3) broad shoulder, 419 (3.4), 439 (3.4), 470 (0.8), long tail up to 530.
(C ^N Pz ^C)AuSNp-2 11	319 (13.8), 368 (8.0), 384 (7.6), 405 (6.1), 470 (0.3).

Table 6.2. Absorption data for complexes in CH_2Cl_2 (5×10^{-5} M).

Complex	$\lambda_{em} / nm (\lambda_{ex} / nm)$	
	298 K	77 K
(C ^N Pz [^] C)AuSPh 3	574 (350-500)	558 _{max} , 593 _{sh} (360-500)
(C ^N Pz [^] C)AuSC ₅ H ₄ N-2 4	492 (300-450)	534 _{max} , 579 _{sh} (300-480, 360 _{max} , 430 _{sh} , 460 _{sh})
(C ^N Pz [^] C)AuSNp-2 5	650 (350-600, 480 _{sh})	370 _{max} , 650 (360-550)
(C ^N Pz [^] C)AuSQuin-2 6	[a]	519 _{sh} , 532 _{max} , 553 _{sh} (350-470)
(C ^N Pz [^] C)AuSCoum 7	[a]	540, 577, 621 (360-550)
(C ^N Pz [^] C)AuSAd 8	633 (370-470)	630 (360, 470, 500-570 _{br})
(C ^N Pz [^] C)AuSC ₆ H ₄ ^t Bu-4 9	600 (350-500)	548 _{max} , 593 _{sh} (350-500)
(C ^N Pz [^] C)AuSNp-1 10	618 (360 _{br} -510 _{max})	547 _{sh} , 630 (350-460, 518)
(C ^N Py [^] C)AuSNp-2 11	[a]	514 _{max} , 544 _{sh} (400-450)

Table 6.3. PL properties of the complexes in the solid state. [a] Non-emissive.

Complex	$\lambda_{em} / nm (\lambda_{ex} / nm)$	τ / ns ^[a]	$\phi / \% (\lambda_{ex} / nm)$ ^[b]
3	530 _{sh} , 616 _{max} (320-390); 616 (500)	355.2±4.4(95%), 44.5±2.0(5%)	< 1
4	540 _{max} , 573 _{sh} , 614 _{sh} (320-350, 400, 420) ^[c]	342.2±5.7(96%), 25.0±2.1(5%)	< 1
5	611 (320-560, 380 _{sh} , 470 _{max})	366.9±6.9(94%), 51.8±2.5(6%)	3.7 (480)
6	508 (340-450, 390 _{max})	369.5±4.8(95%), 46.4±1.7(5%)	4.7 (390)
7	595 (330-450)	376.0±1.2(94%), 56.7±4.8(6%)	< 1
8	642 (350-600, 320 _{sh} , 470 _{sh} , 550 _{max})	374.3±5.7(95%), 46.1±2.3(5%)	< 1
9	622 (340-580, 370 _{sh} , 510 _{max})	345.6±3.9(96%), 38.2±3.9(5%)	3.4 (510)
10	516 _{sh} , 615 _{max} (350-580, 515 _{max})	368.8±3.0(95%), 47.7±1.2(5%)	1.8 (515)

11	~480 ^[b]
-----------	---------------------

Table 6.4. PL properties of complexes **3-11** in 10% PMMA matrix at 298 K. [a] Measured at λ_{max}^{em} [b] Determined by absolute methods using an integrating sphere. [c] Weak emission.

Matrix	$\lambda_{em} / \text{nm} (\lambda_{ex} / \text{nm})$	$\tau_{av} / \text{ns}^{[a]}$	$\phi / \% (\lambda_{ex} / \text{nm})^{[b]}$
1% in PMMA	600 (350-540, 375 _{max} , 450 _{sh} , 490 _{sh}) weak	82.2	< 1
5% in PMMA	611 (320-560, 380 _{sh} , 470 _{max})	186	1.9 (480)
10% in PMMA	619 (350-575, 380 _{sh} , 500 _{max})	204	3.7 (480)
20% in PMMA	628 (350-580, 505 _{max})	194	4.1 (480)
30% in PMMA	630 (350-590, 380 _{sh} , 505 _{max})	204	5.0 (480)
40% in PMMA	644 (350-600, 540 _{max})	198	6.6 (480)
50% in PMMA	649 (350-650, 520 _{max})	267	11.2 (480)
10% in PS	626 (350-580, 380 _{sh} , 515 _{max})	223	4.4 (480)
10% in PVK	632 (350-580, 380 _{sh} , 505 _{max})	226	3.3 (480)

Table 6.5. Steady State properties of complex (C^{Npz}C)AuSNp-2 **5** at 298 K in different polymeric matrix [a] Measured at λ_{max}^{em} . Fit to tri-exponential decay functions in all cases. Only the average lifetime is given and used to calculate the radiative and non-radiative constants. [b] Determined by absolute methods using an integrating sphere.

Matrix	$\lambda_{em} / \text{nm} (\lambda_{ex} / \text{nm})$	$\tau_{av} / \text{ns}^{[a]}$	$\phi / \% (\lambda_{ex} / \text{nm})^{[b]}$
10% in PMMA	508 (340-450, 390 _{max})	28	4.7 (390)
30% in PMMA	508 (340-450, 390 _{max})	30	1.2 (390)
50% in PMMA	517 _{br} (350-450)	94	< 1 (390)

Table 6.6. Steady State properties of complex (C^{Npz}C)AuSQuin-2 **6** at 298 K in different polymeric matrix. [a] Measured at λ_{max}^{em} . Fit to tri-exponential decay functions in all cases. Only the average lifetime is given and used to calculate the radiative and non-radiative constants. [b] Determined by absolute methods using an integrating sphere.

Complex	T / K	λ_{em} / nm (λ_{ex} / nm)	τ [λ / nm]	$\phi / \%$ (λ_{ex} / nm) ^[a]
3	298	[b]		
	77	540 _{sh} , 600 _{max} (370-480) (10^{-4} M) ^[c]	28.7±1.1 μ s [600]	
4	298	516 _{max} , 546 _{sh} (320-350, 400, 420) (10^{-4} M) ^[c]	11.0±0.1(40), 156.4±5.8(60) ns [516]	
	77	540 _{max} , 580 _{sh} (350-600, 370 _{max} , 480 _{sh}) (10^{-4} M) ^[c]	84.3±1.5 μ s (10^{-4} M) [540]	
5	298	680 (300-480) (10^{-4} M) // 683 (300-600, 540 _{max}) (10^{-2} M)	17.3±0.1 ns [680]	2.62×10 ⁻³ (436) ^[e]
	77	605 (360-460) (10^{-4} M) // 614 (540 _{max}) (10^{-2} M)	35.3±0.4 μ s [614]	
6	298	508 (340-420) (10^{-2} M) ^[d]	10.6±0.2(14), 211.2±6.4(86) ns [508]	
	77	544 _{max} , 579 _{sh} (300-470) (10^{-4} M) ^[c]	118.4±3.7 μ s [540]	
7	298	621 (350-570, 370 _{sh} , 520 _{max}) (10^{-2} M) ^[d]		2.34×10 ⁻³ (436)
	77	587 _{max} (320-470, 514 _{max}) (10^{-2} M) // 541 _{max} , 574 _{sh} (320-420) (10^{-4} M)	63.8±1.0 μ s [541]	
8	298	670 (350-470) (10^{-4} M) // 665 (360-600, 500 _{max}) (10^{-2} M)	16.2±0.07 ns [670]	1.45×10 ⁻² (436)
	77	540 _{sh} , 609 (320-480, 365, 430, 450) (10^{-4} M) // 629 (320-570, 370, 460) (10^{-2} M)	12.6±0.2 μ s [629]	
9	298	680 (350-500, 360 _{max} , 430 _{sh}) (10^{-4} M) ^[c]	17.1±0.1 ns [680]	1.94×10 ⁻⁴ (436)
	77	539 _{sh} , 555 _{sh} , 616 _{max} (320-480) (10^{-4} M) // 616 nm (340-500) (10^{-2} M)	106.8±2.6 μ s [540], 30.2±1.9 μ s [616]	
10	298	685 (400-600, 530 _{max}) (10^{-4} M) ^[c]	8.7±0.1 ns [689]	5.58×10 ⁻³ (436)
	77	516 _{sh} , 529 _{max} , 565 _{sh} (320-420) (10^{-5} M) // 516 _{sh} , 529 _{sh} , 599 _{max} (320-550) (10^{-4} M) // 529 _{sh} , 617 (320-550) (10^{-2} M) ^[c]	43.8±1.0 μ s (10^{-2} M) [617]	

11	298	[b]
77	517 _{max} , 552 _{sh} (300-460, 370 _{max} , 410 _{sh} , 440 _{sh}) (10 ⁻⁴ M) ^[c] 50.2±0.1 μs [517]	

Table 6.7. PL properties of complexes **3-11** in CH₂Cl₂. [a] Relative to standard.⁵⁷ [b] Non-emissive. [c] Same at 10⁻² M. [d] Very weak at 10⁻⁴ M [e] 2.30×10⁻³ (372), 2.47×10⁻³ (419), 2.62×10⁻³ (436), 9.59×10⁻³ (472), 1.70×10⁻² (495).

		$\lambda_{em} / nm (\lambda_{ex} / nm)$	
Solvent	Conc.	298 K	77 K
CH ₂ Cl ₂	10 ⁻⁴ M	680 (350-500, 360 _{max} , 430 _{sh})	515, 535 _{sh} , 605 (320-550, 365 _{max} , 440 _{sh})
	10 ⁻² M	680 (350-600, 540 _{max})	622 (500)
THFMe-2	10 ⁻⁴ M	weak	520, 591 _{max} (380-470)
	10 ⁻² M	660 (360-450, 540)	522, 542 _{sh} , 584 (380-470)

Table 6.8. Steady State emission of (C^{N^{Pz}}C)AuSC₆H₄^tBu-4 **9** in different solvents.

		$\lambda_{em} / nm (\lambda_{ex} / nm)$	
Solvent	Conc.	298 K	77 K
CH ₂ Cl ₂	10 ⁻⁴ M	680 (300-480)	605 (360-460)
	10 ⁻² M	683 (300-600, 540 _{max})	614 (540 _{max})
THFMe-2	10 ⁻⁴ M	663 (300-500, 365 _{max} , 440 _{sh})	520, 591 _{max} (360-450)
	10 ⁻² M	664 (350-600, 540 _{max})	520, 585 _{max} (360-460)
Toluene	10 ⁻⁴ M	642 (300-500, 370 _{max} , 430 _{sh})	604 (350-450)
	10 ⁻² M	642 (350-600, 540 _{max})	600 (540 _{max})

Table 6.9. Steady State emission of (C^{N^{Pz}}C)AuSNp-2 **5** in different solvents.

6.5 Diffusion NMR

Diffusion NMR was used in 2.7 to determine the proportion of aggregates in solution and in 3.13 to determine the hydrodynamic dimensions of the species obtained after C–C reductive elimination from **20**.

6.5.1 Investigating aggregation tendency Dr Luca Rocchigiani

¹H PGSE NMR measurements were performed by using a double stimulated echo sequence with longitudinal eddy current delay on a Bruker DRX 300 spectrometer equipped with a smartprobe and Z-gradient coil, at 297K without spinning. In the typical PGSE experiment, the dependence of the resonance intensity (I) on a constant waiting time and on a varied gradient strength G is described by Equation 1.

$$\ln \frac{I}{I_0} = (g\delta^2)D_t \left(d - \frac{D}{3} \right) G^2$$

Equation 6.1

where I is the intensity of the observed spin echo, I_0 the intensity of the spin echo in the absence of gradient, D_t the self-diffusion coefficient, Δ the delay between the midpoints of the gradients, δ the length of the gradient pulse, and γ the magnetogyric ratio. The shape of the gradients was rectangular, their length δ was 4–5 ms, and their strength G was varied during the experiments. All spectra were acquired for 64K points and a spectral width of 6200 Hz and processed with a line broadening of 1.0. The semi-logarithmic plots of $\ln(I/I_0)$ versus G^2 were fitted by using a standard linear regression algorithm. Different values of G and number of transients were used for different samples.

The self-diffusion coefficient D_t , which is directly proportional to the slope of the regression line obtained by plotting $\ln(I/I_0)$ versus G^2 , was estimated by evaluating the proportionality constant for a sample of HDO (5%) in D₂O (known diffusion coefficients in the range 274–318 K)¹⁷ under the exact same conditions as the sample of interest. The solvent was taken as internal standard. The actual concentration of the samples was measured by relative integration to an external standard.

The relationship between D_t and hydrodynamic dimensions is expressed by the modified Stokes-Einstein equation:

$$D_t = \frac{kT}{\rho h f c \sqrt[3]{abd}}$$

Equation 6.2. The modified Stokes-Einstein equation

where k is the Boltzmann constant, T is the temperature, η is the solution viscosity, c is the “size factor”, which depends on the solute-solvent radius ratio and f is the “shape factor”, which takes into account the deviation from sphericity of the diffusing molecule. a , b and d are the semi-axes of the ellipsoid that better approximates the shape of the diffusing molecule.¹⁸

Structural parameter values ($P = fc\sqrt[3]{abd} = kT / \rho h D_t$) were derived from the measured D_t values at different concentration in CD_2Cl_2 and the data are collected in Table 6.2.

Assuming a monomer/dimer equilibrium, the observed P values can be treated as the average between the parameters of both monomer (P_M) and dimer (P_D), according to the following relationship:

$$P_i = P_M x_M + P_D x_D$$

where x_M and x_D are the molar fractions of monomer and dimer at a given concentration.

P_M and P_D parameters are depending on the dimensions of monomer (a_M, b_M, d_M), dimer (a_D, b_D, d_D) and solvent (r_{solv} , approximated at the van der Waals radius of CD_2Cl_2). P_M parameters can be derived from X-ray structures of monomers, by approximating their shape to ellipsoids. P_D parameters have been calculated by using packing data derived by X ray diffraction (see below).

c (mM)	$10^{10}D_t$ ($m^2 s^{-1}$)	P (Å)	mol-% dimer
1 ($C^{\wedge}N^{Pz^{\wedge}C}$)AuCl $P_M=27.9$ Å; $P_D=39.6$ Å			
0.8	11.0	27.8	<1
4.3	11.0	27.8	<1
11.8	10.9	28.0	1.5
23.9	10.6	28.8	13
3 ($C^{\wedge}N^{Pz^{\wedge}C}$)AuSPh $P_M=29.3$ Å; $P_D=39.8$ Å			
2.9	10.4	29.5	2
8.8	10.2	29.9	5
17.5	10.1	30.3	9
22.3	10.1	30.4	10
23.5	10.0	30.5	11
53.8	9.8	31.3	19
55.5	9.7	31.5	21
5 ($C^{\wedge}N^{Pz^{\wedge}C}$)AuSNp-2 $P_M=30.4$ Å; $P_D=44.0$ Å			
0.6	10.0	30.7	2
1.3	9.8	31.1	5
1.9	9.8	31.2	6
4.1	9.7	31.5	8
19.3	9.5	32.3	14
42.6	9.3	32.8	18
72.5	9.0	34.0	26

Table 6.10. Diffusion coefficient (D_t), structural parameters (P) and estimated percentage of dimers (%D) for **1**, **3** and **5** as a function of concentration in CD_2Cl_2 at 297 K.

The amount of dimers was quantified by using standard equations for monomer-dimer equilibrium:¹⁹

$$d_i = d_M f_M + d_D f_D = \frac{[A]}{[A]_0} d_M + \frac{2[A_2]}{[A]_0} d_D$$

$$d_i = d_M + (d_D - d_M) \frac{(1 + 8K[A]_0)^{1/2} - 1}{(1 + 8K[A]_0)^{1/2} + 1}$$

where f_m and f_d are the molar fractions of monomers and dimers, δ_M and δ_D are the limit chemical shift values of monomer and dimer, respectively, K is the association constant. After fitting chemical shift versus concentration trends, the molar fractions of dimers were obtained as:

$$f_D = -1 + \frac{2[A]_0}{[A]_0 + \frac{\sqrt{1 + 8K[A]_0} - 1}{4K}}$$

C (mM)	f_D (%)
(C ^{N^{Pz}} C)AuCl $K=3.6 M^{-1}$	
0.8	<1
4.3	3
11.8	7
23.9	13
(C ^{N^{Pz}} C)AuSPh $K=1.0 M^{-1}$	
2.9	<1
8.8	2
17.5	3
22.3	4
23.5	4
53.8	9
55.5	9
(C ^{N^{Pz}} C)AuSNp-2 $K=1.8 M^{-1}$	
0.6	<1
1.3	<1
1.9	<1
4.1	1
19.3	6

42.6	12
72.5	18

Table 6.11. Table Molar fraction of dimers derived by fitting chemical shift vs. concentration trends for (C^{^N}P^zC)AuCl (**1**), (C^{^N}P^zC)AuSPh (**3**) and (C^{^N}P^zC)AuSNp-2 (**5**) (CD₂Cl₂, 297 K).

6.5.2 Hydrodynamic dimensions of [ClAuSAd]_nH_n in collaboration with Dr Luca Rocchigiani

Diffusion NMR was used to investigate the hydrodynamic dimensions of the species obtained after C–C reductive elimination of **20** in the presence of adamantyl thiol. As described in section 3.13, at the end of the reaction, the mixture is composed by free adamantyl thiol, **23** and an additional adamantyl species, reasonably assigned to the Au(I) complex formed upon elimination of the ligand.

¹H PGSE NMR experiments were again performed by using a double stimulated echo sequence with longitudinal eddy delay on a Bruker DRX 300 spectrometer equipped with a smartprobe and Z-gradient coil, at 297K without spinning. The decay of the signals (I) as a function of the applied gradient (G, Figure 6.1) were used with Equation 6.1^{18a} to obtain the diffusion coefficient. The modified Stokes-Einstein equation (Equation 6.2) was used to calculate the hydrodynamic data values, under the spherical approximation, these are shown in Table 6.12. The CD₂Cl₂ solvent was used as internal standard.

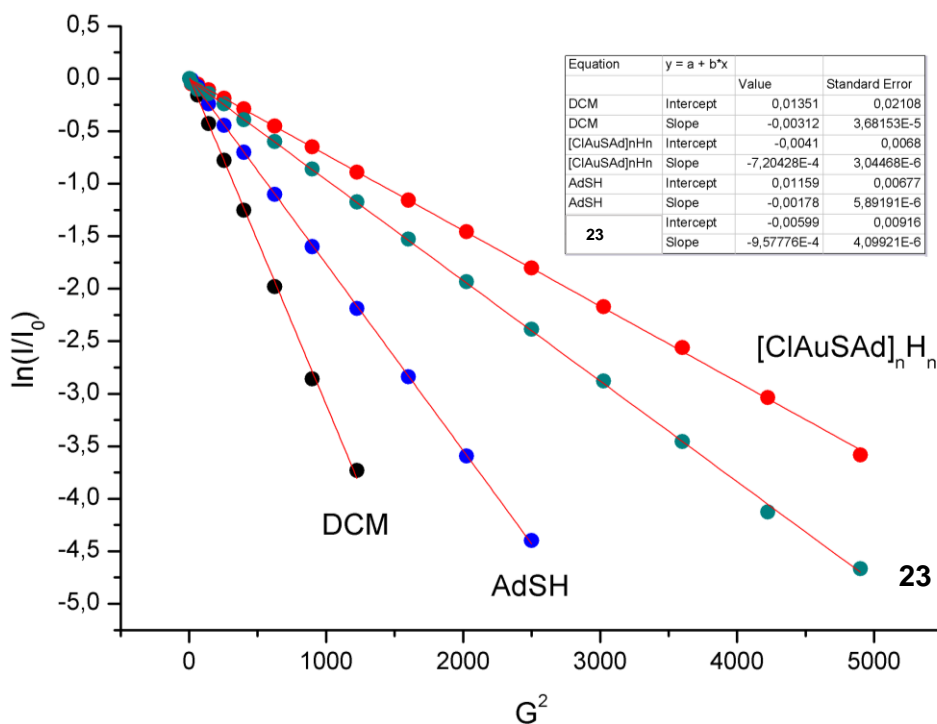


Figure 6.1. Trends of $\ln(I/I_0)$ versus G^2 for the components of the mixture obtained after the reaction of **20** with AdSH.

Species	Hydrodynamic Radius	Hydrodynamic Volume
AuSAd	7.1 Å	1500 Å ³
HSAd	3.53 Å	184 Å ³
23	5.58 Å	727 Å ³

Table 6.12. The hydrodynamic radii and volumes of species measured by PGSE NMR experiments.

The hydrodynamic volume values of 184 and 727 Å³ for adamantyl thiol and **23**, respectively. The Au(I) complex showed a hydrodynamic volume of 1500 Å³, which is about 8 times larger than free thiol. Therefore, it can be reasonably assumed that the Au(I) product exists as a small [ClAuSAd]_nH_n cluster, with an average n close to 7.

6.6 Kinetic Investigations

1/2 (0.005 g, 0.0087 mmol) was dissolved in dry CD₂Cl₂ (0.6 mL) in a J-Young NMR tube and an initial ¹H NMR spectra was recorded to lock and shim the sample. In open air, adamantyl thiol (at varying concentrations) was added to the NMR tube and the reaction was followed in situ by ¹H NMR spectroscopy. Different intervals between the spectra were used according to the thiol concentration.

Absolute concentration values were evaluated by comparing the relative integration to an external standard (4,4'-diiodobiphenyl in CDCl₃ at 3.6 mM) at a known concentration using identical NMR parameters. The spectra were processed and the normalized concentration of **1/2** was monitored over the course of the reaction by comparing the intensity of t-butyl signal with the spectrum at t = 0.

6.7 Biological testing

6.7.1 Antiproliferation assay (Dr Benoit Bertrand)²⁰

Human A549 cancer cell lines (from ECACC) were cultured in RPMI 1640 medium with 10% fetal calf serum, 2 mM L-glutamine, 100 units/mL penicillin, and 100 µg/mL streptomycin (Invitrogen). Cells were maintained in a humidified atmosphere at 37 °C and 5% CO₂. Inhibition of cancer cell proliferation was measured by the 3-(4,5-dimethylthiazol-2-yl)-5-(3-carboxymethoxyphenyl)-2-(4-sulfophenyl)-2H-tetrazolium (MTS) assay using the CellTiter 96 Aqueous One Solution Cell Proliferation Assay (Promega) and following the manufacturer's instructions. Briefly, A549 cells (8 × 10³ /100 µL) were seeded in 96-well plates and left untreated or treated with 1 µL of DMSO (vehicle control) or 1 µL of complex diluted in DMSO at different concentrations in triplicate for 72 h at 37 °C with 5% CO₂. Following this, the MTS assay reagent was added for 4 h, and the absorbance measured at 490 nm using a Polarstar Optima microplate reader (BMG Labtech). IC₅₀ values were calculated using GraphPad Prism version 5.0 software.

6.7.2 FRET assay²¹

The experiments for 5.9 were carried under the supervision of Dr Zoe Waller and Dr Elise Wright.

The initial FRET melting screen was performed using a FRET DNA-melting-based assay. The oligonucleotides are labelled with a donor fluorophore, FAM (6-carboxyfluorescein) and an acceptor TAMRA (6-carboxytetramethylrhodamine).

Name	DNA sequence	Transitional pH
hTeloC _{FRET}	5'-FAM-[TAA-CCC-TAA-CCC-TAA-CCC-TAA-CCC]-TAMRA-3'	6.0
c-MycC _{FRET}	5'-FAM-[TCC-CCA-CCT-TCC-CCA-CCC-TCC-CCA-CCC-TCC-CCA]-TAMRA-3'	6.6

hif-1 α _{FRET}	5'-FAM-[CGC-GCT-CCC-GCC-CCCTCT-CCC-CTC-CCC-GCG-C]-TAMRA-3'	7.2
hTeloG _{FRET}	5'-FAM-[GGG-TTA-GGG-TTA-GGG-TTA-GGG]-TAMRA-3'	7.2
DS _{FRET}	5'-FAM-[TAT-AGC-TAT-A-HEG(18)-TAT-AGC-TAT-A]-TAMRA-3'	7.2

Table 6.13. FRET labeled DNA sequences used in Section 5.9 and corresponding transitional pH values.

The solutions of the oligonucleotides were prepared as 0.2 μ M solutions, with 10 mM sodium cacodylate and 100 mM sodium chloride buffer at the specified pH. This was thermally annealed by heating the prepared samples for 5 minutes at 95 °C, then allowing them to cool to room temperature over 16 hours. Strip tubes (QIAGEN) were prepared by aliquoting 20 μ L of the annealed DNA followed by 0.5 μ L of 2 mM solutions of the complexes **40** – **48** dissolved in DMSO to deliver a final concentration of 50 μ M of complex. Control samples for each run were prepared with the same quantity of DMSO with the DNA in buffer. Fluorescence melting curves were determined in a QIAGEN RotorGene Q-series PCR machine. Measurements of fluorescence were made with excitation at 470 nm and detection at 510 nm. Final analysis of the data to determine melting temperatures for each secondary structure when exposed to complexes **40** – **48** was carried out using QIAGEN RotorGene Q-series software and Excel.

The dose response FRET assays were completed using the same method. A serial dilution of complexes **44** and **47** gave a series of solutions at the following concentrations: 2 mM, 1.2 mM, 800 μ M, 400 μ M, 200 μ M, 80 μ M, 40 μ M, 20 μ M and 10 μ M. The preparation of the samples was the same, using strip tubes (QIAGEN) containing 20 μ L of the annealed DNA followed by 0.5 μ L of solutions of the prepared solutions of **44** and **47** dissolved in DMSO to deliver the final concentrations of 50 μ M, 30 μ M, 20 μ M, 10 μ M, 5 μ M, 2 μ M, 1 μ M, 0.5 μ M and 0.25 μ M of complex.

References

- (1) Fernandez-Cestau, J.; Bertrand, B.; Blaya, M.; Jones, G. A.; Penfold, T. J.; Bochmann, M. *Chem. Commun.* **2015**, *51*, 16629
- (2) (a) K.-H. Wong, K.-K. Cheung, M. C.-W. Chan, C.-M. Che, *Organometallics* **1998**, *17*, 3505. (b) Wong, K. M. C.; Hung, L. L.; Lam, W. H.; Zhu, N. Y.; Yam, V. W. W. *J. Am. Chem. Soc.* **2007**, *129*, 4350.
- (3) D. A. Rosca, D. A. Smith, M. Bochmann, *Chem. Commun.* **2012**, *48*, 7247

- (4) I. Chambrier, D.A. Roşca, J. Fernandez-Cestau, D. L. Hughes, P. H. M. Budzelaar, M. Bochmann *Organometallics* **2017**, *36*, 1358
- (5) S. J. Lancaster, A. Rodriguez, A. Lara-Sanchez, M. D. Hannant, D. A. Walker, D. L. Hughes, M. Bochmann, *Organometallics* **2002**, *21*, 453
- (6) Pintus, A.; Rocchigiani, L.; Fernandez-Cestau, J.; Budzelaar, P. H. M.; Bochmann, M. *Angew. Chem.-Int. Edit.* **2016**, *55*, 12321.
- (7) J. Fernández-Cestau, N. Giménez, E. Lalinde, P. Montañó, M. T. Moreno, S. Sánchez, M. D. Weber and R. D. Costa, *Dalton Trans.*, **2016**, *45*, 3251
- (8) L. Rocchigiani, J. Fernandez-Cestau, P. H. M. Budzelaar, M. Bochmann, *Chem. Commun.* 2017, *53*, 4358
- (9) Rosca, D. A.; Smith, D. A.; Hughes, D. L.; Bochmann, M. *Angew. Chem.-Int. Edit.* **2012**, *51*, 10643
- (10) Schutz, J.; Herrmann, W. A. *J. Organomet. Chem.* **2004**, *689*, 2995.
- (11) *Programs CrysAlisPro*, Oxford Diffraction Ltd., Abingdon, UK (2010).
- (12) Sheldrick, G.M. SHELX-97 and SHELX-2014 – Programs for crystal structure determination (SHELXS) and refinement (SHELXL), *Acta Cryst.* 2008, **A64**, 112.
- (13) A. L. Spek, (2006) PLATON – A Multipurpose Crystallographic Tool, Utrecht University, Utrecht, The Netherlands. A. L. Spek, *Acta Cryst.* 1990, **A46**, C34
- (14) L. J. Farrugia, *J. Appl. Crystallogr.* 1999, **32**, 837.
- (15) ‘*International Tables for X-ray Crystallography*’, Kluwer Academic Publishers, Dordrecht. Vol. C. 1992, pp. 500, 219 and 193.
- (16) U. Resch-Genger, K. Rurack. *Pure Appl. Chem.* **2013**, *85*, 2005-2026. A. M. Brouwer, *Pure Appl. Chem.* **2011**, *83*, 2213-2228 and references therein.
- (17) (a) Tyrrell, H. J. W; Harris, K. R. *Diffusion in Liquids*; Butterworth: London, 1984.
(b) Mills, R. *J. Phys. Chem.* **1973**, *77*, 685.
- (18) (a) Macchioni, A.; Ciancaleoni, G.; Zuccaccia, C.; Zuccaccia, D. *Chem. Soc. Rev.* **2008**, *37*, 479. (b) Zuccaccia, D.; Macchioni, A. *Organometallics* **2005**, *24*, 3476.
- (19) Chen, J.–S., Shirts, R. B. *J. Phys. Chem.* **1985**, *89*, 1643.
- (20) Bertrand, B.; Fernandez-Cestau, J.; Angulo, J.; Cominetti, M. M. D.; Waller, Z. A. E.; Searcey, M.; O'Connell, M. A.; Bochmann, M. *Inorg. Chem.* **2017**, *56*, 5728.
- (21) (a) De Cian, A.; Guittat, L.; Kaiser, M.; Sacca, B.; Amrane, S.; Bourdoncle, A.; Alberti, P.; Teulade-Fichou, M. P.; Lacroix, L.; Mergny, J. L. **2007**, *42*, 183. (b) Wright, E. P.; Day, H. A.; Ibrahim, A. M.; Kumar, J.; Boswell, L. J. E.; Huguin, C.; Stevenson, C. E. M.; Pors, K.; Waller, Z. A. E. *Sci. Rep.* **2016**, *6*, 39456.